NEW METHODS
IN
SHALLOW SEISMIC REFLECTION

BY

ZUHAR ZAHIR TUAN HARITH

BSc. (Malaya); MSc. (London); DIC (Imperial College)

November, 1998

This thesis is submitted for the degree of Doctor of Philosophy

to

The Faculty of Science,
Department of Geology and Applied Geology,
University of Glasgow

ProQuest LLC.
789 East Eisenhower Parkway
P.O. Box 1346
Ann Arbor, MI 48106 – 1346

Dedicate to

my wife, my parents and all my families....

"Your undying love and support have assisted me in

putting me where I am today"

This thesis represents work carried out between January 1996 and November 1998.

I declare that this thesis is entirely my own work except where explicitly declared in the text. All published and unpublished materials used in this thesis have been given full acknowledgement in the text.

This thesis has not been submitted for a degree at any other higher institution.

Zuhar Zahir Tuan Harith

ACKNOWLEDGEMENTS

I would like to acknowledge the University of Science Malaysia and Malaysian Government for giving me an opportunity by granting me a three year scholarship so that this project can be completed despite economic turbulence in the South East Asian region. An additional acknowledgement is also expressed to John Nevett of Glasgow Development Agency (GDA) for giving permission to experiment with the first full 3-D shallow seismic survey on their site and who agreed to fund the cost of the field work. Without this financial help, this project could not have been done.

This project was initiated by Prof. D. K. Smythe and who supervised the whole project. Besides supervising the project, he also gave lots of guidance, support and advice on all matters whether it project, career or personal. He also even postponed his retirement to make sure that I could finish on time. For that I would like to express my thanks and appreciation.

I would also like to express my gratitude to the two other geophysical lecturers – Dr. Doyle Watts and Dr. Ben Doody – for their valuable insight into this work.

Appreciation is also due to the technical staff who assisted (as well as kept me entertained) throughout the years – Bob Cumberland and George Gordon. Also thanks to Colin Farrow and Kenny Roberts for computer support work, Mr. Douglas McLean for photographic work and Mr. Roddy Morrison (chief technician).

Thanks to all the other postgraduates who also go through years of torture in order to contribute to new knowledge –Bel, Andy, Carsten, Al Hamali, Fitchy, Joan, Keijan, Hadi, Gloria, Andy Cav., and others.

Also thanks to

1 Peter Fraenkel and Partners (the GDA consulting engineers) and J. W. H. Ross and Co. (drilling engineers) for their help during the planning stage and kindly providing drilling reports.

2 Roger Caldwell of OYO UK Ltd. for generously providing the recording and minivibrator equipment at a very economic cost, and for supplying free training in its use.

3 The Department of Archaeology for kindly loaning its semi-total station equipment (EDM theodolite).

4 The Robertson Trust for a substantial grant to the Department of Geology and Applied Geology to enable purchase of the 3-D seismic processing package ProMAX/3D.

5 Prof. Ewald Brückl of the Technical University of Vienna for his comments and suggestions in tackling the processing problems and also for the

willingness to test the author's first break data in his refraction modelling program.

6 Sarah Hamilton, Catherine McGee, David Sullivan and Claire Harrison – the student field assistants – for their hard work.

Thanks also to my family who give their blessing and 'doa' during my three years here.

Finally I would like to thank my wife for her understanding and willingness to go through two 'agony' years together even though it means sacrifice of two years of priceless experience as an engineer.

ABSTRACT

The seismic reflection exploration technique has long been established in the oil industry as one of its most successful geophysical exploration tools. It has evolved from a very simple technique (2-D line profiling) to become the most advanced geophysical exploration technique of all (the 3-D reflection technique). Besides its successful use in the oil industry, seismic reflection can also be used to investigate shallow targets. To date, most shallow seismic investigation practitioners have only used the 2-D line profiling technique, as it is easy and cheap to carry out.

Depending on the target, some geophysical investigation techniques can provide an answer to archaeological needs, since they are fast, reliable and above all non-destructive. However, this is not the case for the 2-D seismic reflection method, as it is generally considered to be an unsuitable technique. One of the aims of this dissertation is to test the 2-D line profiling technique with a spatially highly condensed geometry to detect the now-buried vallum (defensive ditch) of a Roman fort at Inveresk, Edinburgh, Scotland. The results are compared with the results of two previously obtained resistivity profiles. An excavation programme around the site had established the existence of only one ditch fort, although this is unusual for a Roman fort, as most of them had at least two ditches enclosing them. The qualitative resistivity results revealed four low apparent resistivity anomalies, with two of them being possible ditch-related anomalies in the area where the ditch (or ditches) was predicted. The 2-D seismic reflection profile acquired a very condensed dataset using a CDP jump-roll geometry. The geophones with a hammer source were spaced at 0.25 m interval along a 50 m long line, yielding a total of 2992 traces. The result of this seismic reflection profile confirms the presence of two ditch-like structures about 3 m and 1 m deep, as inferred from the resistivity profiles. Since one of them is too shallow to be a Roman ditch, the seismic results appear to confirm the existence of only one ditch at this fort. The condensed 2-D method is thus capable of imaging very shallow buried structures such as ditches only one or two metres deep.

The use of current 3-D seismic reflection oil industry technology technique in shallow investigation work is still in an early phase. The limiting factor of transferring this technology is primarily the cost. There is also a problem in scaling down the survey to suit a shallow target. The primary aim of this dissertation is to describe a case history of an attempt to map out the underground tunnels of an abandoned coal mine using 3-D seismic reflection methods, suitably adapted from the 3-D seismic reflection technology used in the oil exploration industry. The site selected for the survey is located in a brownfield site, part of West of Scotland Science Park, Glasgow, Scotland. The 3-D survey was designed to acquire a highly condensed dataset with a full range of source-receiver azimuths, very high fold of coverage, and in the fastest acquisition time possible. For that, a combination of a full and random 3-D survey geometry methods was applied. The data were recorded using a 144-channel, 24-bit recording system. A 100-700 Hz sweep of the mini-vibroseis source was used to try to obtain high frequency broad-band data. To randomise the common mid-points, each source was placed pseudo-randomly within a 4 m^2 area at every 4 m interval. The single element geophones formed a rectangular swath of 8 by 18 on a 2 m grid. The data were processed using industry standard 3-D processing software, using three different

approaches successively. The results reveal an undulating top bedrock surface 3-7 m below ground surface. Although convincing images of underground voids or coal seams were not successfully obtained, the results reveal a general pattern of possible mineworks (or a thick coal seam), showing that such 3-D work is feasible and cost-effective. In retrospect, both the geology and the abandoned workings at the chosen site were probably too complex as a test target.

A by-product of the 3-D reflection study is the development of a new simple and robust mapping technique. This new technique is named 'surface tomography' as it utilises the tomography concept in a simplified form. The aim is to develop a semi-automated method which may pinpoint areally small velocity anomalies on the top bedrock velocity map (say a 2 m diameter anomaly due, for example, to a buried mineshaft). Only the first breaks from all the source-receiver pairs corresponding to the refracted arrival from the top bedrock surface are used. Any propagation through a low velocity zone within the bedrock will experience a time lag (an increase in travel time) and *vice-versa* for a high-velocity zone. The first arrival times are reduced to a representative average velocity. Any reduced time that is higher than the average reduced time is considered to have experienced a time lag and *vice-versa*. To ensure that only raypaths propagating along the bedrock surface were used, the first arrivals from a distance less than the crossover distance of the bedrock arrival and the direct arrival (from the layer above) are deleted. Colour-coded maps of some 80,000 reduced times from the 3-D first breaks were produced to display the anomalies. The results show a systematic pattern of colours striking in the same direction as the general strike of the area. The combined information from this study, the 3-D reflection work and borehole information has been used to revise the geological model of the area.

TABLE OF CONTENTS

CONTENTS

LIST OF FIGURES

LIST OF TABLES

LIST OF PHOTOS

CHAPTER ONE

INTRODUCTION

1.1 Seismic reflection – an overview

One of the greatest things about humankind is the ability to make use of bad experiences as a starting point to a better life. The sinking of the 'unsinkable' *Titanic* in 1912 during its maiden journey after being struck by an iceberg, claiming thousands of lives, was one of the greatest human disasters. In attempts to prevent the same such disaster happening again, many inventions have been produced. Among them, Reginald Aubrey Fessenden comes up with a great idea, in which he developed a model submarine telegraph which had the capability to detect an iceberg. This was a turning point in geophysical exploration. After some modification and improvement, in 1917 he registered with United State Patents Office his method and apparatus for locating ore bodies (Allen 1980, Sheriff and Geldart 1995). The basis of his method was *"being given the distance between two points in a mine, and having determined the time taken by a sound wave to travel between the two points, it is possible to draw conclusions in regard to the probable nature of the rock between the two points, or if an echo be observed, or refraction of the sounds, it is possible to estimate the distance of the reflecting or refracting vein* (Fessenden 1917)". Later, this idea became a main concept in the seismic reflection technique.

Beside being a tool for locating ore minerals, this technique was also capable of locating salt domes, oil wells, etc., as recorded by his wife: *"It is a great pleasure to record their successful use in a totally different and important field – that of locating salt domes, oil wells, sulphur beds etc.* (Fessenden 1940 *in* Allen 1980)".

Because of its capability in locating oil fields which were in demand during that era, during the introduction of petrol engined cars and in search for a more environmentally friendly fuel than coal, lots of capital was spent in improving this technique. The computer revolution starting in the 1960's accelerated the advance of this technique. The introduction of the CDP surveying method and magnetic tape recording for data storage were two of the milestones in seismic reflection history. Prior to 1970's all surveys were done based on 2-D line profiling technique. The introduction of the 3-D

reflection method in the 1970's was another milestone in seismic reflection technique. Nowadays, 3-D reflection is common practice in petroleum exploration. Most petroleum companies will require to shoot a 3-D reflection survey prior to deciding on the location of wells. Thus the seismic reflection method has evolved from a very simple technique to become the most successful geophysical technique of all. In nearly 80 years of constant improvement, it is now almost mature. The chronology of seismic instrumentation and methods is listed in Table 1.1.

Table 1.1 Chronology of seismic instrumentation and methods (after Sheriff and Geldart 1995).

1914	Mintrop's mechanical seismograph	1952	Analog magnetic recording
1917	Fessenden patent on seismic method	1953	Vibroseis recording; weight drop
1921	Seismic reflection work by Geological Engineering Co.	1954	Continuous velocity logging
		1955	Moveable magnetic head
1923	Refraction exploration by Seismos in Mexico and Texas	1956	Central data processing
		1961-2	Analog deconvolution and velocity filtering
1925	Fan shooting method	1963	Digital data recording
	Electrical refraction seismograph	1965	Airgun seismic source
	Radio used for communication	1967	Depth controllers on marine streamer
1926	Reflection correlation method	1968	Binary gain
1927	First well velocity survey	1969	Velocity analysis
1929	Reflection dip shooting		Transit satellite positioning
1931	Reverse refraction profiling	1971	Instantaneous floating point amplifier
	Use of uphole phone	1972	Surface consistent statics
	Truck mounted drill		Bright spots
1932	AGC	1974	Digitisation in the field
	Interchangeable filters	1975	Seismic stratigraphy
1933	Use of multiples geophones per group	1976	3-D
1936	Rieber sonograph; first reproducible recording		Image ray migration (depth migration)
		1984	Amplitude variation with offset (AVO)
1939	Use of closed loops to check misties		DMO processing
1942	Record section	1985	Workstation interpretation
	Mixing	1986	Towing multiple streamers
1944	Large scale marine surveying	1988	S wave exploration
	Use of large patterns		Auto-picking of 3-D volumes
1947	Marine shooting with Shoran	1989	Dip and azimuth display
1950	CDP method	1990	GPS positioning
1952	Medium range radio navigation	Today	4-D; Neural networking

The future development of the seismic reflection technique depends very much on the price of oil. Today, with the help of computer technology, the research is concentrated

in 4-D (time lapse 3-D) methods (Thomas 1997), and how to move into 4-C technology (Greenberg 1997). 4-D technology is done by comparing a new set of 3-D data (shot over an area that has already been shot with 3-D) to the existing 3-D data (Greenberg 1997). It is not strictly an exploration technique, as it is normally done in the oilfield production stage to measure the changes in fluid flow. This can improve recovery and make development and production of a field more efficient. 4-C technology on the other hand is the latest technological development in petroleum exploration, where at each location the reflected signals are recorded by 3 component geophones - attached to the sea bed - for shear wave detection as well as by hydrophones (Greenberg 1997).

1.2 Shallow seismic reflection

1.2.1 Introduction

Beside its successful use in petroleum exploration, the application of seismic reflection can also be found in engineering site investigations, hydrogeological studies, shallow stratigraphy or even in archaeology, in other words for all manner of shallow subsurface investigations. The term 'shallow' is here defined as all such work done using a portable engineering seismograph with a simple source. Most of the time, the target for shallow reflection work is less than 100 m deep. The reason for this branching away from 'deep' seismic methods is the advance in computer and electronic technologies, which have reduced the size and cost, and at the same time have increased the capability of the engineering seismograph.

Basically, shallow subsurface reflection investigators copy the technology from petroleum exploration with some alteration to suit the shallow investigation needs. As shallow investigation work usually proceeds with relatively small amounts of funding, adopting the latest 3-D seismic reflection methods from the well-funded petroleum exploration industry is almost impossible. Most of the shallow investigation practitioners who apply the seismic reflection investigation methods have therefore

limited their work to the use of the 2-D line profiling technique, some 30 years behind the current reflection technology (3-D). Compared to petroleum exploration where seismic reflection is now considered a mature exploration tool, in shallow investigation work, it still has lots of room for improvement.

Shallow seismic reflection practitioners adopt the technique from petroleum industry with the assumption it should give as good results as in petroleum exploration. However, most of the time the results are not very promising compared to other simple geophysical methods such as seismic refraction (bedrock mapping for engineering) and resistivity (for hydrogeological and archaeological studies). Failure to get good results sometimes leads to prejudice about seismic reflection: "why bother spending your money if it is not guaranteed to work".

1.2.2 Some problems

One of the greatest problems in adopting the technique originally designed for exploring deep targets, covering huge areas and requiring lots of capital, to suit an investigation of a shallow target in a limited area with a small amount of money, is the scaling down factor. Most of the time the shallow seismic practitioners did not know how to scale down a simple reflection survey to a specific requirement to utilise the advanced techniques used in the petroleum industry (Bay Geophysical Inc. 1998). Beside the scaling problem, the success of the shallow seismic reflection method also depends on many other factors such as the source and receiver used, the acquisition design, noise etc. But the most important of all is the ground condition.

In many cases, the shallow reflection surveys were designed based on 'rules of thumb' or so-called 'experience'. This is a dangerous approach, as no two sites have the same characteristics. Recorded signal and noise are very site dependent. Their characteristics should be known prior to the design of the survey. Walk-away noise tests are one technique where the signal and noise characteristics can be studied. Besides giving an

idea of the signals and noise, a walk-away test also can be used to set the optimum window (Hunter *et al.* 1984, 1987).

Ground conditions also control the mean frequency of the data. The uppermost earth layer is imperfectly elastic in its response to the passage of seismic wave. Therefore high frequency energy is lost while propagating through the earth. In some conditions, most of the high frequency components are attenuated leaving only low frequency components. Within a few metres of the surface, seismic wave velocities can drop as low as 30 m s^{-1} (Rice *et al.* 1990) and the quality factor (Q) for seismic propagation drops to values as low as 0.3 in unconsolidated, uncompacted soil which results in the attenuation length (the distance over which amplitude decreases by 1/e) being as short as 0.3 m for 100 Hz P-waves (Rice *et al.* 1990). This leads to resolution problems. Since shallow seismic reflection investigation deals with very shallow reflectors which may appear as early as 10 ms, separation of the reflected from the direct or refracted signals is almost impossible. This is the biggest problem in processing shallow reflection data. In addition, the problem of static and lateral variation is also a challenge in processing shallow reflection data.

1.3 The research

1.3.1 Research outline and aims

The nature of the uppermost few tens of meters below the earth surface needs to be determined for several applications. For example, knowledge of this region is required for underground water and mineral resources exploration, as well as foundation qualities for engineering projects. Geophysics offers the tools for investigating this region. The choice of geophysical tools used depends on the target. For example, the magnetic method only can be used to detect a magnetic target, and the gravity method on the other hand can only be used if there is a significant contrast in density of the target relative to its surroundings. Among all geophysical tools available, the seismic

reflection method is the most advanced, and it is widely been used in petroleum exploration. However, usage of seismic reflection in shallow subsurface investigation is still limited.

For decades, seismic reflection was assumed to be useless for imaging the near surface. The reason was that the normal seismic wavelengths used are too long to detect small features or thin beds. Furthermore, near source shallow reflections were always masked by noise while farther away they were hidden by refraction and surface waves. Recently, major improvements in bandwidth, noise abatement and processing capability have produced dramatic improvements in the capability of this method. These can be seen by the increasing numbers of publications of the applications of 2-D seismic reflection for imaging shallow subsurface as discussed in section 1.5.

Despite the increasing number of publications on 2-D seismic reflection for imaging the shallow subsurface, there is still room for improvement. A list of possible research topics relating to near-surface imaging was discussed by Steeples *et al.* (1997). Among them are the application of 3-D seismic reflection methods for shallow subsurface imaging (less than 150 m) and the application of seismic reflection (especially 2-D seismic reflection) imaging methods to image very shallow (ultrashallow) subsurface.

This research was carried out in two stages. An initial stage involved testing the suitability of the Oyo-1600 McSeis recording system for intensive or serious reflection investigation. In this stage a 2-D reflection experiment with closely spaced geophone stations was introduced to image an ultrashallow archaeological structure. The same techniques were applied to the main stage of this research to establish the design parameters for a 3-D survey. The experience in the early stages of the investigation lead us to acquire a DAS-1 recording system to give a greater number of channels, dynamic range, and sensitivity necessary for the 3-D investigation.

3-D seismic reflection surveys are widely used in the petroleum industry, but in general have not been applied to the near surface. Publications on this topic (discussed with

details in section 3.3, chapter 3) are very limited and the earliest date to only 1996. Some of the problems with shallow 3-D reflection include the high level of cost and effort necessitated by small geophone intervals as well as the difficulties posed by the spatial aliasing of ground roll.

Like the 3-D shallow seismic reflection, ultrashallow 2-D seismic reflection surveys are far from routine. Although several examples of reflection in studies the 3-15 m depth range have appeared in some scientific literature, especially in archaeological work, more case histories and continued research are needed to improve the capabilities in this range, particularly for geological conditions in which GPR does not work well.

This research project is primarily about finding the best way of adopting the latest successful 3-D seismic reflection technology, as used in petroleum exploration, to investigating the shallow subsurface. With a small grant from the Glasgow Development Agency (GDA) we (the Geophysics Group at Glasgow University) carried out what is believed to be the first small-scale full 3-D seismic reflection survey over an abandoned coal mine. The main objective of this work is to map out the rooms and pillars of the mine. This technique is adopted from latest technology used in petroleum exploration. Besides adopting the latest technology, this research also concerned with developing a fast, simple and robust subsurface mapping technique that can be produced during the 3-D fieldwork. No additional data collection is needed in this study as it only utilises the first arrival times from the 3-D reflection data. This new technique is named surface tomography as it uses the ideas of seismic tomography. These are two main objectives of this research.

In archaeology, seismic reflection is the least popular geophysical investigation method compared to others such as resistivity, ground penetrating radar or even gravity and magnetic. Most of the time the target is not suitable for the use of seismic reflection. It is either too small or lacks sufficient contrast in acoustic impedance. Despite those two main objectives, the secondary objective of my studies is to image a very shallow (ultrashallow) subsurface which is less than 7 m deep using highly condensed 2-D

seismic reflection method. To prove that the seismic reflection technique can also be used as an archaeological geophysical investigation tool, work was also done in locating archaeological remains, a Roman Fort ditch. The aim of this work is to show that, given the right conditions, seismic reflection can offer a better result than the other techniques.

1.3.2 Funding

These studies were sponsored jointly by the Malaysian Government (MG) and University of Science of Malaysia (USM) as part of the USM Academic Staff Training Scheme program for a duration of 3 years starting from January 1996 to December 1998. These sponsors, MG and USM, paid for tuition fees and a monthly allowance for this period. The 3-D fieldwork was funded by a grant of some £13K from Glasgow Development Agency (GDA) to the University of Glasgow. Without this fund, it would have been impossible to continue this work.

1.4 Thesis presentation and organisation

The presentation of this thesis is based on the British Standard Institution 'Recommendation for the presentation of theses (BS 4821: 1990)'. It is organised into five chapters, where each chapter discusses different topics related to the shallow seismic reflection work. After discussion (Chapter 1) of the brief history and the advances in seismic reflection, the importance of seismic reflection for investigating a shallow subsurface region, and the difficulties and aims of the project, Chapter 2 discusses the application of shallow seismic reflection method in archaeological work. Although this is not the main project, this work came first chronologically, and only involved simple fieldwork and modest amounts of processing time.

The main part of the thesis is the full small scale 3-D seismic reflection survey. This work is discussed in Chapter 3. As we believe this is the first ever such survey, the

discussion on planning, pre-fieldwork survey, data acquisition, processing, and interpretation is discussed in great detail for future reference. Chapter 4 deals with developing the new mapping method known as surface tomography. The last chapter discusses the conclusions from all the work, the future of the shallow seismic reflection method and also some recommendations for future improvement of such shallow seismic reflection work.

1.5 Previous work

As the reflection technique used in shallow investigation work is an adaptation from the more advanced technology used in petroleum exploration, it obviously needs lots of modification and improvement before it can give as good results as in its original field.

First, the seismograph (recording system) needs to be as portable as possible without compromising its capability. Advances in electronic and computer industry have helped a lot in scaling down the huge recording systems used in petroleum exploration to a portable machine. Today there are a number of commercial portable engineering seismographs such as the OYO McSeis 1600, Bison, OYO DAS-1 etc. All these commercial seismographs claim the capability of recording high-resolution seismic reflection data and are suitable for shallow subsurface investigations. In choosing a seismograph, the most important factor is its dynamic range – the ratio of the largest recoverable signal to the smallest recoverable signal. The dynamic range of the seismograph is linked closely to the number of bits used in the A/D (analog to digital) converter. As each signal bit represents very nearly 6 dB (Knapp and Steeples 1986a), by multiplying the number of A/D bits in the converter by 6, an estimate of the seismograph's dynamic range can be obtained. Besides the seismograph, the use of the detector (geophone) is another important factor in any seismic reflection investigation. Shallow seismic reflection needs high-resolution detectors. Most of the geophones used in petroleum exploration are not appropriate for shallow work (Lepper 1981).

Choosing appropriate acquisition parameters are also important in shallow seismic reflection work, as the results strongly depend on it. The choice of recording parameters is determined by the objectives of the survey, the solid geology, top layer conditions and also the resources available (Knapp and Steeples 1986a). Pre-acquisition knowledge of the site and/or a walk-away noise test is helpful in choosing the recording parameters. In order to record reflected signals with minimal noise, Hunter *et al.* (1984, 1987) introduced the concept of the optimum window. The optimum window is a range of offsets (source to receiver separations) that allow the target reflectors to be observed without interference from other events. It can be determined from analysing the walk-away noise test record.

Almost anything can be used as a seismic generator (source) for shallow reflection work, as long as it is capable of imparting sufficient energy to provide reflections from the reflecting target, and is cheap, safe, portable and repeatable. In practice it ranges from a simple hammer source to a complicated minivibrator. However, the selection is dependent on the objectives of the survey, the target depth and also the ground conditions. Pullan and MacAullay (1987) and Miller *et al.* (1994) discussed the characteristics of various sources on various sites, and found that the source characteristics are largely site dependent. Rules of thumb for source selection as addressed by Miller *et al.* (1994) are, *'If the near surface is saturated and fine grained, a downhole source is the best. If it is hard and dry, weight drop should be a top choice. Always try to bring several types of sources but the first choice should be based on near surface conditions, site restrictions and target of interest'.*

Ground coupling is another important factor in shallow reflection work, as bad coupling can severely distort the quality of the recorded data. Distortion can cause the response wavelet to be longer and more complex, and the changes in the wavelet character of key reflections could be misinterpreted as a stratigraphic change (Knapp and Steeples 1986b). The coupling between receiver and ground can be represented by a damped oscillatory system (Lamer 1970), whose properties depend upon the geophone mass, the diameter of earth contact and local soil conditions (Hoover and O'Brien 1980). An

efficient geophone ground coupling requires a lightweight geophone and a long spike to firmly couple it into the ground (Hewitt 1980).

An understanding of the difficulties and their solution related to the shallow seismic reflection work leads to its appropriate utilisation. The application of shallow seismic reflection can be classified into three main categories, which are:

- Engineering site investigations (Hunter *et al.* 1984, Pullan and Hunter 1985, Hill and Ali 1988, Miller *et al.* 1989, and Jeng 1995),
- Hydrogeology (Birkelo *et al.* 1987, Hunter *et al.* 1987, Miller *et al.* 1990, Johnson and Clark 1992a, Johnson and Clark 1992b, Kidd *et al.* 1990, Clark *et al.* 1994), and
- Mining or void monitoring (Al-Rawahy and Goulty 1995, Brückl *et al.* 1997, Kourkafas and Goulty 1996, Gochioco and Cotton 1989, Gendzwill 1990, Steeples and Miller 1986).

Besides these, there is also work done in mapping mineral veins or even in locating archaeological remains (Stright 1986, Karastathis and Papamarinopoulos 1997).

Most of such surveys are limited to the use of 2-D line profiling and using a conventional compressional wave (P-wave) source such as hammer, weight drop or buffalo gun. There was also some work (2-D reflection) utilising shear waves (S-waves) as their source (Clark *et al.* 1994, Johnson and Clark 1992a, Jeng 1995, Pullan *et al.* 1990, Norminton 1990). The advantage of using S-waves as a source in shallow reflection investigation is that the effect of water table (giving a false geological reflector) is minimised. S-wave propagation is not influenced by the saturation level as its propagation is controlled only by the shear modulus of the medium. The other advantage is that the wavelength of S-waves is shorter than P-waves, which means that they can resolve thin layers better than P-waves. One problem of employing S-wave reflection, on the other hand, is that it may consume twice the time as the equivalent P-wave survey, since it requires each shot-point to be shot in both directions (perpendicular to the line) to obtain a difference record. Besides that, the data also need to be recorded for twice as long as P-wave data for the same target depth as they have travelled more slowly than the P-waves.

The problem of using the old-established 2-D line survey method is that it does not give the whole picture of the area, and sometimes the image is unclear due to the lack of resolution. Brückl *et al.* (1997) and Kourkafas and Goulty (1996) both suggested that their unclear image could be improved by running a 3-D survey. The suggestion from these two projects led to the idea of conducting a 3-D reflection survey (within a limited budget) over an abandoned coal mine. The essence of the 3-D method is areal data collection followed by the processing and interpretation of a closely spaced data volume (Brown 1996) which increases the resolution.

3-D is considered to be a very recent trend in shallow reflection investigation, although the technique was introduced in the petroleum industry in early 1970's. Corsmit *et al.* (1988) carried out a shallow 3-D survey on a tidal flat to investigate the shallow stratigraphy. Their work was purely academic and pedagogic, as the prime objective was to demonstrate to students how to conduct a 3-D survey and how to process it. Smythe (1994, 1995) also conducted a 3-D survey to study the fault patterns in volcanic rock to assess its suitability as a site for radioactive waste disposal. Smythe (1994) used the same 3-D technique as normally used in petroleum exploration, however the target is too deep (around 500 m) for this experiment to be considered as shallow reflection work. The details of other preliminary 3-D experiments will be discussed in Chapter 3.

The latest 3-D survey conducted using portable seismograph was done by Miller *et al.* (1997) where they deployed a low fold 3-D survey to evaluate better lateral variability of the interpreted faults at a sinkhole. The target (around 400 m) was also deep for an ordinary shallow reflection survey. Bay Geophysical Inc. (1998) also claim to have done a 3-D survey using a shear wave source in their web pages, however no published article is available for reference.

At the time of writing (August 1998), Büker *et al.* (1998b) published a paper on the same area 'Shallow 3-D seismic reflection surveying' discussing acquisition technique and preliminary processing strategies in mapping a glacial sediments deposit. Details of this paper are discussed in Chapter 3.

CHAPTER TWO

SEISMIC REFLECTION IN ARCHAEOLOGY

2.1 Introduction

Excavation – coring and trenching - is a normal practice in archaeological investigation. Their objectives are to acquire cultural and biological artifacts for subsequent laboratory and statistical studies, and to document the three-dimensional relationships between artifacts by using accurate, on-site recording procedure as the work progresses (Wynn 1986). The decisions on where to excavate are normally taken by the field archaeologist based on historical documentation, surface artifacts, surface morphology or on aerial photographs suggesting an earlier human occupation. In the absence of surface indicators, random coring is done and based on that, trenches are dug. This routine is time consuming. As time is often very precious in less well-funded projects like in archaeology, fast and reliable investigation methods are needed. In addition to that, those methods should be non-destructive. A non-destructive method is very important in all archaeological investigation as it preserves the spatial relations between the artifacts.

Depending on the target, a geophysical investigation survey can provide an answer to archaeological needs. It is fast, reliable and non-destructive. Because of that, most geophysical survey methods have found some application in the archaeological context, either as site exploration (the search for an undiscovered site) or as intra-site mapping - used to guide excavation programs within an already discovered site (Wynn 1986). Although many methods have been used in archaeological investigation, only a few are frequently used. Magnetic, resistivity, electromagnetic (EM) and ground penetrating radar (GPR) are the premier methods, while the gravity method is sometimes used. Seismic methods – refraction and reflection – on the other hand, are usually found to be unsuitable for archaeological investigations (Reynolds 1997).

In this chapter, I compare the results from two contrasting geophysical methods – resistivity and seismic reflection - used in archaeological investigation. The first was chosen to represent the most common geophysical investigation method in archaeology, while the latter was chosen to represent an unsuitable geophysical investigation method

in archaeology, even though it is one of the most successful methods in other fields such as in petroleum exploration.

2.2 Aim

The aim of this project is to locate a Roman fort ditch (vallum), which was filled and covered by surface material. We use a spatially highly condensed seismic reflection method. The results from the seismic profile were then compared to the results of the resistivity survey done earlier by Baker (1996). Besides locating the target, it is also hoped that it will give a new perception about this method in archaeological investigation, from being considered as an unsuitable investigation method to at least being thought of as a secondary if not a primary investigation method.

2.3 Previous work

Not many archaeological investigators are keen on using the seismic method, as it is expensive and involves a complex field procedure compared to other geophysical investigation methods (Wynn 1986). Furthermore, the success of this method depends on the presence of a contrast in elastic properties between the target and the surroundings. The bigger the contrast the higher the chances are of success. The size of the target also plays an important rule in the success of seismic reflection work. In most cases the target is either buried metal, foundation stone or man-made structures, and is thus too small for a normal shallow (hammer source) reflection survey. Only certain targets which are big and show a significant contrast in elastic properties are suitable. Goulty *el al.* (1990), and Goulty and Hudson (1994) employed the refraction method to delineate the 8 m wide Hadrian Wall's vallum, while Karastathis and Papamarinopoulos (1997) applied both refraction and reflection techniques in detecting the 35 m wide King Xerxes' canal. Both of these works showed promising results.

Baker (1996) compared the results from several geophysical surveys such as seismic refraction and reflection, resistivity and magnetic methods in detecting the Roman fort ditch at Inveresk. Her failure to get a good result in the seismic surveying methods led to a conclusion that this technique was not suitable for the detection of the vallum, compared to the other two methods.

This work is a continuation of Baker's project. However, instead of applying both refraction and reflection as Karastathis and Papamarinopoulos (1997), a highly condensed reflection survey was employed. The results are then compared with two resistivity profiles reinterpreted from Baker's work.

2.4 The site

2.4.1 Introduction

Discussion on this subject is based on three archaeological papers by Dennison and Coleman (1996), Richmond (1978), and Baker (1996). As the nature of this study is an application of geophysical techniques in archaeology, I have no intention of explaining in detail the excavation history that the site underwent and its findings, except to give a general perception of the site history and its relation to the target. Furthermore the author has no basic background in archaeology.

2.4.2 Location

Inveresk is part of modern day Musselburgh. It is situated within the East Lothian District of East Lothian Region approximately 10 km east of Edinburgh, Scotland (Figure 2.1). The fort at Inveresk lies on the slightly higher ground facing the Firth of Forth, surrounded by the river Esk on three sides.

Today, nothing of the fort itself is visible on the ground. Most of it is buried under the ground of St. Michael's Kirk. The field where the surveys were undertaken is also part of St. Michael's Kirk. It is a reserved cemetery ground. Physically it situated on the gentle westerly sloping flank of the hilltop.

2.4.3 Geology

The south of Scotland can be divided into three major zones, which are the Highlands, Midland Valley and Southern Uplands. Two major faults, the Southern Upland Fault and the Highland Boundary Fault separate the two outer zones, and the Midland Valley is a graben bounded by those two faults. The Highland zone is made up of metamorphic rock while the Southern Uplands are formed mainly of folded Ordovician and Silurian strata. On the other hand, younger rocks such as an Old Red Sandstone and Carboniferous sandstone and shale are the main rocks of the Midland Valley (MacGregor and MacGregor 1948). Around the Edinburgh area, the youngest rock recorded after the Carboniferous rock is Quaternary glacial deposits, which implies that this area was subjected to weathering and erosion for a long time.

During the last two million years, most of northern Britain has been subjected to repeated glaciation periods. The latest was 15,000 years ago. The meltdown of the ice produced a vast amount of running water, which transported glacial debris before it lost its energy and settled on top of the Carboniferous rocks. The meltdown also raised sea level by a few tens of metres. Most of the lowland areas were submerged and the beach deposits were deposited further inland, which later became raised a beach deposit after the sea level fell again.

The geological events around Edinburgh and the Midland Valley can be summarised as in Table 2.1. Musselburgh is situated in this Valley and is developed on raised beach sand and glacial deposits.

Figure 2.1 Inveresk: Site and physical setting.

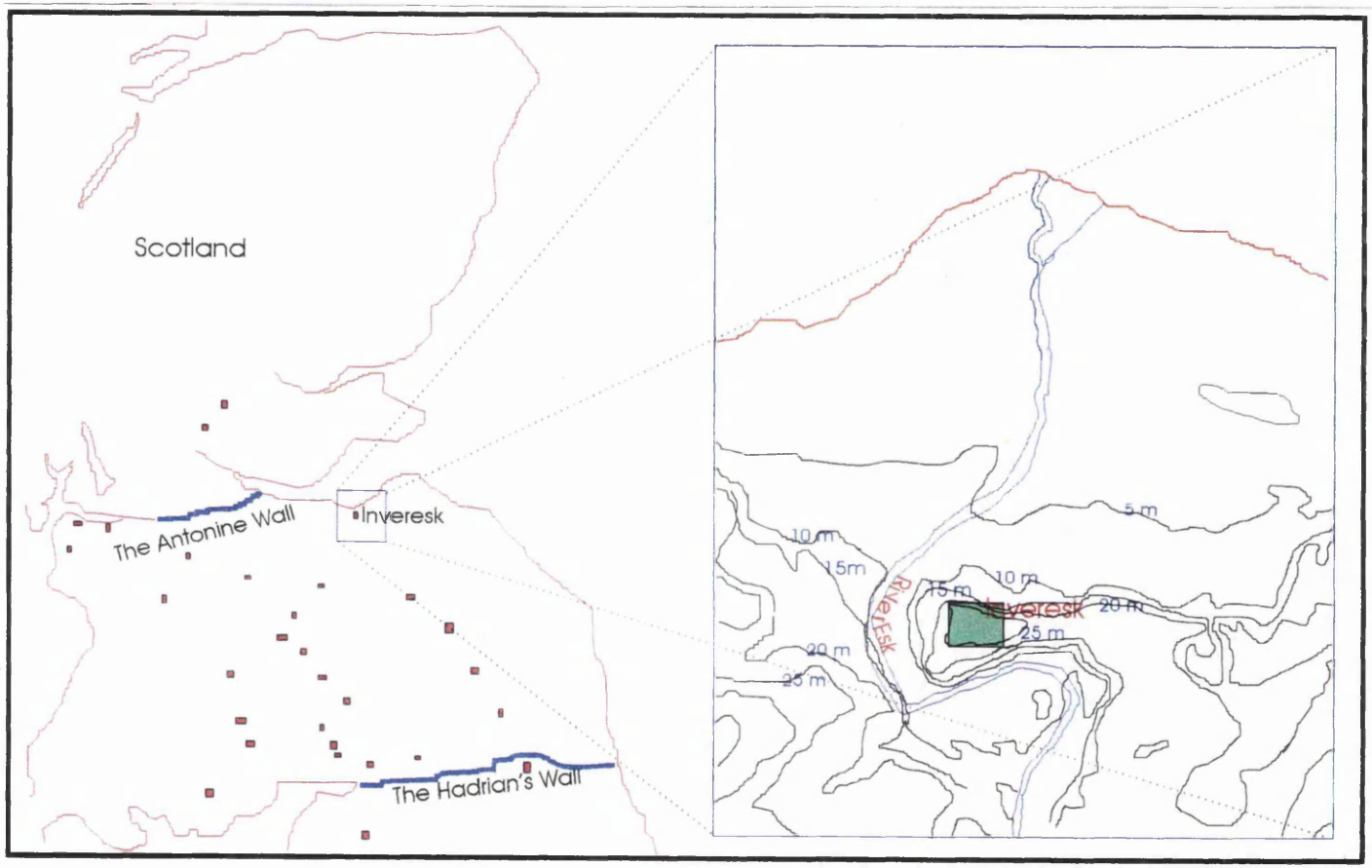

Main map shows location of the Roman Forts (in red).
Detailed map (right) shows topographic contours at Inveresk (5 m contour interval).

Table 2.1 Summary of the geology of the Midland Valley (after MacGregor and MacGregor 1948).

Era	System and Subdivision		Depositional Condition	Contemporaneous Igneous rock	Intrusive Igneous rock
Quaternary	Recent and Pleistocene	Blown sand Peat Fresh water alluvium Marine alluvium Sand and gravel Moraines Boulder clay	Aeolian (coastal) Humid continental Fluviatile; lacustrine Littoral; marine Fluvio-glacial Glacial Glacial		
Pronounced unconformity following erosion of Tertiary times					
Tertiary					Dykes of Tertiary age
Mesozoic strata absent in Midland Valley but represented in Arran					
Upper Palaeozoic	Permian	Mauchine Sandstone	Aeolian (desert)	Lavas and tuffs	Volcanic necks and plugs
	Beginning of Permo-Carboniferous Earth Movements				
	Carbon-iferous	Barren Red Coal measures Productive Coal measures Millstone Grit Carboniferous Limestone series Calciferous sandstone series	Deltaic and estuarine Mainly lagoonal Deltaic and fluviatile Marine; estuarine; lagoonal Lagoonal	 Lavas Lavas and tuffs Lavas	
	Old red Sandstone	Upper Old Red Sandstone Lower Old Red Sandstone	Fluviatile; lacustrine Semi-arid;fluviatile; lacustrine	 Lavas	
Main period of Caledonian Orogenic (Mountain – Building) movements					
Lower Palaeozoic	Silurian	Downtonian Ludlow Wenlock Llandovery	Semi-arid; fluviatile Marine Marine Marine	Spilitic lavas and tuffs	Serpentine, gabbro, etc
	Ordovician	Ashgill Caradoc Arenig	Marine Marine Marine		

2.4.4 History

The settlement of Scotland took place around 7000 BC (in the Mesolithic or Middle Stone Age), however no evidence for humans' existence in this area has been found. The earliest evidence found, such as a stone axe for clearing woodland (SE of Musselburgh) and the stone macehead used for ceremonial purposes (at Woodside Garden, Musselburgh) suggest that people began to settle around this area at around 3500 BC, which is the Neolithic or New Stone Age (Dennison and Coleman 1997). The evidence found (refer to Ritchie and Ritchie 1972, for details) shows that the settlements around Musselburgh have continued until today. Among the archaeological findings, the findings from an early Iron Age settlement are dominant. This settlement continued until the Romans arrived in the first century AD.

The conquest of Britain by the Romans started in 43 AD with the invasion of Emperor Claudius. Under the general Gnaeus Julius Agricola (Ritchie and Ritchie 1972), they reached as far as the northeast of Scotland and circumnavigated islands during the first century of campaigns in Scotland. These campaigns met with much resistance by the local people, and the Romans were forced to retreat from most parts of Scotland in AD 87 - 88. In order to keep their southern region (Britain) away from the northern rebellious factions, Hadrian's wall was built in 120 AD. During the invasion, forts were also built as part of their defensive and support system. After their retreat, most of the forts were abandoned or demolished.

After the death of Emperor Pulius Aelius Hadrianus (Hadrian's wall was named after him), his successor – Emperor Antoninus Pius - ordered Lollius Urbicus, the governor of Britain at that time, to recapture Scotland. A second barrier – the Antonine wall - was also built stretching for 60 km from the Forth (Edinburgh) to the Clyde (Glasgow) for the same purpose as Hadrian's Wall. Associated with that, forts were also built. The fort at Inveresk was built during this time. As it is located on the mouth of the Esk, it is believed that this fort functioned as a port or a harbour.

2.4.5 Target

No two Roman forts are the same (Breeze 1983), however most of them shared basic common features. For example, a fort is normally rectangular in shape, and faced either the enemy, the line of march or east. The forts are surrounded by a defence system which usually consists of ramparts of tuff or stone with at least two ditches (Collingwood and Richmond 1969, Breeze 1983).

The Roman fort at Inveresk was first investigated by Ian Richmond in 1946-47, when he established the lines of ramparts on the north, south and west sides, enclosing an area of around six acres with the main entrance facing to the west. These ramparts are made of beaten clay standing to a height of 1 m, edged by a neat kerb of fresh hammered dressed sandstone blocks, and is approximately 7 m wide (Richmond 1978). In one trench on the west of St. Michael's Kirk, the kerb rampart front was discovered at 2 m depth.

The ditches were normally dug beyond the ramparts (Breeze 1983). The excavation on the southern wall revealed the outer scarp and the bottom of a V-shaped ditch some 10 m wide. The ditch was dug in a yellow sand and clearly outlined by a filling of chocolate-coloured silt and by a coating of red clay almost 10 cm thick (Richmond 1978). Only one ditch was found, which is rather unusual for a Roman fort defence.

Between the rampart and the ditch lies the intervallum or roadway. Two superimposed intervallums were found at the site. The lower is 4 m wide, while the upper is 11 m wide. These intervallums were found lightly gravelled, standing upon an artificial terrace of clay 60 cm thick (Richmond 1978). Based on his excavation records, the fort plan and a cross-section of the defences are shown in Figures 2.2 and 2.3, respectively.

Our target is to detect the V-shaped ditch, which is part of the defence system as described above.

Figure 2.2 Richmond's proposed plan for Inveresk Fort.

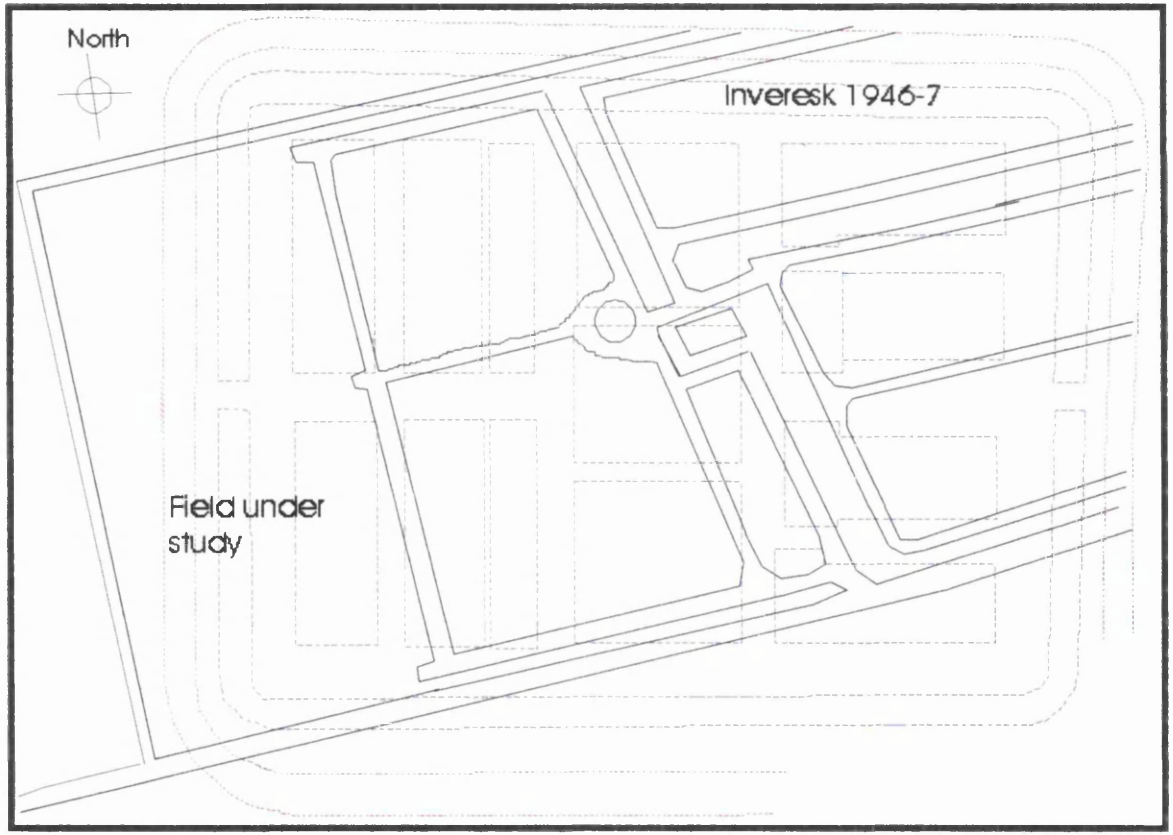

Coloured dotted line is the outline of the Inveresk Roman Fort as outlined by Richmond (1978).
Red dotted line is the outline of the ditch.

Figure 2.3 Schematic cross-section of the defence (Western Wall) (after Richmond 1978).

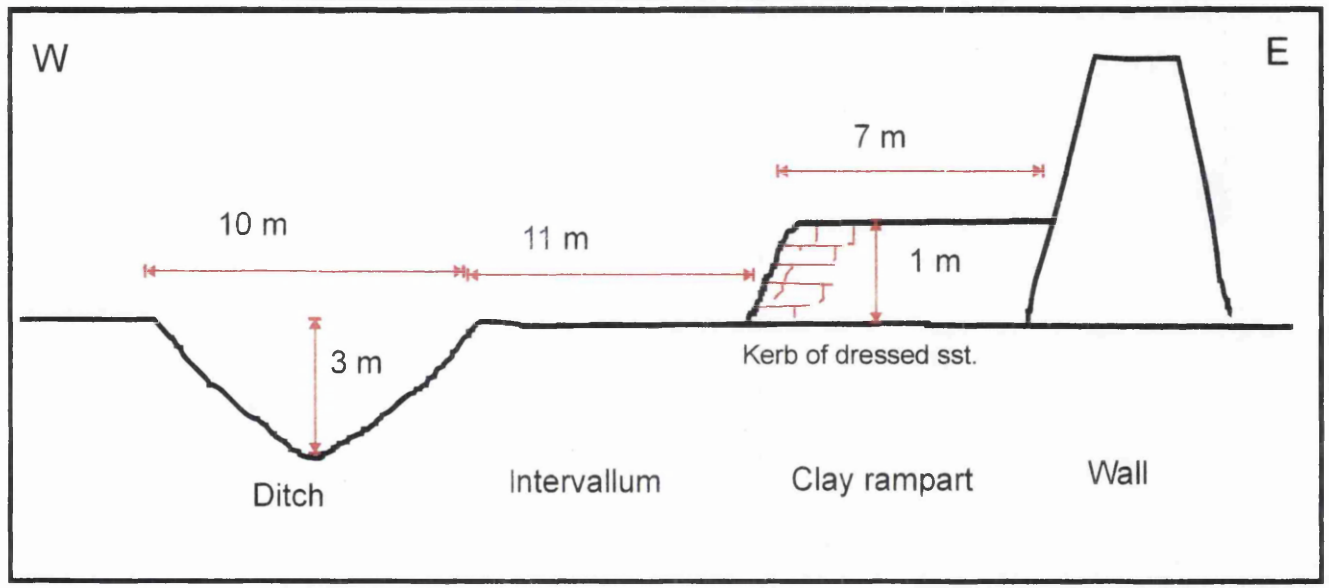

2.5 Resistivity survey

2.5.1 Introduction

Resistivity surveys are one of the most common geophysical surveying methods employed by the archaeologist, simply because they are both cheap and easy to conduct. However the interpretation of resistivity profiles sometimes can be very difficult. To discriminate the interpretation's ambiguities, good geological or non-geological control is required.

Here, two resistivity lines - L3 and L4 - were surveyed by Baker (1996) prior to the seismic reflection work. L3 was acquired on the same line as the planned seismic line whereas L4 was acquired 10 m to the north of L3 and parallel to it (Figure 2.4). As a control, L3 was designed to run through two man-made features, an archaeological trench at the eastern end and an area of stripped topsoil at the western end.

In order to obtain a 2-D model (i.e. a picture) of the subsurface, an expanding Wenner array with a moving central point (a combined of vertical electrical sounding (VES) and constant separation traversing (CST)) was used. Since the target is less than 4 m deep, the readings were read at only 1, 2, 3 and 4 m electrode spacings before the central point was moved down the line by a 1 m interval.

2.5.2 Interpretation theory

The apparent resistivity reading is controlled by the presence of conductive material such as water or metal. Since our target is the buried Roman ditch, we would expect a low resistivity anomaly because the ditch had subsequently been filled up, normally by loose material, and such material traps a quantity of conductive water.

Figure 2.4 Details of the study area.

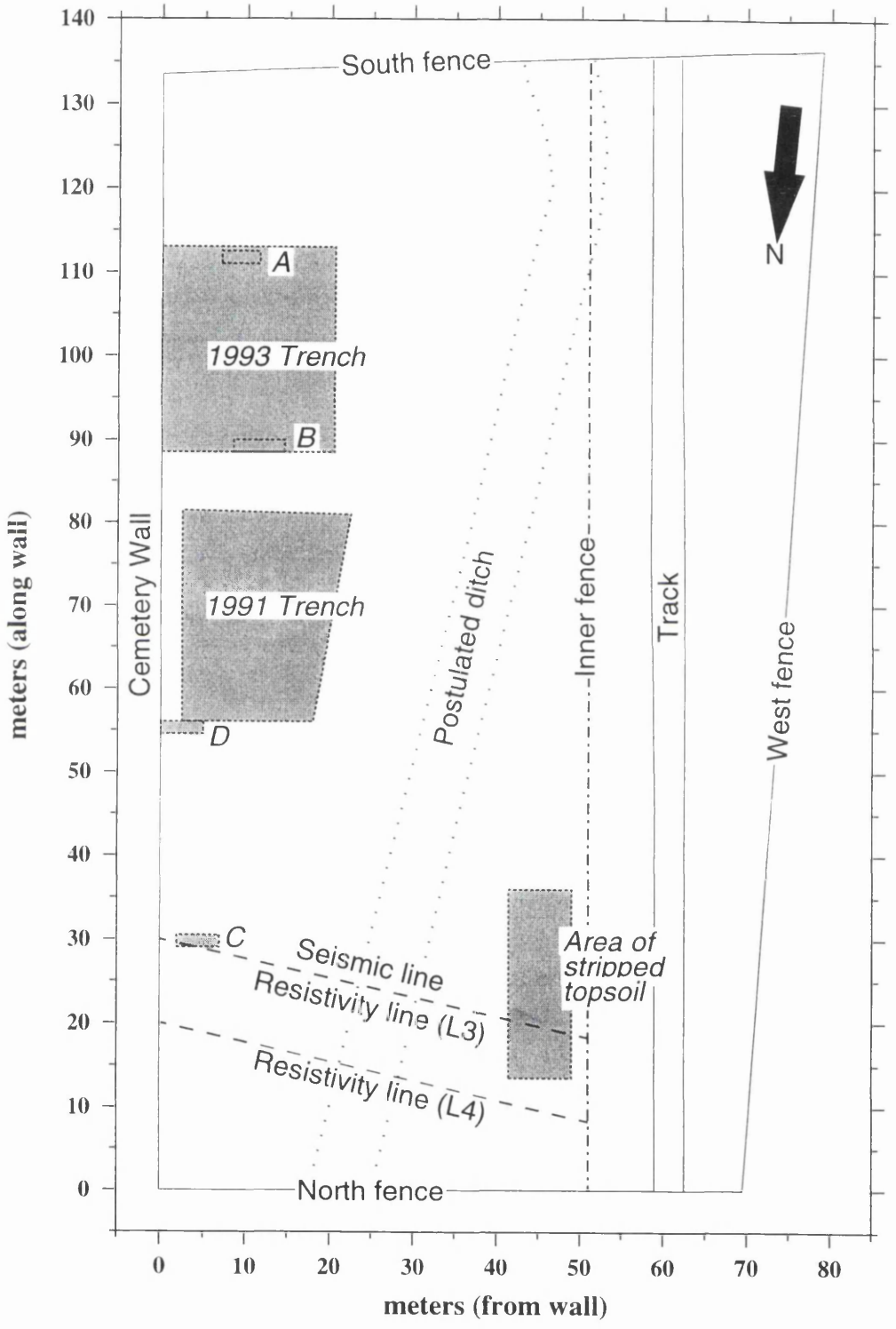

Note: A, B, C, D and the shaded area are GUARD trenches.

Figure 2.5 shows an example of how the resistivity profiles over the buried ditch normally look like. We would also expect to see a high resistivity anomaly on the profile due to the presence of the dressed sandstone at the edge of the clay rampart and the heavy paved berm.

Figure 2.5 Resistivity profiles (CST) across a buried ditch. Note that relatively low resistivity value on the right (10 – 20 m) is associated with poorly compacted infill materials (ditch)(from Kearey and Brooks 1996).

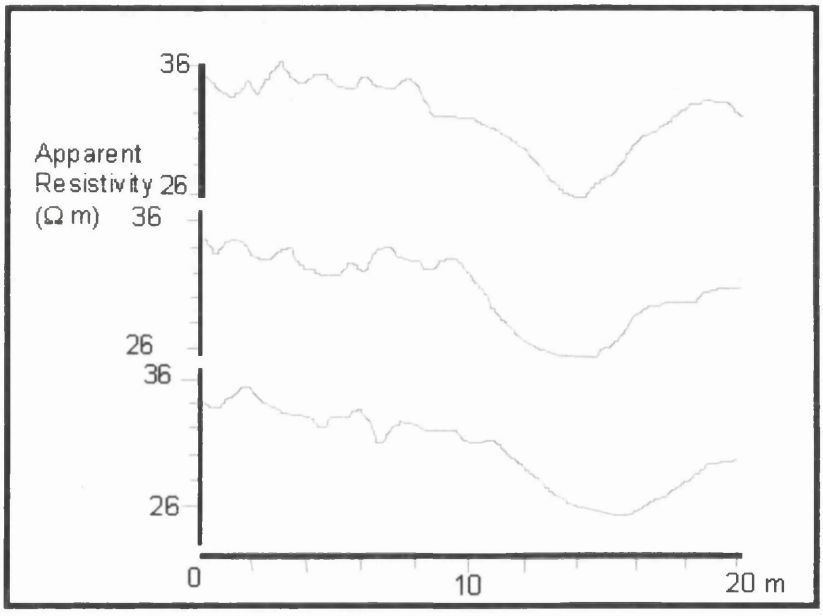

The effect of the topography and the near surface resistivity variation should also be taken into consideration during the interpretation of resistivity profile, since these can mask the deeper resistivity values.

2.5.3 Results and discussion

The resistivity readings were plotted on an Excel spreadsheet graph for qualitative interpretation before transfer to the Generic Mapping Tools (GMT) program for presentation purposes. In general the profiles for L3 (Figure 2.6a) and L4 (Figure 2.6b)

show resistivity values following the same pattern as the topography, which is decreasing towards the western end of the lines. This is a good example of how the topography can mask the effect of the deeper variations.

The 1 m electrode spacing profile on both lines shows the most variable profile of all. The reason is simply that it reads the resistivity values of a highly disturbed topsoil. As the target is deeper (2 - 4 m), the variation of this profile is less significant than the variation in the deeper profiles. This shallow profile is important for checking the interpretation validity of the resistivity profiles.

The interpretations of the resistivity data are made based on the low resistivity value on all the profiles on lines L3 and L4. Comparing the resistivity profiles on both lines, four resistivity low anomalies were identified, namely A, B, C and D (Figure 2.6a and 2.6b).

Anomaly A is picked up on line L3, and is characterised by a narrow and strong low anomaly. This anomaly, however, is absent on L4. Anomaly B, on the other hand, is clear on L4 but very subtle on L3. It is characterised by a strong but broad low anomaly.

Anomaly C appears on both lines L3 and L4. It is also a broad anomaly; however it is not as strong as anomaly B. It only appears on the 1 m spacing profile on both lines. Anomaly D only exists on the 1 m electrode spacing profile of L3. It is a very weak low anomaly.

Note that the 'strength' of the anomaly as referred to here is based on maximum depth at which the anomaly can be detected. A 'strong' anomaly means that the anomaly can been seen on the deeper profile (2, 3 or 4 m electrode spacing profiles); on the other hand, a low or weak anomaly only appears on the 1 or 2 m electrode spacing profiles. The summary of the low resistivity anomalies is given in Table 2.2. All these anomalies are difficult to explain unless they can be related to a physical control.

Figure 2.6a L3 resistivity profiles.

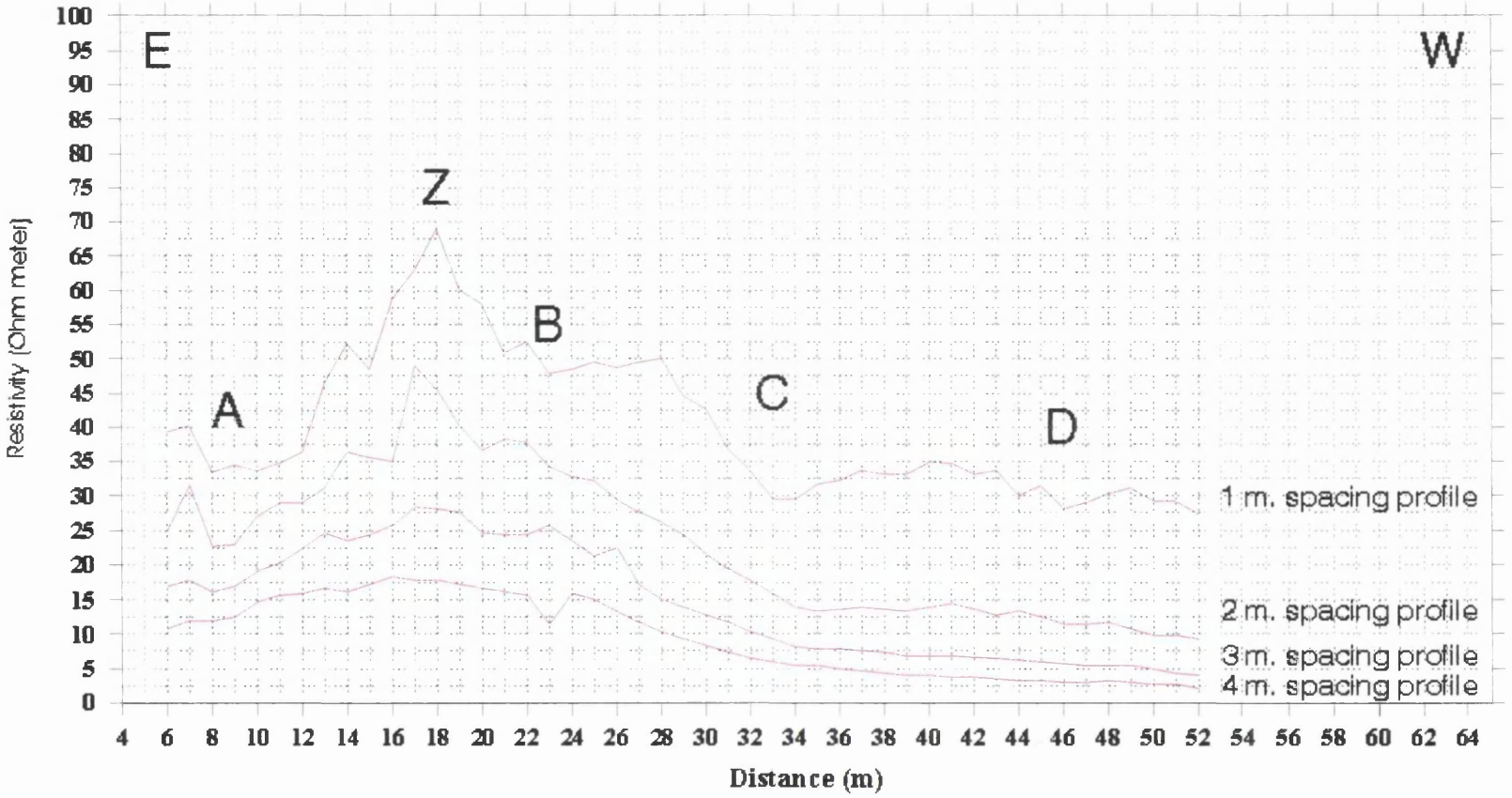

A, B, C, D and Z are the anomalies discussed in the text.

Figure 2.6b L4 resistivity profiles.

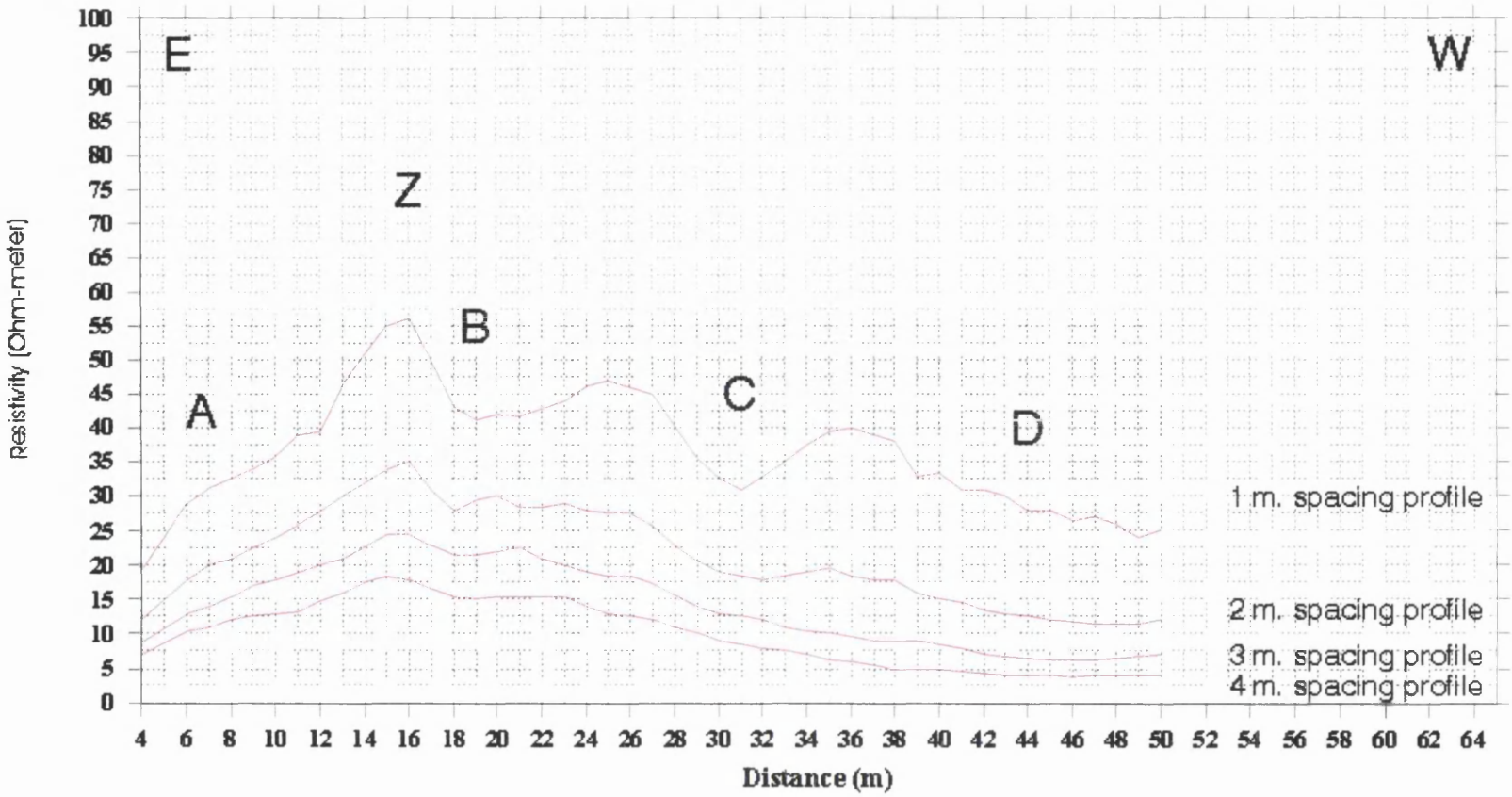

A, B, C, D and Z are the anomalies discussed in the text.

Table 2.2 Summary of the low apparent resistivity anomalies.

	Anomaly A		Anomaly B		Anomaly C		Anomaly D	
	L3	L4	L3	L4	L3	L4	L3	L4
Appearance	√	X	√	√	√	√	√	X
Centre of the anomaly (m)	9	-	23	19	33	31	45	-
Width	narrow	-	wide	wide	wide	wide	narrow	-
Max. depth of resis. minima (m)	3	-	?	4	1 or 2	1 or 2	1	-
Strength	strong	-	?	strong	weak	weak	weak	-

Figure 2.7 shows the relationship between these anomalies and the field. Anomalies A and D on L3 lie directly over the trench C and an area of stripped topsoil respectively. These were the control of the interpretation. The trench was 2 or 3 m deep and it is filled by loose excavated materials.

Anomaly A is very prominent on 1 and 2 m electrode spacing profiles, however the anomaly is weak on the other two (3 and 4 m electrode spacing profiles). This anomaly is believed to be a result of the trench C. The appearance of the anomaly on the deeper profile (3 and 4 m electrode spacing profiles) is an example on how a strong near surface resistivity reading can affect the readings of the deeper section.

Anomaly D (on L3) is also believed to be a result of the stripped topsoil area and this was confirmed with the result of the twin probe resistivity survey (Baker 1996). Since only the topsoil was stripped off, we would expect this anomaly to be only picked up by the shallow profile (1 m spacing profile) and not by other profiles as shown in Figure 2.6. The reason why the anomalies A and D did not appear on the L4 profile is simply because that line was deliberately chosen to avoid these two known man-made structures.

Anomalies A and D can be confidently interpreted since they have good control. But the anomalies B and C are still unexplained. These anomalies lie in the area where the target ditch was postulated. From the excavation in the nearby area, only one ditch was found, and the idea of a Roman fort with one ditch is always questionable, since most of them had two or more ditches as their defence.

Can the pair of anomalies B and C be taken as a proof of the existence of two trenches around this fort?

Figure 2.7 Relation between resistivity anomalies (A-D and Z) and their near surface features.

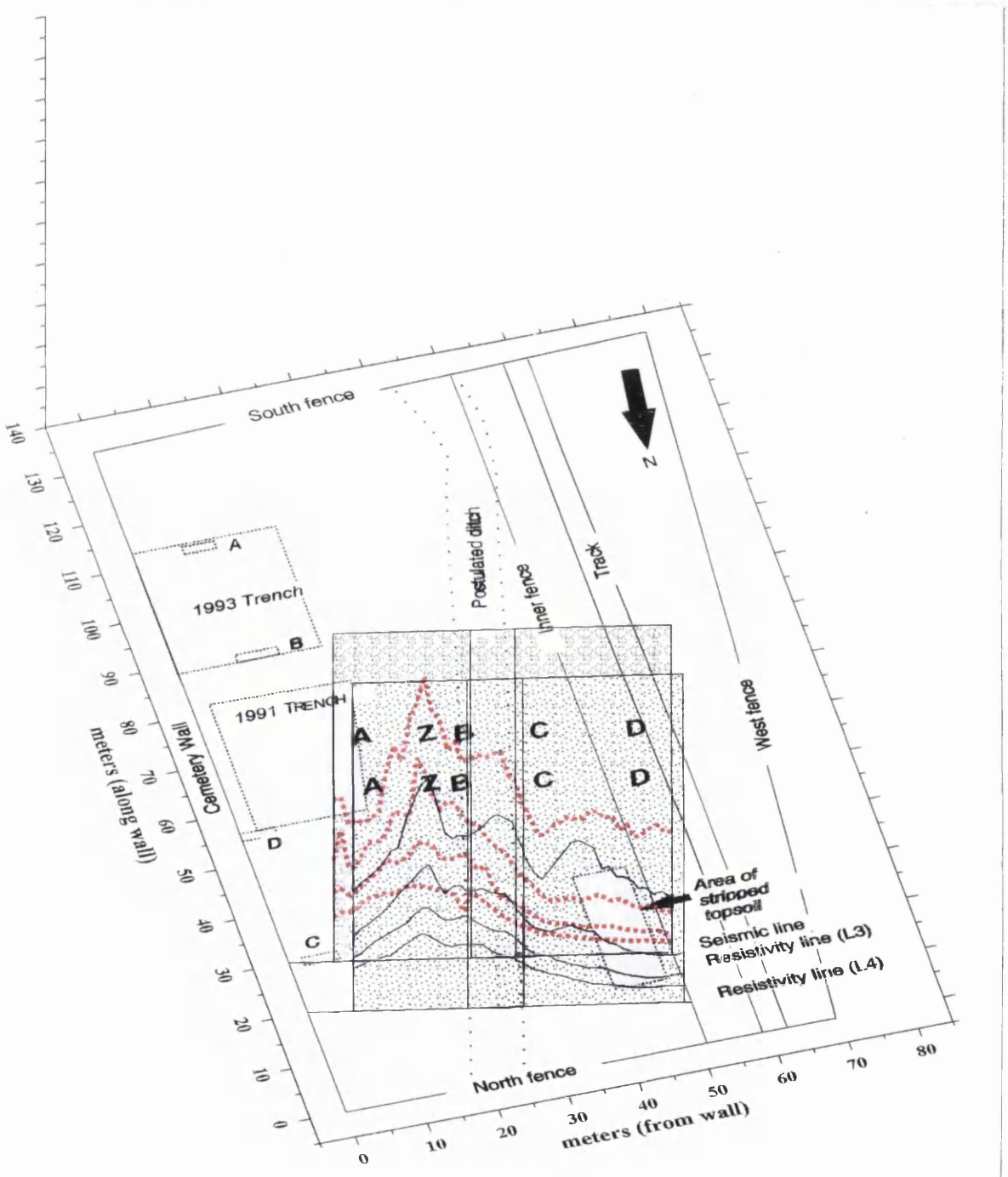

Without a careful analysis, we might agree with the idea of the existence of two ditches, since the anomalies B and C are very strong on both 1 m spacing profiles on both lines; however this idea contradicts what the field evidence shows. On the other hand, if we agree with the idea of a single ditch, which of these two anomalies represents the ditch, and why are there two low resistivity anomalies?

Anomaly B is a wide and strong low anomaly. It appears on all profiles of L4, however on the L3, only the shallow profile shows the effect. The other profiles in that region are undulating, and the recognition of the anomaly is very difficult. By comparing the anomaly B on L4 and anomaly A on L3, we can say that this anomaly results from the deep trench-like structure. However, the difficulties in recognising any anomaly on the deeper profile on L3 may indicate that the structure is not continuous. Comparing anomaly C on both lines to anomaly B on L4 and to the anomaly D on line L3, we can say that this anomaly also results from the trench-like structure. However the maximum depth of this structure is less than 1 m, since the deeper profile did not show the same anomaly.

Although a trench-like structure which gave anomaly C is continuous (based on its appearance on both lines), it is unlikely that it can be the Roman ditch since it is too shallow. Since anomalies A, D and C cannot correspond to the Roman ditch, then the ditch must correspond to anomaly B. However, the problem with anomaly B is that it is discontinuous – i.e. there is no clear indication of the anomaly on line L3.

The other interesting anomaly is a prominent high resistivity anomaly - anomaly Z (Figure 2.6a and 2.6b). This anomaly is very narrow and its centre is at 14 m on L3 and 16 m on L4. This anomaly can be seen on all profiles on both lines L3 and L4. Normally, a high resistivity anomaly results from the presence of less conductive material such as a rock boulder. From the knowledge of the area, this anomaly may correspond to the dressed sandstone in front of the clay rampart.

In conclusion, although there is good excavation control, the interpretation of the resistivity data is still subject to many ambiguities. The reasons why resistivity is very popular amongst archaeologists are simply because it is cheap and easy to operate.

Although the interpretation of the resistivity data is ambiguous, it can however give a rough idea of where to dig a trial pit. To overcome those ambiguities, other geophysical surveys should be conducted in the same area. Since the seismic reflection method has shown great success in imaging the subsurface for engineering and hydrological work (not to mention its huge success in petroleum exploration), it also can be used in archaeology if the conditions are right.

2.6 Reflection survey

2.6.1 Can reflection work?

The success of the seismic reflection survey method depends on the acoustic contrast between layers. Here, our target is to locate the ditch which was dug into the yellow sand. The target was probably filled by building stones (archaeological remains) or other materials and covered by loamy topsoil. Excavations done in 1993 (the 1993 trench shown in Figure 2.4) by the Glasgow University Archaeological Research Division (GUARD) team shows that the thickness of the loamy material (top soil) was less than 0.75 m. The archaeological remains sat on loose sand, which was believed to be a beach deposit of Quaternary age (Figure 2.8).

In another area (west of St. Michael church), a rampart front was found at approximately 2 m depth (Richmond 1978). Depending on topography, the thickness of the topsoil varies. Normally it is thinner on the higher ground relative to the down slope. As the site slopes to the west, the thickness of the eastern part (near to the cemetery wall) is thinner compared to the end of the line (down slope).

Figure 2.8 The excavation cross-section showing the relation between archaeological remains and their surroundings (after GUARD personal communication).

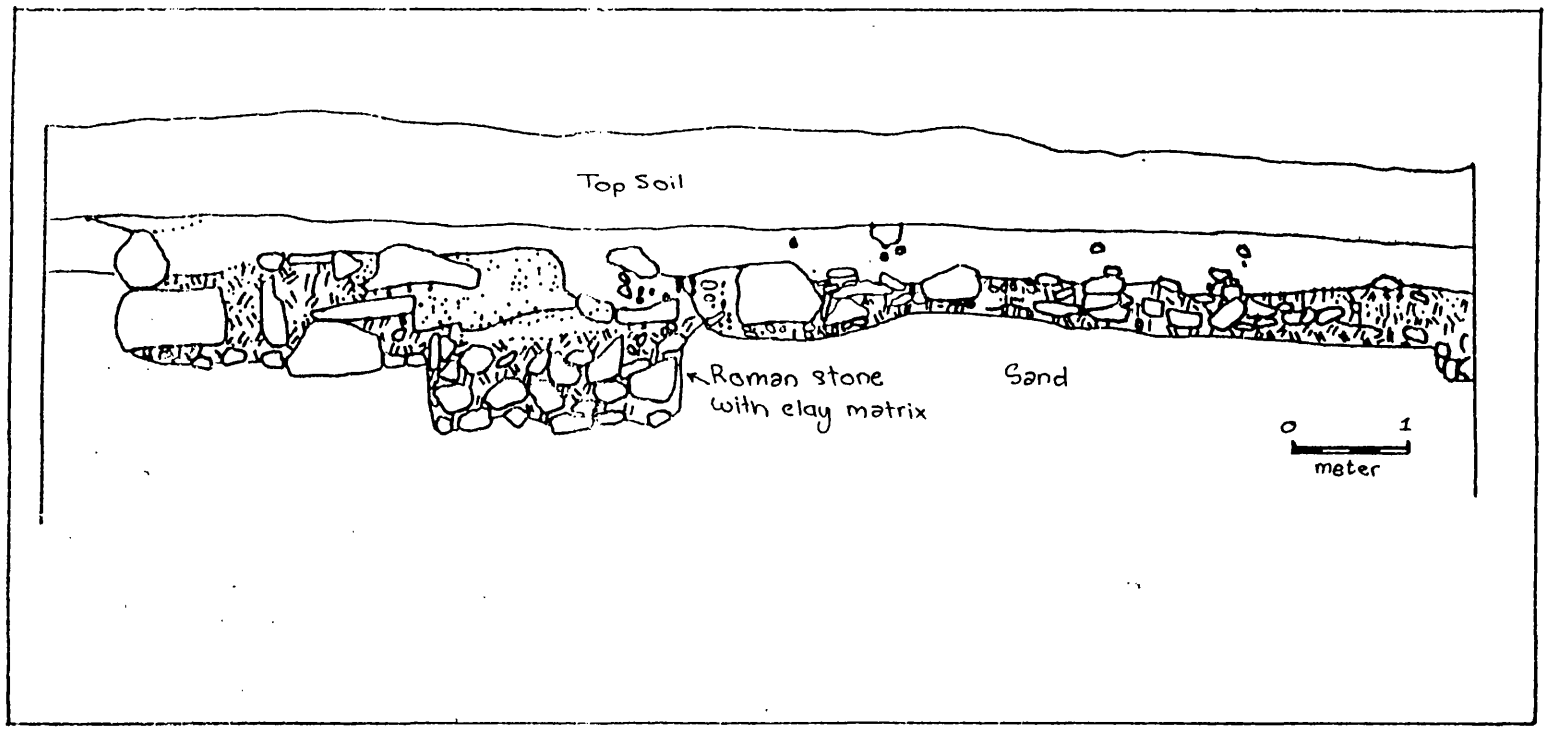

The loamy topsoil has a lower acoustic impedance (the product of density and velocity) than yellow sand. As long as there is a contrast in acoustic impedance, the reflection technique can be applied. However, the success rate is much higher in the area where the contrast is bigger. Besides the necessary acoustic impedance contrast, the target size and geometry are also important. The horizontal dimension must be bigger than the first Fresnel zone otherwise it is undetectable, since the major contribution to the reflected signal comes from this zone (Sheriff and Geldart 1995). The width (radius) of the first Fresnel zone (w) is controlled by the dominant wavelength (λ) and the reflector depth (z) and their relation is

$$w \approx \left(\frac{z\lambda}{2} \right)^{\frac{1}{2}}$$

For the target of less than 3 m depth and if the normal mean frequency produced by a hammer source is 80 -100 Hz, the first Fresnel zone is only about 1.8 m in radius. As the target is wider than first Fresnel zone, horizontally it can be detected by the reflection method. The success of the reflection method in detecting King Xerxes' Canal (6-8 m below the surface, and 25-35 m wide) using a sledge hammer as a source by Karastathis and Papamarinopoulos (1997), shows that our target should also detectable.

2.6.2 Data acquisition

As the aim of this work is to detect the Roman fort ditch using the reflection technique and to compare it to the resistivity profile, the decision was made to lay the reflection line along the L3 resistivity line (Figure 2.4). Before any recording was done, the line was first sighted for elevation. The sighting were done using a Sokkisha Automatic Level (Model C3E) and only elevations relative to the observation point (assumed as 0 m) were read. The actual height of the observation point is 37.82 m above sea level.

Topographically, the site is sloping gently toward the west without any variance. Because of that, only four points of elevation (one at each end and two in the middle) were sufficient, as shown in Table 2.3. The elevations for other points along the line can be interpolated from these four points by assuming a linear relation.

Table 2.3 Elevation of the reflection line.

Distance (m)	Relative Elevation (m)
0	0.82
30	-1.16
40	-2.18
50	-3.24

The data were recorded using a 24 channel OYO McSeis-1600 (version 3.1) seismograph. One of the advantages of this seismograph is that it can facilitate high-speed multicomponent sampling with high resolution. 48 Hz low cut and 1000 Hz high cut pre-filters were applied during the recording. This range was chosen to allow the seismograph to record its maximum possible range of frequency. The 1000 Hz high cut was also chose to eliminate the frequency fold-back problem (aliasing) which can deteriorate digital signals. Low frequency noise was further reduced by using single 100 Hz high-resolution geophones.

The signal was generated by hammering a 3 kg steel hammer on a steel plate. It is the cheapest and commonest source in shallow seismic exploration. It produces peak amplitudes in the frequency range 80-100 Hz. Each record is displayed on the OYO display unit and depending on a visual estimate of quality, it can be stored in memory, deleted or stored directly to floppy disk. The signal stored in memory can be stacked with the later records, if necessary. To improve the signal to noise ratio, a stack of 6 good shots was generally recorded at each shot location.

Depending on the offset (how far it is from the source) and the reflector conditions (acoustic impedance contrast), the energy of the signal detected by the geophone varies. The near offset geophones normally detect high signal amplitudes, which most of the time are so high that they mask other signals on the display of the seismograph, while

the far offset geophones signal levels is so low that it sometimes hardly seen. To overcome those problems, appropriate gain was applied on the all channels. The near offset channels were assigned a lower gain in order to scale down the high energy signal while the far offset channels had a higher gain in order to amplify the signal.

The survey was designed to acquire a very condensed dataset using a 24 channel seismograph across a 50 m wide field. For this, a common depth point (CDP) jump-roll geometry was designed, where 24 geophones equally spaced at a 0.25 m spacing and 13 shots at every 0.25 m starting between geophone 6 and 7 were shot. Then geophones 1 to 12 were moved down the line (to become geophones 25 to 36) (Figure 2.9). Each spread was only 5.75 m long and moved 2.75 m down the line at each 'jump'. 208 shots were recorded on the line, giving a total of 4992 traces. The subsurface reflecting points, which are at half of the receiver spacing are thus every 0.125 m, with maximum coverage of 13 fold (1300%).

In order to get the highest resolution possible, the signal was sampled at every 0.1 ms interval for 102.3 ms. 102.3 ms is known as the record length and is controlled by the pre-triggering record length set (1024 samples) and the sampling rate. The pre-triggering record length is fixed depending on the seismogram, and for the OYO McSeis 1600 it can be selected between three values of 1024, 2048 and 4096 samples.

As the signal is sampled at a very small interval (0.1 ms), the sampling frequency is 10^4 Hz. The Nyquist frequency, the maximum frequency that can be recorded before aliasing occurs is defined to be half of sampling interval, i.e. 5000 Hz. However by applying the 1000 Hz high cut pre-recording filter, aliasing, which folds back frequencies higher than Nyquist frequency, is unlikely to occur.

Figure 2.9 CDP jump-roll geometry.

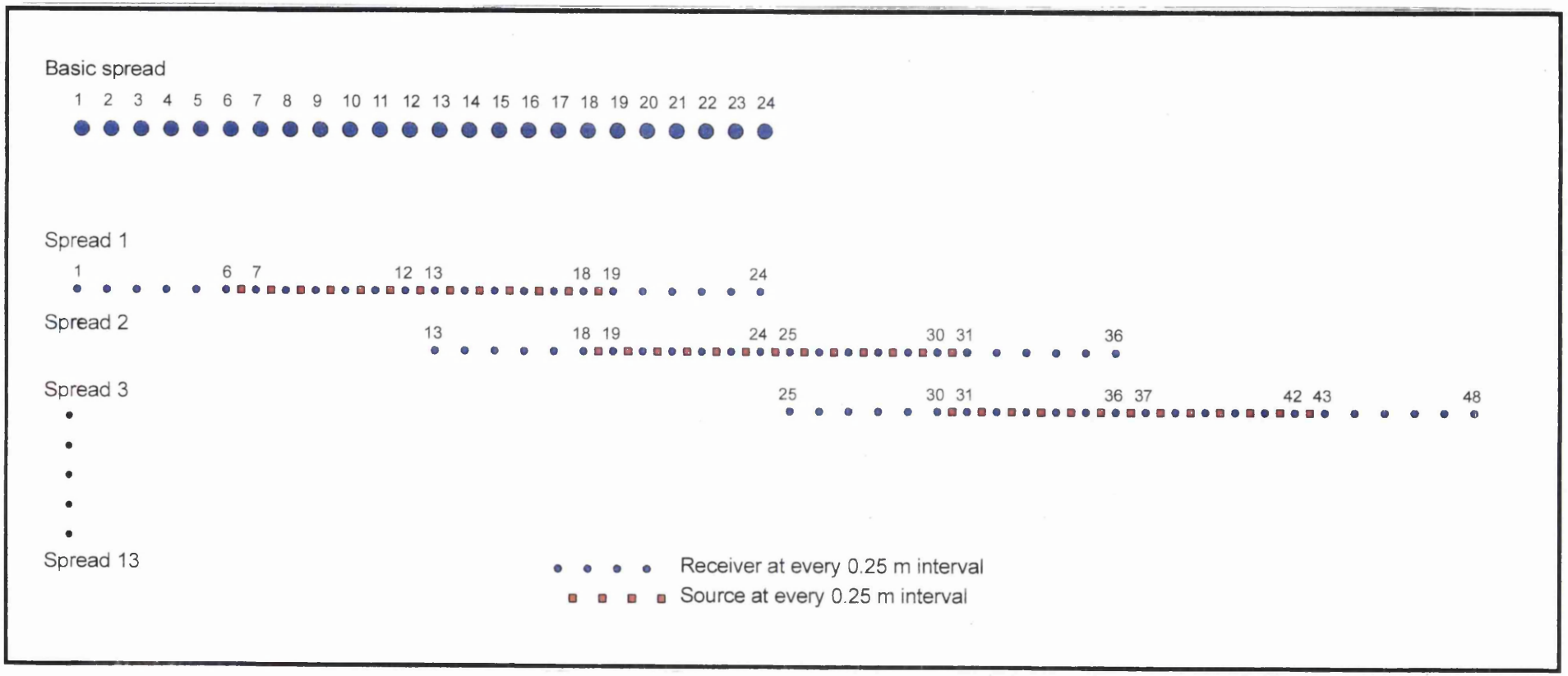

Table 2.4 Summary of the recording parameters.

Spread type	Jump roll
Geophone	100 Hz single element vertical component 'carrots'
Source	3kg hammer and steel plate
Geophone spacing	0.25 m
Source spacing	0.25 m
Nominal fold of coverage	13
Record length	1024 samples
Sample rate	0.1 ms
Record length	102.3 ms
Pre- filter	1000 Hz high cut 48 Hz low cut

2.6.3 Seismic data processing

The data were processed using ProMAX/2D (v 6.1) industry standard software on a Sun SPARCstation-20, with the exception of figure 2.13 which was produced using SierraSEIS processing software.

Before any processing was done, the correct FFID (field file identification number) from the observer's log sheet was added to each file. Noise tests and other non-production files were edited out. Then the geometry was loaded from ProMAX/2D database spreadsheet and stored in the header of each trace. Once the geometry was installed the noisy and bad traces were killed and any reversed traces were corrected. Shot gathers show that the near offset data were dominated by refracted waves and ground roll and it is hard to recognise any reflection signature, on the other hand, the far end records shows an interesting reflection-like signature at around 20-30 ms TWT (two way time) (Figure 2.10). This reflector-like signature shows as a linear event in some records but in most of the records it is a slightly hyperbolic curve. Examples are found in source index number (SIN) 135 and SIN 161 in Figure 2.10. The reason is that refraction arrivals are strong and mask the reflection signal since the target is very shallow.

The length of the spread also contributes to this problem. Since the length of the spread was only 5.75 m, only a small part of the hyperbolic reflector event was recorded. The longer the offset, the better the hyperbola that is recorded.

In order to get a better hyperbolic curve, the edited data were sorted into common depth point (CDP) gathers prior to any further processing. By doing this the reflection signal can be confidently recognised especially on the western end gathers such as CDP 330 in Figure 2.11. The CDP gathers also show the same as shot gathers, where the near offset traces was dominated by ground roll and refraction arrivals. Only the far offset traces on gathers at the western end of the line showed a clear reflection signature (e.g. CDPs 303 and 330 in Figure 2.11).

Figure 2.10 Shot gathers.

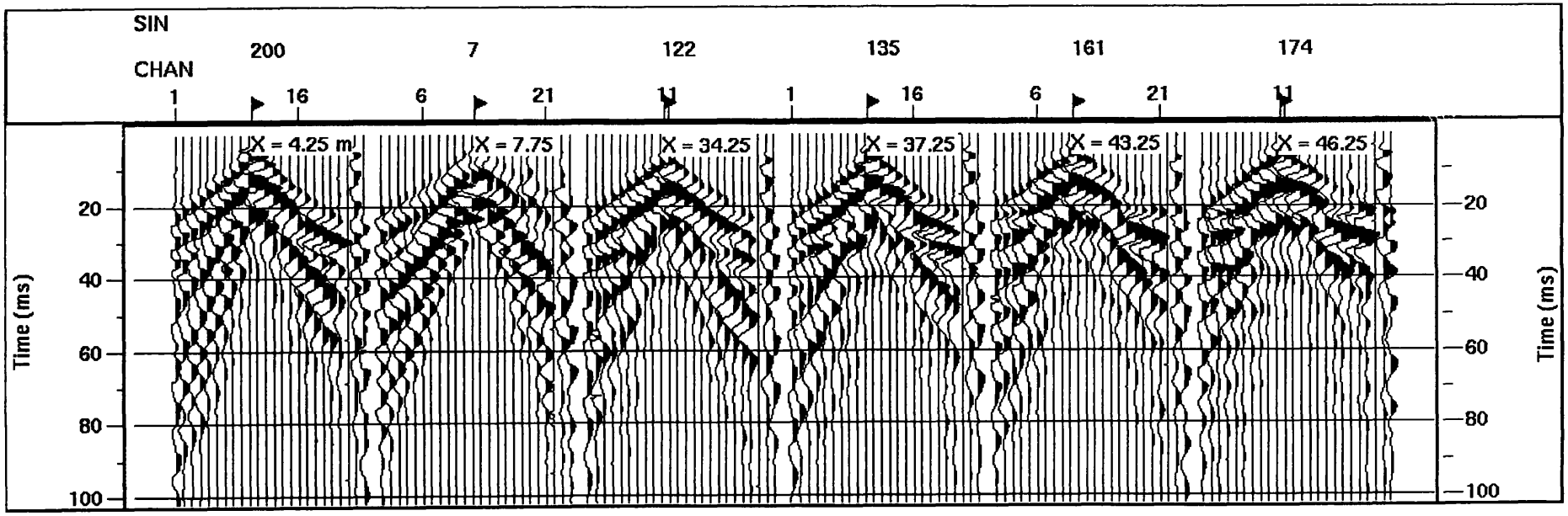

Figure 2.11 CDP gathers.

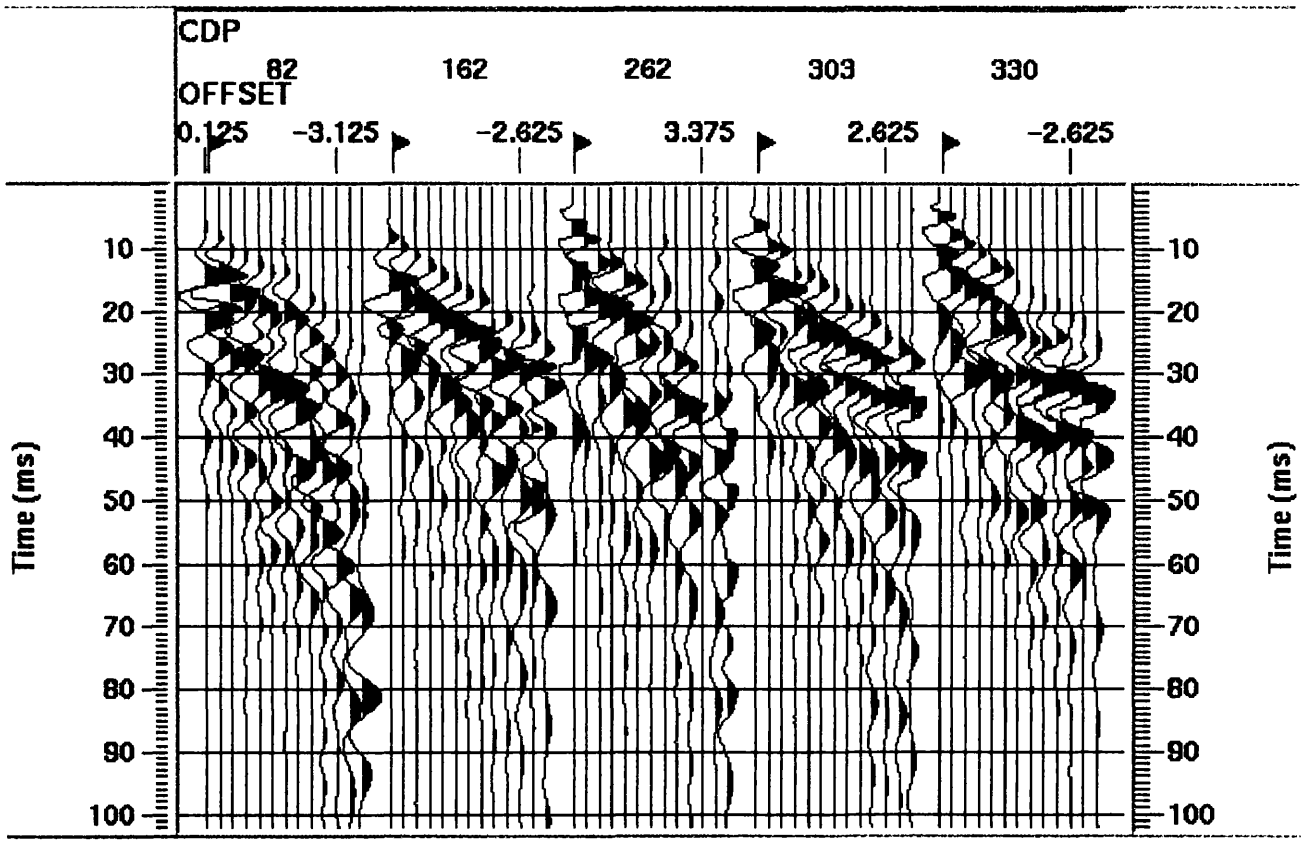

Frequency analysis of the CDP gathers shows that energy is concentrated in the 80 - 120 Hz range (Figure 2.12). F-K analysis of the shot gathers using SierraSEIS processing software shows the data in this domain are dominated by early arrivals (Figure 2.13). These early arrivals were a combination of refraction and reflection arrivals as the reflector is very shallow. It was impossible to separate these arrivals in the F-K domain. An F-K filter was therefore not applied, in order to avoid the removal of the reflected signals.

The first arrival was only muted out on the gathers where the reflection signal was clearly recognised (Figure 2.14). In the noisy gathers, or in gathers where the reflection signals was questionable, the first arrival mute was applied based on the nearest clearly recognised reflection signals. This was to ensure that no reflected arrivals were muted and to ensure that only the refracted arrival were muted.

Reflection times on the seismic traces recorded on land have to be corrected for time differences resulted from near surface irregularities. These irregularities have the effect of shifting reflection events on adjacent traces out of their true time relationship. Two major sources of irregularities are 1) elevation differences between shots and receivers, and 2) the presence of a weathered layer of extremely low seismic velocity (weathering effect). The thickness of weathered layer ranging from a few meters to tens of meters. Although it is thin, its abnormally low velocity can caused large time delay to passing rays which may lead to false identification of significant features on seismic section.

A flat horizon can sometimes appear as a dipping event in topographically uncorrected section, with the thinner end appearing to be shallower than the thicker part. This is one of example how the surface irregularity can effect the reflection result, thus it need to be corrected prior any other processing. The correction for these effects is known as 'field static or static correction'. The static corrections remove the effect of the low velocity layer and reduced all reflection time to a common height or datum.

Figure 2.12 Frequency content.

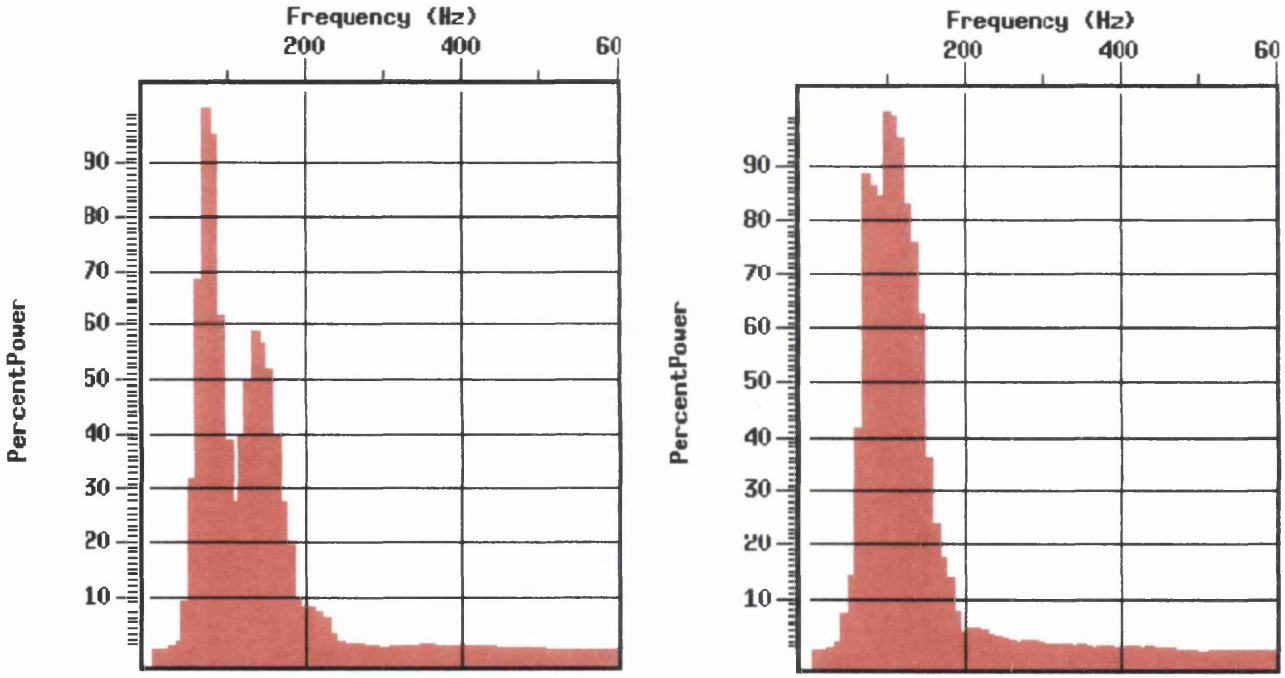

Left and right panels are the frequency content for CDP 136 and 200 respectively.

Figure 2.13 F-K analysis.

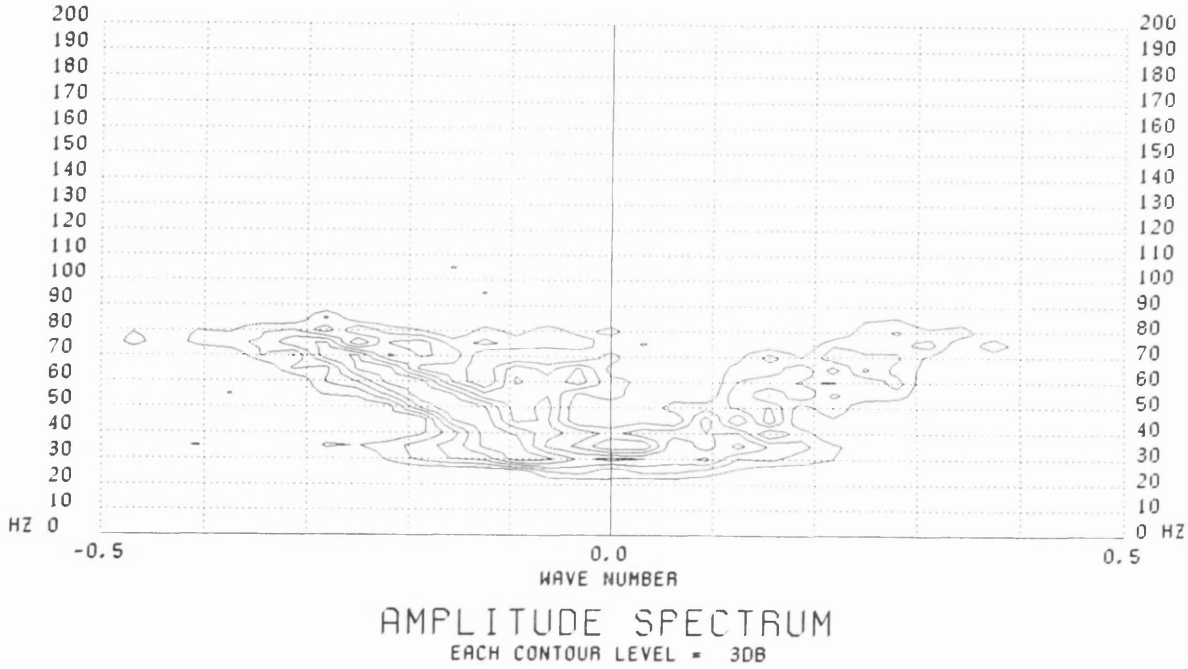

This figure was created earlier using SeirraSEIS processing software.

Figure 2.14 CDP's gathers with front or top mute applied.

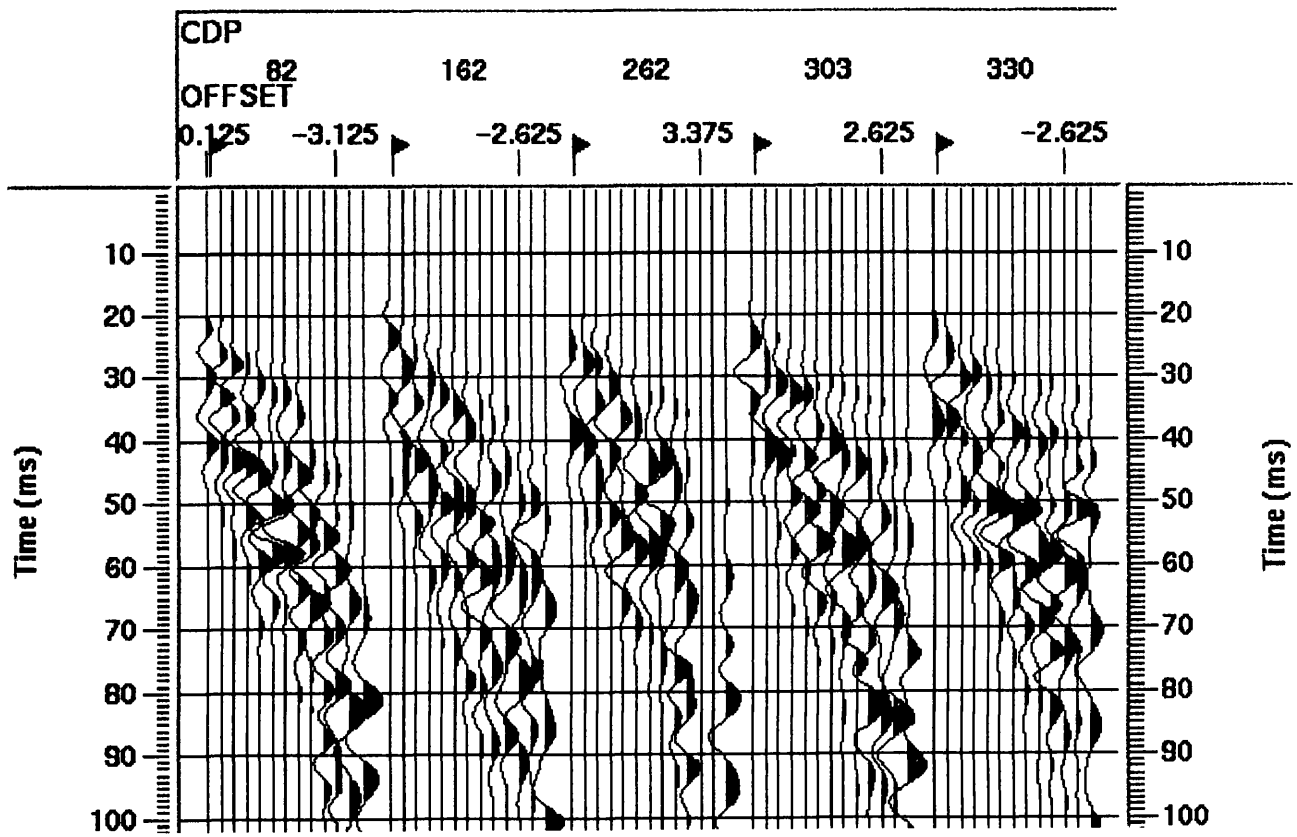

Calculation of the static correction requires knowledge of the velocity and thickness of the weathered layer and the velocity of the underlying layer under all shot and detector locations. It is also need to assume that the rays travel in vertical path through the low velocity layer.

The first step in static corrections is to remove the effect of low-velocity layer (weathered layer). In this 'weathering' correction, we effectively change the low-velocity layer (weathered layer) with the un-weathered velocity value. In mathematical form, the weathering corrections time (t_w) can be represent as follows.

$$t_w = \frac{h_w}{v_w} - \frac{h_w}{v_f}$$

where h_w is the thickness of the weathered layer beneath the shot or receiver and v_w and v_f are the velocity for weathered and fresh layers, respectively.

The second step of static correction is the correction for topography elevation irregularities. The correction for this effect involves correcting the signal to one arbitrary horizon, normally known as the datum. If the value chosen is lower than the surface elevation level, the trace is shifted so that the arrivals are earlier by the correction time (excess height divided by replacement velocity). On the other hand, if the value chosen is higher than the surface elevation level, the correction will shift the arrival time so it is later by the amount of the correction time. If the processing system is such that events above zero time – datum, are lost or muted, then shallow data can disappear. Ideally the datum is chosen so that the corrections are as small as possible.

In shallow reflection work where the early arrivals are significant, the choice of a processing datum is important (Rogers 1981). For a small-scale survey and where the topography does not vary much, the lowest point is normally taken as the datum (Burger 1992). In the study area the topography changes by approximately 4 m (Table 2.3) along the 50 m line. Thus taking the lowest point as the datum will mean truncating up to 16 ms of valuable records from the higher region traces. To overcome this over-truncation of the traces, the datum is chosen to be the middle of the field. The reason for

this is that the thickness of the weathering layer was unknown, and if the datum is too deep, the elevation correction will 'remove' the surface layers by bringing the traces up. Since the target is shallow, an over-truncating of the traces should be avoided to preserve the near surface information. An elevation correction with a 250 m s^{-1} replacement velocity was applied to the data. This value was an estimation of the first (glacial till) layer velocity taken from the direct wave velocity in the shot gathers.

Figure 2.15 shows the CDP gathers after all the corrections and data enhancements were applied. The relatively small dataset enabled a constant velocity stacking analysis to be done to find the suitable stacking velocity. A normal semblance velocity analysis was very hard to do since the record length was short (only 100 ms) and the velocity changes were not very clear. Using this technique, an approximation of a stacking velocity function was obtained (Table 2.5) and used in normal moveout correction and stacking process. Only the reflectors between 10 - 40 ms were important in this survey because the target is less than 5 m deep. A summary of the processing flow applied to the data is given in Figure 2.16.

A brute stack section (Figure 2.17a) shows a strong reflector starting from 20 m (CDP 160) to the western end of the line. The first 20 m of the section were contaminated by steep dipping events. The autostatic horizon for static correction was picked based on this reflector. However, after this static correction, the data shows only a slight improvement. To remove the steeply dipping linear events, a dip scan stack was applied (Figure 2.17b). The section was further improved by applying post-stack Kirchhoff time migration using the same stacking velocity (Figure 2.17c).

Table 2.5 Stacking velocity function

Time	Velocity m/s
0	200
30	400
60	1000
100	1600

Figure 2.15 CDP's gathers after pre-stack processing (refer to text for details) applied.

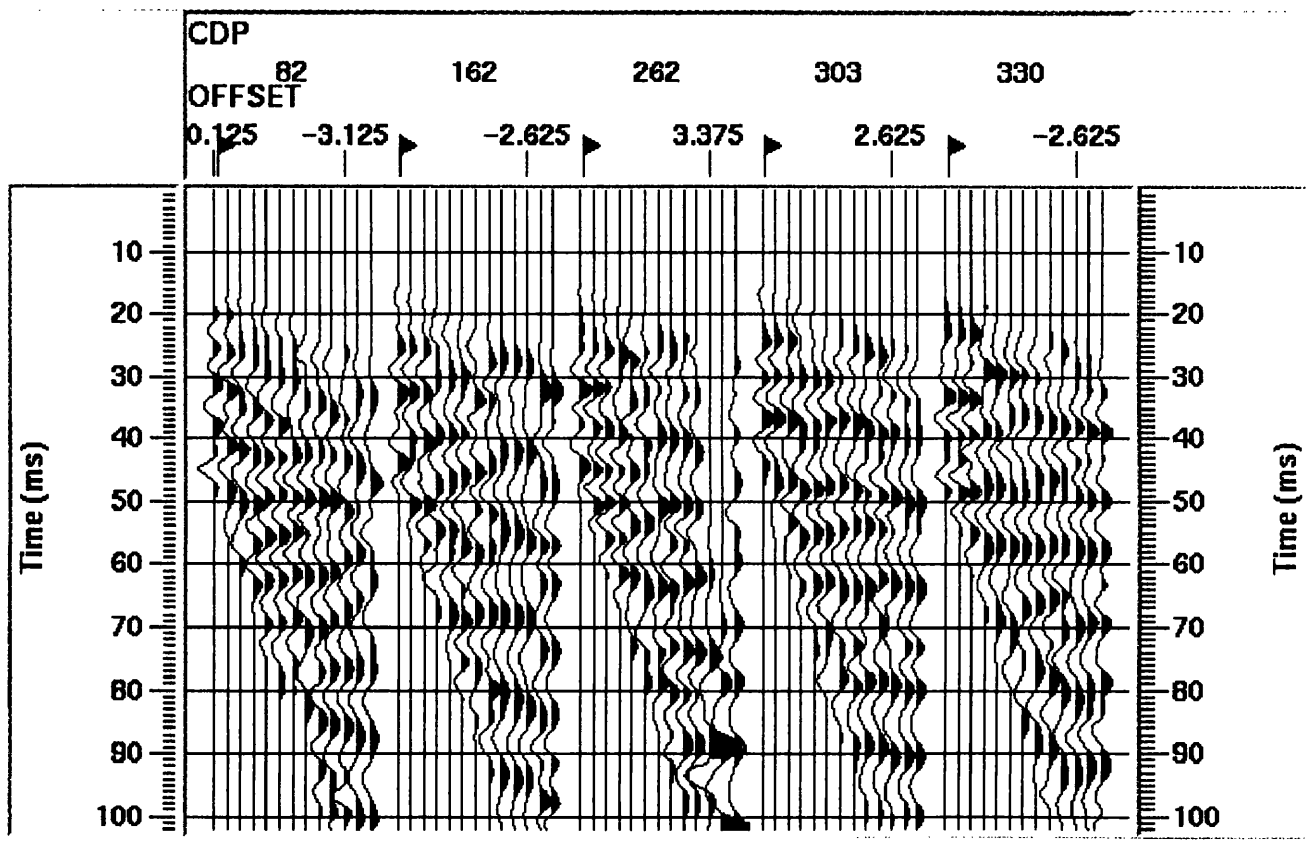

Figure 2.16 Processing flow chart.

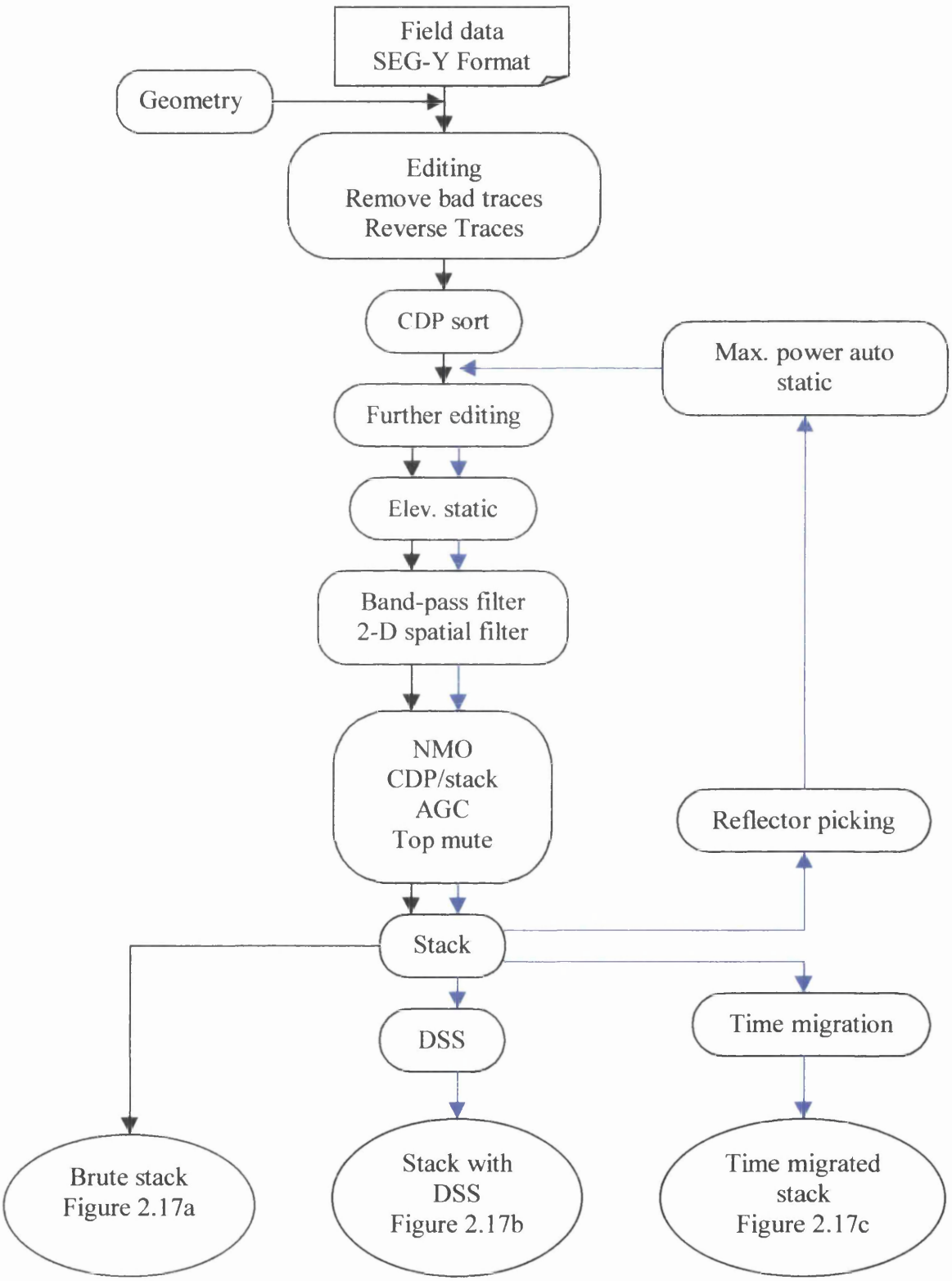

Figure 2.17a Brute stack.

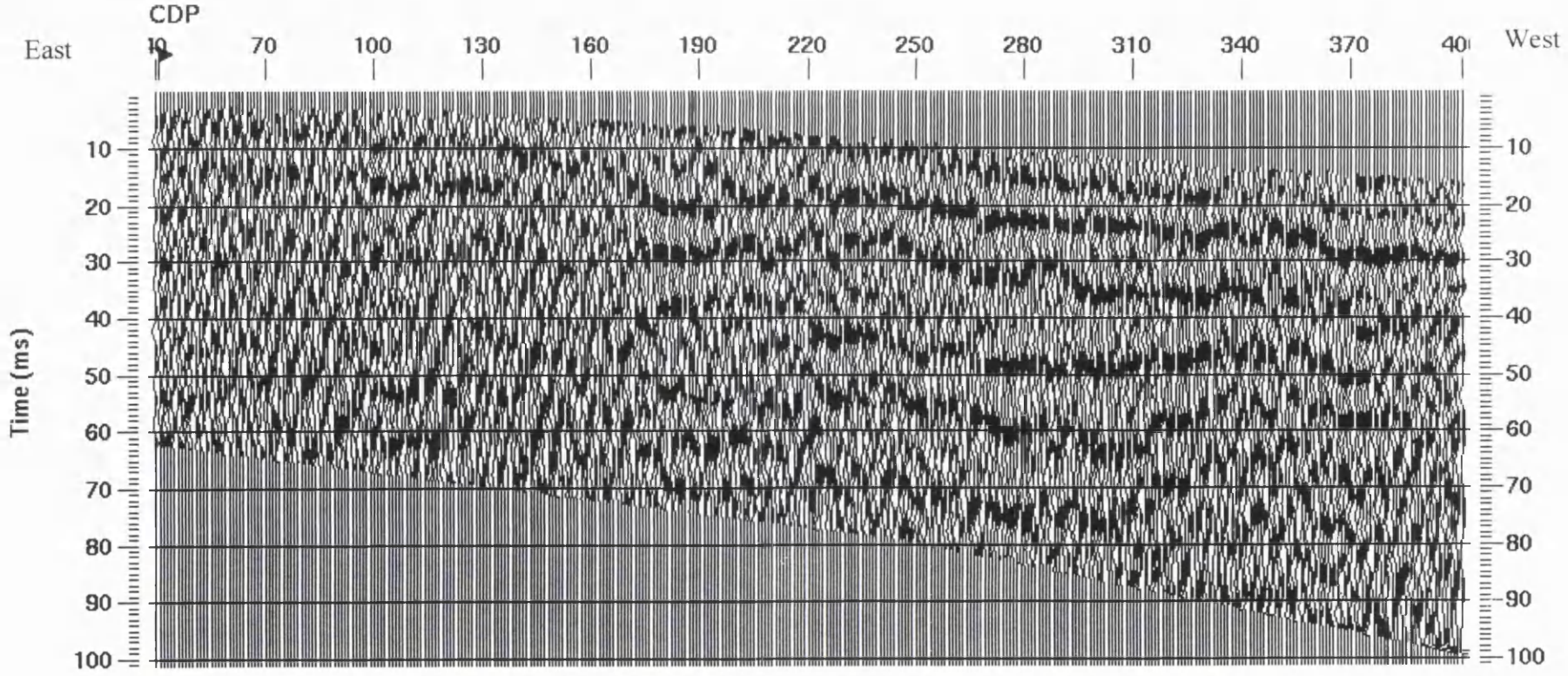

Figure 2.17b Stack section with DSS applied to remove linear dipping events.

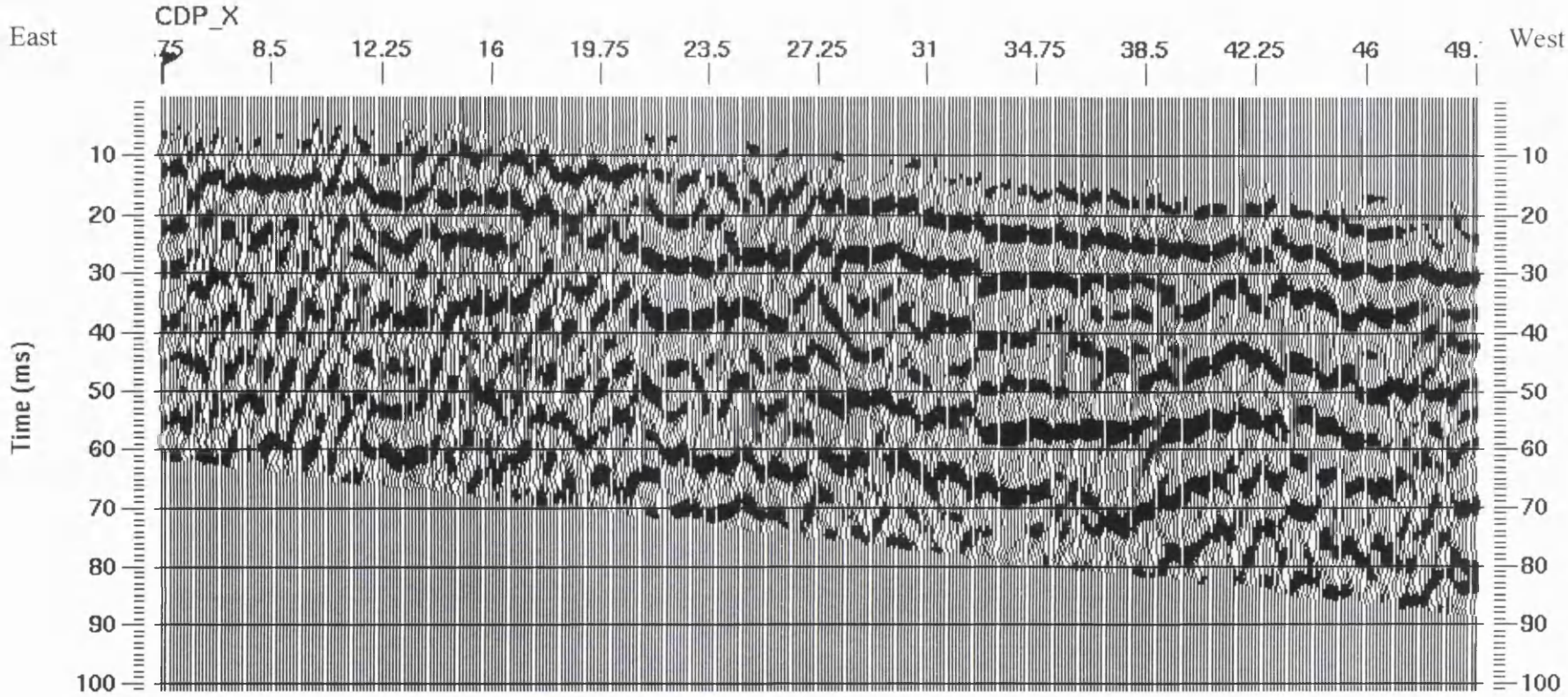

Figure 2.17c Time migrated section.

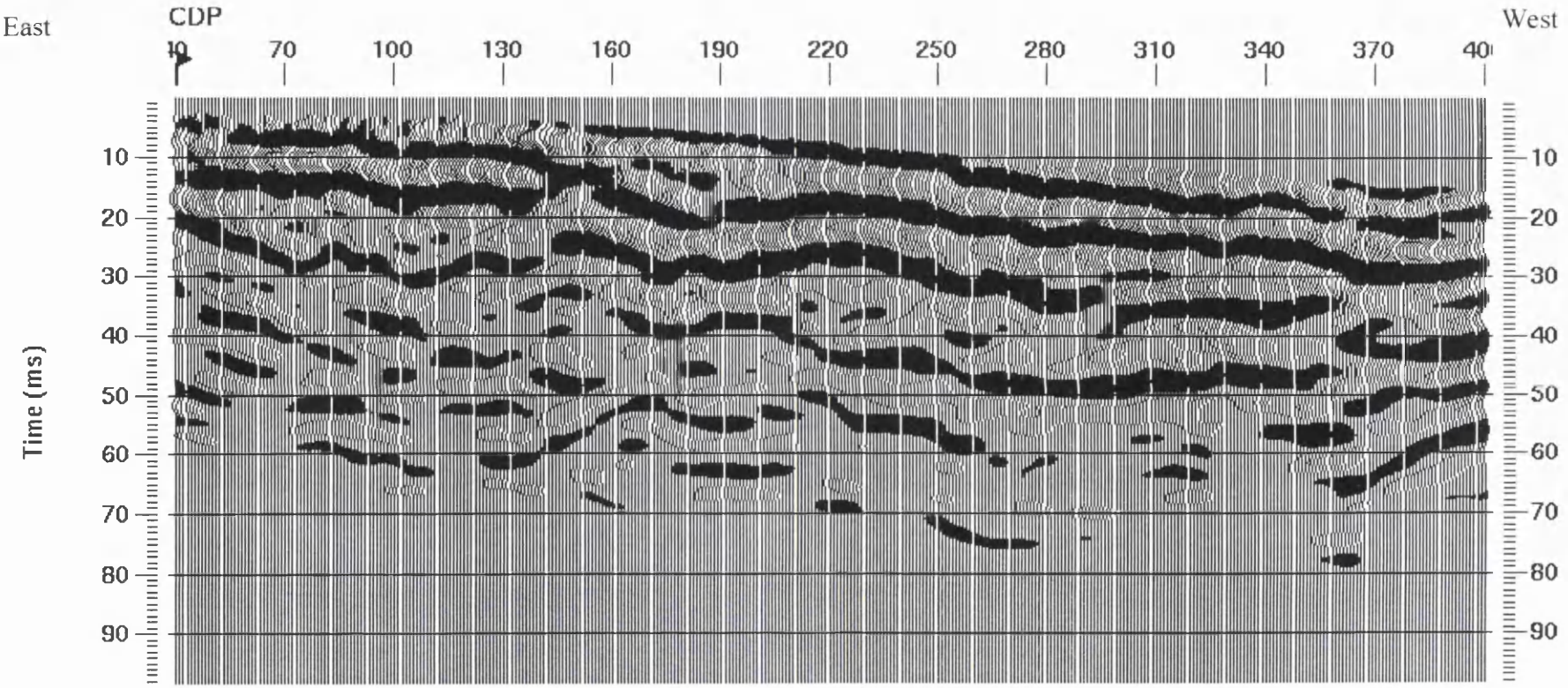

2.6.4 Discussion

Figure 2.18 shows the interpreted final result of the reflection survey. The reflector (red) is found dipping to the west, following the topography. At the eastern, leftmost end of the profile (low CDPs), the reflector is only 8 ms TWT deep, while at the western end the depth increases to approximately 30 ms TWT. The most interesting feature in the profile is the 'synclinal' pattern in the middle of the section, between CDPs 150 and 200. This feature is approximately 10 m wide and about 10 to 15 ms TWT deep.

From the archaeological excavation evidence, the Roman fort was built on the sandy beach deposit and was subsequently covered by loamy topsoil. From the exposure in the nearby area, the sandy beach deposit was deposited on top of Carboniferous Coal Measures group (sandstone and shale). The velocity of the topsoil was measured from the direct arrival analysis and it is in the range of 180 m s^{-1} to 250 m s^{-1}, with an average of 200 m s^{-1}. This value (lower than the velocity of sound (air blast, 332 m s^{-1})) is a result of the wave travelled through a loamy and grassy wet top surface.

Stacking using the NMO velocity function (Table 2.5) of which was estimated from the CVSs analysis shows the appearance of maximum reflection amplitude at approximately 10 ms TWT to 40 ms TWT. This maximum reflection is indicated by the red marker on Figure 2.18. Calculating the dip of this horizon shows it is a flat horizon. The Dix equation shows that for uniform horizontal layers and small offsets, NMO velocity is equivalent to the root-mean-square velocity (VRMS). The conversion from time to depth section requires interval velocity information, which can be calculated from the relation below;

$$\text{int } vel = \left[\frac{T_2 x VRMS_2^2 - T_1 x VRMS_1^2}{T_2 - T_1} \right]^{1/2}$$

where $T_{1\&2}$ are TWT to the shallow and deeper layers, while $VRMS_{1\&2}$ are the root-mean-square velocities to the respective levels.

Figure 2.18 Interpreted time migrated section.

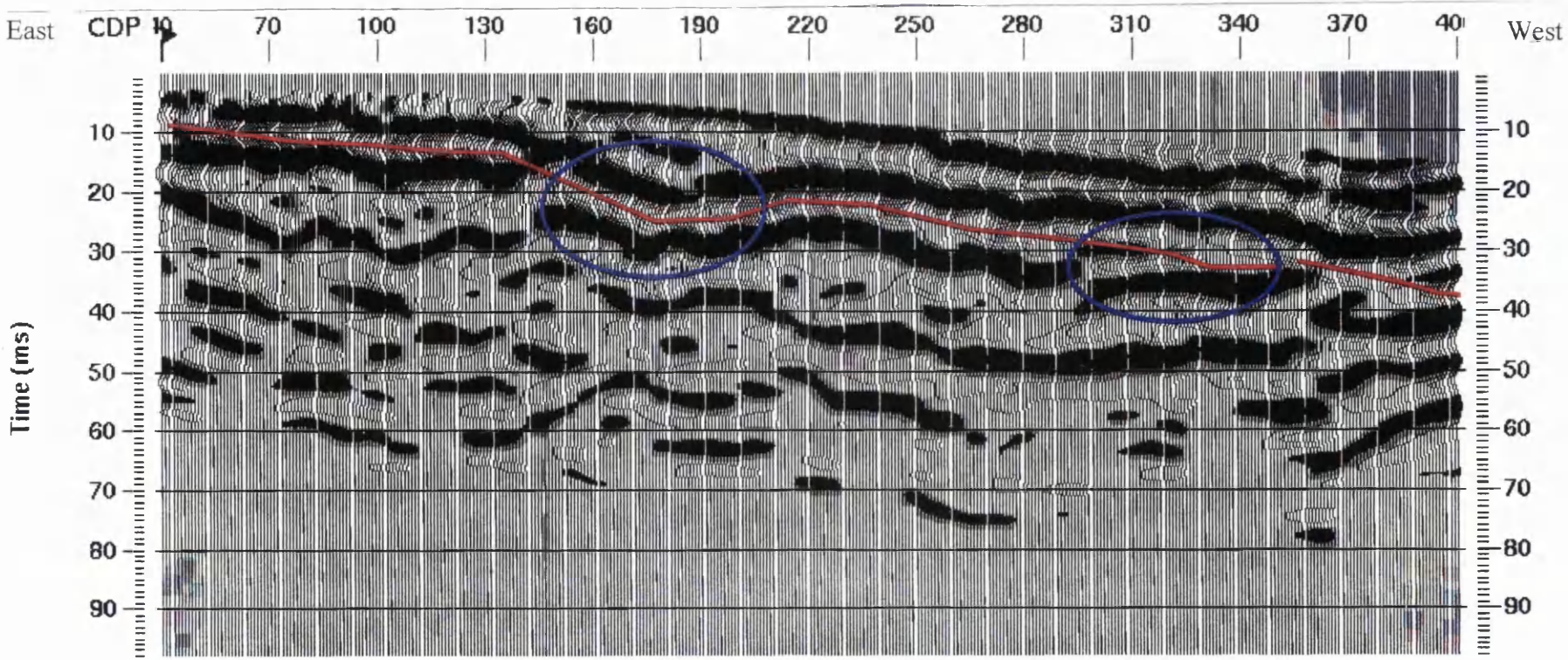

The red line represents the shallow boundary between topsoil and underlying sandy layer.
The blue ellipses correspond to the resistivity anomalies. The left ellipse is the possible location of the ditch.

Based on this relation, the interval velocity for the first interval is approximately 400 m s^{-1}. This value is bigger than the velocity of the direct arrival (200 m s^{-1}). This value is also used to calculate the depth of the red reflector with respect to the datum. Based on the velocity information, the depth of the red reflector is approximately 1.8 m at the eastern end of the line and progressively increases to 7.2 m down the line. The depth of the syncline or pit is approximately 2 m.

This reflector (red) is believed to be a boundary between loamy topsoil and a sandy beach deposit. The synclinal shape of the reflector is presumably the indication of the V-shaped Roman ditch, since it is located at the place where the ditch is expected. Furthermore, the width and the depth of this reflection feature is also about the same as estimated from archaeology.

The brute stack (Figure 2.17a) shows the good reflector from about the 20 m position (CDP 160) to the western (right-hand) end of the line and it is missing (hardly recognisable) from the eastern end to that point (CDP 160). This phenomenon might be expected to appear due to up-slope thinning of the topsoil. Because the topsoil is thin in the higher level (eastern end), the problem of interference between direct wave (travelling along the surface) and reflection signals (from the top of the sandy beach deposit) might be occurred at this end which degrade the quality of the section.

2.7 Conclusions

The result of the resistivity survey suggested there were two possible anomalies related to the ditch - anomaly B and C. However, anomaly C was too shallow, while anomaly B was discontinuous. Anomaly B is more likely to be due to the ditch than anomaly C since it is much deeper, although the presence of the C anomaly on L3 was unclear. On the other hand, on the reflection survey only one ditch-like feature was detected. Compared to the resistivity profile L3, this feature appears to be at the same location as anomaly B.

The seismic reflection survey employed here has produced a better image of the Roman ditch than the semi-qualitative resistivity survey. It confirms that there is only one ditch in this area, and that the centre of this ditch is 21 m from the wall on line L3. The width of the ditch is approximately 9 m wide and has a depth of approximately 2 m.

In conclusion, although the reflection survey is technically more complex than the resistivity method, it did nevertheless produce a better image, and a more definitive detection of the target.

CHAPTER THREE

3-D
SHALLOW SEISMIC REFLECTION

3.1 Introduction

The 3-D seismic reflection exploration method is the latest exploration technique and has been widely used in search for petroleum. From the time when it was introduced in 1972 until now, it has undergone a great deal of improvement and modification. The usage of this technique is widespread all over the world in the search for petroleum. In 1996, approximately 42.5% of world seismic exploration (for petroleum) was done using the 3-D seismic technique, compared to only 35% using the 2-D technique, while the method used for the other 22% is unknown (Stefanic 1997). The deployment of this 3-D exploration method is still increasing. Many major oil companies will not drill oil exploration wells without consulting 3-D seismic data first. After constant improvement throughout the years, it was considered by 1991 to be almost a mature technique (Brown 1991).

Although 3-D is considered a mature exploration tool, only a few attempts have been made at employing this technique for small-scale near surface investigation work. Application of the 3-D petroleum technique to near-surface investigation has been proven not only challenging but also expensive (Lanz *et al.* 1996, Miller *et al.* 1997). As the 3-D technique matures within the petroleum exploration field, involving lots of capital, adapting the technique affordably to shallow investigation work (mainly for engineering purposes) which traditionally involves less capital expenditure is the main restriction.

In this chapter we are going to discuss the application of full 3-D seismic reflection in investigating a very shallow structure for engineering purposes. This work is believed to be the first of the kind ever done. Because it is considered a novel trend in shallow seismic investigation, details from the planning through to presentation of results will be discussed.

3.2 Aims

The main aim of this work was to map out underground tunnels (rooms and pillars) of an abandoned coal mine using 3-D seismic reflection methods adapted from the latest and most advanced 3-D seismic reflection used in petroleum exploration. The fieldwork costs of this project were sponsored by the Glasgow Development Agency (GDA). Designing the 3-D survey or finding the best way to scale down the survey from petroleum exploration to suit engineering work is the most important aspect, as it is believed to be the first of its kind has ever been done. Besides that how the data are processed is also important, as shallow records cannot be treated like deep records.

3.3 Previous work

The application of the 3-D surveying technique in shallow investigation is still in an early phase of development. Corsmit *et al.* (1988) conducted a 3-D survey to study the shallow stratigraphy over a tidal plain. The data were acquired using a 12-channel, 10 bit engineering seismograph with a 30 kg steel ball source dropped from 3 m height on to a 30 kg steel plate. Their 3-D survey was designed so that the data points of different source - receiver pairs exactly coincide, so that the CMPs lie on a regular grid. For that, the geophone stations were located on two parallel lines while the shot locations were placed on four traverses perpendicular to the receiver line (Figure 3.1a). His work was purely academic and pedagogic, as its main purpose was to demonstrate to students how a 3-D survey is conducted, and how the data are handled and processed.

A simple 3-D survey can be designed by placing the line of receivers perpendicular to the line of sources. Using this simple concept (Figure 3.1b) Hasbrouck Geophysical Inc. (1994) conducted a 3-D seismic survey to test the use of 3-D data in defining the near surface structures and properties that control groundwater flow and contaminant transport.

Figure 3.1a Simple 3-D field geometry design (after Corsmit *et al.* 1988).

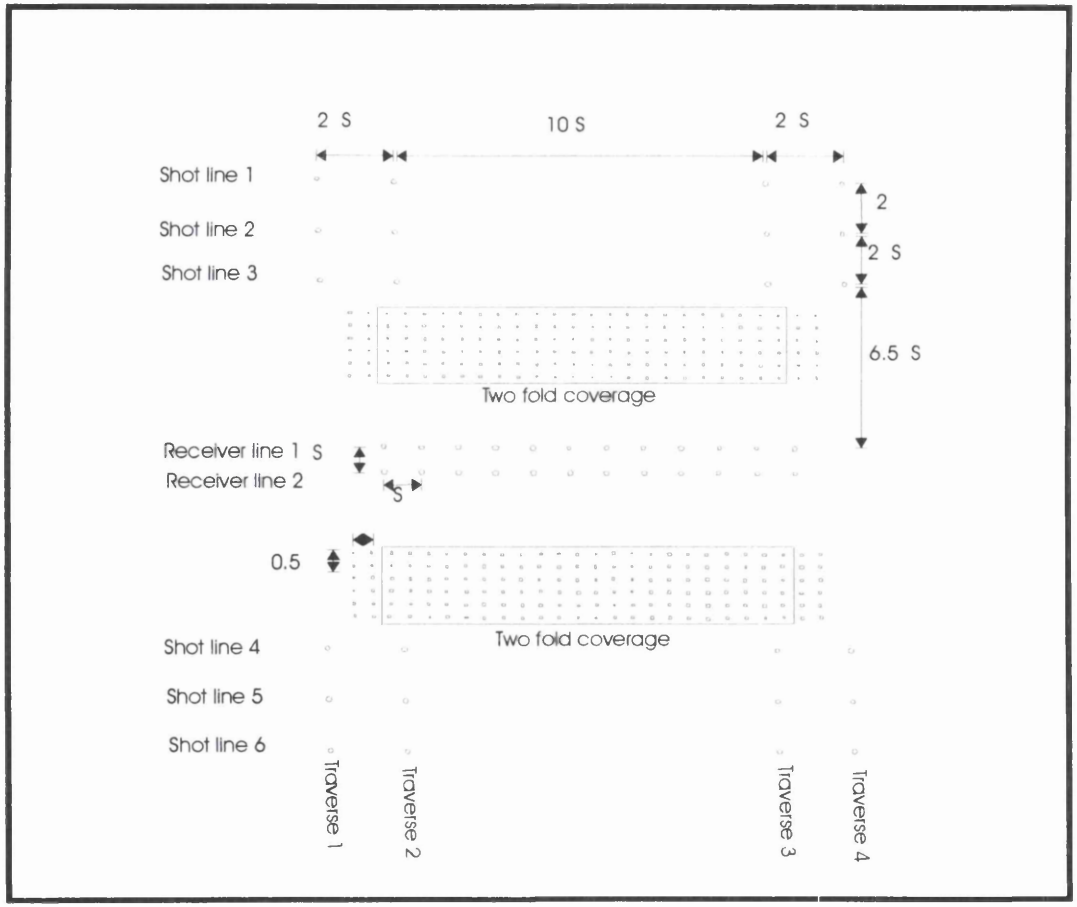

Figure 3.1b Simple 3-D field geometry design (after Hasbrouck Geophysical Inc. 1994).

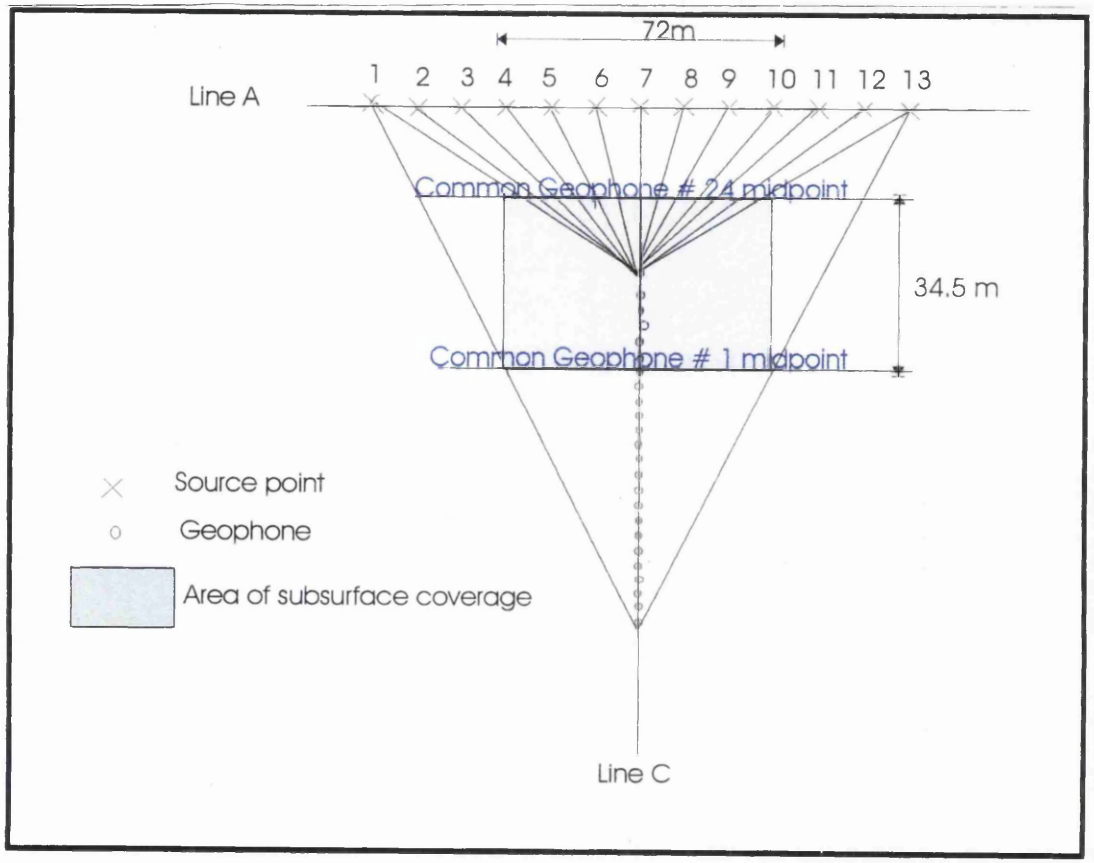

Figure 3.1c Simple 3-D field geometry design (after Lanz *et al.* 1996).

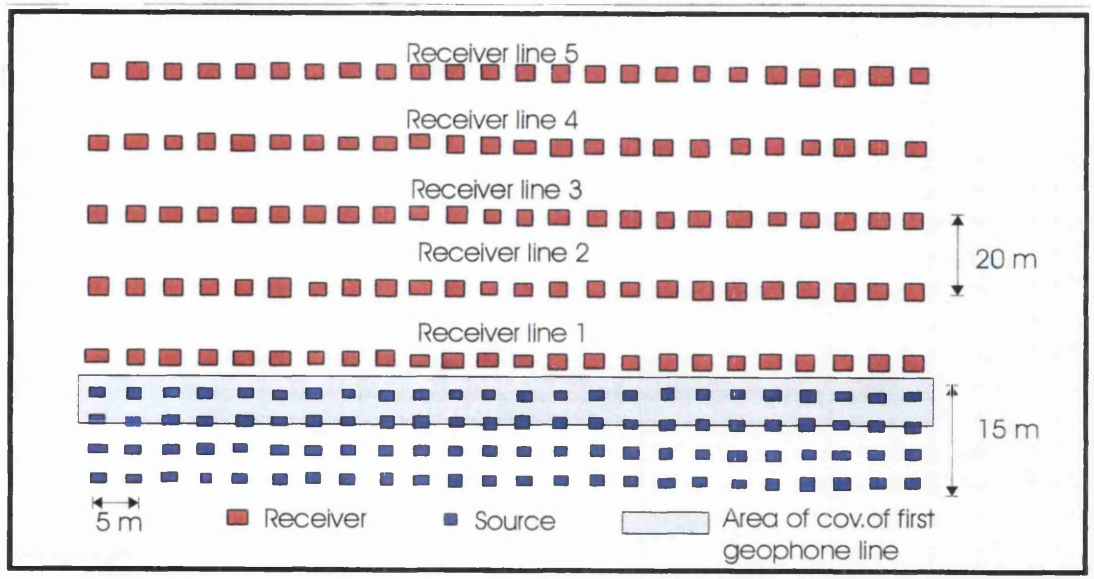

Figure 3.1d Simple 3-D field geometry design (after Miller *et al.* 1997).

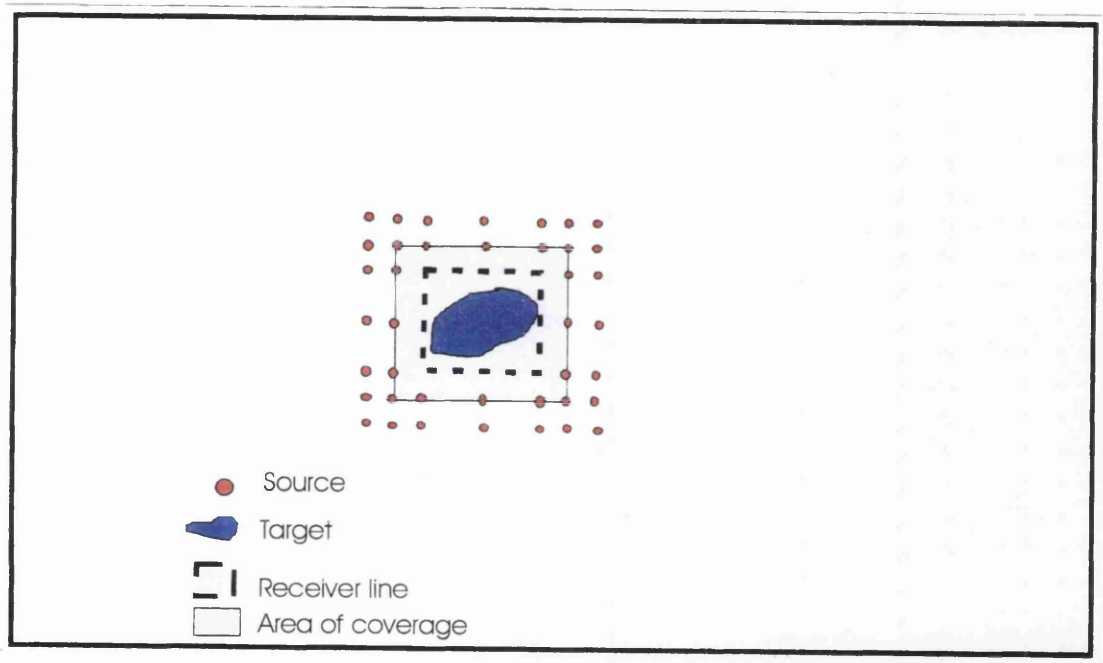

A simple 3-D survey also can also be designed by placing the receiver lines parallel to the source lines. This design (Figure 3.1c) was deployed by Lanz *et al.* (1996) in order to overcome the problems in the 2-D section where the critical parts of the 2-D seismic section were dominated by out-of-plane reflections and diffractions. For each receiver deployment, a total source configuration consisting of four rolling lines of 24 sources (shotgun) points at a 5 m interval was used.

Miller *et al.* (1997) also deployed a 3-D survey to evaluate the lateral variability of the interpreted fault around a collapse feature or sinkhole. The 3-D dataset was recorded using a single fixed square array centred on the sinkhole (Figure 3.1d). This is another simple method of acquiring 3-D data.

All these simple methods were designed so that the midpoints from different source receiver pairs exactly coincide so that the CMPs lie on a regular grid. Because of the regular CMP grid, these simple methods can be considered as a subset of a more general 3-D survey, in which the source receiver midpoints and the azimuths should be as random as practicable, so that there is complete freedom in binning the CMP data. A discussion on 3-D survey design is presented in Section 3.8.

Smythe (1994) pioneering the use of the vibroseis source in imaging the fault patterns for hydrogeological work. The aim of his work was to image the relationship of faults within the target volcanic rocks in 3-D, in order to investigate the suitability of the area as a radioactive waste disposal site. This survey covered 1 km^2 of CMP area with the prime target in a depth range of 400-1000 m. Although the aim was to provide information on fault patterns for an engineering site investigation, the depth of the target excludes this work from being categorised as a shallow investigation work. However, the success of this survey has led to the present shallow 3-D experiment, the author's project.

Based on the success of Smythe (1994) in mapping a complex fault system at a relatively shallow depth (compared to petroleum exploration) and the suggestion from

Brückl *et al.* (1996) and Kourkafas and Goulty (1996) that the 2-D reflection images over a mining area (coal and gypsum) can be improved by conducting a 3-D reflection survey, in early 1996 the decision was made to experiment with full 3-D seismic reflection over an abandoned coal mine.

The year 1996 marked a new era in shallow seismic industry where the transformation to a full 3-D seismic reflection technology (from the petroleum industry) has been brought in. At the time the present project was initiated, it was believed that it was the first ever of its kind, as there were no publications (except for the previously mentioned simple 3-D surveys). However by late 1996, several publications on the same subject had been published (Barnes and Mereu 1996, House *et al.* 1996, Siahkoohi and West 1996).

Barnes and Mereu (1996) studied the limitations of high resolution 3-D seismic reflection techniques for mapping near surface stratigraphy. They also compared a 2-D with a 3-D data set to evaluate the effectiveness of the 3-D method in imaging structures as seen on the 2-D data set. Siahkoohi and West (1996) on the other hand used the 3-D seismic reflection techniques to image complex stratigraphic structures within glacial deposits. Several problems were encountered such as: (1) maintaining the consistency of shot amplitude and spectral content, (2) strong surface wave generated especially at single points shot, and (3) in obtaining a uniform S/N ratio as well as the offsets and azimuth within each bin. The uniform offset and azimuth within each bin can be achieved by using a less linear shot and receiver distribution (Siahkoohi and West 1996).

House *et al.* (1996) also used the 3-D survey method to determine the feasibility of using this methodology to constrain bedrock topography. Based on their work, they also suggested that the targets should have a depth of more than 15 m with a sharp velocity contrast in order to have good results in 3-D shallow seismic reflection work. The latest publication on this subject has been by Büker *et al.* (1998b) who outlined a comprehensive strategy of 3-D seismic reflection data acquisition and processing.

3.4 The site

3.4.1 Location

The site, at national grid 556705, is part of the West of Scotland Science Park. It is located to the NW of and 7.5 km distant from Glasgow City centre. It lies north of the junction of Acre Road and Maryhill Road, and is elongated 320 m along the Maryhill Road with 110 m width. The total area of the Science Park is 35.2 km^2 (Figure 3.2, Photo 3.1). At the time of initial survey, the site was a green field, however later during the course of fieldwork, part of the topsoil was stripped off from the site.

3.4.2 Geology

Glasgow is situated in the Midland Valley. The valley is an ancient rift valley or graben bounded by two parallel faults orientated NE-SW, the Highland Boundary Fault to the north and the Southern Upland Fault to the south. The rocks in the valley are relatively young, with two main systems, the Old Red Sandstone of Devonian age and Carboniferous sediments. Broadly speaking, the Carboniferous rocks are arranged in a wide compound syncline underlain and flanked by strata of Old Red Sandstone age (MacGregor and MacGregor 1948).

In the Glasgow area, most of the solid rocks are covered by glacial moraines and outwash sand (George 1973). The Drift edition of the geological map 1" Sheet 30 clearly shows that the site is covered by boulder clay from recent glacial deposits. This glacial deposit is deposited on the "d^{2b}" rocks, which are the Limestone Coal Group of the Carboniferous Limestone Series (Geological map, Sheet 30, Solid Edition, part of which is reproduced in Figure 3.3). These groups were deposited during Lower Carboniferous time. The cross section drawn through the nearby area (Figure 3.3) shows that the Carboniferous rocks are dipping to the east at a low angle.

Figure 3.2 West of Scotland Science Park, Todd Campus West (green colour): The site location.

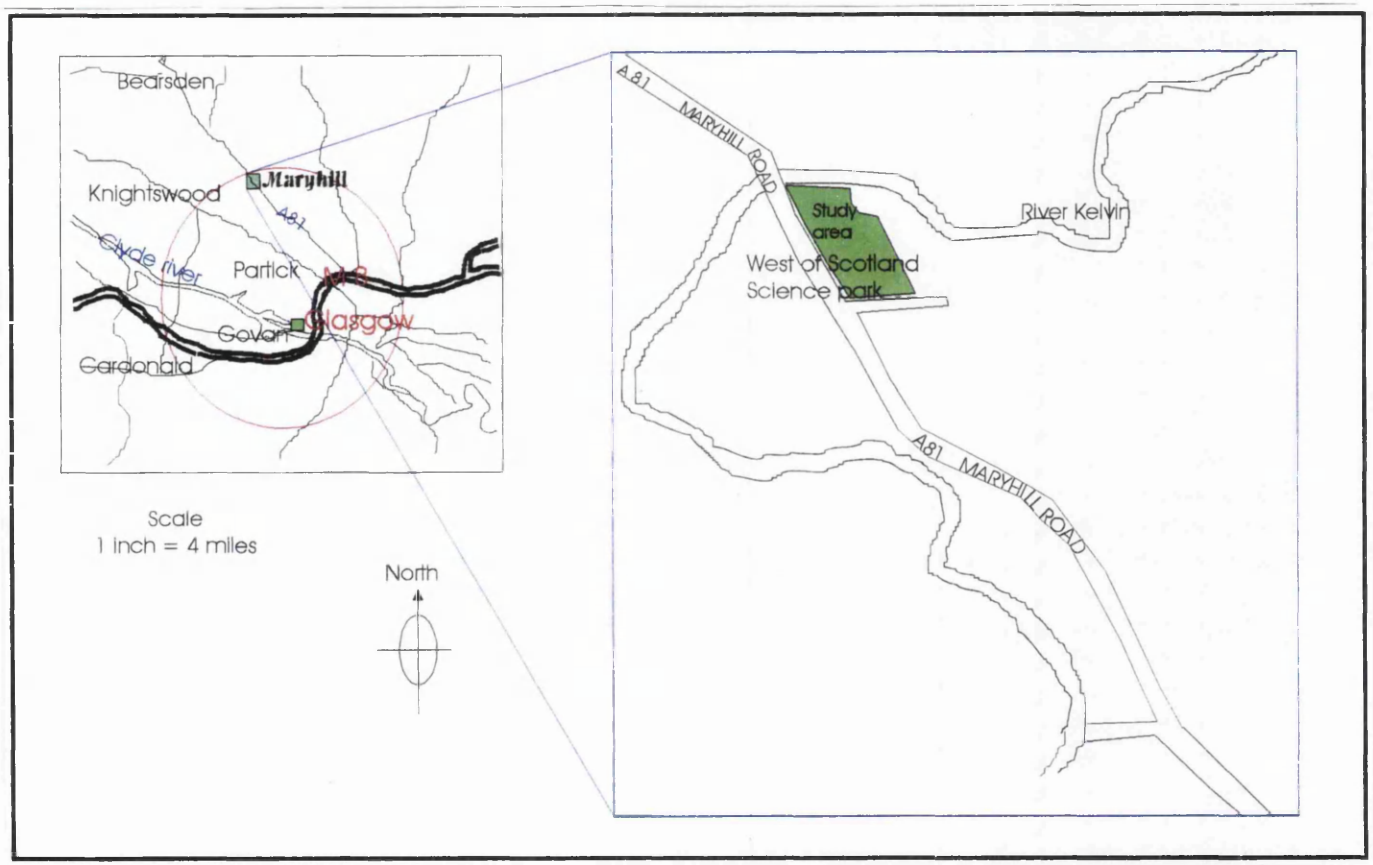

Photo 3.1 Aerial photograph of the site area before the survey. The field is outlined.

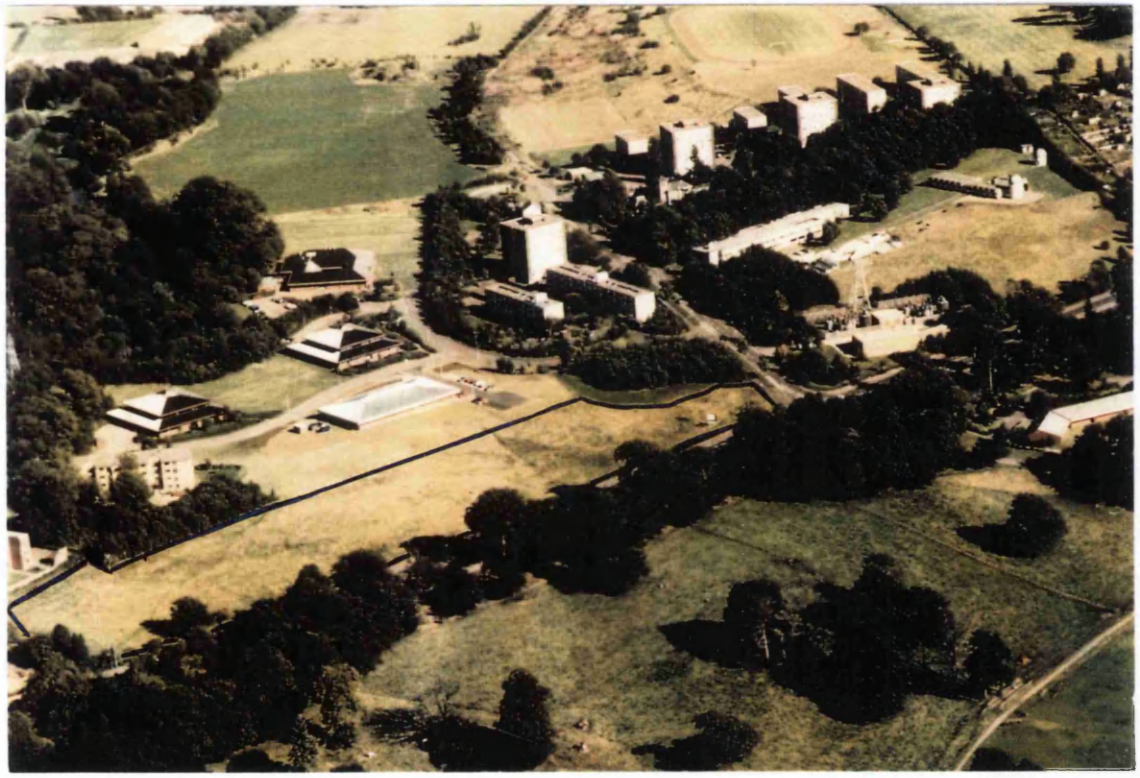

Figure 3.3 Geological map and the cross section of the site and neighbouring area (Geological Survey of Great Britain, sheet 30)

Horizontal scale: 1 inch : 1 mile.

Vertical scale: 1 inch : 0.5 mile.
(twice the horizontal scale)

Stratigraphic column of the sedimentary rocks in the site and nearby area

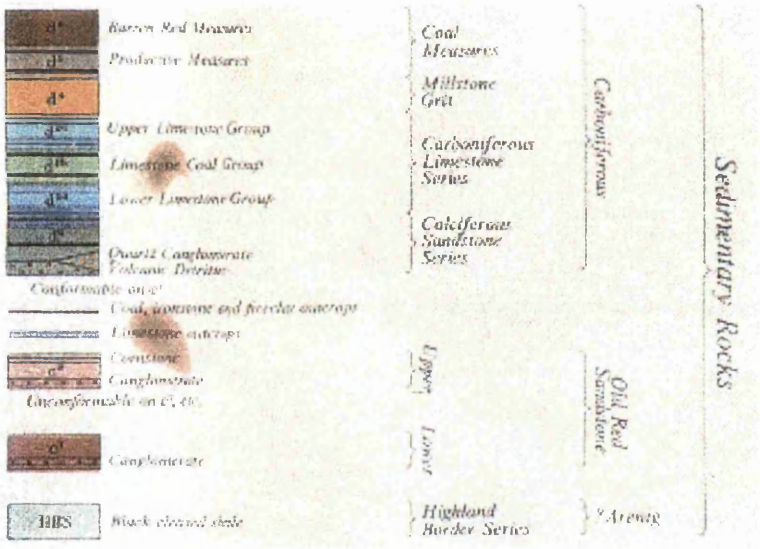

Cross-section of A-B showing northeasterly dips

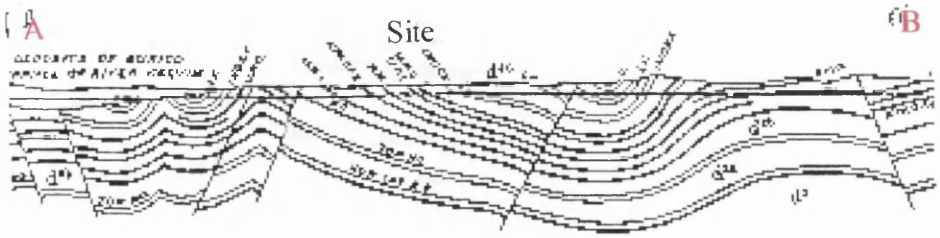

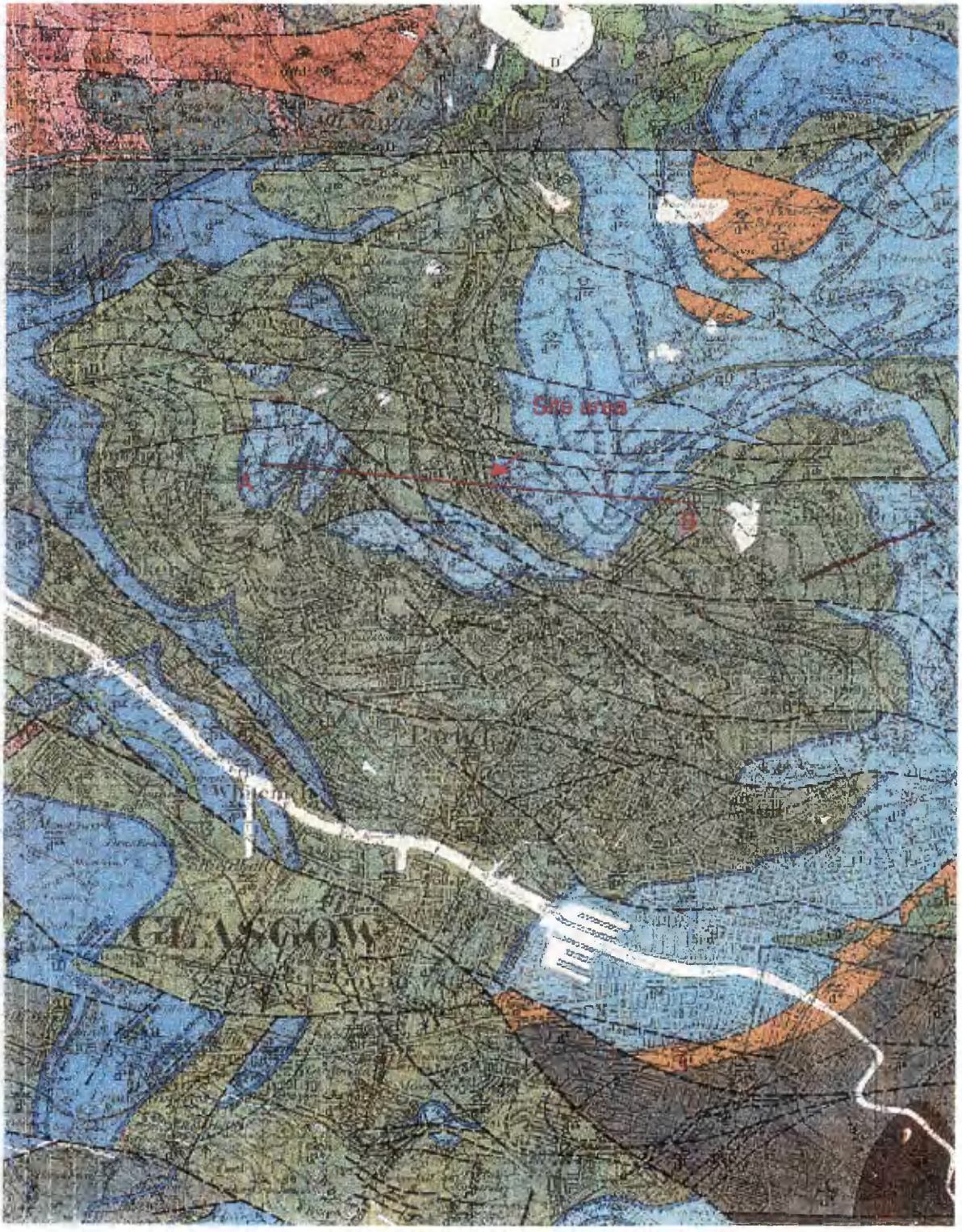
Site area
A
B
GLASGOW

3.4.3 The problem

Many cities in the United Kingdom, especially in the northern England and in the Midland Valley of Scotland, such as Sheffield, Newcastle, Edinburgh and Glasgow are underlain by rocks of Carboniferous age which have been substantially mined not only for coal but also for fireclay, ironstone, clays or even sandstone during the past. These materials were extracted in several fashions depending on the era. In medieval times (15^{th} century), a shaft of about 2 m square was dug down to the coal layer and the coal was extracted radially from the bottom of the shaft until it was difficult to support the hanging roof (Hyde 1987, Waltham 1997). Only then was it abandoned and a new shaft dug nearby. The excavated material from the new working was used to fill old shafts, but normally this fill was not properly compacted. This kind of working was known as a bell pit.

Later, the 'stoop and room' or room and pillar excavating method become popular because more coal can be extracted, and it is safer than the bell pit method. In this method, coal is extracted from the rooms, and pillars are left to support the roof. The extraction of these rocks creates an underground void. Once the area is found uneconomic, the mining stops. After some time has elapsed, the pillars might no longer be able to support the roof, so that the roof collapses into the rooms (Photo 3.2). This may cause a depression or a hole at the surface. Adding additional pressure or weight by building on these areas accelerates the collapse process, which can damage the buildings (Photo 3.3).

For that reason, land over an old mining area, which has old uncollapsed voids at shallow depth is considered unsuitable for redevelopment. However, due to the increasing demand in recent years for city-centre land, either for housing or industrial development, these areas, which were formally regarded as unsuitable, should be reassessed.

Photo 3.2 Exposures of rooms and pillars from an abandoned coal mine.

Photo 3.3 Damage to buildings caused by underground subsidence.

The site used in the present dissertation is situated in a green field with pasture, over an area of an old coalmine within the Garscube Mineral Field. The mine was abandoned in 1897. Figure 3.4 shows a map of the known workings on the site at the time it was abandoned. Associated with the coalmine, three mine shafts – Pit no 7 and Pit no 8, are within the site, while Pit no 5 lies just outside the field. These pits were completely covered by topsoil. The outlines of these pits were only rediscovered in 1981 after extensive trial-and-error drilling. The size of No 7 pit is approximately 3 x 2.5 m^2 (Photo 3.4) and was found after 44 closed spacing boreholes had been drilled (J. W. H. Ross and Co., unpublished report 1981). Pit No 8 (100 m deep) is bigger, at approximately 6.1 x 3 m^2 and was found after 16 boreholes had been drilled (J. W. H. Ross and Co. unpublished report 1981). These two workings were for a deep coal horizon which creates no problems for the foundations of any new buildings. The outlines of No 5 pit were undefined despite the fact that 40 boreholes were sunk at the suspected location (J. W. H. Ross and Co. unpublished report 1981). The boreholes drilled, however, found filled material at approximately 6 and 10 m depth. Compared to the depth of No 8 pit, this working is obviously near to the surface and could give rise to problems to the foundations if any buildings were going to be built.

In this green field, single and double story buildings were planned as an expansion or enlargement of the West of Scotland Science Park. As the subsurface has been mined, the strength of the rocks has also being disturbed. The ability of the rocks beneath the proposed buildings to hold the weight of the proposed buildings needs to be reassessed. The extraction of the coal also creates zones of weakness along the existing sewage tunnels. Assessing the suitability of the site for construction is done by geotechnical engineers as part of the site investigation.

In an area of an abandoned coal mine, the primary aims of the geotechnical investigation are to determine the extraction ratio, the pattern of the layout and the condition of old pillars and rooms. The methods can be either by exploratory drilling, trenching, closed-circuit television or where possible entering old workings, depending on the conditions and depth of the workings (Bell 1979).

Figure 3.4 Plan of the coal mine as abandoned in 1897.

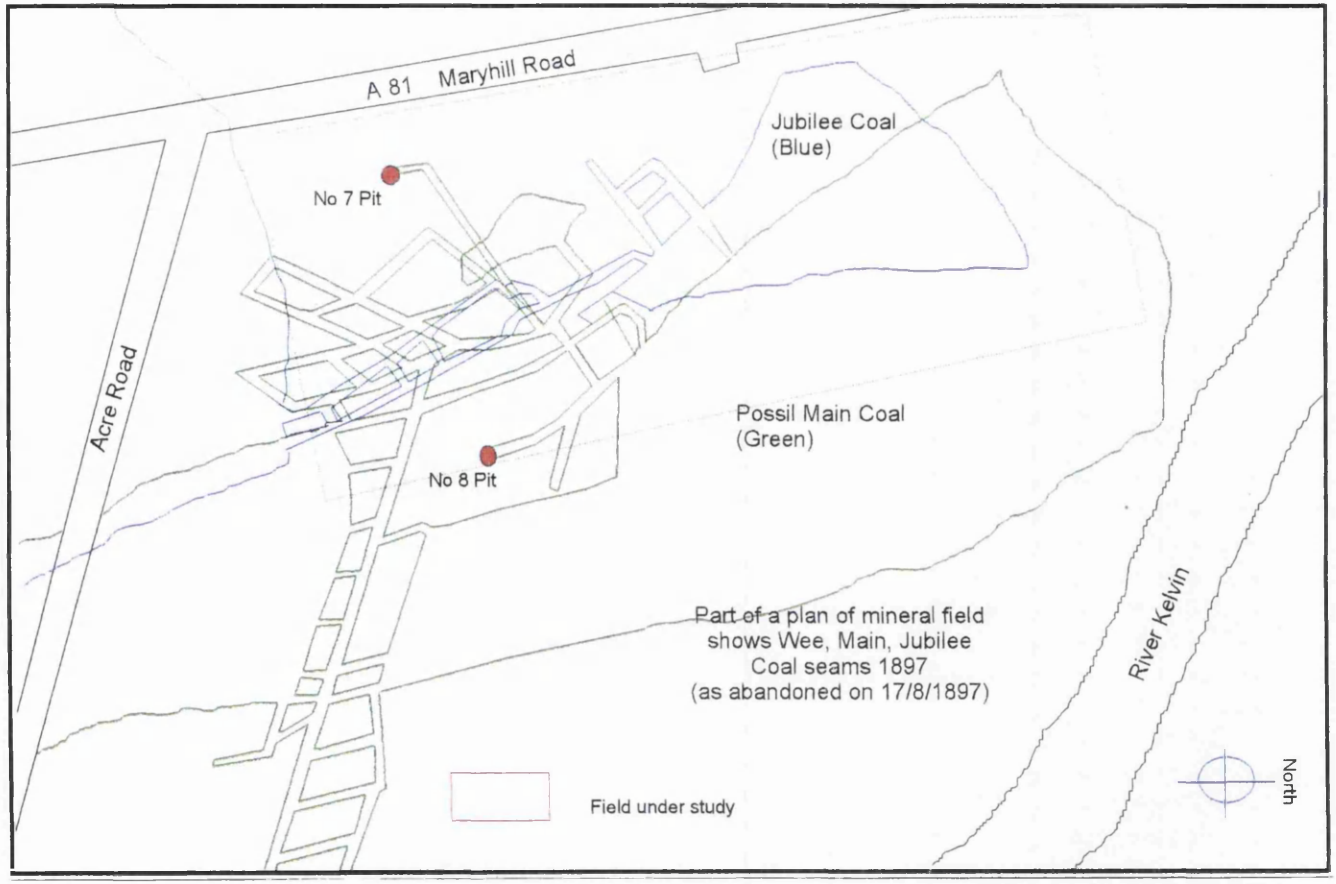

Photo 3.4 No 7 pit, which has been exposed for treatment.

All these methods are already established among geotechnical engineers. For important structures, it requires thorough exploration and sampling of all strata likely to be significantly affected by the structure load. Once the coal working pattern has been recognised, the building can be either moved to a more stable area, or when there is no alternative an appropriate treatment to the subsurface void should be carried out. Normally, the voids are grouted. The amount of grout material used depends on the void volume.

At the present site, the decision had already been made by the consulting engineers to grout the areas which were likely to affect the proposed buildings, prior to this 3-D seismic project being approved.

3.4.4 Suggested solution

As the objective of the geotechnical site investigation is to recognise the pattern of old underground tunnels and other voids, novel methods of accurate subsurface imaging for shallow structures and underground tunnels need to be developed. Ideally the investigating method should be able to picture or image the target with great detail and give a continuous image at minimum cost. The current geotechnical investigating methods such as drilling do not give the continuity needed, and grid drilling is expensive. Entering an old working, on the other hand, is considered to be too dangerous.

One answer to such an engineering site investigation problem is the 3-D seismic reflection method. Although the 2-D reflection method already has been widely used in engineering investigations, it still cannot meet the continuous imaging requirement of the site investigation. Furthermore, the resolution is sometimes poor. The 3-D seismic reflection method on the other hand has long been established in the petroleum industry and proven capable to continuously image the rocks and their structures with great resolution. Few studies have been done to date on how to scale down the advanced oil

industry seismic technologies to suit shallow investigations. The main delay in progressing to 3-D at the site engineering scale has probably been the fact that the processing software and cost are still beyond the capability of engineering companies. 3-D for engineering investigation purposes is considered a new challenge for the shallow subsurface investigator.

3.5 Planning and basemaps

3.5.1 Planning

The success of any work depends on careful planning. The most important factor is financial. Unlike petroleum exploration, shallow investigations (for engineering purposes) are normally provided with very limited funding. This is the main constraint in adopting expensive 3-D survey technologies. Furthermore, the knowledge of the site such as surface material, surface conditions, accessibility, possible noise and problems are also should be taken into account in designing the survey.

After a series of discussions with the Glasgow Development Agency (GDA), the GDA permitted the University of Glasgow to conduct a small-scale shallow 3-D seismic reflection survey over one of their sites. The site, within the West of Scotland Science Park, is part of an area previously classified as unsuitable for development because of the presence of underground voids left over from the old coal-mining work.

The aim of this survey was to find the best methods of adopting the latest full 3-D technologies used widely in petroleum exploration industry to image the shallow underground tunnels of an old coalmine working. The methods developed as a result of this work hopefully can be used to give useful information on the pattern of underground tunnels and their depth at other sites. As part of the agreement, GDA funded the field costs at the site. However, it should be stressed that the results from the

seismic work were not intended to influence the development of this particular site, since a programme of orthodox drilling and grouting was to take place regardless. Rather, the aim was to use the drilling results as a calibration, if possible, for any positive seismic images.

The survey was designed to make it as economical as possible. The costings were designed to allow:

1. A week of on-site topographic survey (refer to Section 4.6.2)
2. 1-2 days of experimental acquisition methods
3. 4-6 days of intensive production mode data acquisition
4. Hiring high resolution recording equipment
5. Paying the field assistants.

Among all these factors, hiring the high-resolution seismic recording equipment was the most expensive.

The fieldwork took place during July 1996. To minimise the cost, only a maximum of eight people were involved, compared to dozens or even hundreds in normal petroleum exploration. They comprised three geophysics academic staff, of whom two were present at anyone time, the author as a postgraduate student, and up to four student field assistants. Besides hiring the recording equipment and paying for the students, other expenses were minimal. Transportation and software for processing (ProMAX/2D & 3D) and interpretation (GMAplus 3D) were already available in the department.

Prior to the actual 3-D survey, preliminary surveys in the form of undergraduate geophysical field training were done to improve our understanding of the site. At the end of the 3-D survey, a conventional 2-D reflection line was also planned for comparison purposes.

3.5.2 Basemaps

Basemaps in the form of paper copies and digital AutoCAD DXF (data exchange format) ASCII files of the site were provided for us by Peter Fraenkel and Partners, Geotechnical Consultants for GDA, using their AutoCAD software. Since it had been decided to make all maps and figures (where possible) using the public domain GMT (Generic Mapping Tools) software, the AutoCAD DXF ASCII generated files were then converted to a suitable format for input to GMT using acad2gmt, a specially written Geophysics Group Fortran program.

The basemaps supplied contained all information relating to the site such as the field and other boundary outlines, main road, neighbouring buildings, and topographic contours (Figure 3.5). However, only the field and main road outlines are relevant to the survey, so for clarity the others were edited out. On the other hand, information on the borehole locations, preliminary refraction survey lines and the outlines of the common depth point subsurface coverage were added into the base map (Figure 3.6).

3.6 Preliminary studies

The objective of the preliminary study is to obtain an idea of the near surface geology and conditions as well as to examine possible noise sources and physical limitations, so that the acquisition of 3-D could be designed to suit all the conditions and limitations.

The preliminary studies consisted of an afternoon site visit to discuss the best time to do the survey as well as to observe and check the accessibility of the site. This was followed by the Honours third year students' geophysical field training week, of which seismic refraction and resistivity surveys were conducted at this site. Besides those surveys, borehole information from mineral and site investigation reports was also studied.

Figure 3.5 Basemap as supplied by Peter Fraenkel and Partners, Geotechnical Consultants for GDA. Contour line is every 0.5 m.

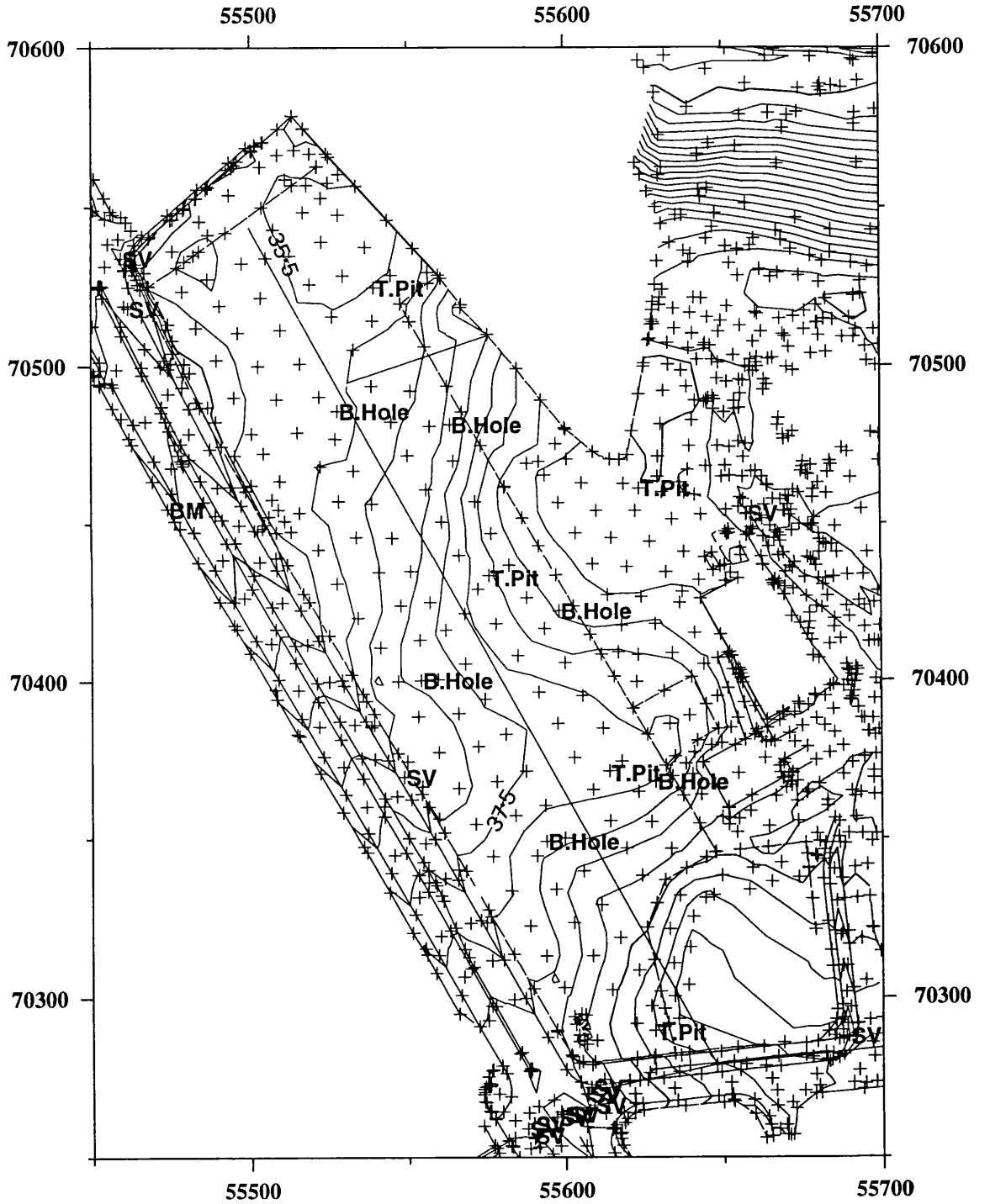

Figure 3.6 Simplified basemap with extra information such as borehole locations and refraction lines added.

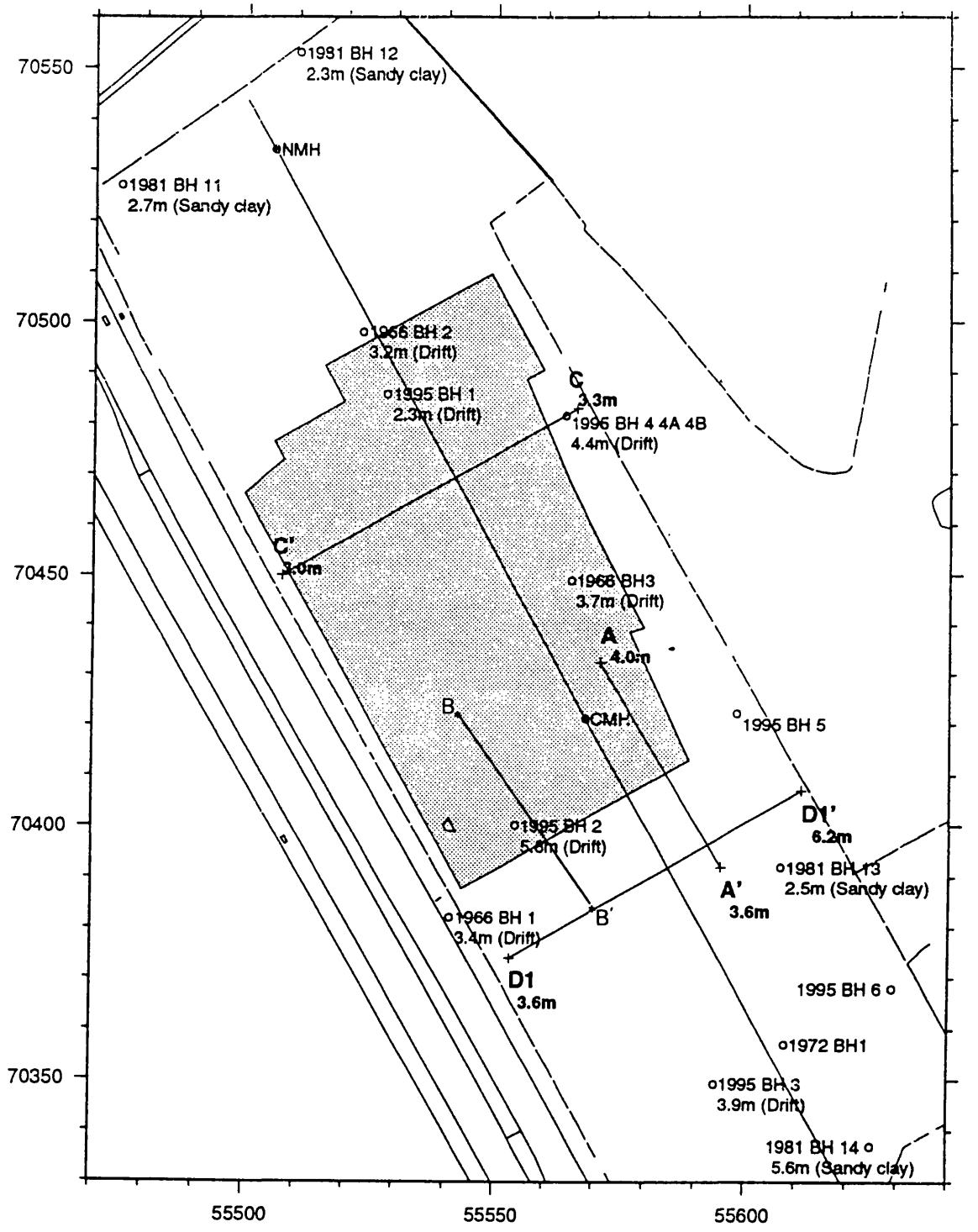

Shaded area is the seismic reflection CMP coverage.
The values (in m) beside boreholes represent the thickness of the overburden.

3.6.1 Preliminary geophysical surveys

Prior to the actual 3-D survey, some of the undergraduate geophysical field training for the 1996-97 Honours Geology class was done at the site. It was supervised by two geophysics lecturers and two postgraduate students including the author. This field training for the students' benefit was also designed so that the author could use the data from this fieldwork to understand the site characteristics and physical limitations in order to design the 3-D survey. The students were divided into four groups and each group spent half of a day on each of two geophysical methods.

Two types of geophysical investigations were conducted - electrical resistivity and seismic refraction. These two investigation methods were chosen as they represent the most common geophysical investigation methods applied in shallow engineering and hydrogeological investigations.

Resistivity

Resistivity is the most common geophysical methods used in shallow investigation works, particularly in engineering and hydrogeological investigations. It is used to study the horizontal and vertical variations in the electrical properties of the earth's subsurface. It works by measuring the potential differences at points at the earth surface that are produced by introducing or directing an artificial current into the ground. The changes in potential difference give information on the subsurface electrical properties.

The movement of the electrical current through the rock is mainly controlled by the content of ions (salinity) in pore waters and pore connectivity. Unlike water, most rock-forming minerals such as silicate are insulators, which means that they do not let current flow. In general terms, resistivity decreases with increasing salinity and connected water filled pore space.

In electrical resistivity investigation practice, two resistivity surveys procedures are routinely done - Vertical Electrical Sounding (VES) or 1-D electrical drilling, and Constant Separation Traversing (CST) or 2-D electrical profiling. Each student group had to conduct at least two VES and one CST. The VES's were conducted using the Wenner electrode configuration where four electrodes, aligned at equal spacing, progressively expanded about a fixed location.

The resistivity values were plotted on log-log graph paper and qualitatively analysed before computer modelling. Figure 3.7 is an example of the resistivity values plotted on the log-log graph, which give an idea of the layers present. The plotted resistivity curve shows a common S or C shape. In the example shown there are at least three different layers. The first layer has a considerably higher resistivity and corresponds to the near surface material, which was dry at the time of the survey. The second layer has a lower resistivity, which implies that this layer is porous and contains lots of connected water. This layer may correspond to the saturated overburden or glacial till. The deeper high resistivity layers on the other hand can be assumed to correspond to the Carboniferous rocks, which are more compacted and therefore with less pore space. Based on the rough idea of the layers present and their resistivities, the estimated depth or thickness of each layer was calculated. The summary of the bedrock depth from the undergraduate studies is given in Table 3.1.

Table 3.1 Summary of the thickness of top two layers from resistivity data.

Thickness (m)	Group A	Group B	Group C	Group D
Top layer	0.5	1	0.9	0.9
Second layer (Glacial till?)	4.5	2.3	2.3	2
Third layer	16	-	4.9	-
Bedrock depth (m)	5	3	3.2	2.9

Figure 3.7 Example of resistivity curve (Wenner array) plotted on log-log graph.

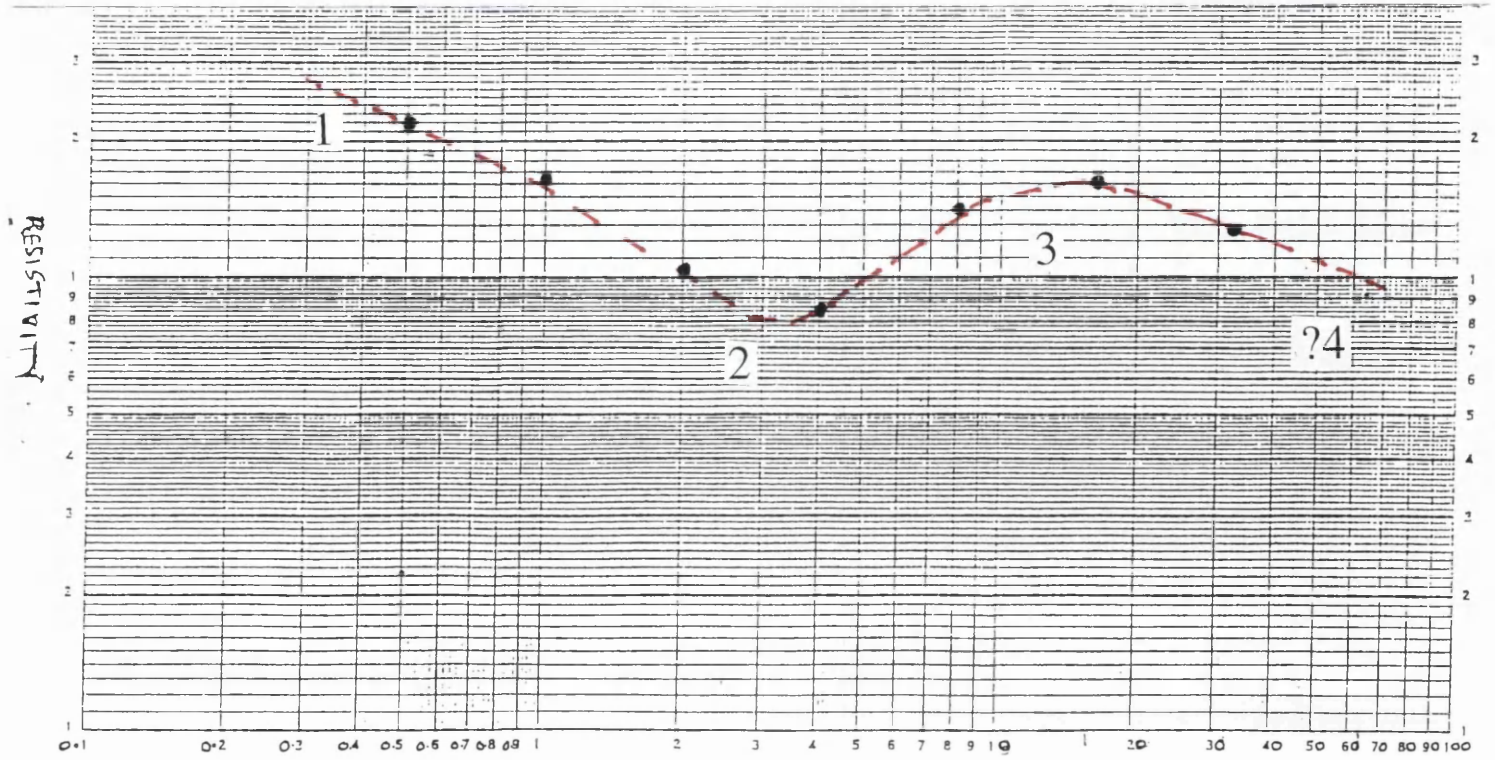

This S-shape curve indicates four layers 1-4 as shown.

Seismic refraction

As with electrical resistivity, the seismic refraction surveying method is another common geophysical tool used in investigating shallow subsurface targets, especially for estimating the depth of the bedrock for engineering works. Besides that, the information gathered from this survey can also be used to assess the rock strength and potential fluid content (Reynolds 1997).

The refraction data were recorded using a 24 channel OYO McSeis 1600 seismograph. Most of the lines surveyed were oriented in the dip direction except line A-A' (Group A) where it was oriented in the strike direction (Figure 3.6). The geophones were arranged on a 46 m line at a 2 m interval while the shots were placed at 2 and 5 m offset from each end and also at the midpoint. Time-distance plots were produced to get the velocity and thickness of the layers at every shot point. A summary of the thicknesses obtained from the refraction survey is listed in Table 3.2.

Table 3.2 Velocity and thickness of the layers from refraction survey.

	Group A	Group B	Group C	Group D
Layer 1 – Velocity ($m\ s^{-1}$)	455	425	385	370
- Thickness (m)	4.5	2.7-3.7	1.87	2.36
Layer 2 – Velocity ($m\ s^{-1}$)	2235	2370	1571	2000
- Thickness (m)	-	-	9.38	-
Layer 3 – Velocity ($m\ s^{-1}$)	-		2647	-
- Thickness (m)			-	

Three of the groups found a two-layer earth except for Group C, where a three-layer earth was recognised. If the two-layer earth is assumed (glacial till overlain by Carboniferous bedrock), the velocity for layer 1 is too low for glacial till, but on the other hand the velocity for the second layer could correspond to shallow weathered Carboniferous rock. Group C's model is somewhat more sophisticated, where the first, second and third layers correlate to the topsoil, glacial till and Carboniferous rock respectively. These results have not been re-interpreted by the author.

3.6.2 Borehole studies

Borehole exploration has long been established as an integral part of any shallow subsurface investigation. Depending on the investigation purposes and cost, the drilling methods can range from cheap and simple auger boring to expensive rock core drilling. It is normally done prior to the engineering construction to examine the subsurface geology and other related issues. The information from the drilling programme is recorded on borehole logs, which record (as tabulated text) the depth, rock types and any special remarks. Samples from rock core drilling can be used to examine the rock quality, minerals present and also the shallow structure such as faults. The advantage of borehole study is that it is a direct investigation method, however the investigation is limited to the immediate vicinity of the hole. Furthermore, subsurface correlation usually cannot reliably be done by borehole since it needs continuous sampling of the borehole, which is expensive.

Drilling on the site had been undertaken since 1966, when three boreholes were sunk in order to investigate the unrecorded mine workings. In 1981 another drilling programme was carried out. The aim was to investigate the mineral (i.e. coal seam) location under the site and adjacent area. The latest drilling programme was conducted in 1995 with the main purpose of providing information on the ground conditions at the site relative to the proposed development. All three drilling programmes are discussed individually as their objectives were different.

The 1966 drilling programme

The 1966 drilling programme was conducted by the Institute of Geological Sciences, Edinburgh and supplied to Glasgow University by Peter Fraenkel and Partners. Three rotary drilling logs - 1966-1, 1966-2 and 1966-3 - were studied. The quality of the borehole logs were so poor that it was difficult to correlate one with another; however

they clearly indicate the bedrock at approximately 3 m depth, and the presence of coal seams at various depths.

The 1981 drilling programme

The 1981 drilling programme was conducted by J. W. H. Ross and Co. as instructed by the GDA. The main purpose of this drilling was to investigate mineral locations under the site and adjacent area. Twenty-nine boreholes were drilled, of which six were drilled within the site. These six boreholes were drilled using the rotary core drilling method where continuous samples were collected and the minerals were analysed for nomenclature and correlation (explained below in Chapter 4). However, due to the lack of borehole information, the nomenclature and correlation of the minerals in all the boreholes drilled in the site might not be correct (J. W. H. Ross and Co. unpublished report 1981).

The borehole information shows that the bedrock belongs to the Carboniferous Limestone Series of Lower Carboniferous age, dipping 9° to 18° toward the NE. The depth of the bedrock, however, varies from approximately 2.3 m to more than 8 m as tabulated in table 3.3.

Table 3.3 Approximate depth of the bedrock in the site based on 1981 drilling.

Borehole Number	Approximate Depth (m)
1981-11	2.7
1981-12	2.3
1981-13	2.5
1981-14	5.6
1981-15	5.1
1981-16	8.5

A more complete analysis of the borehole information is carried out in Chapter 4 in the context of the surface tomography results. The summarised result of the 1981 drilling

programme is shown in Figure 3.8, where the meroon (red) hatched area is unsuitable for development, while the green hatched area is deemed suitable for single storey buildings.

The 1995 drilling programme

The 1995 drilling programme was carried out by Nicholson (Site Investigation) Limited on behalf of Peter Fraenkel and Partners. The aim of this drilling was to provide information on the ground conditions in relation to development of the site. Like the 1981 drilling programme, this programme also evaluated the nearby area. Six out of nineteen borehole sunk were drilled within the site, however only first five were available. Borehole 1995-6 was not supplied. The boring was conducted using the cable percussion method, which is a poor method of sampling rocks. The percussion boring often destroys the parent structure, resulting in a mix-up in identification of the bedrock materials (parent rock), and boulder material is often mixed up (Nicholson Limited unpublished report 1995).

The five borehole logs studied show that drilling was stopped after encountering bedrock or obstruction. Because of that, the use of this borehole information is limited to the estimation of the depth of the bedrock only (Table 3.4).

Table 3.4 Bedrock depth from 1995 drilling programme.

Borehole Number	Approximate Depth (m)
1995-1	2.3
1995-2	5.8
1995-3	3.9
1995-4	Not reached
1995-5	4.1

Figure 3.8 Summary of the 1981 mineral investigation programme (after J.W.H Ross and Co. unpublished report 1981).

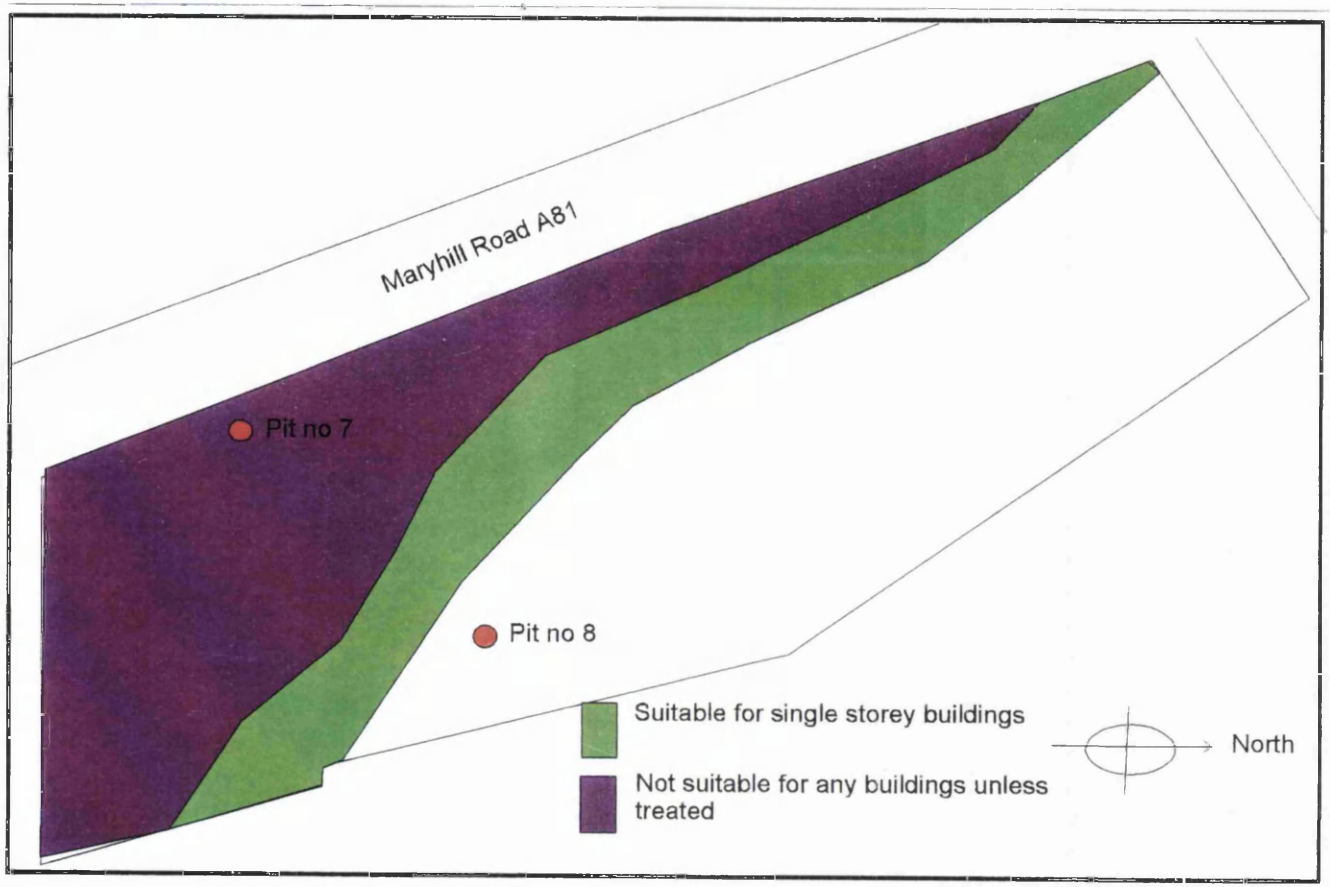

3.7 Topographic survey

Knowledge of the precise location of sources and receivers is very important in all seismic exploration. For a land seismic investigation, positioning is often carried out with the Global Positioning System (GPS) or by a theodolite survey, or by a combination of both GPS and theodolite depending on the area of coverage. GPS readings give the coordinates with respect to the satellite coordinate system, and have to be transformed into local coordinates (Sheriff and Geldart 1995). The accuracy achieved depends on the type of codes (P or C/A-code) observed and the level of SA (selective ability), and it ranges from several tens of meters to tens of centimetres (Leick 1992, Dana 1998).

For a small scale high resolution survey, the accuracy need to be much better than this, which can be achieved by using theodolite surveying. A theodolite system can be used to calculate the distance and bearing as well as the relative height between the station and specific locations. The theodolite positioning technique offers a precision up to 0.06 m with an additional uncertainty of 0.01 m per kilometre of line length (Heliker *et el.* 1986).

3.7.1 Equipment

An Electronic Distance Measurement (EDM) theodolite was borrowed from the Glasgow University Archaeological Research Division (GUARD). It was a Sokkia 5-G-D20816 set (serial no 116057). It consists of three parts, the tripod, EDM theodolite and reflection prism.

EDM theodolite is widely used today as it is easy to operate, is fully automatic and gives a very accurate reading. The precision error depends on the model used. Sokkia set5 (the model used) has an angular accuracy (horizontal / vertical) of 5 second. For measuring distance, it provides very accurate readings with ± (5 + 5ppm x D) mm

accuracy, where D is the measuring distance. In EDM theodolite surveying, a laser beam is aimed at the reflection prism and the time taken for the beam or pulse to travel from theodolite to the prism and be reflected back to the theodolite is calculated to give the distance as well as the horizontal and vertical angles. The vertical angle can be used to calculate relative height between the station (theodolite position) and the prism location.

3.7.2 Surveying strategy and aims

The Autocad DXF file (supplied by Peter Fraenkel and Partners) containing the outline of the site was used to guide the theodolite surveying work. As the site is elongated parallel to the Maryhill Road, a 2 by 2 m grid was plotted to cover the site with the Y axis or column parallel to the baseline which also parallel to the main road. The site was covered by 34 columns and 140 rows (Figure 3.9). The location of the grid points were denoted by a five digit notation, where the first three digits represent the row number and the other two represent the column number. This map is known as a prearranged layout, and forms the basis of the acquisition pattern design. Using a specially written Fortran program, the range and bearing (azimuth) of all the grid positions with respect to certain known points are calculated.

The aim of this theodolite survey was to mark the actual location on field with a peg, as defined in the prearranged layout, so that the geophones and sources can be positioned, and at the same time to calculate the elevation differences between the grid point location and the fixed (control) point. To save time, only 8 m by 8 m grids were sighted using the theodolite and then interpolated to a 4 m by 4 m grid using measuring tape. All the positions, whether sighted using theodolite or by tape, were marked by sticking specially constructed peg into the ground. The pegs were constructed of softwood, 250x5x10 mm^3 in size and numbered uniquely on a white background using the five-digit notation.

Figure 3.9 Prearranged layout map for a grid of survey pegs at 2 m spacing.

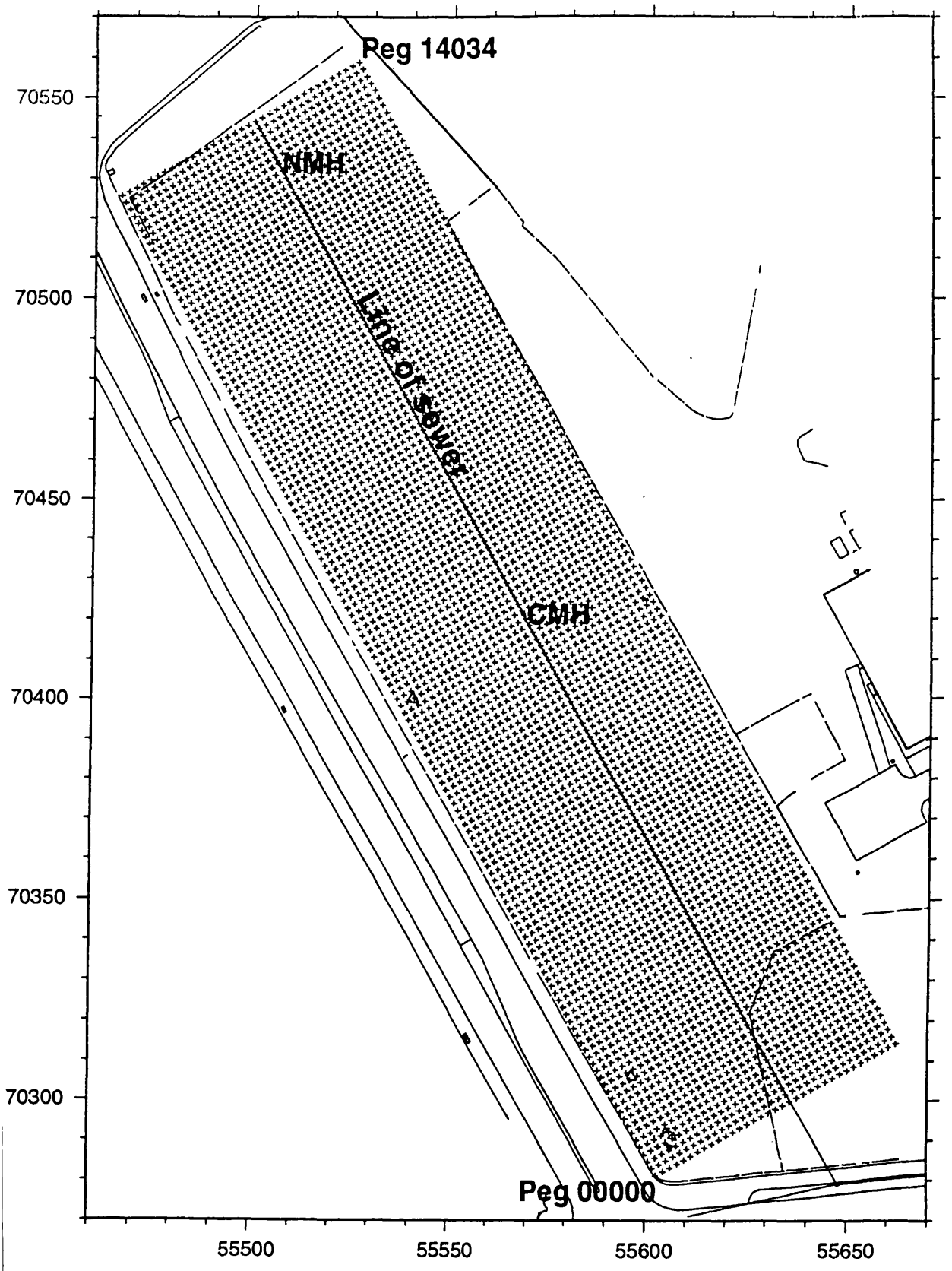

3.7.3 Controls

The digital base maps supplied by Peter Fraenkel and Partners define the position of two manhole covers in the site, one in the middle and the other one at the north end of the field. The central manhole is noted by CMH while the north end one is denoted by NMH. These two manholes were the control points and all the distances and azimuths for theodolite survey were calculated with respect to either these two points. The line connecting these two points is taken as the baseline, used to align the azimuth of the theodolite. The elevation and the national grid (easting and northing) of these two points is recorded in Table 3.5.

Table 3.5 Survey control points.

Station	Easting (m)	Northing (m)	Height (m above OD)
CMH	55568.08	70421.31	37.80
NMH	55505.12	70534.07	35.51

3.7.4 Conversion from column, row to National Grid

As rows and columns were aligned with respect to the baseline (an arbitrary line connecting CMH and NMH) the column and row coordinates need to be converted into National Grid coordinates (easting and northing). The conversion process was done in two phases where firstly they are rotated into an arbitrary grid and then secondly shifted to true National Grid coordinates.

The rotation was being done by taking the 00000 position as the rotational axis and rotating the column/row coordinates clockwise by 29°.645. The rotated coordinates were then shifted to their true coordinates by adding the actual Easting and Northing coordinate of the 00000 position.

3.7.5 Precision and errors

Setting out the pegs, based on the pre-arrangement layout by walking the prism to the correct range and bearing, following instructions from the surveyor at the theodolite, resulted in field accuracy of better than 0.1 m. This is within the precision required of the high-resolution seismic reflection method, in which errors of the order of 0.1 m in horizontal and vertical coordinate are acceptable. The accuracy of the peg positioning can be observed by checking the line-up of pegs along rows and columns. Vertical errors were checked at the processing stage by re-gridding and contouring the data, to see any anomalous peg positions stand out, as well as comparing the height with the gridded topographic elevation supplied by Peter Fraenkel and Partners.

Comparing the calculated CMH and NMH eastings and northings with the values supplied give zero error, which means the calculated coordinates are correct. Eastings and northings were calculated to a precision of 0.01 m.

3.7.6 Problems

The main problem in the theodolite survey was that sometimes the pegs disappeared. The reasons were either that they had been removed especially in the area where the topsoil was stripped for drilling injection boreholes, or they were run over by vehicles. The missing pegs were normally replaced by using tape measuring from the neighbouring pegs, however in case of pegs removed for topsoil stripping, new pegs were replaced by re-sighting the position using theodolite.

3.8 3-D survey design

A good survey design is a design of which achieves the investigation goal and at the same time minimises the cost and time of acquisition and processing. Designing the 3-D

survey varies depending on survey objective, cost and time. In the late 1970's, 3-D surveys were shot using a three-line swath (Figure 3.10). A 3-D three-line swath is actually an expansion of the ordinary 2-D line survey, where the centre line is an in-line spread while the other lines are simply off-line spreads. The data were processed using the same concepts as for 2-D data. All the traces with the same CMP number were grouped and NMO-corrected before stack. The NMO for off-centre lines needed an azimuthal factor and proved a little more difficult than anticipated (Stone 1994).

Figure 3.10 3-D three-line swath (after Stone 1994).

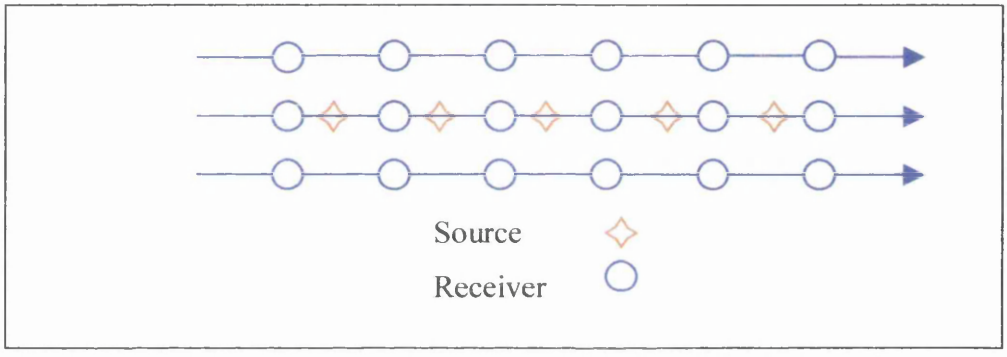

Today, 3-D surveys are often designed so that the source and receiver lines are arranged perpendicular to each other. The CMP concepts were replaced by the binning concept, as developed for crooked-line 2-D CMP gathering. The bin is a small area, normally rectangular, into which the 3-D data are sorted. For each bin, the fold, offset and azimuthal distribution is important although the exact position of each CMP within it is (by definition) unimportant.

Some of current 3-D land design methods are parallel, cross-spread and perimeter techniques. Dickinson *et al.* (1990) compared these techniques and concludes that the results from the first two techniques differ little. The perimeter survey method is not as good as other two due to low fold, on the other hand it is cheaper. Other methods such as swath, full 3-D and loop were explained in detail by Stone (1994).

In a swath survey the receiver array is much greater in length in one direction than in the other and the source moves through them orthogonally (Figure 3.11). The source-receiver azimuths are almost unidirectional. The limited range of azimuths make this design unsuitable for exploring complex targets. This design is recommended for survey that are large but have relatively simple structure in one direction (Stone 1994).

Figure 3.11 Basic swath design for 3-D.

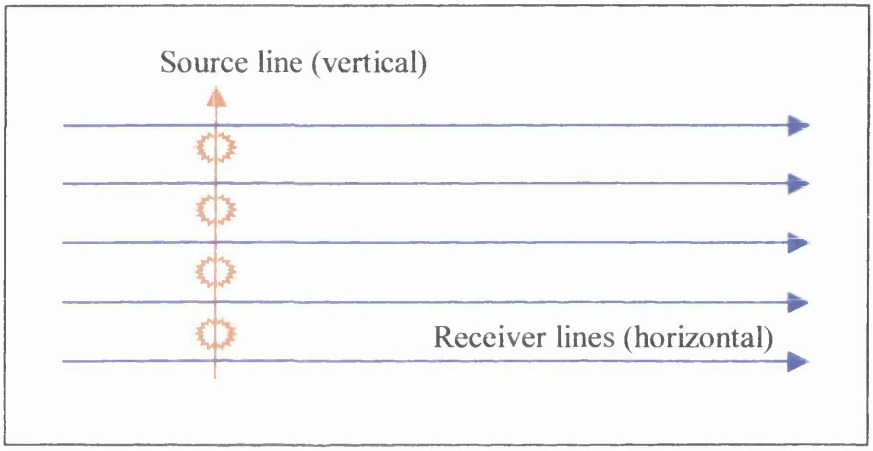

To investigate a more complex target, the survey must be designed so that a full-range of azimuths can be obtained in each bin. This can be achieved by a full 3-D survey design. A full 3-D survey can be designed by arranging the receivers in a rectangular grid and for each receiver position the shot is placed adjacently. This kind of design will produce a full 360° range of azimuths within most of the bins.

A simple full 3-D design survey (Figure 3.12) in which a rectangular fixed receiver pattern covers the survey area is relatively easy and cheap to conduct. However if the survey requires moving the receiver pattern to cover the whole area, it becomes rather expensive, as lots of time is needed to move the cables and geophones. Traditionally, moving the receiver pattern in a full 3-D seismic survey is done by moving one or two grid units to either the right, left, up or down after a line of shots has been observed (Figure 3.13). This kind of survey requires lots of equipment to be laid beforehand. In addition, telemetry type receivers must be used to enable efficient switching.

Figure 3.12 Example of simple fixed receiver pattern full 3-D survey.

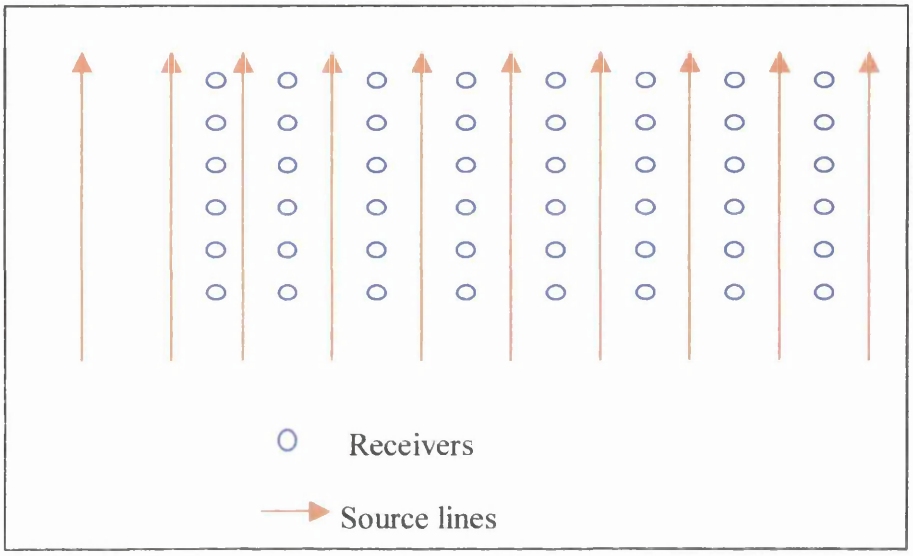

Figure 3.13 Traditional moving receiver full 3-D survey.

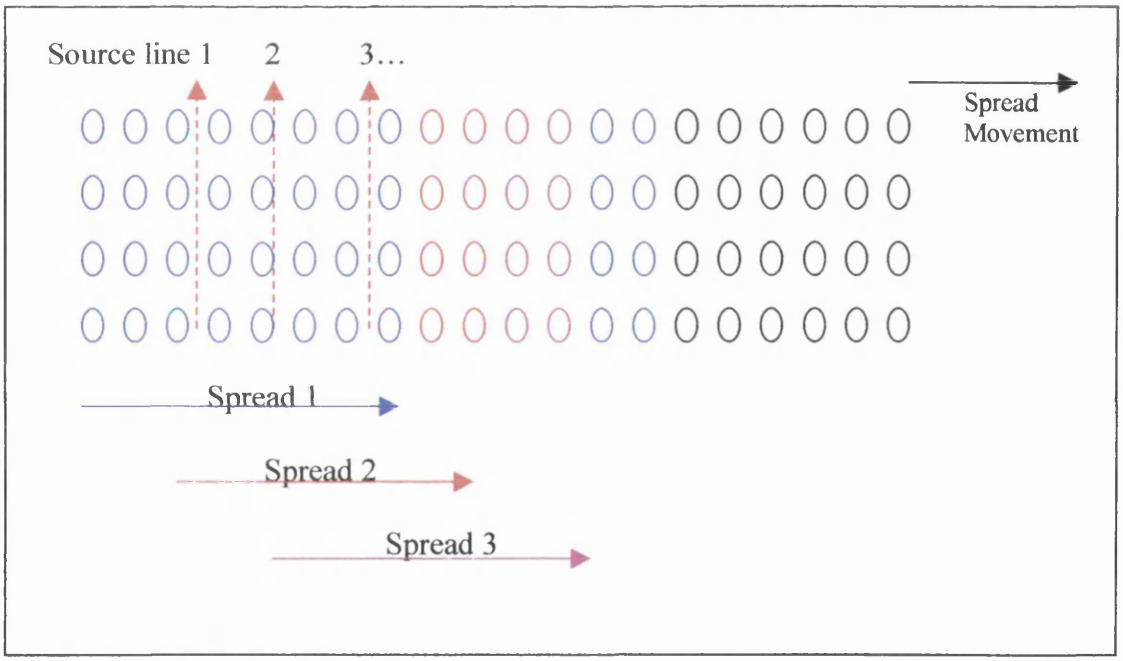

In highly cultivated and populated areas where a normal 3-D survey such as a swath or full surveying technique is difficult to design (due to obstructions), Bertelli *et al.* (1993) introduced a new kind of survey which could overcome the coverage restriction while at the same time increasing the spread efficiency as well as improving the field operations flexibility. This new technique is known as the 'random' technique.

This technique is based on the assumption that in order to achieve the desired 3-D coverage of an area it is sufficient to subdivide the surface into basic elements, and put into each of them the average number of sources and receivers positions that provide the desired coverage (Bertelli *et al.* 1993). In the random survey, the basic recording block, according to the number of seismic channels available, includes a number of the elementary areas.

3.8.1 3-D field layout

In order to achieve the desired 3-D coverage of the area as well as achieving the full source-receiver azimuth range, a combination of full and random 3-D survey methods was deployed. Basically, the receivers and sources were arranged and moved in or along a grid pattern similar to the full 3-D survey, however instead of moving the whole spread after each shot line is completed, the recording block is divided into three elementary areas (groups) as in the random 3-D survey design so that only parts of it are moved. The full 3-D survey will ensure a full range of source-receiver azimuths, while the random 3-D survey will ensure that most of the survey area will be covered with a desirable fold, which is important in the binning process.

Using 144 channel recording equipment, the receivers were divided into three groups of 48 receivers each. This division is constrained by the input cabling to the recording instrument. The receivers in each group were arranged in 6 rows and 8 columns or 8 rows and 6 columns. In geophysical terms, this group is known as a spread. Each spread was connected to the recording instrument by a separate set of cabling. Three spreads

were placed next to each other to form a rectangular layout of 18 rows and 8 columns or 8 rows and 18 columns. This rectangular receiver layout is known as the swath (Figure 3.14). Each row and column has a 2 m interval. Figure 3.15 shows the layout of all the spreads employed in the 3-D survey.

The sources were arranged in a variable pattern over each swath. Figure 3.16 shows an example of the area of shot coverage for two of the swaths. After all shots for the pattern were fired, one or two spreads were moved instead of the entire swath. This strategy was employed as it maximises acquisition efficiency.

Spreads and swaths were defined over the whole area of interest (Figure 3.15). Ideally the swath geometry (consisting of three adjacent spreads) should have a rectangular shape, however in some cases due to unavoidable obstructions such as drilling rigs, the geometry of the swath was set in a L or even a T shape (Figure 3.16). The spreads are labelled in alphabetical order. Although there is no overlap of receiver spreads, many shot positions were observed or shot several times (Figure 3.17). This is a more efficient method than a geometry in which each shot position is observed only once, but in which many more movements of the receiver spreads would than have to be made.

3.9 Acquisition

3.9.1 Instrumentation

OYO DAS-1 recording system

The data were recorded using an OYO 144 channel DAS-1 system. It is a multi-purpose high performance seismic acquisition system designed for engineering, environmental and hydrocarbon exploration. It can be used for all seismic investigation such as P- and S-wave reflection and refraction, VSP, and crosshole tomography.

Figure 3.14 An example of three spreads (CDE) making one swath.

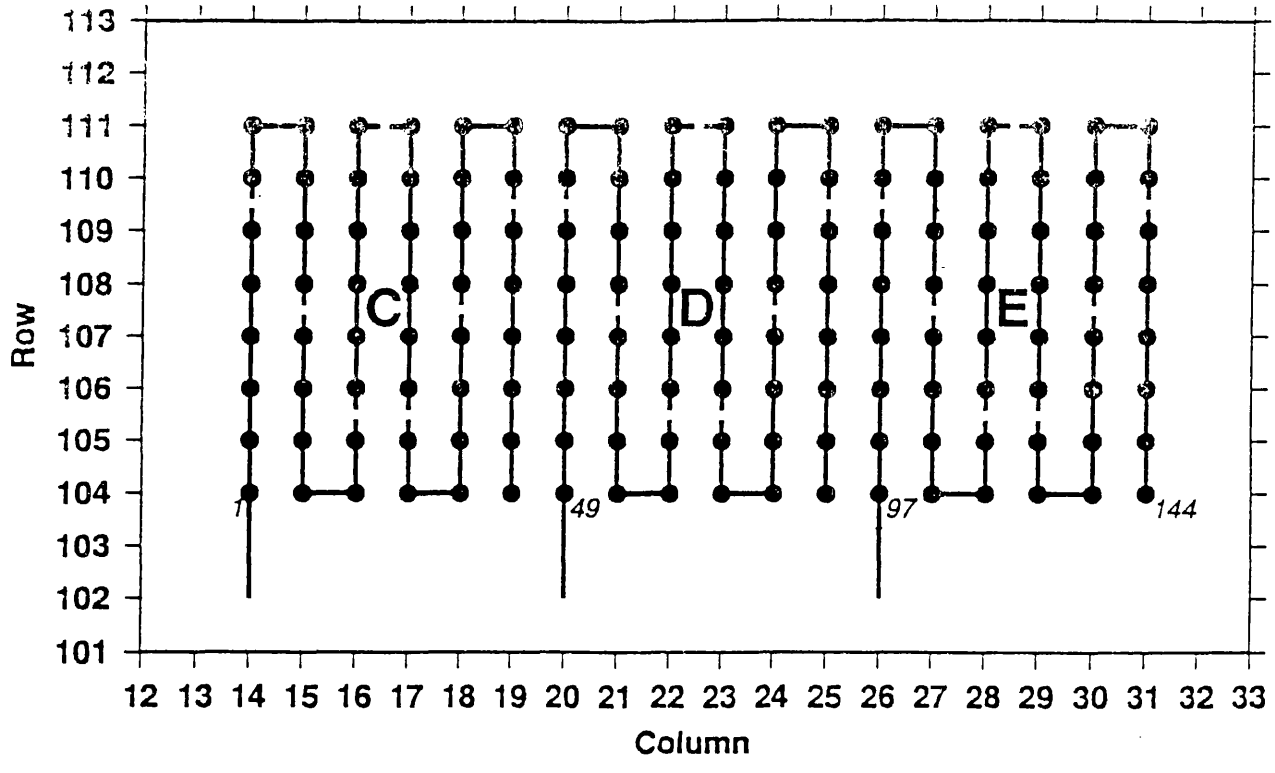

Each spread comprises 48 channels labelled with a letter. The three cables are connected at channels 1, 49,97. The rectangular layout of 3 such spreads is the swath of 144 channels. Receiver spacing is 2 m.

Figure 3.15 Layout of all spreads.

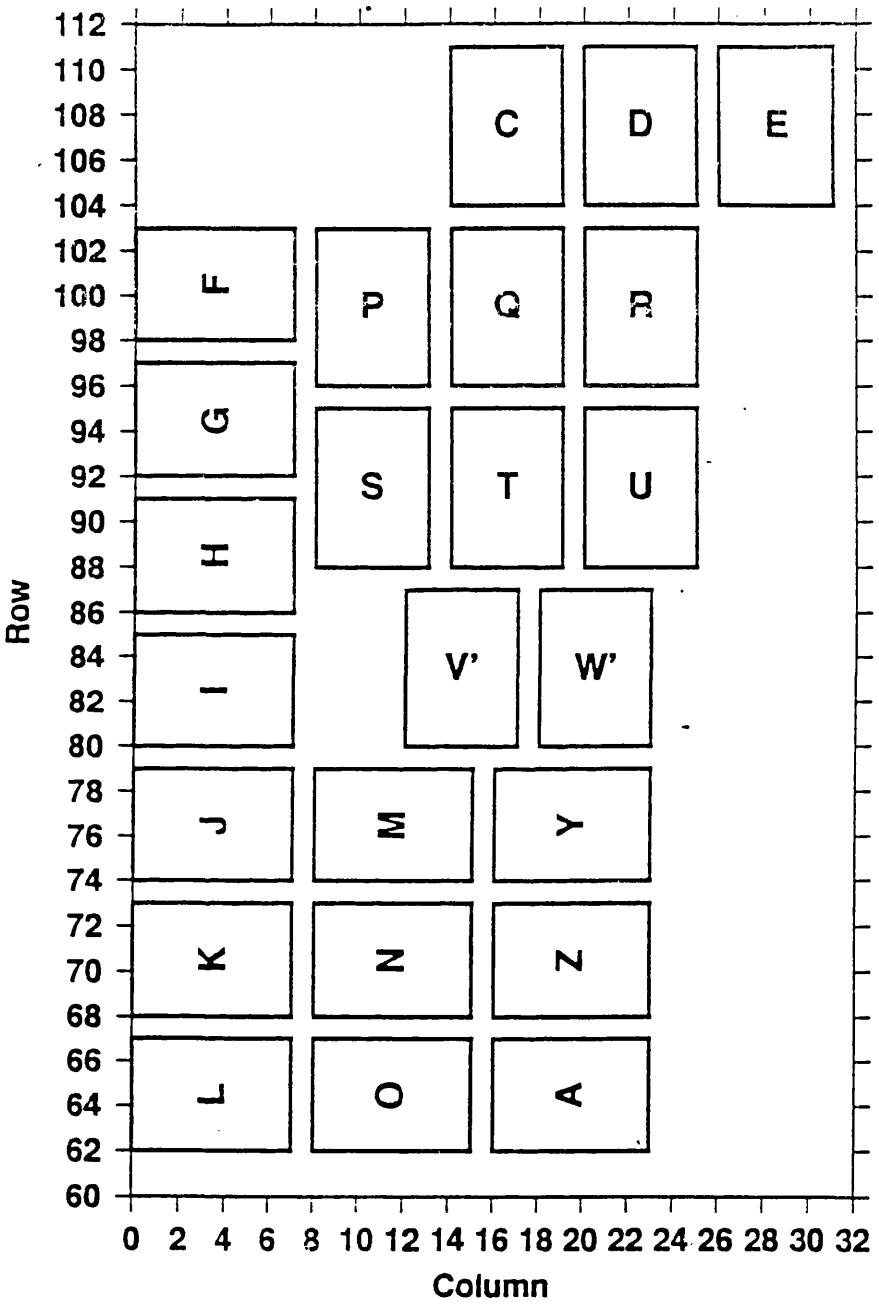

Spreads of 48 channels are labelled A, C-W, Y, Z. Spreads V and W were moved right from their original positions to V' and W' respectively due to an unavoidable obstruction

Figure 3.16 Layout of patterns CDE and V'W'Y – a detailed example.

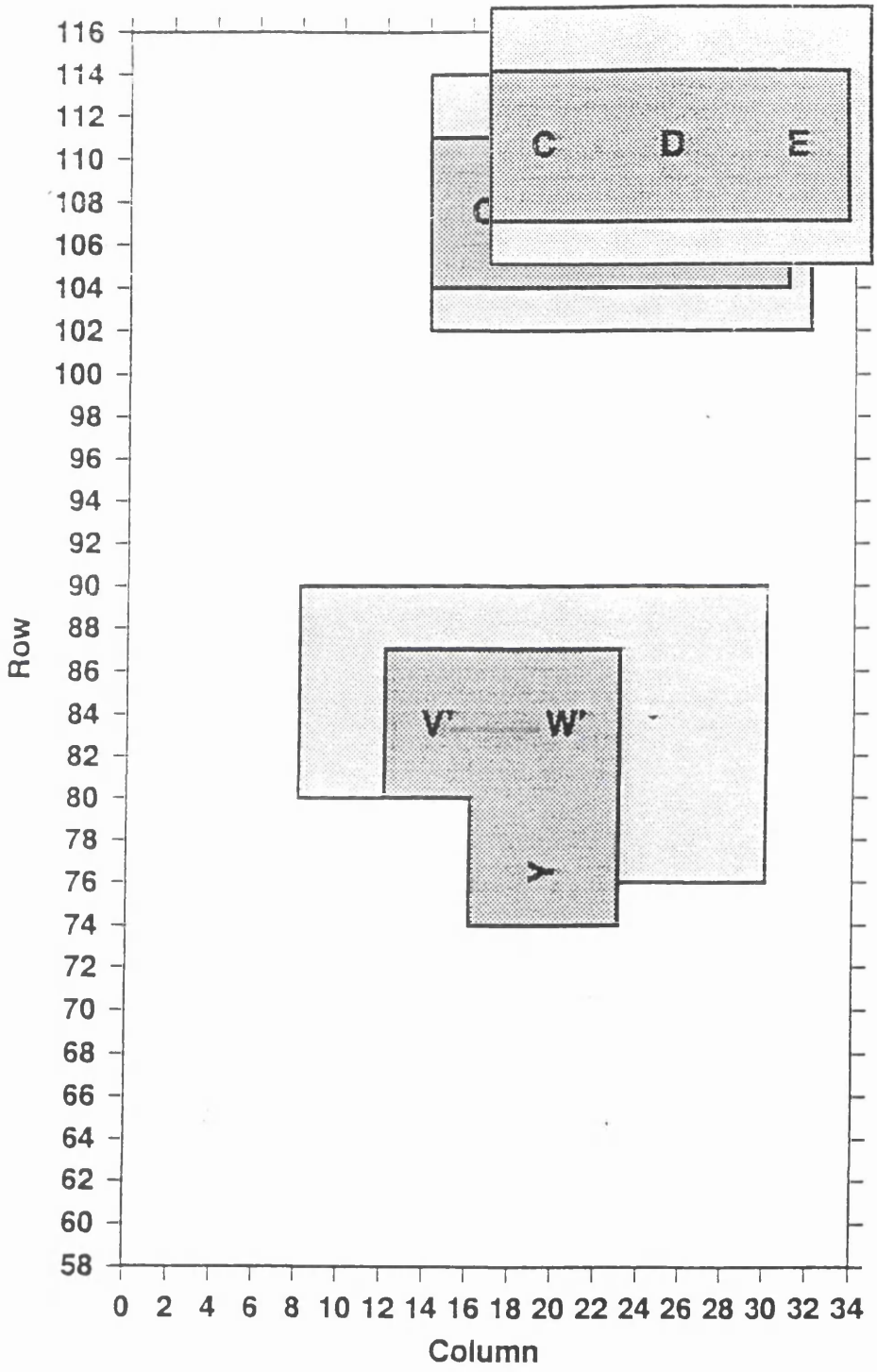

Dark shading indicates swath receiver area while lighter shading indicates area of the shots into the swath

Figure 3.17 Layout of all patterns.

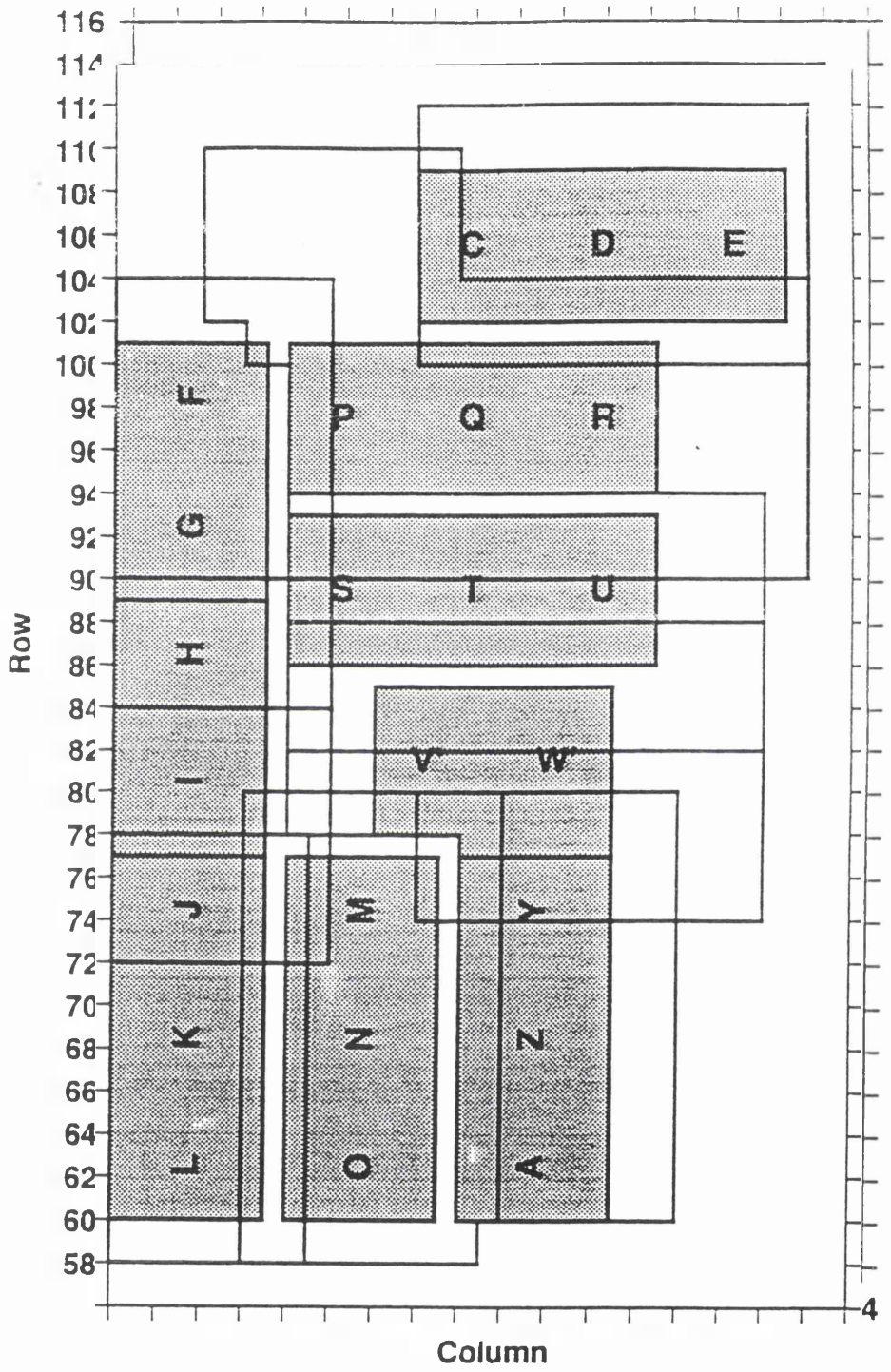

Dark shading with alphabet represent the receiver swaths while the outlines represent the area of the shots into the swaths. Note that the area of shots overlap each other to obtain a good fold of coverage even at the edge of the swath.

The DAS-1 uses 24 bit Sigma Delta Technology, which increases the system dynamic range by 18 dB and the instantaneous dynamic range by 24 dB, to give superior digital recording resolution according to its manufacturers OYO.

Sources

Three types of sources were tested in order to find the best source to be deployed on the site. These were a portable mini vibroseis, a 7 kg sledgehammer and 7.26 kg weight drop.

The vibroseis was supplied by OYO as part of the recording system equipment. The Oyo minivibrator is a compact portable electromagnetic device weighing about 75 kg. It has a cylindrical shape, and is approximately 40 cm diameter and 60 cm in height (Photo 3.5). Two people are needed to move it around and for that it is fitted with handles. The vibrator is connected to its power source and the DAS-1 by a 100 m long armoured umbilical cable.

Beside the vibroseis source, more common shallow seismic sources (7 kg sledgehammer and 7.26 kg weight drop) were also tested. Both of these strike a steel plate of 40 cm in diameter, 2.5 cm thick and weighing about 20 kg. The weight drop was dropped manually by field assistance from 1.75 m height measured by sighting rod. The plate has approximately the same diameter as the base plate of the vibrator. The plate has a tangentially drilled cylindrical hole into which is put the trigger. For better coupling with the earth, the plate and the vibrator are placed in a pre-prepared hole.

Photo 3.5 Mini-vibrator for vibroseis source.

3.9.2 3-D data recording

Crew

Recording the 3-D data was done by the Glasgow University Geophysical Team comprising 3 academic staff and one postgraduate student (the author). Additional to that, 4 students were paid on a daily basis as field assistants. Although 8 people were involved during the recording phase, not all of them were present on the site at one time. Academic staff took charge, but only one or two were involved each day. The permanent members in the field were the author and two student labourers. On average, there were 5 personnel present at any time during the seismic survey period.

Receiver swath

The receiver swaths were based on the columns and rows of the 4 m grid. However, for part of the survey area the receivers were laid out at a 2 m interval in order to acquire the densest data possible. The 2 m ranging rod was used to mark a 2 m position from the peg. As the pegs are very important for location, to avoid removing them the receivers were offset to the right and upwards by 0.1 m from the pegs (Figure 3.18).

Randomised source location

The source was moved along columns or rows of the survey grid. However, it was not placed exactly on the grid, to avoid a regular common shot point (CSP) pattern. The combination of randomised CSPs in conjunction with the regular grid of receivers leads to a randomised coverage of CMPs. This is desirable in all 3-D so that CMP binning can be carried out in any desired fashion.

Figure 3.18 Pegs, receivers and randomised source positioning.

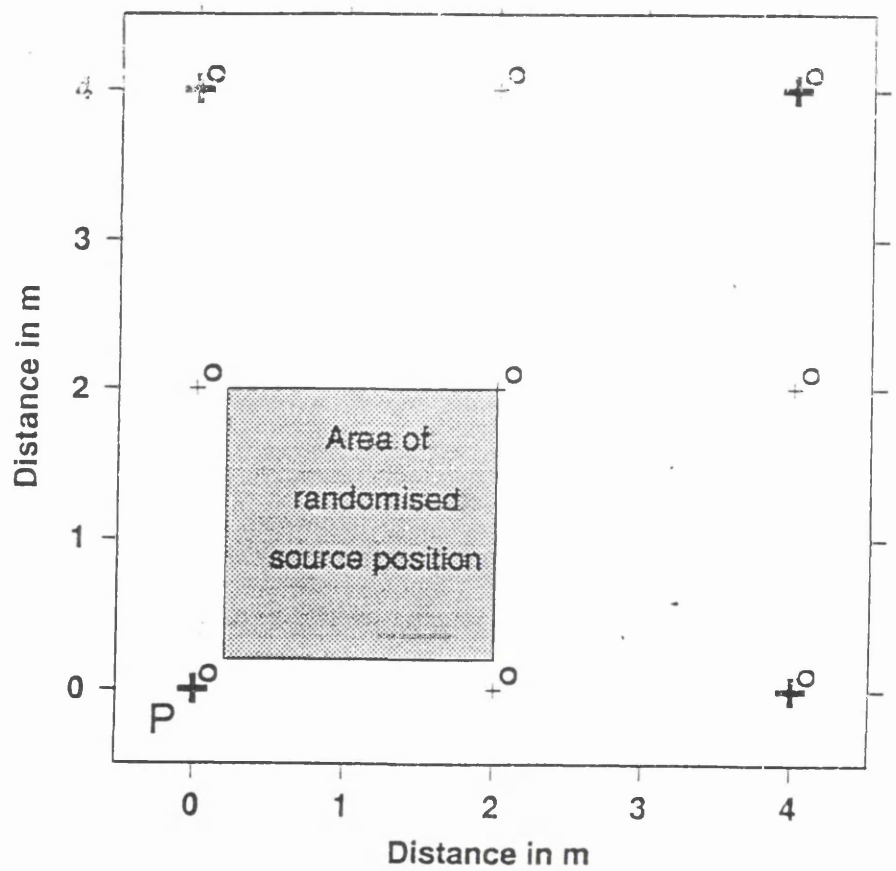

The bold crosses are pegs physically marking every second row and column
while light crosses mark the intervening rows and columns. Geophones (marked by circles) are planted every 2 m.

The shot position was placed randomly within a 1.8 x 1.8 m^2 area from the pegs, as shown by the shaded square in Figure 3.18. In helping to determine the shot location so that the CSP is as random as possible, a random number generator was used to generate a table of offsets in the row and column direction for every possible shot position, in increments of 0.2 m. With 10 permissible such offsets in each coordinate, there is a total of 100 possible positions within the randomised area.

In advance of each shot, a field assistant consulted the table and measured the offset required in the row and column direction using a ranging rod. On the turf-covered sites, the position was then marked by digging a 40-cm radius hole as a preparation for placing the source. On the stripped topsoil site, the position was marked by an un-numbered peg. To avoid confusion with the grid pegs, these pegs were coloured yellow (Photo 3.6).

Vibroseis sweep

In all high-resolution work, the ideal source is the one that can generate lots of high frequency energy. However, depending on the near surface materials, most of the high frequency components are attenuated. Unlike impulsive energy sources, which generate the energy during a very short time, the vibroseis source transmits energy at a low rate (i.e. low power) into the earth for several seconds. This long-duration encoded quasi-sinusoidal signal contains a range of frequencies at a constant amplitude, and is known as a sweep.

The sweep can be designed to start at the high frequency and end at the low frequency (downsweep), or *vice-versa* (upsweep). Usually the change of frequency over time is linear, however in some cases a non-linear sweep may also be deployed. The non-linear sweep is usually designed so that the sweep spends relatively more time at the upper end of the sweep spectrum, to compensate for losses due to the attenuation from the top layers.

Photo 3.6 Yellow coloured pegs mark source locations to avoid confusion with the grid pegs (white).

In an attempt to record the broadest bandwidth of frequencies possible, a 100-700 Hz linear upsweep was chosen. The reason behind this was if the higher frequency signals were badly attenuated, the lower end of the band can still be used since low frequencies are less affected by the attenuation. Although a non-linear sweep can be used to compensate for the loss of high frequency components, the decision was made not to use it, as a non-linear sweep increases the recording time. Furthermore, a non-linear sweep might have been too risky if the high frequencies did prove to be elusive, unless the total duration of the sweep were also lengthened to maintain sufficient time at the lower frequencies.

The value 3850 ms of sweep duration is derived from the DAS-1 set up parameters of 4000 ms total recording time. The total recording time is a combination of the sweep duration and the listening time (the time after the sweep is finished). 150 ms of listening time gives a correlated length of 150 ms, the same as the record length chosen for an impulsive record.

Recording parameters

The recording parameters were chosen during the planning phase with the aim that the acquisition would acquire the data in the densest and broadest band mode as possible. Most of them are limited by the equipment capability. Although the recording parameters were chosen during the planning phase, some of them were changed during the actual fieldwork due to unavoidable problems.

To get the spatially densest data possible, the receiver station interval was set to 2 m. The shots were at a 4 m interval, i.e. at every second row or column. In the southern corner of the area, where the topsoil had been cleared, the shot interval was changed to 2 m.

The 144 channel DAS-1 system is made up of a 48 channel main unit and two 48 channel analogue input extension units. Each unit handles each spread, which means that the swath is handled by 3 units of 48 channels.

The primary seismic source was the OYO minivibrator. The impulsive sources (sledgehammer and weight drop) were only done for 3-D preliminary tests. The signals were detected using SM4 30 Hz single channel geophones already available in the department. Although 100 Hz geophones have in the past been considered more appropriate for high resolution shallow work, their primary purpose was to filter out ground roll. Modern high dynamic range recording systems now make this analogue filtering unnecessary.

As the aim of this work is to map the abandoned mineworkings at less than 60 m depth, only short records were required. For impulsive sources, the record length was 150 ms, however for the vibroseis data, 4 s of uncorrelated data were recorded. After correlation, the record length is only 150 ms. The data were sampled every 0.5 ms. The sweep was also tapered using a 50 ms cosine taper. A list of recording parameters is summarised as in Table 3.6.

Both correlated and uncorrelated vibroseis data were recorded in the field. The field-correlated data is done using a convolution function available in the DAS-1. To increase the signal to noise ratio, uncorrelated vibroseis data were stacked 4 times and the impulsive data 8 times before storage. This vertical stacking method will increase coherent signals such as reflection by 'n' times and reduce the random noises by the power of '$n^{1/2}$'. This hopefully can increase the signal-to-noise ratio by the factor of '$n^{1/2}$', where 'n' is the number of stacking times.

Table 3.6 3-D recording parameters.

Recording instrument	OYO 144 channel DAS-1 system
Source type	OYO mini-vibrator, sledgehammer and weight drop
Receiver type	Sensor SM4 30 Hz
Station interval	2 m
Source interval	4 m and in some areas 2 m
Station array	None
Source array	None
Receiver Geometry	144 receivers arranged in 18x8 or 8x18 rows and columns
Stack	4 (uncorrelated Vib) , 8 (hammer and weight drop)
Recording format	SEG-2 32-bit
Sample interval	0.5 ms
Record length	4 s (uncorrelated Vib), 150 ms (hammer, weight drop)
Low cut	3 Hz, 6 dB/Oct
High cut	-
Early gain	48 dB
Sweep length	3850 ms
Sweep	100-700 Hz
Sweep type	Linear
Start and end tapers	50ms, cosine

3.9.3 2-D data recording

Introduction

On completion of the last of the 3-D acquisition, it was decided to run a single 2-D reflection using all available sources in turn - mini-vibrator, sledgehammer and weight drop. Only one line of 2-D was recorded as there was only one afternoon (and evening) left before the termination of the recording equipment hire. The 2-D profile was shot along row 072, where the topography was nearly flat. Furthermore, half of the line was stripped of topsoil, while the other half was still covered. This would provide a further comparison of the effect of topsoil.

Geometry

The total length of row 072 is 70.5 m. To acquire the densest data possible, all 144 channels were used, which means the receiver spacing was 0.5 m. The geophones were placed directly at the pegs without the offset as in the 3-D survey. The pegs at every 2 m were shifted to the left of the line to make room for placing the geophones. The first was placed on column 00 while the channel 140 was on column 34. As there was no more room at the NE edge of the field, channels 141 to 144 were not connected.

The source was moved towards the higher column number at every 2 m or at every column starting on column 01 and ending on column 34. As the peg position was occupied by the receivers, instead of placing it directly on the location, the source was offset by 0.5 m towards the higher column number. All sources were placed in a 0.5 m wide, 10 cm deep pre-prepared hole for better coupling.

Recording parameters

Most of the recording parameters used for 2-D profiling were the same as those used for 3-D surveying. The only differences were the receiver and source geometry and their interval. A summary of the 2-D recording parameters is tabulated in Table 3.7.

3.9.4 Data recording and transfer

The recording took place inside the recording truck (Photo 3.7). The recording truck is equipped with three independent 12 VDC power supplies. These power supplies were used to supply the power to the DAS-1 seismograph. The power for the vibrator was supplied by an external power generator. This external generator was placed quite a distance from the swath in order to reduce the noise generated from it.

Summing the data to improve signal to noise ratio and correlation of the uncorrelated vibroseis data were done automatically by the DAS-1. The data were written to an external SCSI 500 Mb hard disk. Both correlated and uncorrelated vibroseis data were recorded. Each time the data were written on to the external hard disk, information such as shot number, source position and source type were recorded on the observer's logsheet. At the end of the day, the recorded data were transferred into a processing Sun workstation back in the Department *via* a networked personal computer into which the hard disk was plugged. Visual checks of the data were made before the contents of the disk were erased for the next day's surveying.

In order to save time re-laying the spread every morning, the spreads were left on the ground overnight. The risk of theft or vandalism was considered to be minimal, as the site is fenced. Furthermore, there was also a guard on duty in the yard at the south end of the field. The DAS-1 and other hired equipment were locked up in the recording truck. The portable generator was left outside the security guard's hut.

Table 3.7 2-D recording parameters.

Recording instrument	OYO 144 channel DAS-1 system
Source type	OYO mini-vibrator, sledgehammer and weight drop
Receiver type	Sensor SM4 30 Hz
Station interval	0.5 m
Source interval	2 m
Station array	None
Source array	None
Receiver Geometry	Fixed Geometry, 140 receivers spread equally at 0.5 m interval along row 072
Stack	4 (uncorrelated Vib) , 8 (hammer and weight drop)
Recording format	SEG-2 32-bit
Sample interval	0.5 ms
Record length	4 s (uncorrelated Vib), 150 ms (hammer, weight drop)
Low cut	3 Hz, 6 dB/Oct
High cut	-
Early gain	48 dB
Sweep length	3850 ms
Sweep	100-700 Hz
Sweep type	Linear
Start and end tapers	50ms, cosine

Photo 3.7 Recording truck.

After the last day of production (Day 11) the morning of the last field day (Day 12) was spent in removing all ground equipment and the remaining pegs.

3.9.5 Progress

The actual 3-D field work started on Monday 15 July 1996 with the arrival of the hired DAS-1 and portable mini-vibroseis. Day 1 and most of day 2 were devoted to laying out the cable – swath CDE, and to test shots. The 3-D data production started on the evening of the second day using the vibroseis source. After all 70 shots fired into this swath the production acquisition was repeated using the hammer and weight drop sources. The first swath – CDE – was completed in four days. At the end of day 4, based on the time consumed to complete just one swath, it was decided not to proceed recording the data from both hammer and weight drop, but to concentrate only on the vibroseis source. It appeared to produce the broadest-band data.

The surveys were also done during the weekend when the drilling engineers were on weekend break. This meant that there was no drilling noise and we were also able to work on the stripped top soil area especially at the southern end of the site. Most of swaths MNO and PQR were shot with a 2 m source spacing, so that that area has an extra dense coverage. Starting on the following Monday, the survey had to continue in the presence of five active rigs drilling grouting holes. The noise from these rigs has undoubtedly reduced the quality of the data to some extent.

In general, moving a whole swath (three spreads) took around two hours. The geophones were left connected to the cable and each spread was loaded hand over hand into the Landrover. This method of speeding up the survey progress also had the additional advantage that the two or three bad channels remained at the same relative place within the swath. This made the equipment checking easier at the start of recording of each new swath.

Table 3.8 summarises the progress rate of the 3-D acquisition. Table 3.9 summarises the total number of vibroseis shots collected for the whole area.

Time lost to production recording because of unforeseen events, breakdown, etc. is known as down time. It includes the necessary daily travel time and equipment checking. Over the 12 survey days, the amount of down time was approximately as follows:

1) Spread faults	5 hours
2) Recording truck problems (flat batteries)	4 hours
3) DAS-1 problems (setting up configuration files)	1 hour
4) Severe rain (Day 8)	3 hours
Total	13 hours

The working day average about 10 hours, so there was a loss of about 1 hour per day. Additional to this time was the period spent each evening downloading the data from the hard disk, which took another 2-3 hours.

Table 3.8 Summary of the seismic recording daily production.

Date (July 96)	Day No.	Work	Swaths	Shots	Weather	Comments
Mon. 15	1	Field testing	CDE	0	Very good	First swath laid; test shots
Tues. 16	2	Testing; production	CDE	42	Very good	Vib. only
Wed. 17	3	Production	CDE	73	Very good	Vib. and WD
Thu. 18	4	Production	CDE	31	Very good	WD
Fri. 19	5	Production	FGH, HIJ	132	Very good	Vib. only; Impulsive source terminated
Sat. 20	6	Production	JKL	197	Very good	
San. 21	7	Production	MNO	194	Hot, cloudy	
Mon. 22	8	Production	PQR	0	Heavy rain	Drilling started
Tues. 23	9	Production	PQR, STU	154	Good	Drilling noise
Wed. 24	10	Production	STU V'W'Y'	173	Good	Drilling noise
Thu. 25	11	Production	YZA	104	Good	End of 3-D: 2-D line shot
Fri. 26	12	Clear up	-	0	Good	All spreads and pegs removed

Table 3.9 Spreads of the swath and the number of vibroseis shots fired into each.

Pattern no.	Swath	No of Stations	No of pairs of files	FFIDs	Remarks
1	CDE	70	70	101-240	
2	FGH	66	68	241-376	
3	HIJ	60	64	377-504	
4	JKL	197	197	505-898	2m shot spacing
5	MNO	194	194	899-1286	2m shot spacing
6	PQR	139	139	1287-1564	
7	STU	90	90	1565-1744	
8	V'W'Y	98	98	1745-1940	
9	YZA	70	70	1941-2080	

Each pair of files comprises an uncorrelated and a field-correlated file.

3.10 Seismic data processing

3.10.1 Introduction

All the reflection data - 2-D and 3-D - were processed with ProMAX/2D and ProMAX/3D, industry standard software installed on a Sun SPARCstation20, with a capacity of 132 Mb RAM and 27 Gb hard disk storage. As ProMAX does not have the capability of data picking and displaying time slices, the processed stacked data were transferred to a 486 PC running GMAplus 3-D software, a software for viewing, manipulating, and interpreting 3-D data sets.

The seismogram (seismic record) is basically a record of the amplitude of a wave disturbance (together with background noise) that is detected by a detector at different times. The amplitude of the wave is controlled by the reflection coefficient (R) which depends on changes in acoustic impedance (I). Acoustic impedance (I) is defined as the product of velocity (V) and density (ρ) of the material:

$$\text{Acoustic Impedance} \quad I = V.\rho$$

$$\text{Reflection Coefficient} \quad R = \frac{V_2\rho_2 - V_1\rho_1}{V_2\rho_2 + V_1\rho_1}$$

In seismology, the layered earth can be represented by a series of reflection coefficient values at different times (depths). If the earth's surface is disturbed, the wave generated at the disturbance centre will travel through the earth as well as along the surface. Normally the disturbed wave is generated by a sudden release of energy, which leads to the generation of a very short pulse known as a wavelet. An initial waveform (wavelet) travelling through the earth will travel at various speeds, depending on the properties of the medium. The changes in physical properties that the wave encounters are like a filter. When the initial waveform (wavelet) passes through the boundaries of layers with different properties, the shape of the wave will change. Figure 3.19 shows graphically

the changes of the wavelet when it meets the boundaries represented by the reflection coefficients of different value (left panel), thus producing the seismogram.

The changes in shape can also be understood mathematically as being a convolution operation between the disturbing wave and the reflection coefficient response series.

Vibroseis correlation

Since reflections occur at intervals smaller than the sweep length, the returned signal detected by a receiver is the superposition of the reflected wave trains (Figure 3.20) together with the noise. It is a very long and complex seismic record, and it is impossible to interpret. It must therefore be converted into a more conventional seismic record form (as would be gathered from an impulsive type source). To do that, the field data must be cross-correlated with the pilot sweep.

Cross correlation measures the resemblance between two time series. When both time series are identical, the cross-correlation between them is known as the autocorrelation. The autocorrelation of the sweep is known as the Klauder wavelet. Note that the autocorrelation value is a maximum where two functions are superimposed without a relative time delay (at zero lag), and the resulting function is symmetrical.

Processing strategies

Processing of the recorded data started with the 2-D data as it involved a relatively small amount of data. Furthermore, the results from these three different data types (vibroseis, hammer and weight drop) would hopefully give an idea of the layers present and their velocity. The phase relationships between the three sources and in particular the vibroseis polarity could also be checked by comparing the signatures of the first arrivals.

Figure 3.19 Seismogram concept (after Yilmaz 1987).

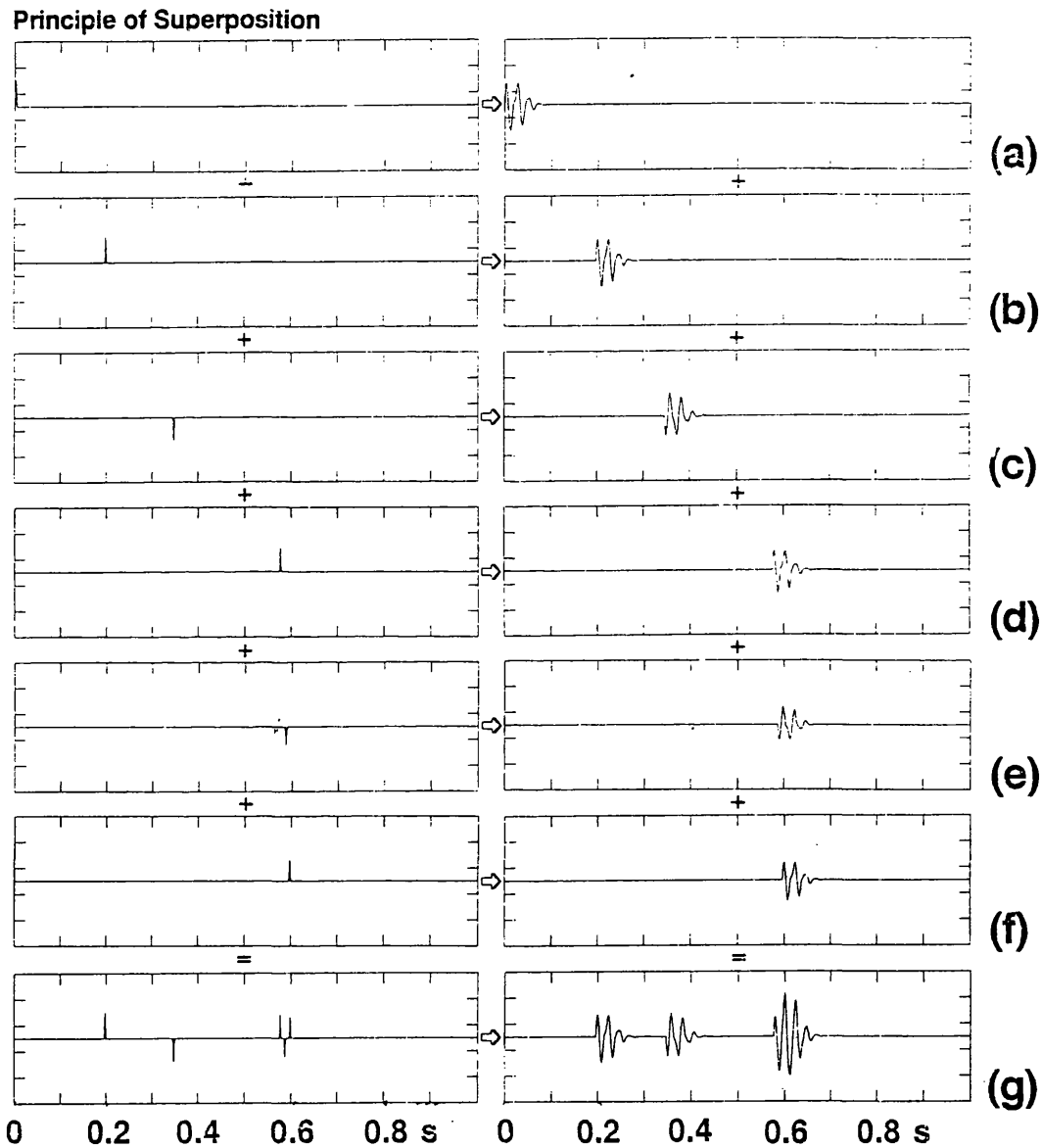

A wavelet (a) travelling in the earth repeats itself when it encounters a reflector along its path (b, c, d, e, f). The resulting seismogram (g, right) represents the composite response of earth reflectivity (g, left) to the wavelet (a, left).

Figure 3.20 Graphical illustration of the superposition concept of vibroseis data and the cross-correlation effect (after Raymond 1997).

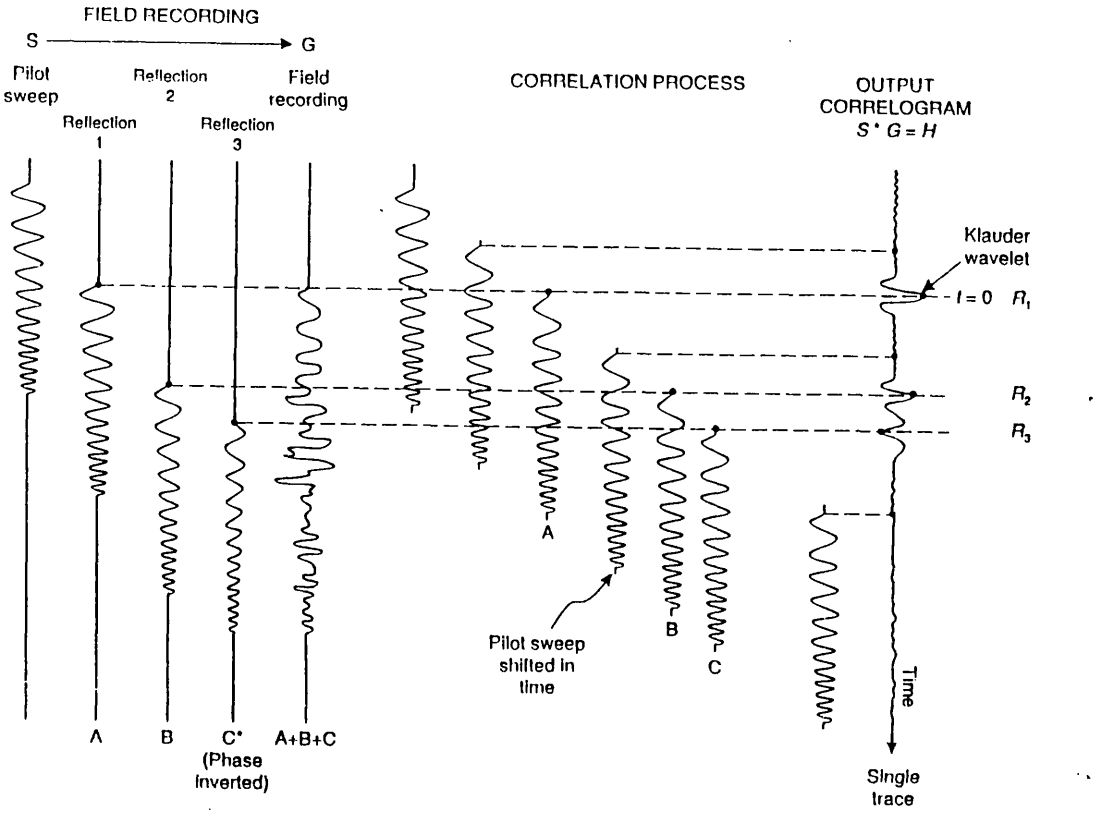

Although all the sources were tested for the first swath (CDE), only the vibroseis source was continued to the end of the 3-D survey. The other two were terminated due to shortage of time. As both correlated and uncorrelated vibroseis data were recorded, it was decided to correlate the uncorrelated data again in the laboratory using a synthetic sweep, and to compare the quality to the field correlated data. Processing of the 3-D data was done in three different stages, as discussed in section 3.10.3.

3.10.2 2-D data processing

Introduction

All the data were processed using ProMAX/2D. The data used for 2-D profiling were hammer, weight drop and vibroseis lab correlated data. Although vibroseis field correlated data were recorded, they were not used, for reasons discussed below.

Frequency analysis

All the data were stacked in the field vertically 4 times for the vibroseis data and 8 times for the hammer and weight drop data. Figure 3.21 and Figure 3.22 are examples of shot gathers from the three methods at the same location. The quality of the data ranges from poor to moderate. Most of the shot gathers were dominated by direct waves, ground roll and air blast. The far-offset traces were badly contaminated by noise. To make processing even more difficult, there was no clear sign of reflectors present on any shot gathers.

Figure 3.21 Shot gathers of three different types of source at the same location.

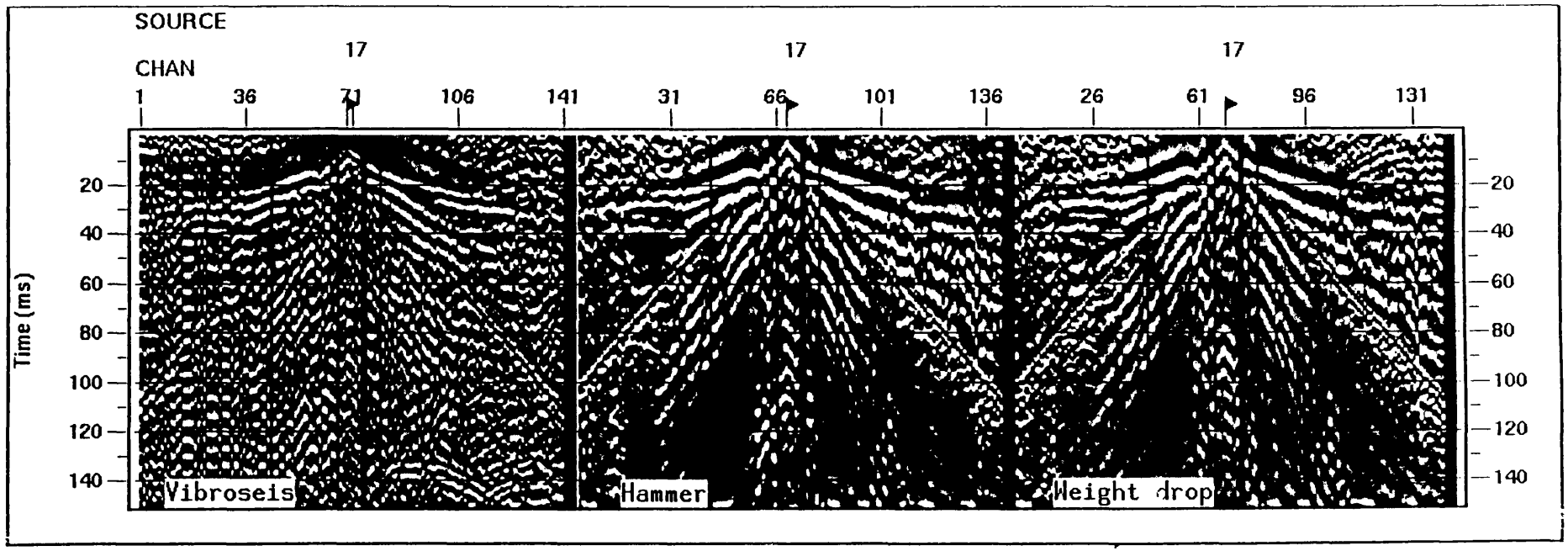

Figure 3.22 Vibroseis shot gathers from three different shot-points.

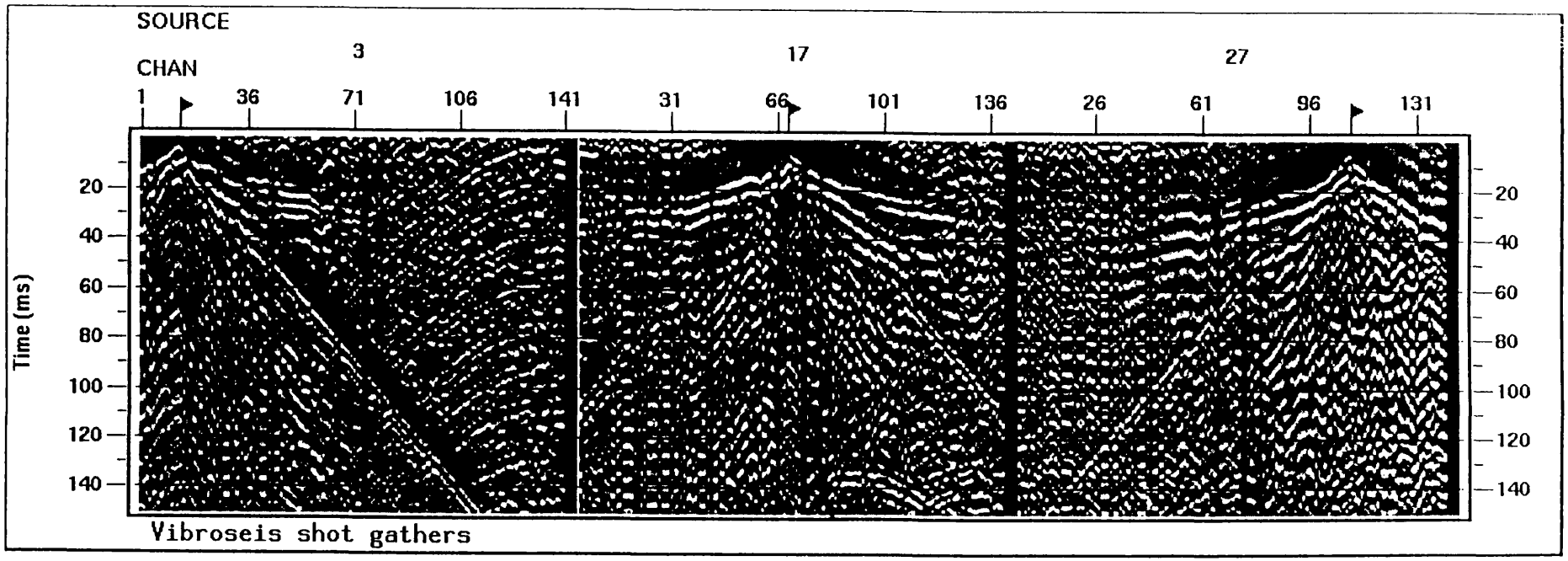

The frequency content of the shot gathers shows that the amplitude spectrum of the vibroseis data is confined essentially to the correlation range of 100-700 Hz, with the peak amplitudes at the low end of this range, around 150 Hz (Figure 3.23a). The spectrum shows a severe loss of the higher frequencies, at a rate of about 10 dB/oct. In contrast, the impulsive source records have a lower frequency spectrum, in the range of 20 to 100 Hz with the peak at 30 to 80 Hz.

Figures 3.23b and 3.23c show a shot record with its corresponding amplitude spectrum for hammer and weight drop respectively. The figures show a great similarity between the hammer and weight drop records. There appear to be no useful source frequencies higher than 100 Hz.

The 30 to 80 Hz effective bandwidth for the impact source records implies they are not suitable for high resolution work, as the minimum thickness that can be resolved is approximately 6 m (assuming a velocity of 1200 m s^{-1} and mean frequency of 50 Hz). On the other hand the peak value of the returned frequency for the vibroseis data is around 150 Hz, which means the minimum thickness it can resolve is approximately 2 m, using the same criteria.

Phase comparison and first break picking

The SEG signal polarity convention is that for an upward ground motion, the signal is represented by a negative number on the tape which in turn means a trough on the displayed trace. The polarities for all records were checked by comparing the first arrival signatures from all the records.

The aim of this was mainly to ensure that the polarity of the vibroseis data matched that of the impulsive source data, because the zero-phase nature of the former was not clear on the shot records.

Figure 3.23a Shot gather and frequency spectrum – vibroseis.

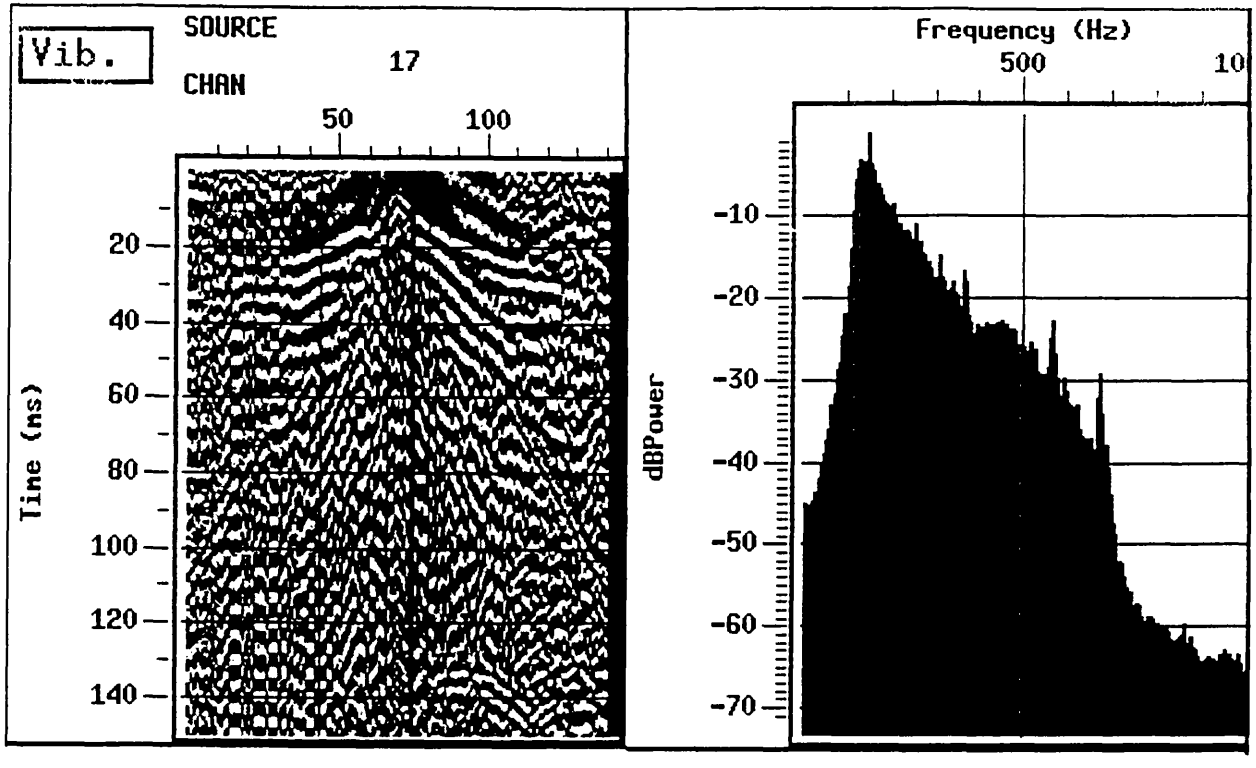

Figure 3.23b Shot gather and frequency spectrum – hammer.

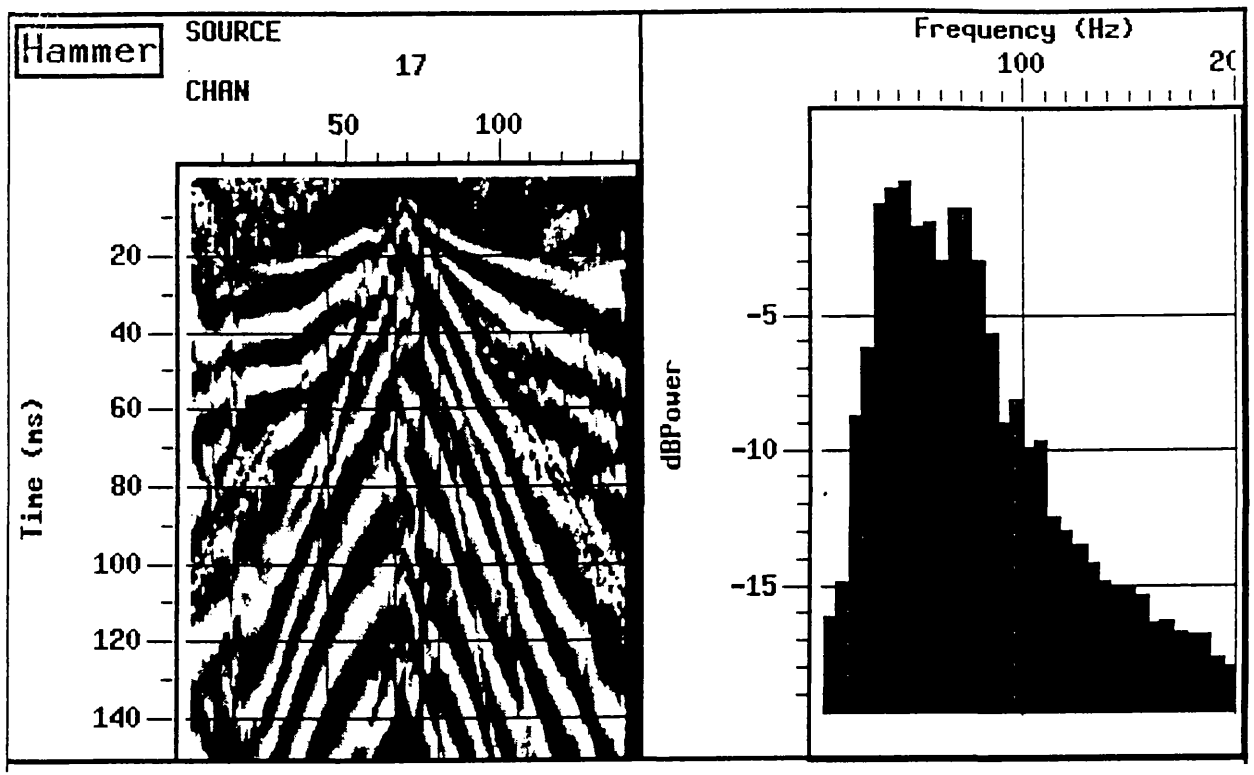

Figure 3.23c Shot gather and frequency spectrum – weight drop.

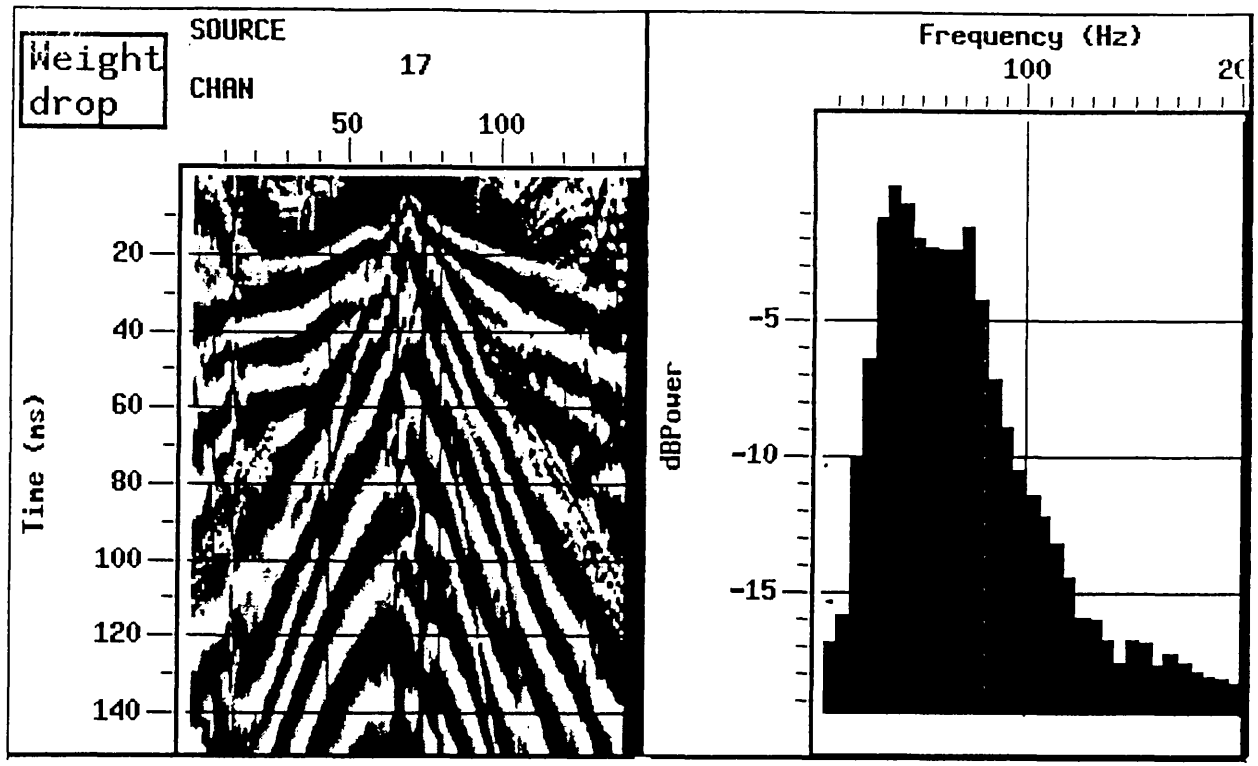

Figure 3.24 shows that the first breaks are to the left (trough) on both impulsive sources. The first 'kick' represents the first arrival signature. Comparing short offset data (where the signal is strong) between impulsive and vibroseis data, it is seen that the first arrival in the impulsive records corresponds to the first trough on the vibroseis record. This confirms that the polarity for all three datasets is same. First break times were picked using the ProMAX first break picker. On impulsive records, the onsets (the first 'kicks') were picked, while on the vibroseis records, the corresponding first troughs were picked. Only clear first breaks were picked, and noise-contaminated traces were not picked.

Refraction model

To obtain the near surface velocity structure, the first break times picked on the hammer data for the 2-D line were sent to Professor Ewald Brückl of the Technical University of Vienna for refraction inversion. His results show that the average velocity of the first layer is about 350 m s^{-1} (Figure 3.25). This value has been used in elevation and static corrections applied subsequently to all the data, both 2-D and 3-D.

Pre-processing

The field recorded data were assigned with their appropriate field file identification number (FFID). The FFID number is unique and is based on the Observer's logsheets. Any non-production files such as noise tests were deleted prior to applying geometry. All 34 shot records of vibroseis data and 31 shots each of hammer and weight drop were carefully inspected to look for any signs of anomaly or inconsistency. Visual inspections of the data were also done to look for any signs of reflector; unfortunately the data were dominated by low frequency noise which would mask any reflectors. After visual inspection of the files on the screen, any dead and noisy traces were zeroed and reverse traces were corrected.

Figure 3.24 Comparison of the polarity of the signal of three different sources.

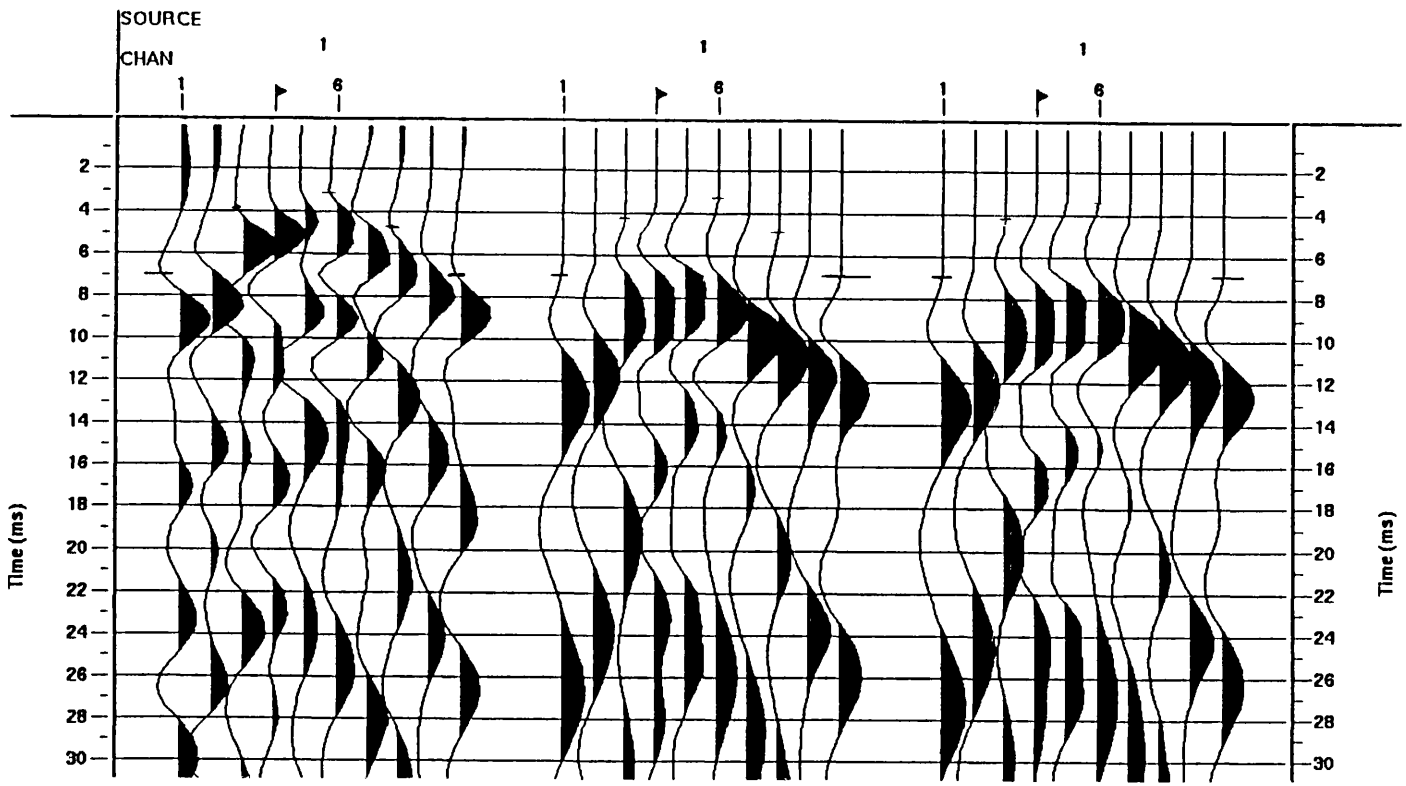

Left, middle and right panels are represent the vibroseis, hammer and weight drop data respectively.

Figure 3.25 The refraction model produced by the Technical University of Vienna from 2-D line (vibroseis source).

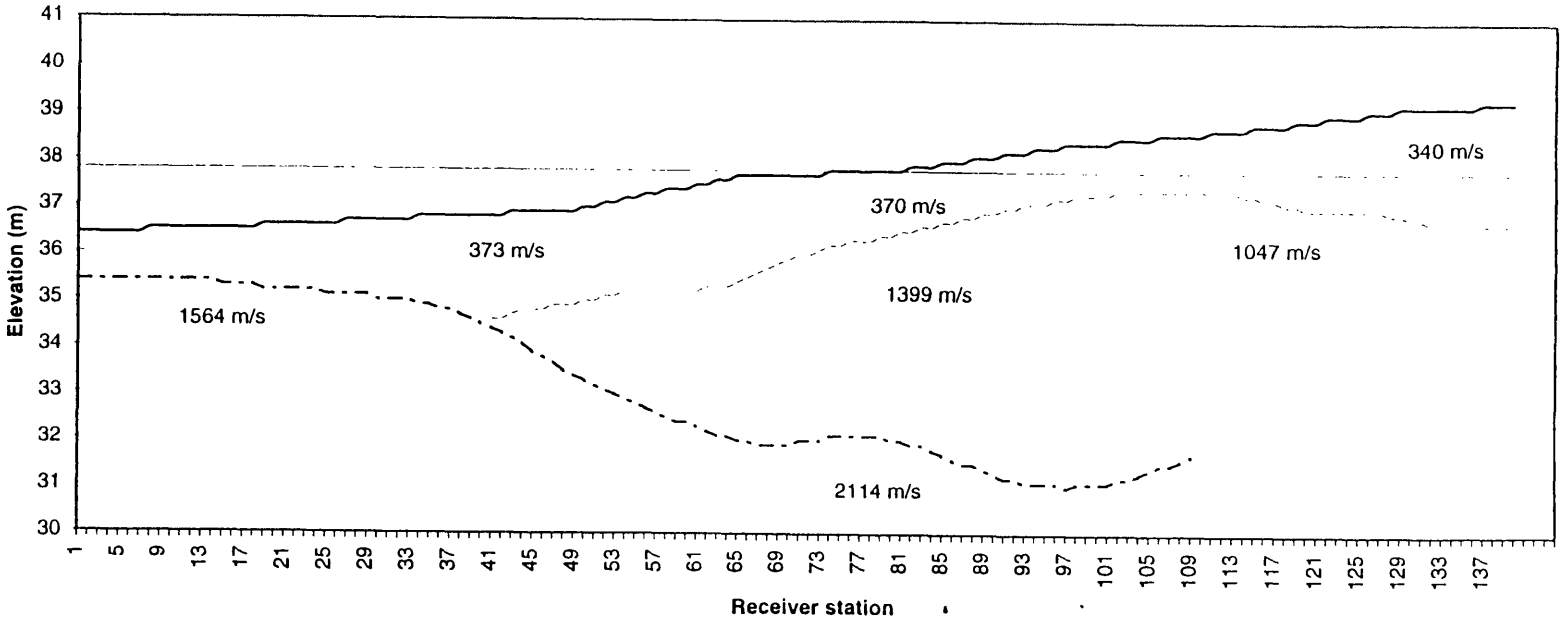

Processing - approach-I

As the vibroseis source has a higher amplitude frequency spectrum, the vibroseis data were processed first. The aim of this strategy was to process the data following common practice in petroleum industry or in other words, the data were treated the same as for deep seismic records. Shot gathers (e.g. Figure 3.26) are very noisy. The most interesting noise appears on the far end of the shot record, where it shows a hyperbolic pattern. This noise also appears on the impulsive source shots, which means it is not a correlation artefact of vibroseis data, nor is it from the external generator for the vibroseis source. It is probably reflected air blast energy from a building off to one side, in line with receiver channel 125.

The raw data (Figure 3.27) were first automatically scaled by a factor of 35 and corrected for spherical divergence based on a simple spherical spreading equation $(\frac{1}{dist})$ correction with true amplitude recovery (TAR) velocity function as listed in Table 3.10. Air blast signal was also attenuated (Figure 3.28). An elevation static with 350 m s^{-1} replacement velocity was applied to the data. Datum for this elevation static was set at 37.0 m.

Since only high frequency signals were important in this work, the data were filtered using a frequency band pass filter (60-100-300-400 Hz). A dip scan stack (DSS) was also applied to the shot gather, with the main aim to scan and filter out the linear dipping noise events such as air blast and ground roll.

Table 3.10 TAR velocity function.

Time (ms)	Velocity (m s^{-1})
0	350
10	800
20	1200
50	1500

Figure 3.26 Raw vibroseis shot record showing that the gather is dominated mostly by unwanted noise. Geophone spacing is 0.5 m.

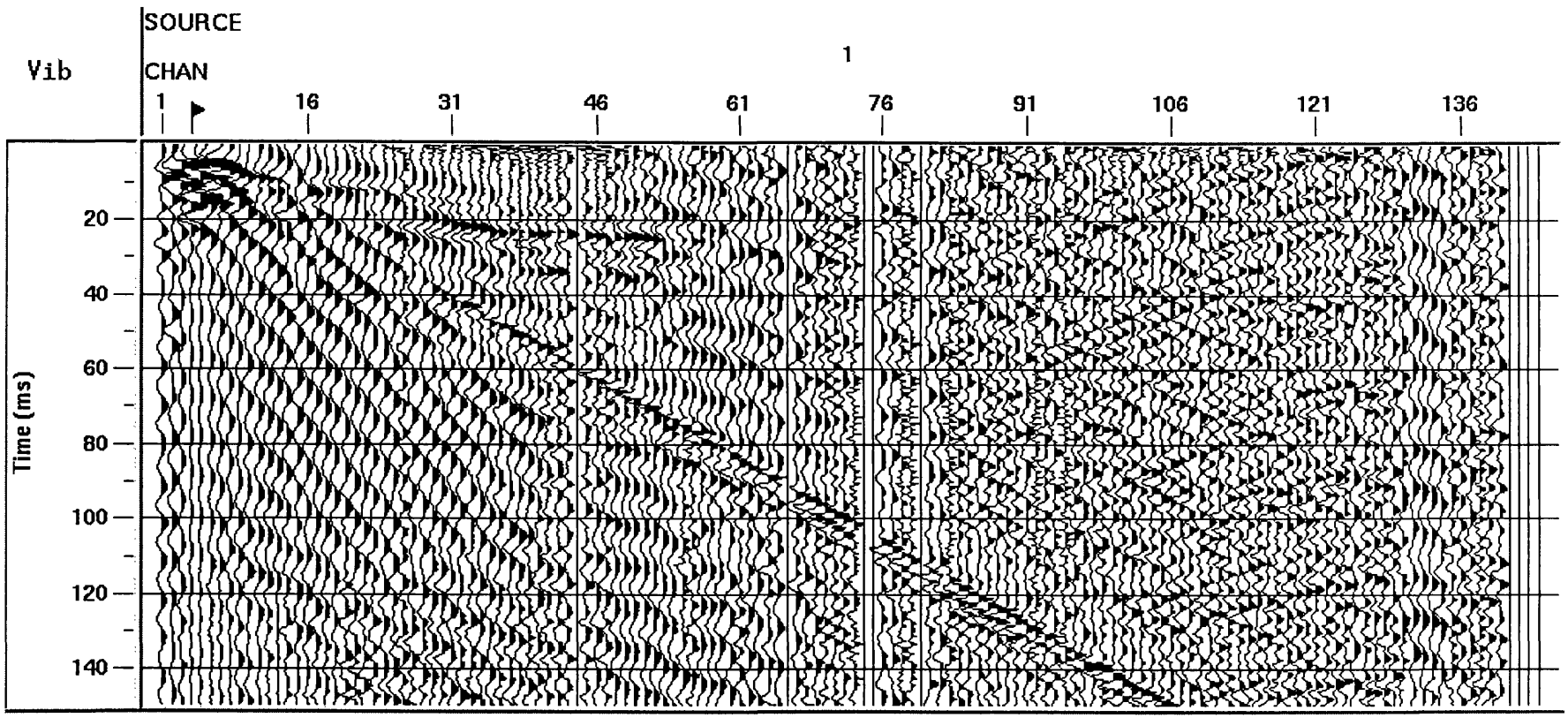

Figure 3.27 Shot gather no. 13 from vibroseis data.

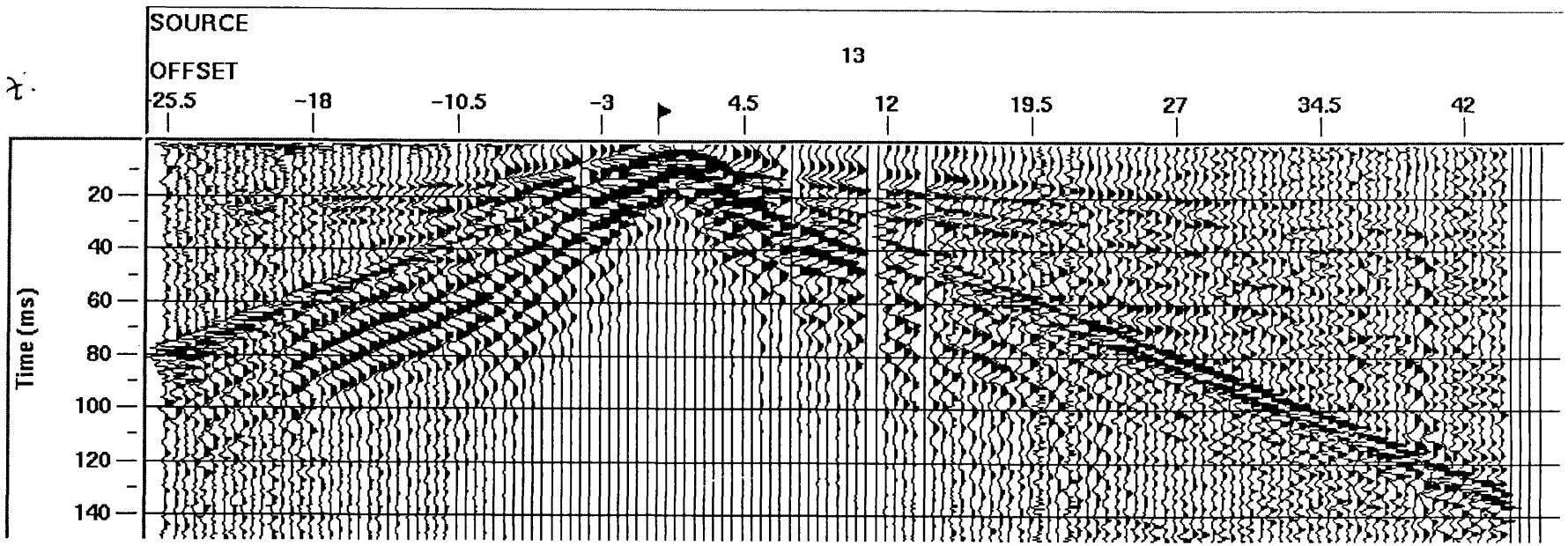

Offset value is given in meter.

Figure 3.28 Shot gather no. 13 after AGC, TAR, 60-100-300-400 Hz frequency band pass, DSS and another AGC.

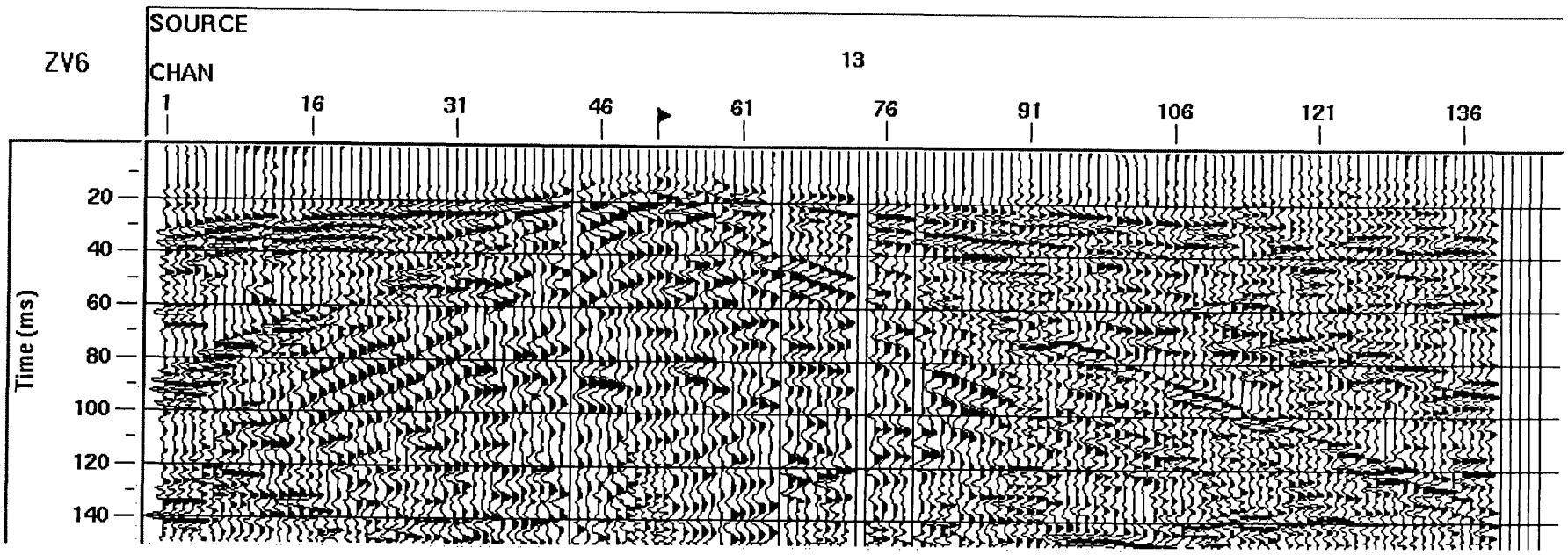

Geophone spacing is at every 0.5 m.

Although the deconvolution process can increase the temporal resolution (by compressing the wavelet into a spike), it was not applied to the vibroseis data since it only works best with a minimum or maximum phase wavelet. The vibroseis data has a zero phase wavelet. In order to enhance the signal and remove the noise, an F-K filter was applied. This was designed using F-K analysis (Figure 3.29). The F-K filtering removed most of the noise (Figure 3.30). The data were not muted for the first arrivals, as reflectors of interest were suspected to appear at very early times, less than 20 ms. After the F-K filtering, the data were then sorted into CDP (common depth point) gathers.

As a fixed spread geometry is used, the maximum fold is the same as the number of shot records, i.e. 34 fold. Because the record length is short (150 ms) and dominated by the unwanted signals, the velocity analysis for CMP gathers was difficult. Furthermore there was no clear or sharp contrast between the glacial till and the bedrock as the top of bedrock was weathered (thus lowering the velocity). The difficulties of velocity analysis were compounded by lateral velocity variations that distort the expected hyperbolae. So instead of using a velocity function, the data were stacked using several constant velocities or CVS's (constant velocity stacks).

Figure 3.31a, 3.31b, and 3.31c show the stacked section using 600 m s^{-1}, 1350 m s^{-1} and 2054 m s^{-1} constant velocities. It seem that by using stacking velocity of 1350 m s^{-1} the maximum reflection amplitude appear continuously uninterrupted around 20 ms. No residual static were applied to improve the quality of the reflector. This stacking velocity value is assumed to be an appropriate stacking value for the interface of the bedrock. A summary of the approach-I processing flow is tabulated in Table 3.11.

Figure 3.29 F-K analysis used for designing the F-K fan filter parameter.

ZV 7

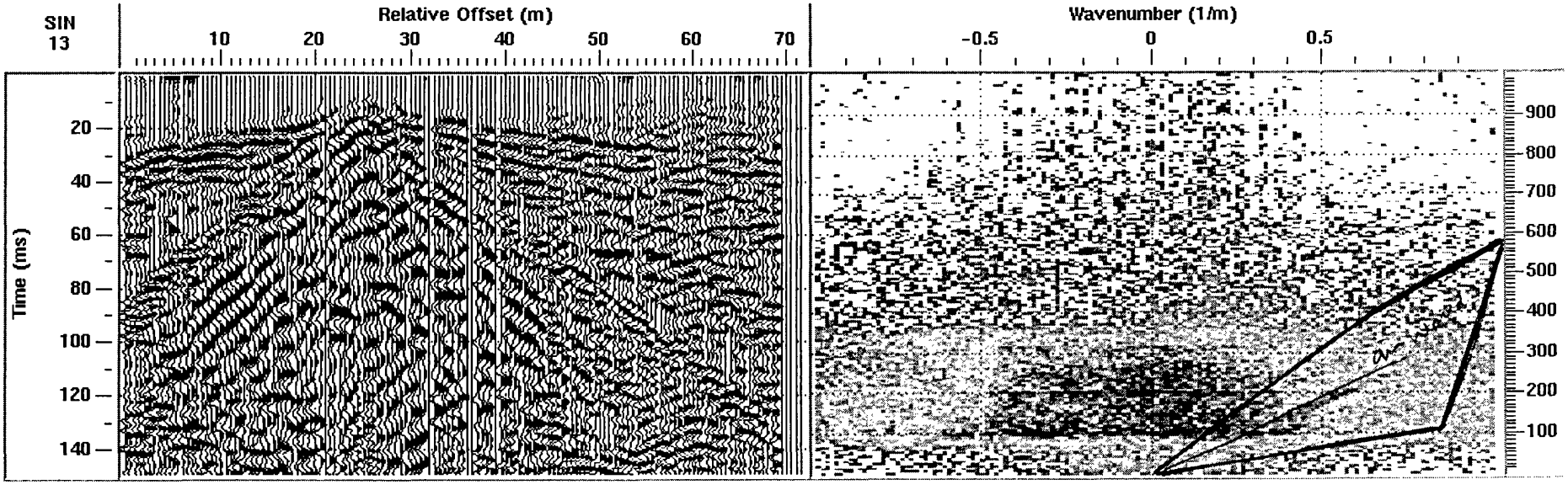

Figure 3.30 Shot gather after F-K filtering.

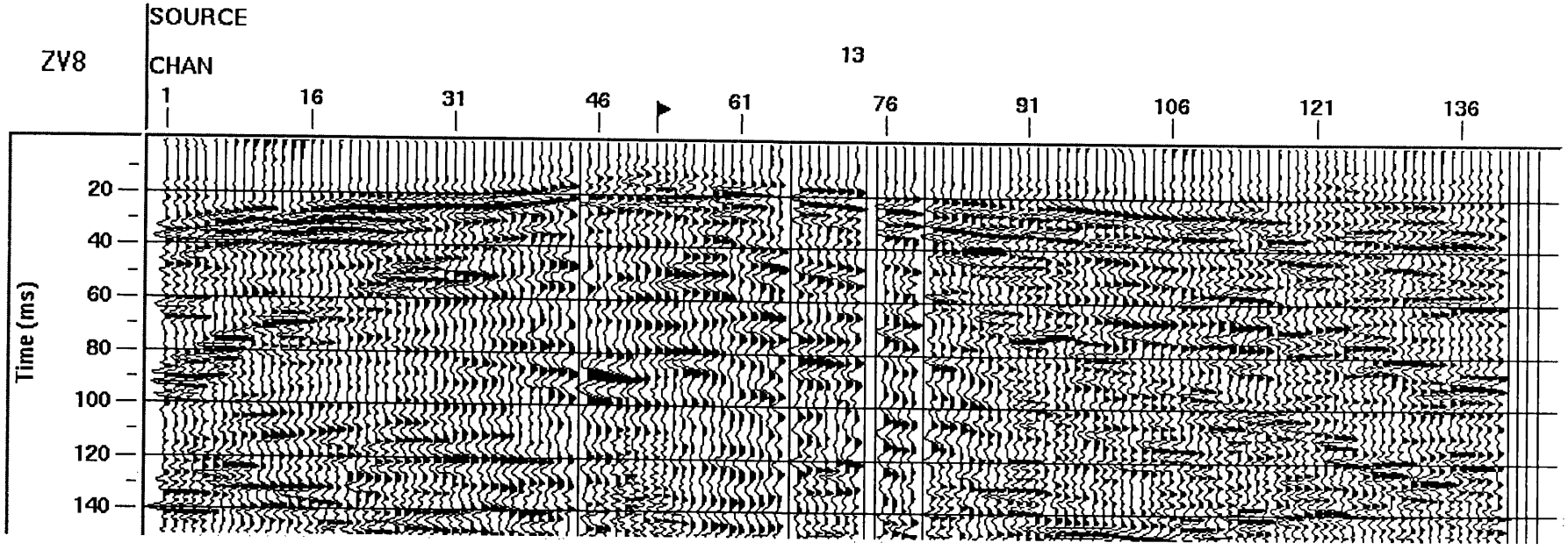

Channel spacing is 0.5 m.

Figure 3.31a Stacked section using 600 m s^{-1} constant velocity.

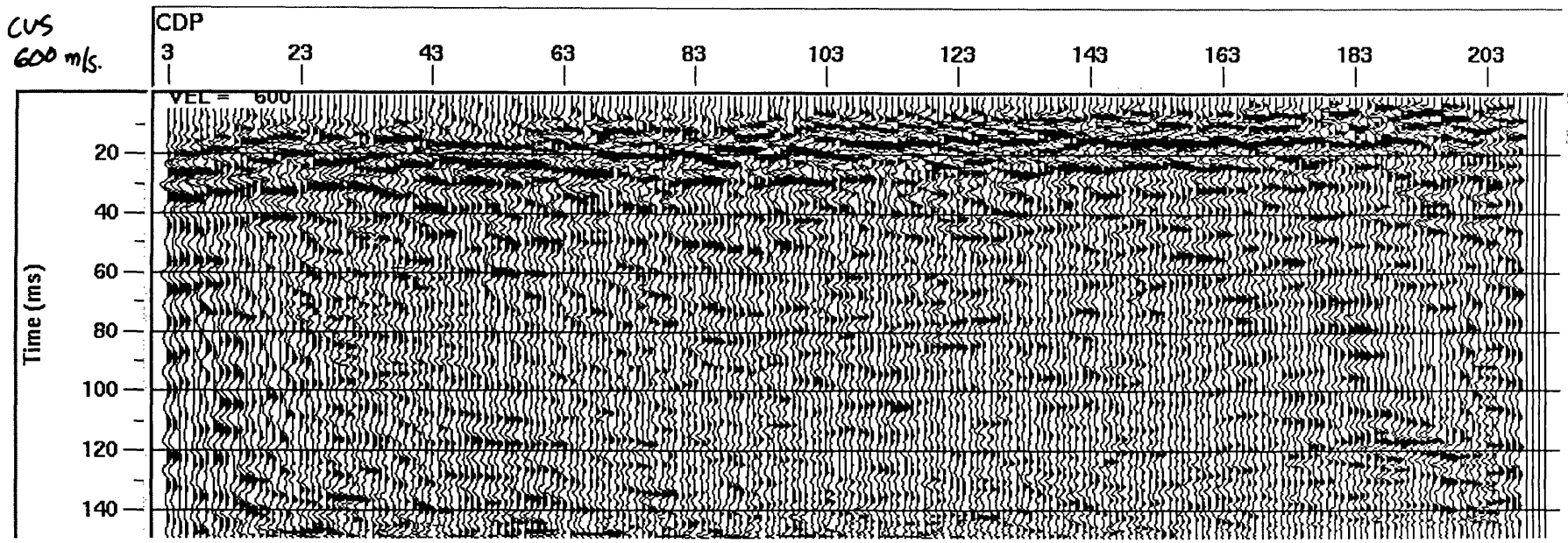

CDP spacing is at every 0.25 m.

Figure 3.31b Stacked section using 1350 m s^{-1} constant velocity.

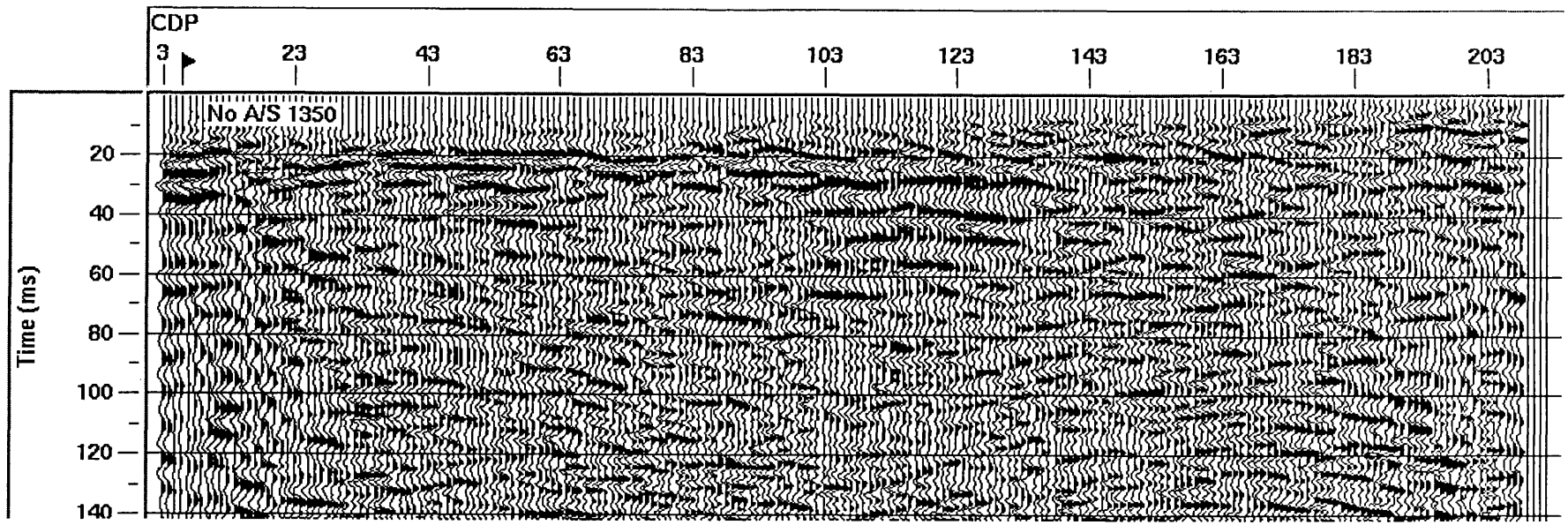

CDP spacing is at every 0.25 m.

Figure 3.31c Stacked section using 2054 m s^{-1} constant velocity.

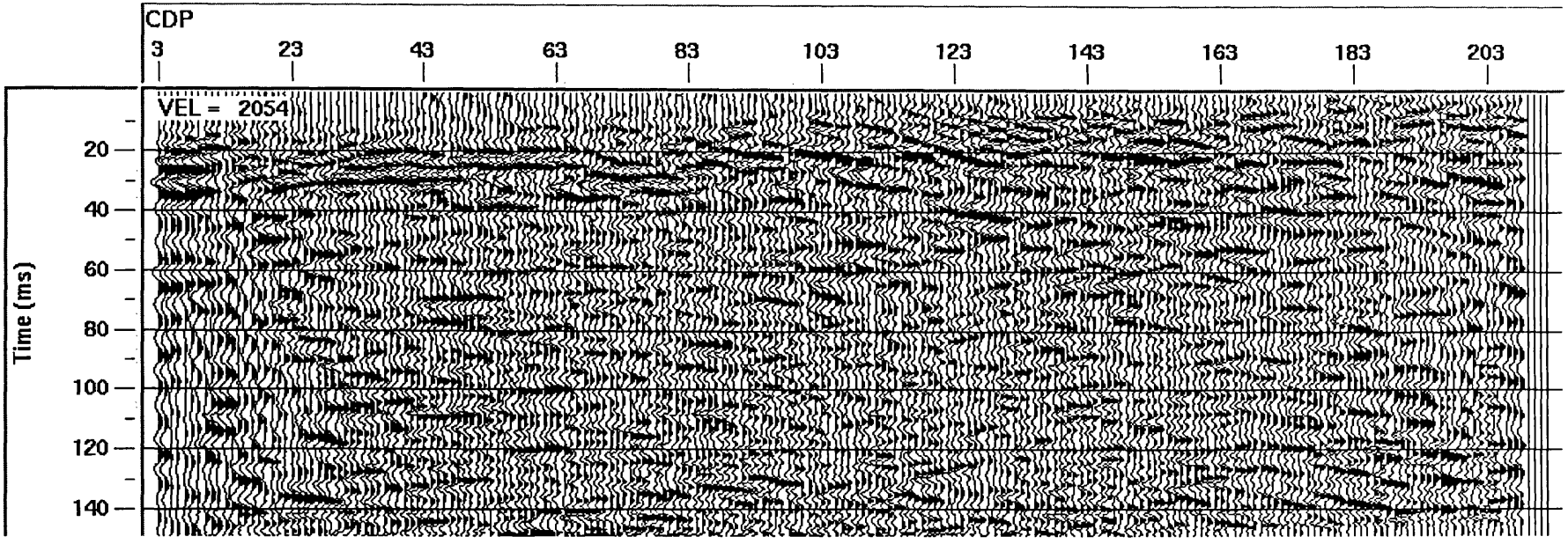

CDP spacing is at every 0.25 m.

Table 3.11 Summary of approach-I processing flow.

Input Data	Vibroseis 100-700 lab correlated data
Geometry	2-D land geometry; fixed spread; 0.5 m receiver spacing; 2 m source spacing.
Editing	Kill channels 44, 66, 74, 75, 140-144 (bad traces)
AGC	35 ms
TAR (s: m s^{-1})	0:350; 5:800; 10:1000; 20:1500; 40:1700; 150:2700
Elevation static	Datum 37.0m; replacement velocity 350 m s^{-1}
Air Blast Attn.	334 m s^{-1}
Band Pass filter	60-100-300-400
F-K (vel.: freq.)	Fan filter on both sides.
CDP sort	
CVS stack	600 m s^{-1}; 1350 m s^{-1}; 2054 m s^{-1} (3 panels)

Approach-I: result and comments

The section shows a discontinuous reflector at approximately 20 ms TWT on the 1350 m s^{-1} CVS section. Using a simple equation (velocity = distance over time, or distance = 1350 m s^{-1} * 10^{-2} s), the approximate depth to this reflector is around 13 m. The actual depth (the depth calculated from an appropriate velocity function) is less than that as the section is stacked using single value of velocity 1350 m s^{-1}. This reflector may represent the top of the bedrock (Carboniferous sandstone and shale) since it is flat-lying.

If it represents the bedrock reflector, it should be continuous over the whole section. Since the line was oriented parallel to the dip direction, the deeper dipping reflectors are also to be expected under this horizontal reflector (according to the refraction model). Because of these unsatisfactory results there was little point in proceeding to process the impulsive data using the same processing flow.

Processing – approach-II

In approach-II, the data were processed using a bare minimum of processing. The primary goal was to stack the data without having to worry about adverse processing effects such as the risk of spoiling the wavelet (by deconvolution) or stacking the refracted arrivals (only short offset traces were considered).

In this strategy, the data from all three sources were processed. Since there was no clear indication of any reflectors in shot gathers, and the far offsets were severely contaminated by unwanted noise, all the data were sorted into CMP gathers prior to any processing. The data were sorted into 276 and 263 CMPs for vibroseis and impulsive data respectively. The spacing between each CMP is equal to half of the receiver spacing, i.e. 0.25 m. As the data were collected using a fixed spread with 0.5 m receiver and 2 m source spacing, the fold of coverage increases by 1 every 4 CMPs. The

maximum fold of coverage is same as the number of shots, which is 34 for vibroseis and 31 for both impulsive datasets. Since the source interval was 2 m, the average offset increment between traces in CMP gather is 2 m. Figure 3.32 shows example CMP gathers for each of the sources. The data are severely aliased spatially. In order to cure the spatial aliasing problem, the CMP offset was rounded down to the nearest integer using a simple mathematical expression as follows:

$$Int\left(\frac{(CDP+3)}{4}\right)$$

Then all the CMPs with the same integer number were combined. Thus four CMPs at 0.25 m interval were combined to form supergathers at a 1 m interval. This reduces the number of CMPs by a factor of 4. The total numbers of supergathers is 71. Figure 3.33 is an example of a supergather for each of the three sources. They all show quite an improvement of the raw data appearance, compared to the original gathers (Figure 3.32). However, air blast and ground roll are still dominant. In order to avoid misinterpreting the refraction events as reflections, extra care was taken in muting the first arrivals. However, as the reflection signal was expected to be very shallow (right below or even masked by the refracted signal), the muting process was only applied to positively identified refractions (Figure 3.34). All the signals below the air blast were also muted out (Figure 3.34). The muting was done on the supergather CMPs. A bandpass filter was also applied to the supergathers. An F-K filter was not applied as most of the noise was successfully muted out.

At this point the supergathers were re-sorted back to their original CMPs. To improve the quality of the data, a minimum phase predictive deconvolution with a very small (1 ms) prediction distance was applied for the impulsive data. Because the deconvolution would only be successful if the input signal is of minimum phase, such deconvolution was not applied to vibroseis data. For the vibroseis data, frequencies in the 100 to 400 Hz range were boosted using spectral shaping. The CMPs were stacked using a 1-D velocity function with a 60% NMO stretch mute. Results are shown in Figures 3.35a, 3.35b and 3.35c.

Figure 3.32 Three original CMP gathers (2 m trace spacing) showing severe aliasing.

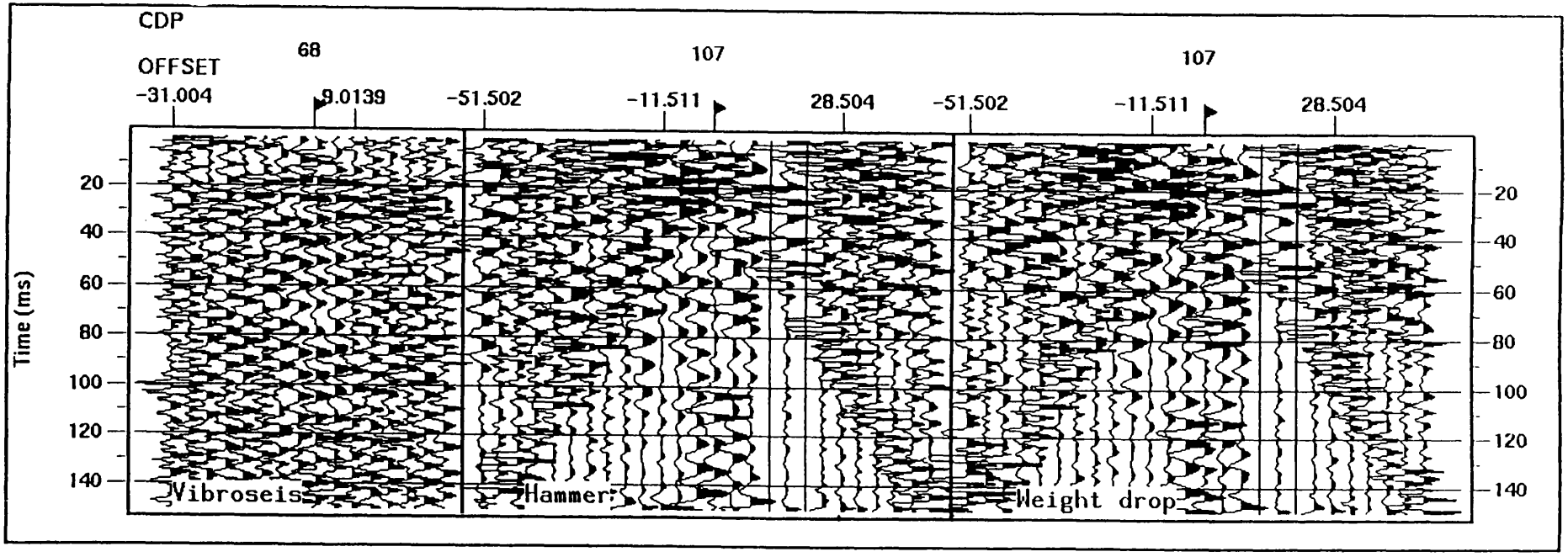

Figure 3.33 CMP gathers after summation of 4 adjacent CMPs.

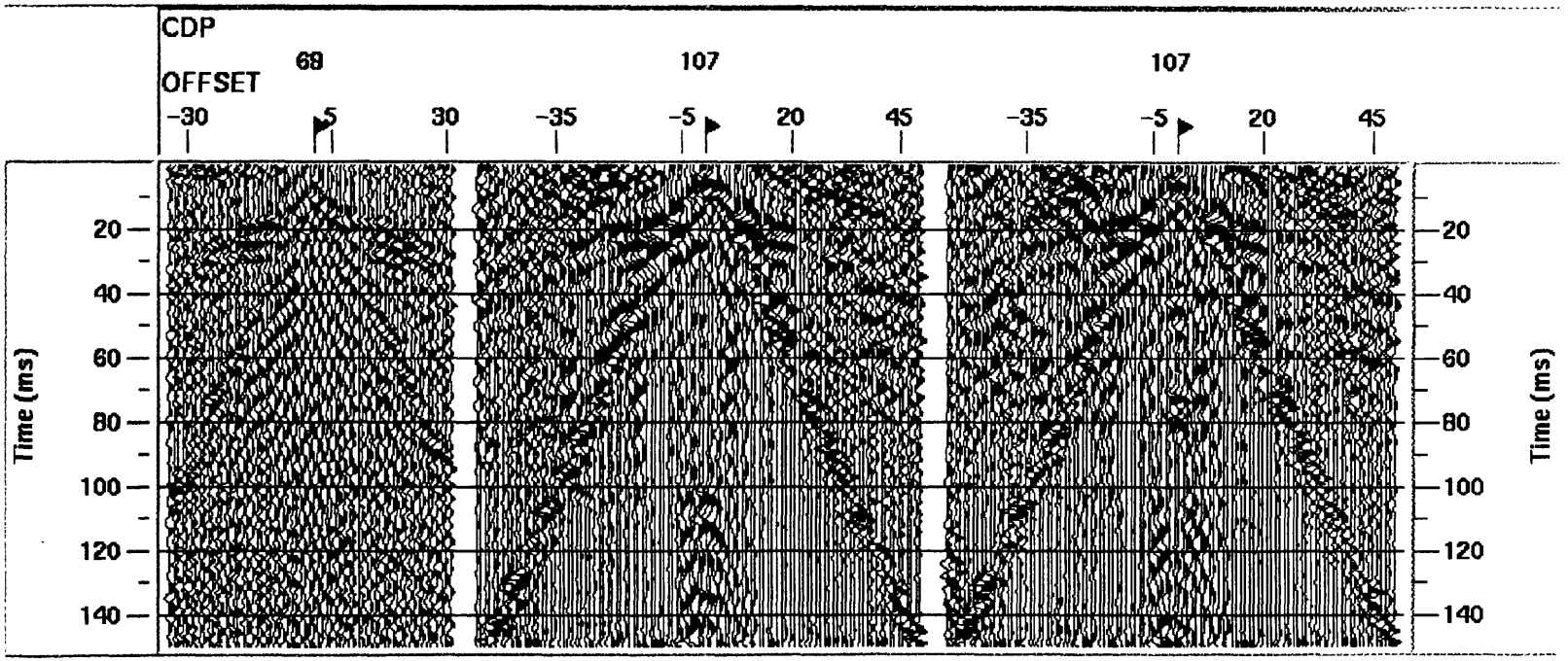

Note that the spatial aliasing problem in Figure 3.32 has been cured.

Figure 3.34 Supergather after severe front and bottom mute applied.

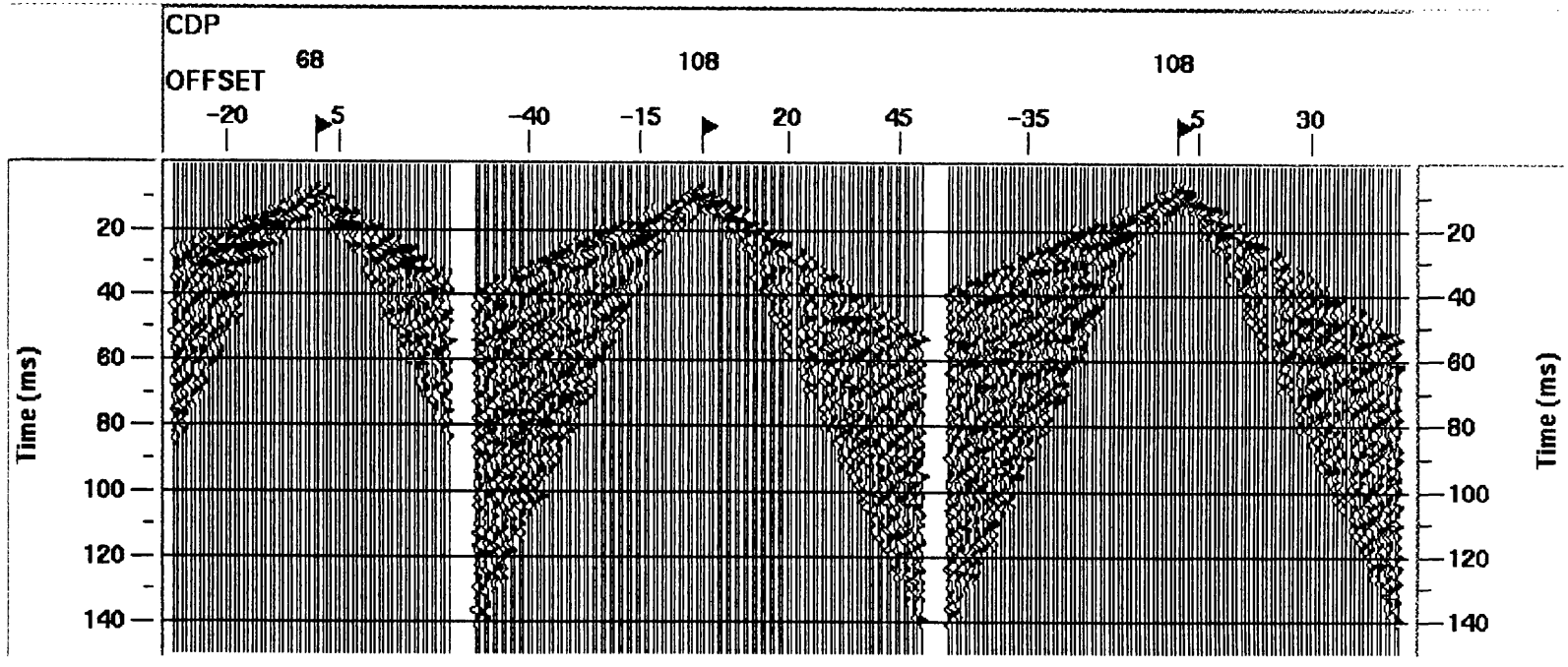

Table 3.12 Processing flow for vibroseis and impulsive data – approach-II.

Input Data	Vibroseis 100-700 lab correlated data
Geometry	2-D land geometry; fixed spread; 0.5 m receiver spacing; 2 m source spacing.
Editing	Kill channels 44, 66, 74, 75, 140-144 (bad traces)
Muting	First arrival and all signal later than air blast
Elevation static	Datum 37; 350 m s^{-1} replacing velocity
Spectral shaping	Vibroseis only: 100-400 Hz
Predictive Decon.	Impulsive only: 40 ms operator length with 1 ms predictive distance
AGC	30 ms centred (vibroseis); 15 ms centred (impulsive)
Band pass filter	Ormsby frequency band pass filter 100-400 Hz (vibroseis); 60-100 Hz (impulsive)
NMO/ Brute Stack	1-D velocity function: 60% stretch mute

Figure 3.35a 2-D vibroseis data – brute stack.

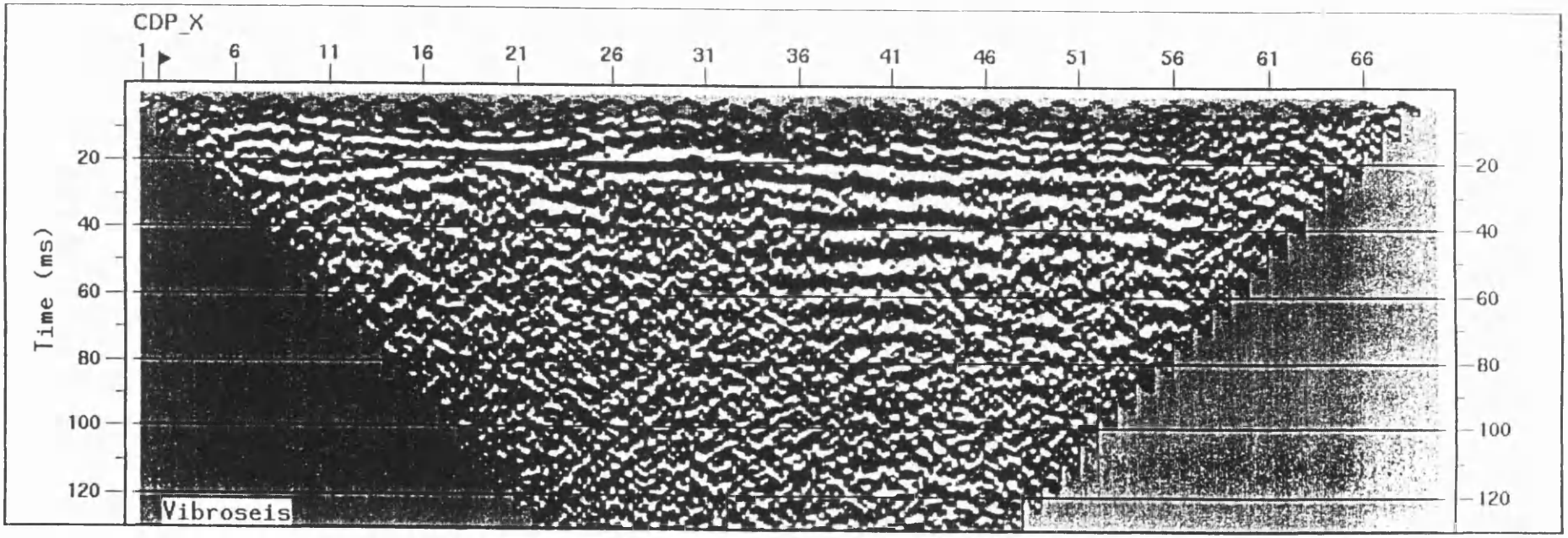

Figure 3.35b 2-D hammer data – brute stack.

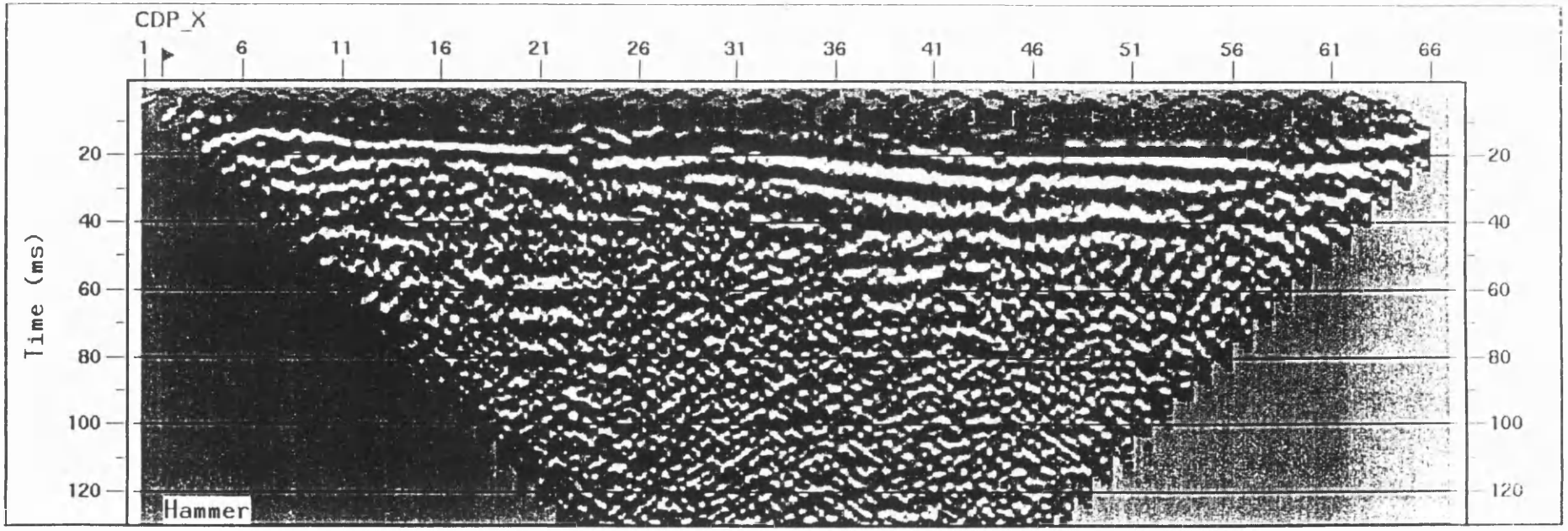

Figure 3.35c 2-D weight drop data – brute stack.

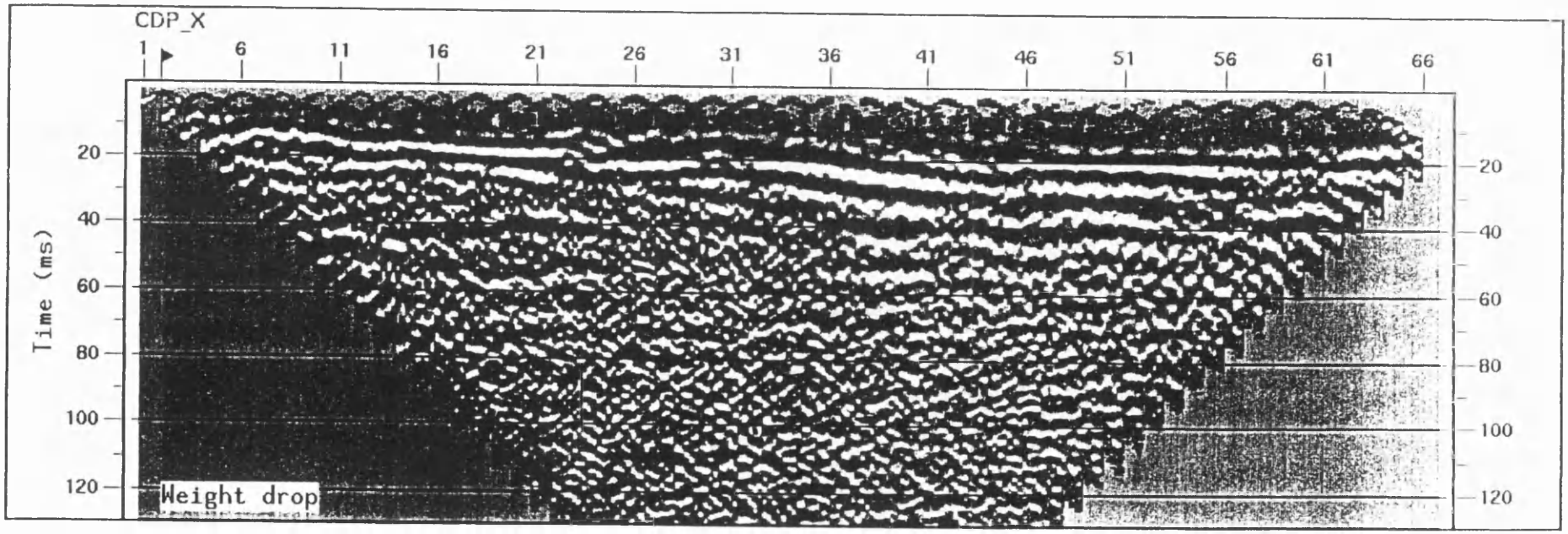

Approach-II: result and comments

The results (Figures 3.35a, 3.35b and 3.35c) show much resemblance to each other. As with approach-I, all three sources show a reflector at 15 –20 ms TWT. This is probably the reflection from the top of the bedrock. However, the results of approach-II show another reflector below the bedrock reflection. This reflector dips to the right (NE), in the approximately down-dip direction for layers within Carboniferous bedrock. The refraction model (Figure 3.25) also shows this feature.

3.10.3 3-D seismic data processing

Introduction

Although the actual idea of this project was to conduct the first combination of full and random 3-D survey for shallow investigation using three possibles sources – vibroseis, sledgehammer and weight drop, the decision had been made to acquire the majority of the 3-D data using only the vibroseis source. The reasons were that to use all three sources would have required triple the field work time, which was not available. After analysing the frequency content of the three different sources from the first swath (CDE), it was evident that both sledgehammer and weight drop have lower dominant frequencies (30-80 Hz) than the vibrator.

Both correlated and uncorrelated vibroseis data were recorded. The uncorrelated data were stacked four times to increased the signal to noise ratio before they were cross correlated with their pilot sweep to produced the correlated data. Like the 2-D where the data were processed by ProMAX/2D, the 3-D data was also processed using ProMAX software, however instead of ProMAX/2D, the 3D version was used. Only the vibroseis data were processed. The impulsive datasets (from the first swath CDE) would only be processed if the results from the vibroseis data were promising.

Field correlation

Correlation is the first process applied to the uncorrelated vibroseis data. Normally, the correlation process is done in the time domain by a purpose-built 'correlator', and it is common practice to record the correlated data only, as the long uncorrelated data use lots of recording space or tape. With the DAS-1 and minivibrator recording system, the field correlation is done slightly differently from the conventional method. Here the baseplate and reaction mass accelerations are measured and recorded on two auxiliary traces. The weighted sum of the two accelerations is used in a convolution filter process, which replaces conventional correlation. This is done in order to get a better estimate of force applied to the ground (Smythe personal communication). This recorded correlated data is defined as the field correlated data. Because the DAS-1 system correlates the uncorrelated signals using an essentially 'blind' convolution process, both correlated and uncorrelated records were recorded. Although the uncorrelated data consume lots of recording space, by recording the uncorrelated data (which were later correlated using conventional methods), comparison between the correlation methods can be done.

Lab correlation

In conventional correlation, a synthetic pilot sweep was generated using ProMAX software. This synthetic sweep matches the sweep used in the field, as listed in Table 3.13. Using the vibroseis correlation processor in ProMAX, all the uncorrelated data were then correlated and stored as '100-700 Hz Lab. Corr.' datafiles.

The correlation process can also be used to filter the data; for example if the uncorrelated data are correlated with a matching sweep as before, but only having finite amplitude over 200-500 Hz, the correlated data will only contain frequencies in that range.

With that idea, a secondary dataset was constructed by correlating the uncorrelated data with a 200-700 Hz synthetic sweep. Thereby the low frequencies (lower than 200 Hz) are filtered out. The original 100-700 Hz sweep was a linear sweep, meaning that the rate of increase of frequency is linear. So for the frequency range of 200-700 Hz, the sweep must be 3208.33 ms in length to keep the same linearity relation:

$$\frac{700Hz - 200Hz}{x} = \frac{700Hz - 100Hz}{3850ms}$$

$$x = 3208.33 \text{ ms}$$

But if we generate a synthetic sweep of 200-700 Hz over 3208.33 ms in the same way as generating the 100-700 Hz sweep, we create a sweep which has different phase from the 100-700 Hz sweep. So this sweep cannot be used to correlate the uncorrelated vibroseis data.

To generate the 200-700 Hz synthetic sweep with same characteristics as the 100-700 Hz sweep and maintain the linearity relation, we generate a 100-700 Hz sweep with the front end muted up to 200 Hz. Since the sweep has a linear relation, the amount of muting can be calculated precisely using a linear equation as follows:

$$\frac{200Hz - 100Hz}{x} = \frac{700Hz - 100Hz}{3850ms}$$

$$x = 641.67ms$$

Because the sweep (100-700 Hz with 641.67 ms time delay) was generated using 100-700 Hz sweep, the relation between these sweeps were same, however this sweep only has frequencies in a range of 200-700 Hz (Figure 3.36).

Table 3.13 Sweep parameters.

Sweep Types	Linear
Start Frequency	100 Hz
End Frequency	700 Hz
Sample Interval	0.5 ms
Sweep Length	3850 ms
Taper Type	Cosine on both ends
Filter	1000 Hz high frequency; 96 dB/octave slop

Table 3.14 Synthetic sweeps parameters used for lab correlation.

Parameter	100-700	200-700	200-700
Delay time (ms)	0	0	642
Start time (ms)	0	0	642
End time (ms)	3850	3208	3850
End tapers (ms)	100	100	100
Result	100-700 Lab Corr.	--	200-700 Lab Corr.

Figure 3.36 Graphical presentation of 100-700 Hz, 200-700 Hz and 100-700 Hz with time delay sweeps.

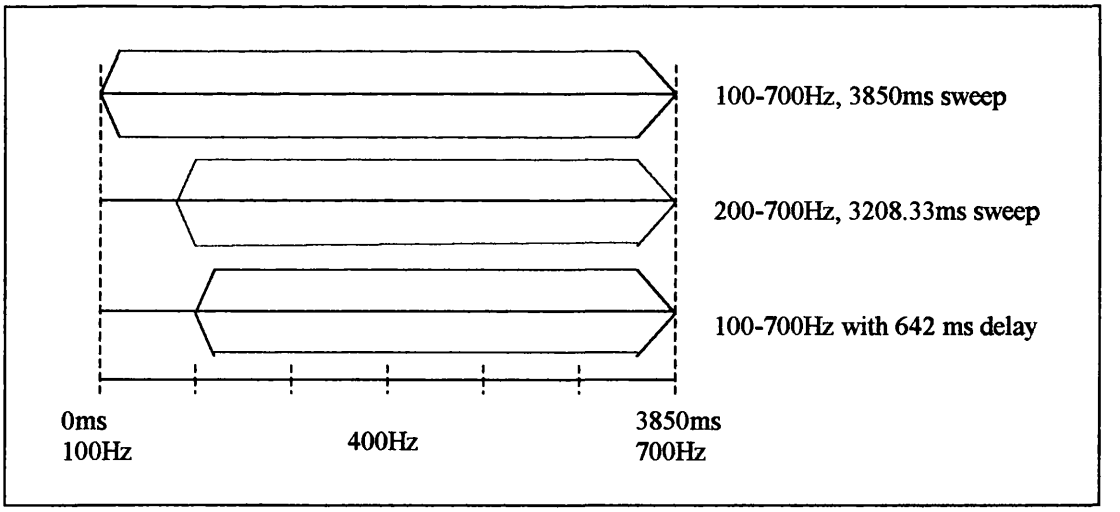

Comparison between field and lab correlated data

Figure 3.37a, 3.37b and 3.37c shows the quality of the field correlated data compared to the 100-700 Hz lab correlated and 200-700 Hz lab correlated data. Each figure has three panels of the same shot gather representing the results of three different correlation methods. The left panel represents the result from the OYO field deconvolution process, while the middle and right panels show the output from the 100-700 Hz and 200-700 Hz lab correlated processes, respectively.

The field correlated dataset shows a different polarity compared to the lab correlated datasets. From the polarity comparison in 2-D of the 100-700 Hz lab correlated vibroseis data and the impulsive datasets, the polarity of the lab correlated vibroseis data was same as the polarity of the impulsive datasets. For that reason the field correlated dataset has been reversed in polarity in the displays of Figures 3.37a, b and c.

Figure 3.37a shows the first 48 channels for shot 401, which represents the typical characteristics of data from small offset (2-15 m) gathers. Figures 3.37b and 3.37c on the other hand show the qualities of the first 48 channels for the shot 101 and shot 51 respectively, which represent typical traces at intermediate (15-30 m) and far (>25 m) offsets. The chevron effect that appears on all shot gathers is the result of the receiver swath geometry where the source-receiver offsets varying up and down the six-column spread (see Figure 3.14 above).

The effectiveness of all the correlation methods can be discerned partly by analysing the relative quality of the air blast on the three panels. As it is a coherent signal, the convolution process in theory should enhance this signal as it enhances the reflection signals; however the field correlation datasets show the air blast in the left hand panel of Figure 3.37c is very poor compared to that on the other two (lab correlated) panels. This effect is less seen in near offset gathers (Figure 3.37a) as it is masked by early arrival signals.

Figure 3.37a Raw shot gather for very shot offsets (2-15 m) correlated in three different ways.

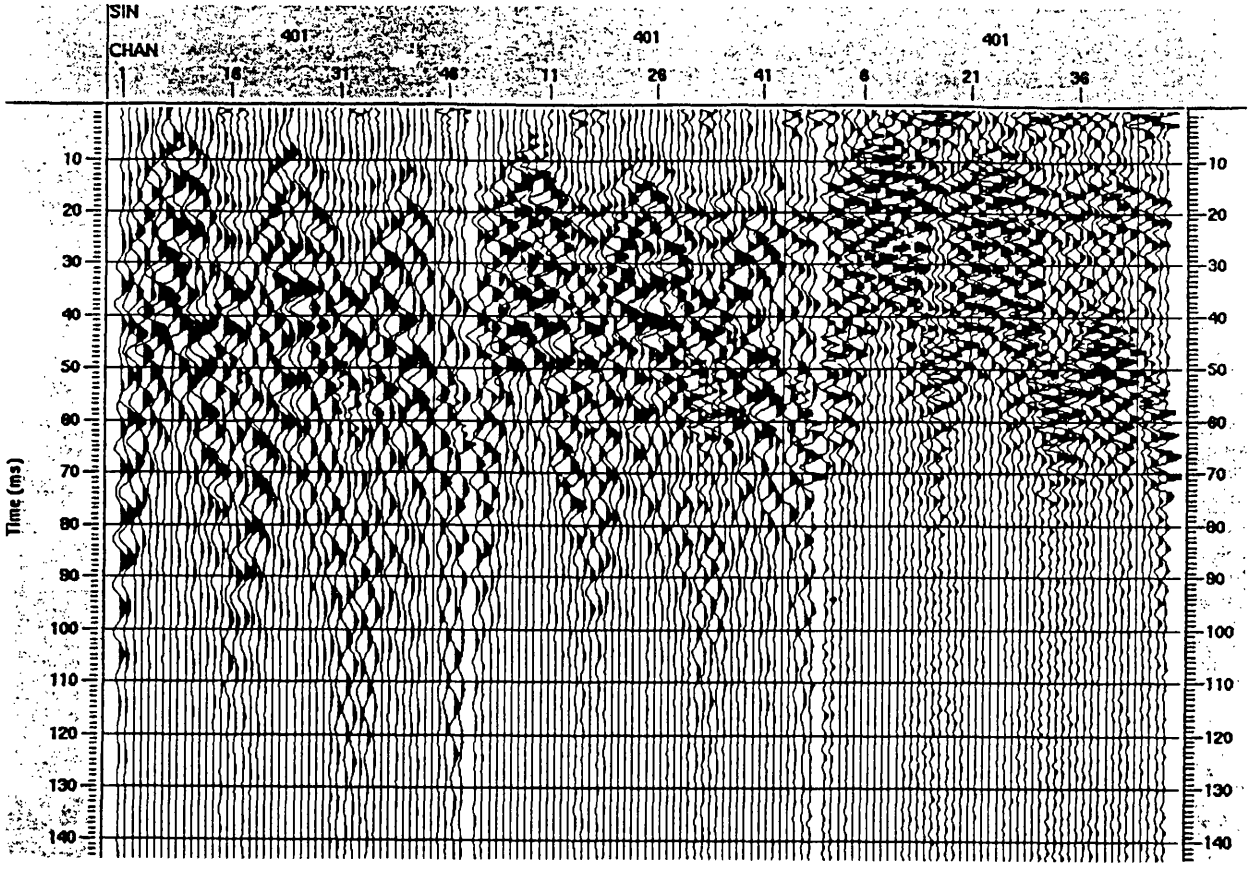

Figure 3.37b Raw shot gather with medium offsets (15-30 m) correlated in three different ways.

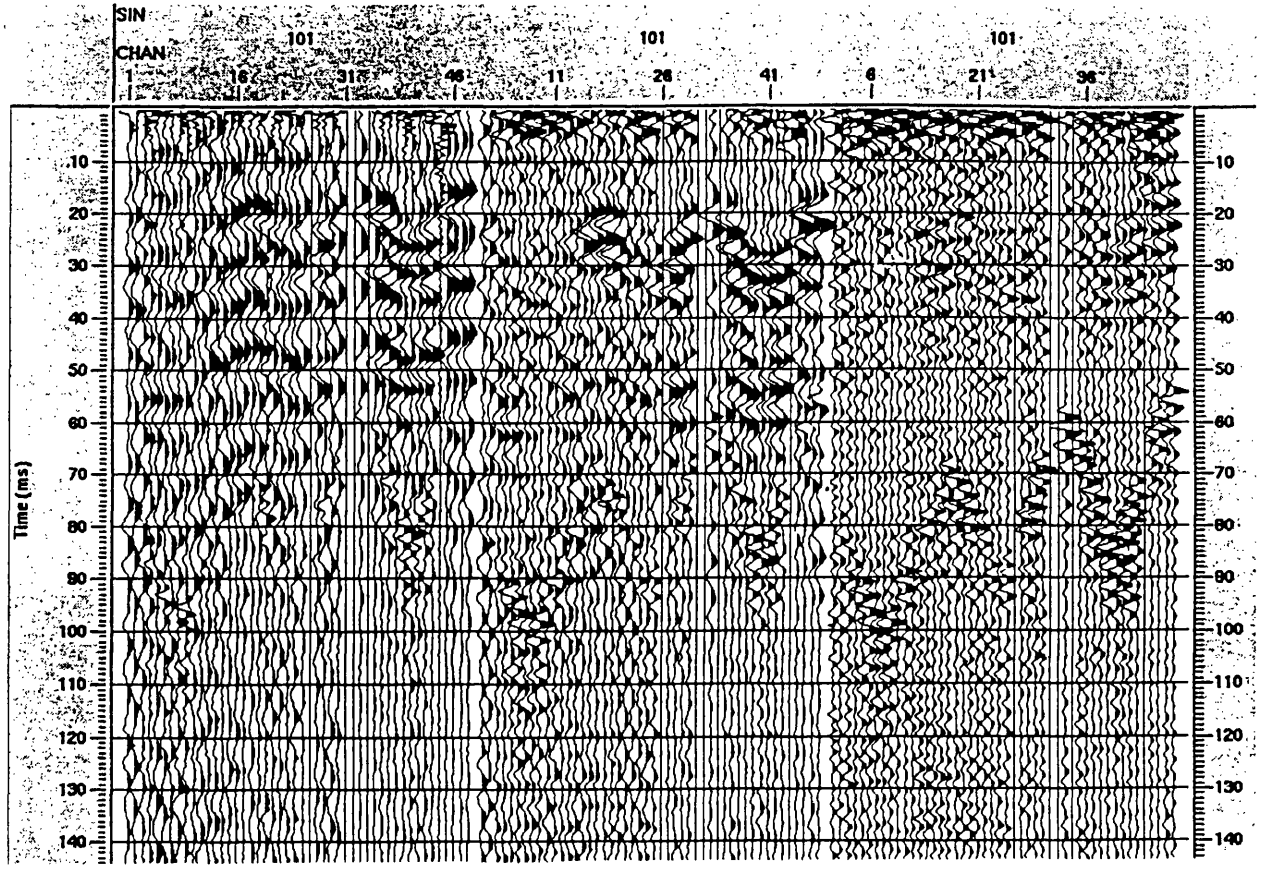

Figure 3.37c Raw shot gather with long offsets (>25 m) correlated in three different ways.

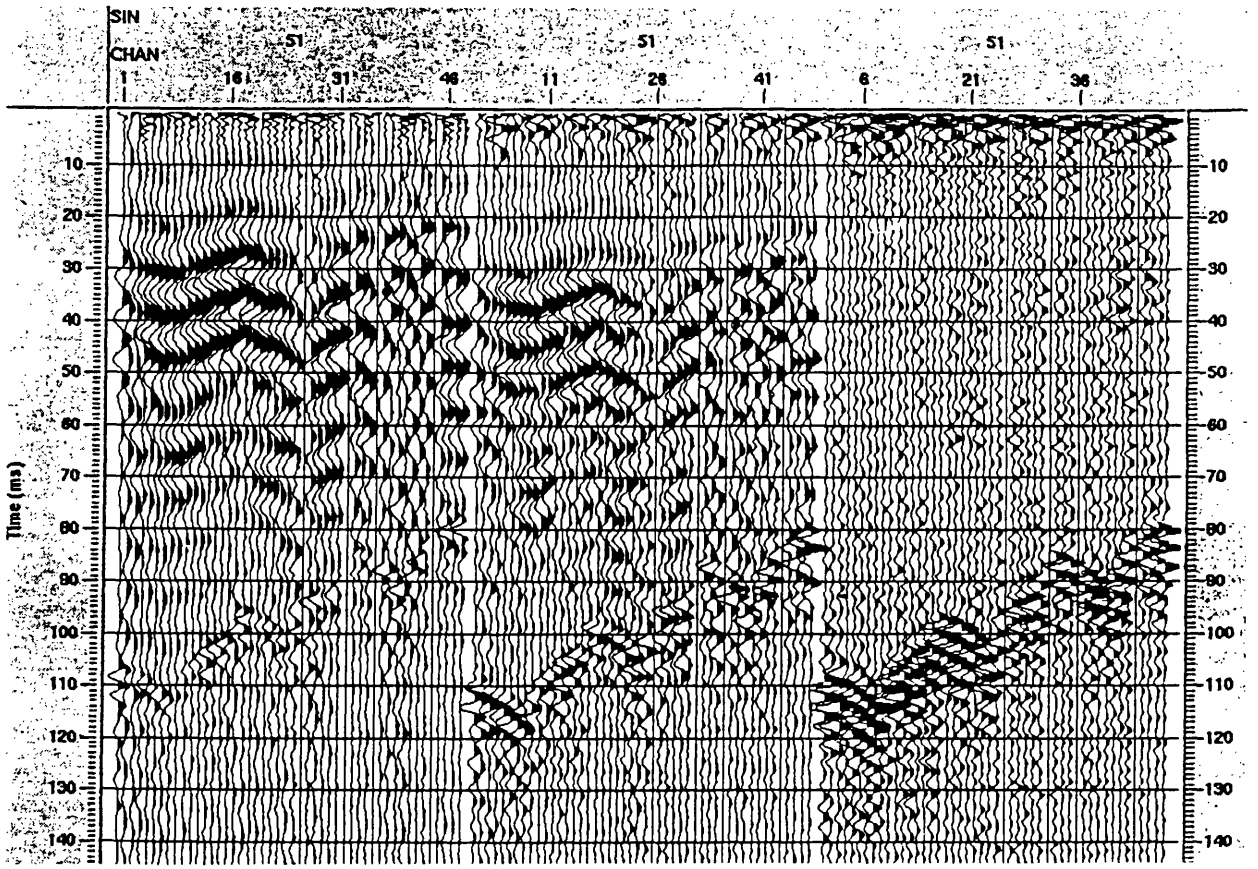

From the air blast effect, we can conclude that the weighted sum of the two accelerations as input to a convolution operator for correlating the vibroseis data is possibly unstable. Because of this, it was decided not to use the field correlated data in any subsequent processing.

Field correlated data are very ringy and dominated by low frequency signals. The figures also show that most of the low frequencies are filtered out from the record when the data are correlated using 200-700 Hz synthetic sweep (Figure 3.37c). The interesting effect from this 200-700 Hz correlation is that the first arrivals (from near offset traces) are very sharp (Figure 3.37a). These results suggested that for near offset processing the highest resolution might be obtained by using 200-700 Hz correlated dataset.

Processing strategies

In order to obtain the best result as possible, both 100-700 Hz and 200-700 Hz lab correlated data were used. The 200-700 Hz lab correlated dataset was processed first. For this data, only the short offset traces were used as the 200-700 Hz. correlated data show a very sharp first arrival (from near offset traces, Figures 3.37a, b, and c). Furthermore, for the long offset traces, the returned signals were very weak and contaminated by random noise. The reflection signal is curving with the offset. The longer the offset, the better the hyperbola that can be observed. The problem with using only near offset traces (as in first approach) is that it is very difficult to differentiate the reflection from the refraction signals, as both appear straight. This may create a problem during the stacking as the refraction signal is assumed to be a reflection signal.

To overcome these uncertainties, longer offset traces were considered for the second approach. However, because the returned signal was very weak and hardly seen in 200-700 Hz shot gathers, the broader range of frequency dataset (100-700 Hz) was used.

Pre-processing

Processing the 3-D data is not fundamentally different from processing the 2-D data. For example, the data need to be labelled with their appropriate FFIDs prior to any processing, then editing bad traces or removing unnecessary or problematic files based on the Observer's logsheets and visual inspections is a task that has to be done. Other processes, such as geometric spreading correction, elevation statics, and data enhancement need to be applied to all seismic reflection data. Basically, almost all the concepts of 2-D seismic data processing apply to 3-D data processing.

Complications in 3-D data processing arise in geometry quality control, statics, velocity analysis and migration (Yilmaz 1987). Unlike in 2-D, where the data are acquired using a linear spread, the 3-D data is acquired in an areal mode spread, in this instance with randomised source locations. This leads to differences in CMP sorting.

The 3-D CMP binning concept is essentially the same as in 2-D processing. However the traces in a 3-D CMP bin have different azimuths. This leads to difficulties in analysing the velocity for NMO stacking, especially in areas where lateral velocity changes are present.

Editing and geometry assignment

The first task before any processing was carried out was to add the correct FFID (field file identification number) to each file. This FFID number is unique, based on the Observer's logbook. Besides referring to notes in this logbook, like the 2-D data, the 3-D data were also visually checked to identify any previously un-noticed bad or reversed traces. These bad traces and any other irrelevant data (such as noise tests) were edited out prior to any processing. The reversed traces were also corrected to their correct polarity.

Before the geometry was assigned to the traces, any discrepancies in shot location must be corrected. This is a very important step in this 3-D survey, since the sources were placed in pseudo-random positions. For that, the shot positions (determined from the randomised table) were sighted using the theodolite after the shots had been taken.

Checking the source locations was done by making detailed GMT maps of the proposed location (from the randomised table) and the actual location (surveyed after the shot had been taken) as shown in Figure 3.38. In most cases the discrepancies between the proposed (from table) and actual (surveyed) position are very small, however in some cases there were also big discrepancies such as in column 12 of Figure 3.38. For such big discrepancies, checks on shot location (to find which one is correct) were done by examining the air blast travel times (and hence shot-receiver distance at the constant velocity of 330 m s^{-1}) on the correlated data. Figure 3.39 shows the entire corrected survey source positions as vectors from the peg to the actual shot.

After the survey information had all been corrected, this geometry information was then loaded into the ProMAX database and then applied to the seismic data. From this stage onwards, every seismic trace carries the geometry information in its trace header.

Binning

Figure 3.40 shows all the source-receiver midpoints. They are so abundant in most of the survey area that they turn the diagram solid black. The one gap (white area) in the middle of the survey area was a result of the spread shifting due to an unavoidable obstruction (drilling rigs). A grid of 2 m square bins was defined and fitted as a uniform grid to the dataset (Figure 3.41a). The binning grid azimuth was defined to be the same as the surface geometry azimuth, although the subsurface grid could have been aligned in any direction. Details of the binned CMPs are shown in Figures 3.41b and 3.41c where the former shows bins at the southern edge with few CMPs in each, while the latter shows central bins with a very high fold of coverage.

Figure 3.38 Detail of offset vectors.

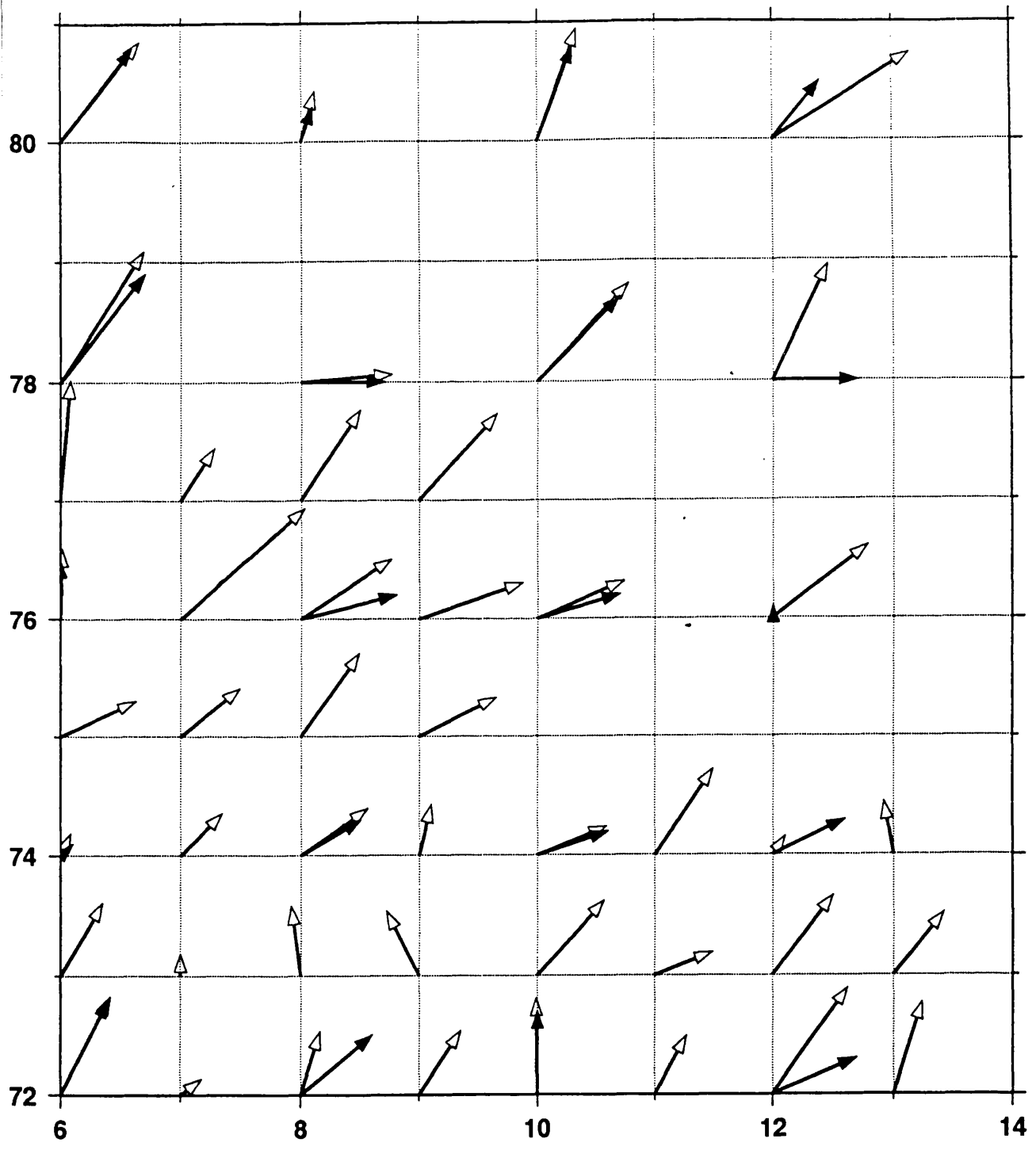

The black arrow vectors are the randomised positions from the table while the white arrow are actual source positions as surveyed after the shot

Figure 3.39 All corrected source vectors.

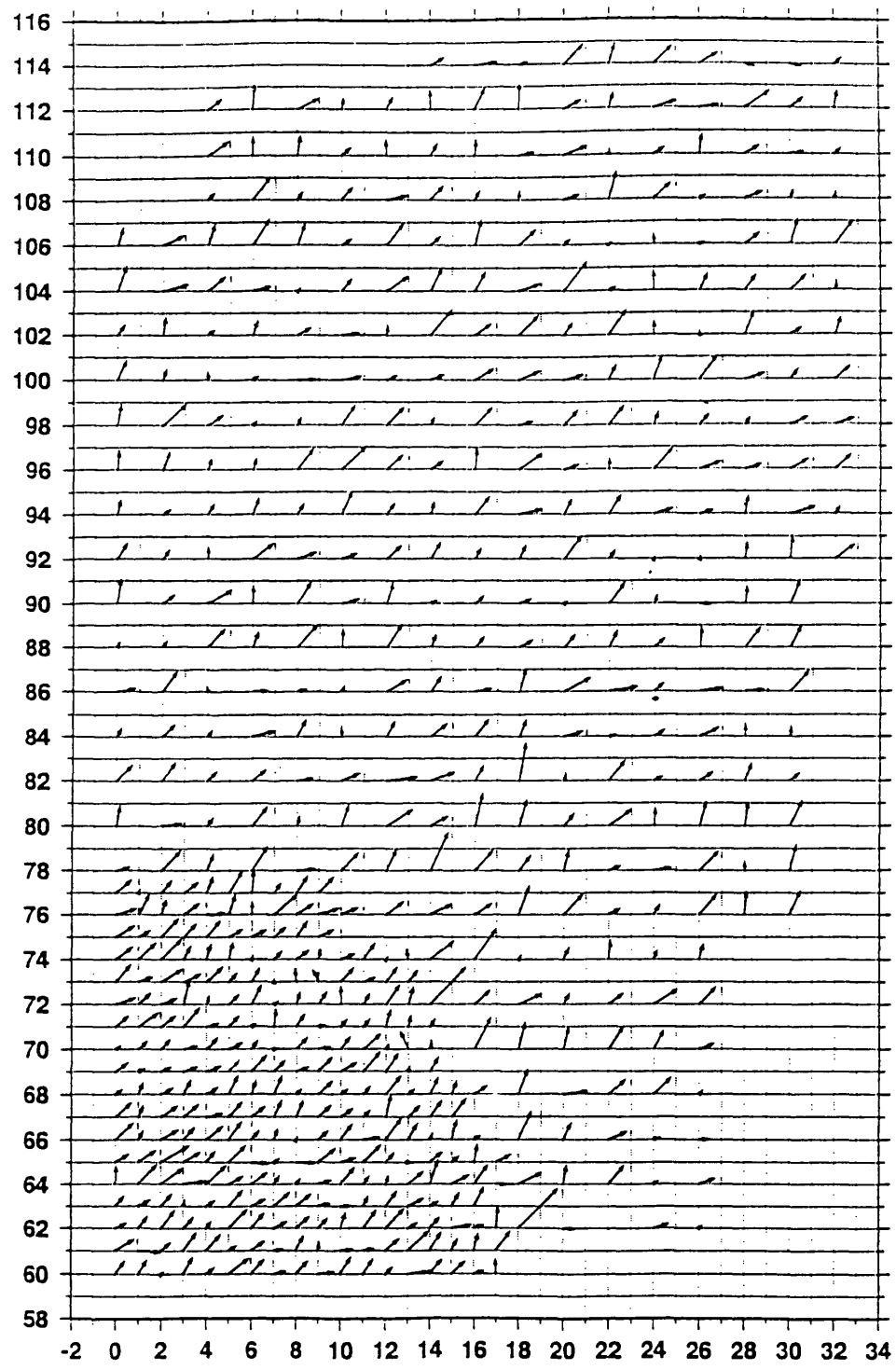

The arrowheads represent the position of the source.

Figure 3.40 CMP coverage map.

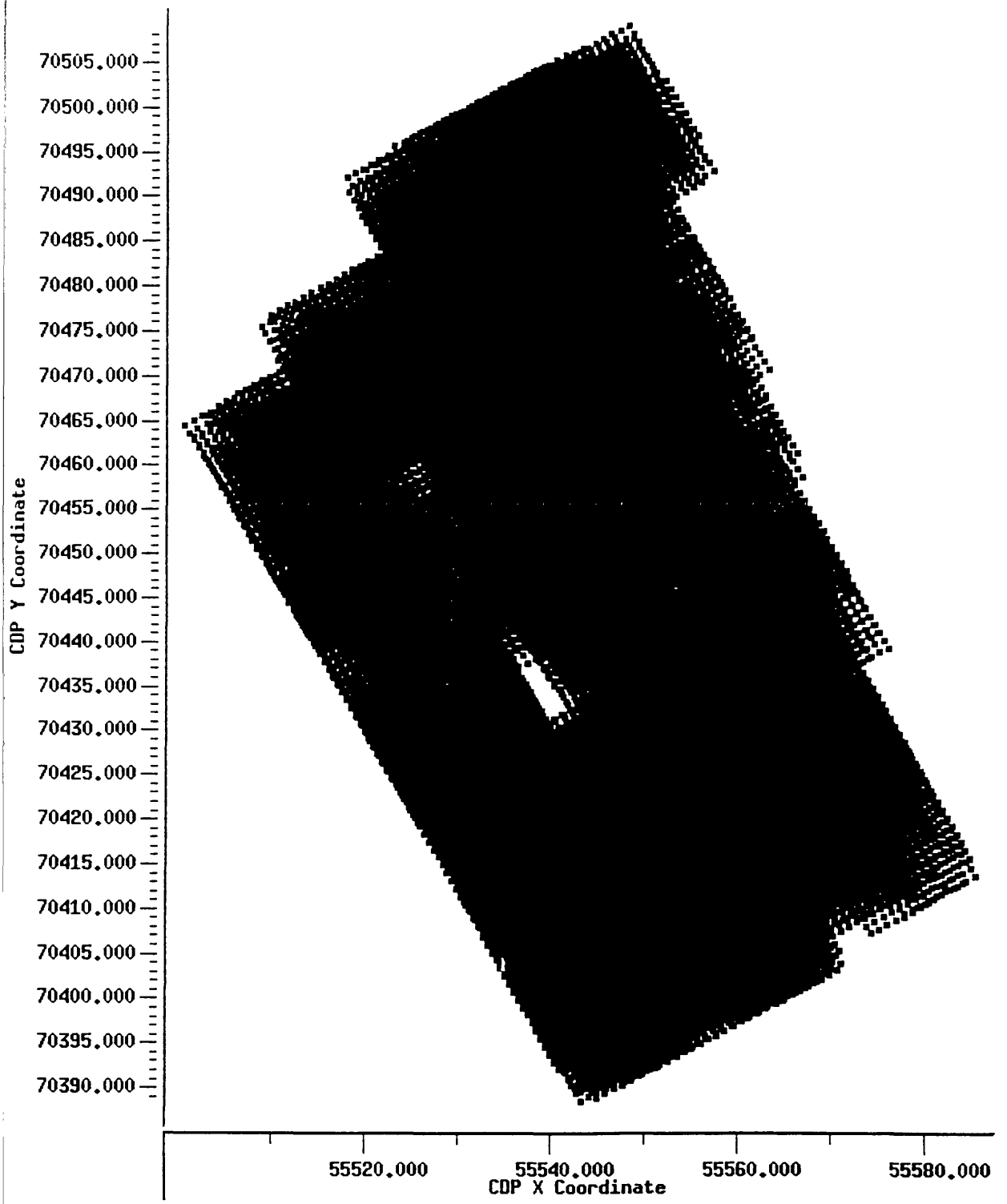

Figure 3.41a CMPs with 2 m binning grid overlain.

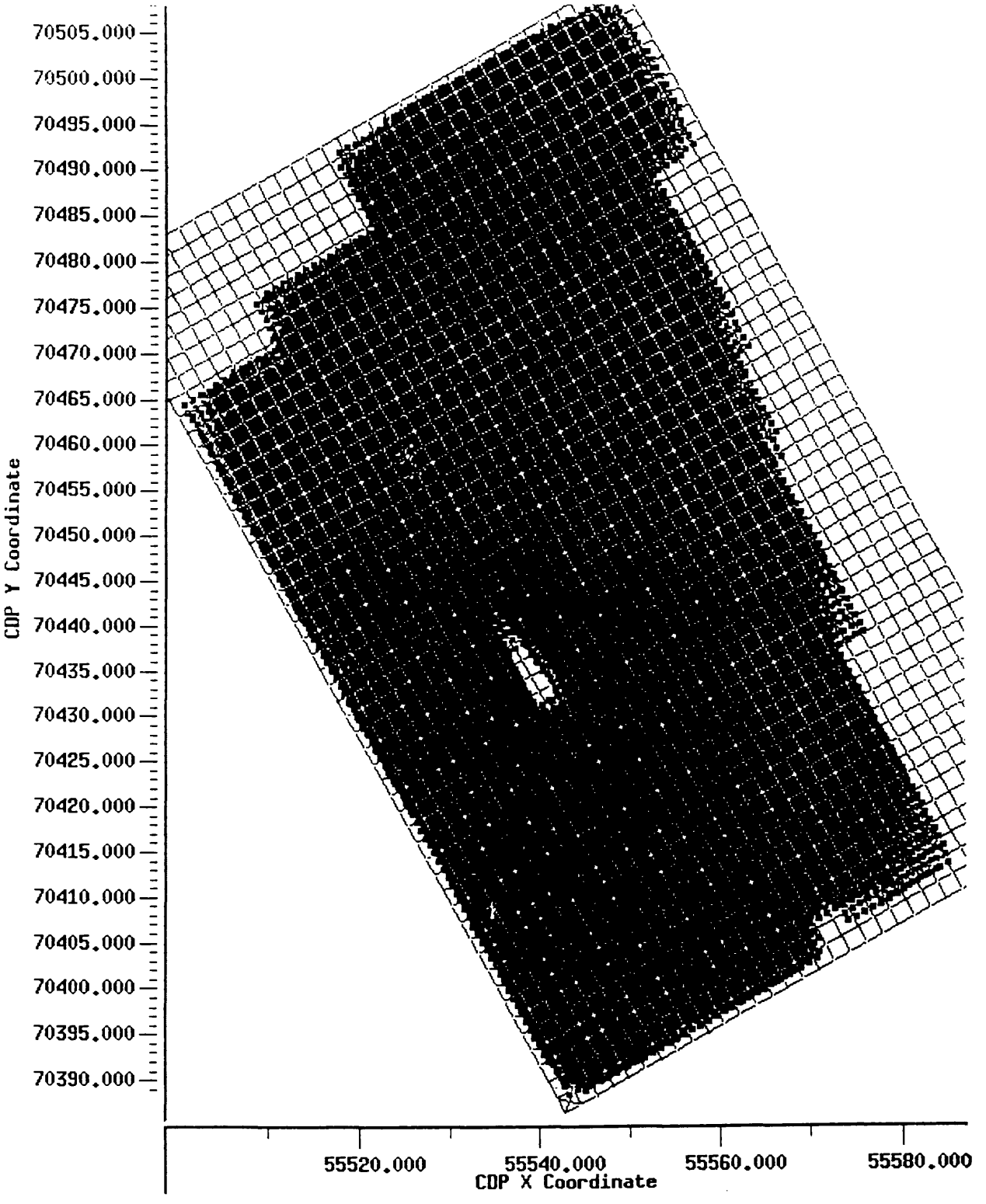

The grid is laid parallel to the surface column and row directions.
In this way it minimises the occurrence of empty bins.

Figure 3.41b Detail of binned CMPs at southern edge of survey.

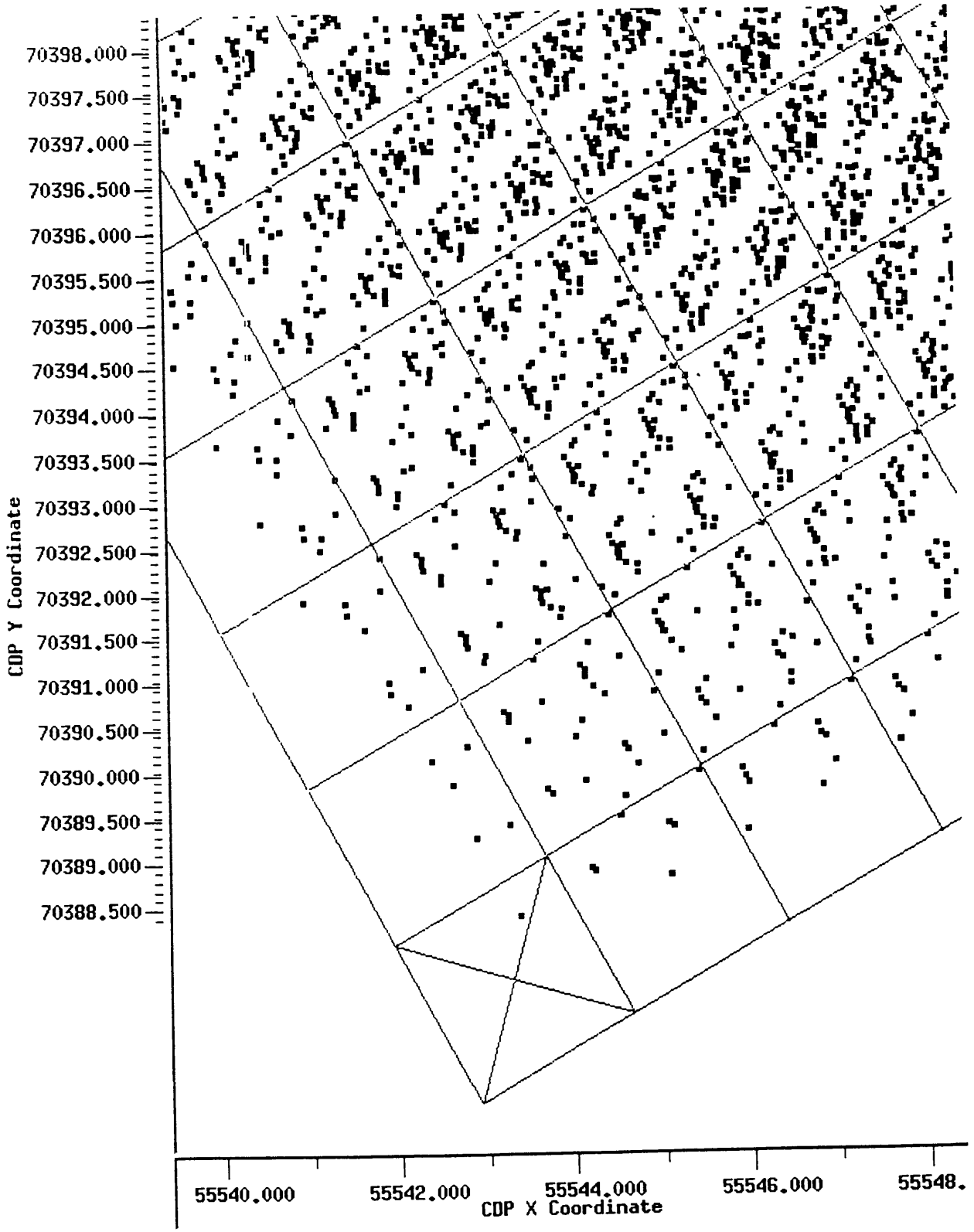

Figure 3.41c Detail of binned CMPs from centre of survey.

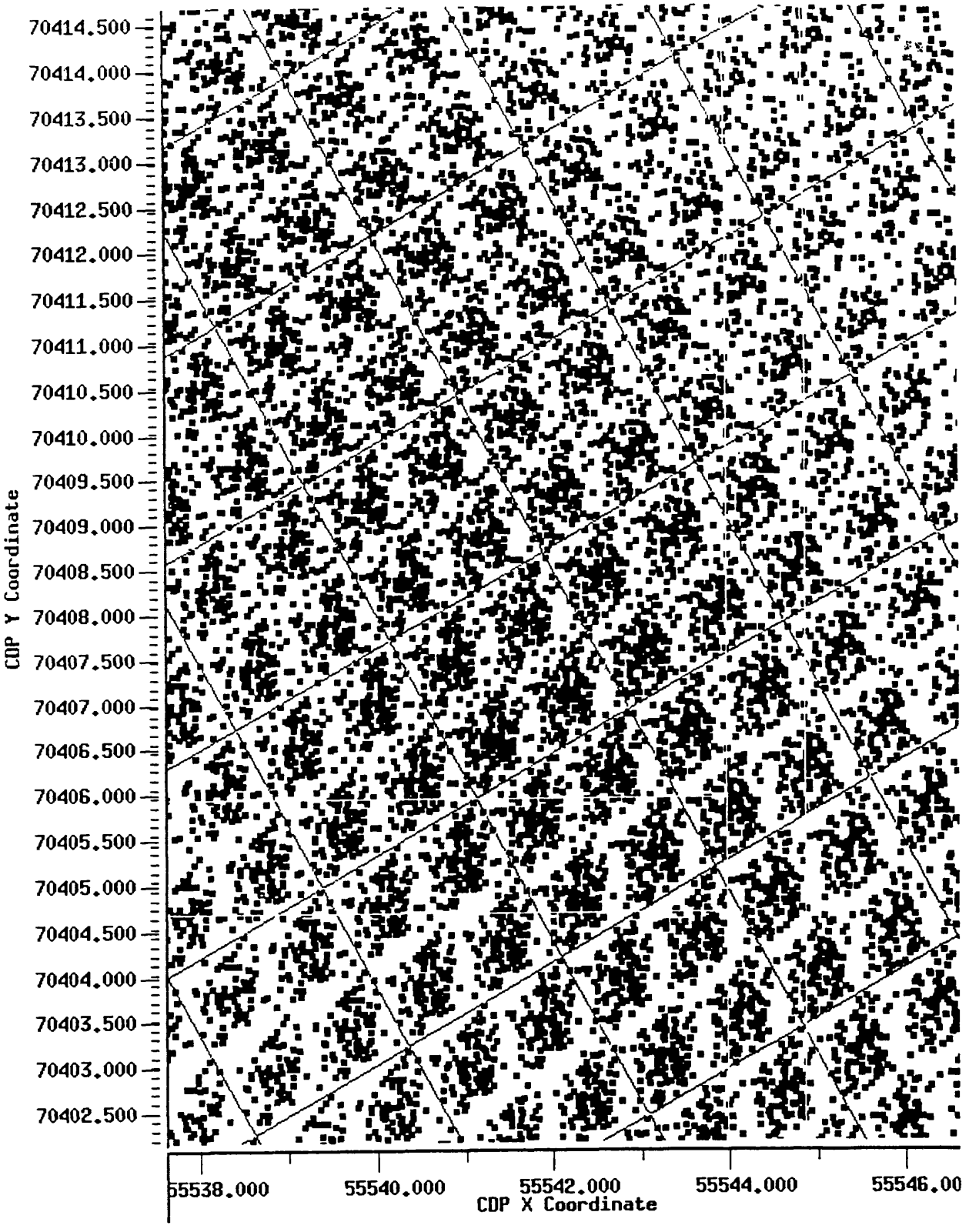

Fold of coverage

Figure 3.42a summarizes the fold of coverage (in plan view), whereas an isometric view is shown in Figure 3.42b. The fold of coverage ranges from a minimum of 1 to extremely high, as high as 570 fold. The exceptionally high value of 570 fold is achieved at two peaks in the lower left corner where the 2 m source spacing was used instead of 4 m spacing. The total number of bins is 53x33 or 1749, with the mean fold coverage being about 80 fold. This is a very high figure compared to 3-D surveys even in petroleum exploration. A summary of the statistical figures for the 3-D data is given in Table 3.15.

Table 3.15 3-D vibroseis data statistics.

Total no. of shots	979
No of receivers per swath	144
Total no. of traces	140976
No. of 2x2 m grid bins	53x33 =1749
Average no. of traces per bin (fold)	80.6

Figure 3.42a Fold of coverage in plan view.

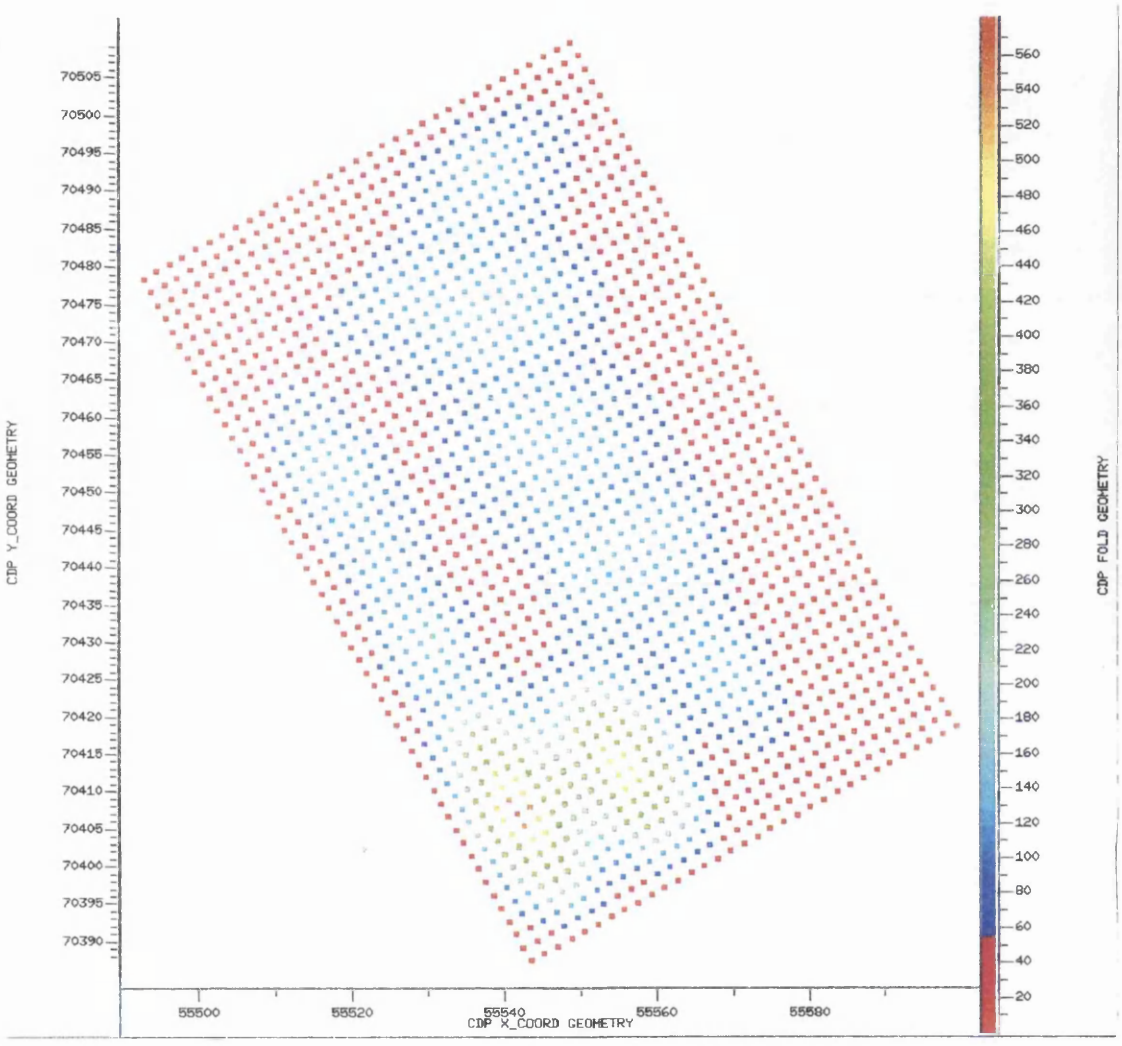

Figure 3.42b 3-D view of fold of coverage.

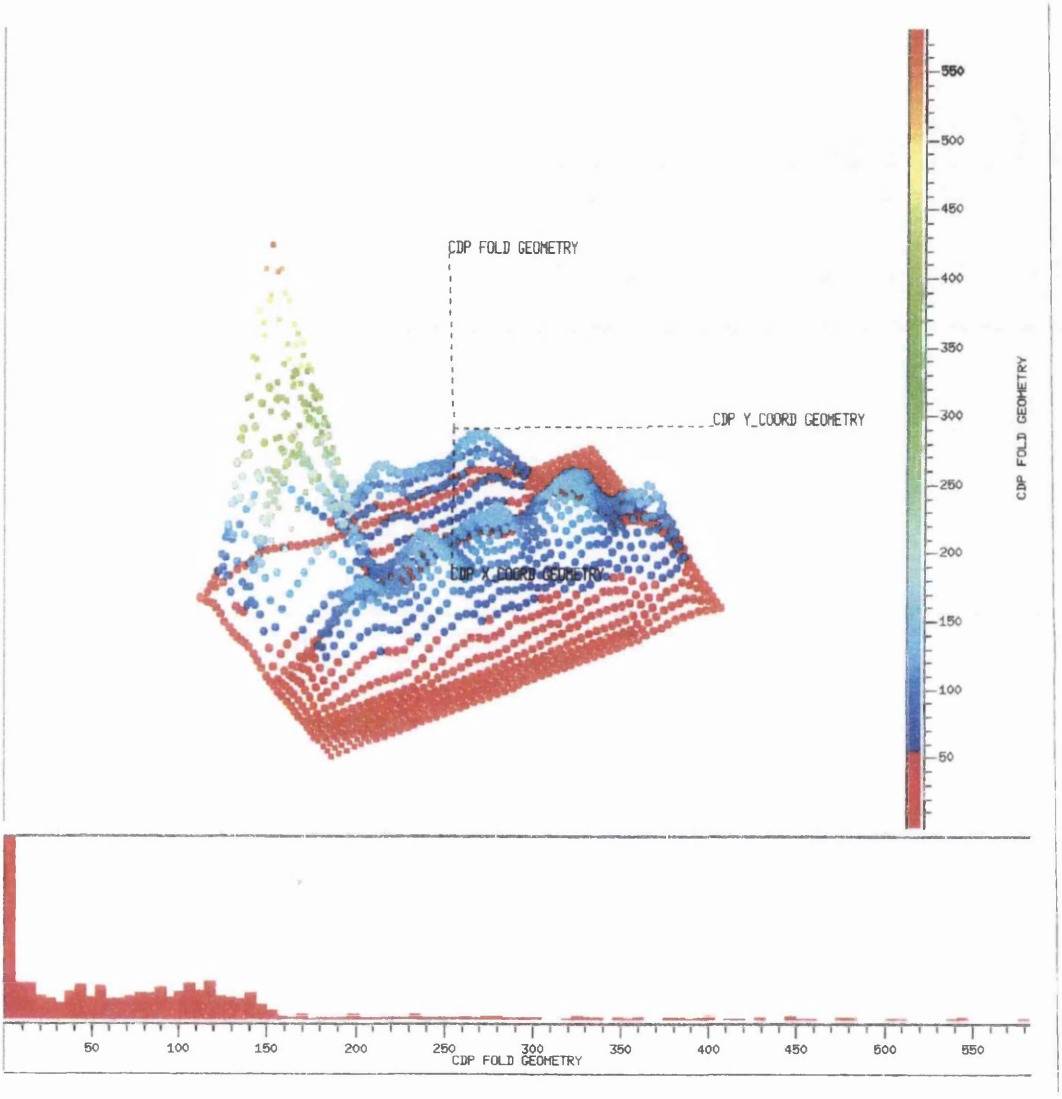

Peak corresponds to the area where dense data were collected.
The average fold is 1-150 although some bins reached 550 fold.

Processing - approach-I

As the aim of this work was to image the shallow underground tunnels as well as the shallow geological conditions, high-resolution data are really important. Therefore the 200-700 Hz lab correlated dataset was used instead of 100-700 Hz lab correlated dataset. By using the higher frequency range dataset, it was hoped that the smallest possible reflection times could be resolved, which would be very useful in mapping the base of the boulder clay (top bedrock surface) at 3-6 m depth. In this approach, the data were reversed in polarity to match the polarity of the field correlated data. It was only discovered subsequently that the polarity of the lab correlated dataset has the correct polarity, based on the analysis of the impulsive 2-D datasets discussed in section 3.10.2 above.

Instead of using all the traces, only small offset (<5 m) traces were used. This was due to the fact that in far-offset traces, the returned high frequency energy was very weak and was hardly recognised in the gather. To ensure only reflected arrivals were stacked, and to avoid any possibility of stacking refracted arrivals, a severe front-end trace mute was applied to the data (Figure 3.43).

This approach also had the aim of not degrading the source wavelet, hence no deconvolution was applied to the data (since the deconvolution only works optimally if the data are minimum phase). However in order to enhance the frequencies of likely use, 200-500 Hz spectral shaping was applied. Spectral shaping keeps the phase of the wavelet unchanged while increasing the amplitude of the frequencies specified.

Because only near offset traces were used and no reflectors were visible in the deeper section (later times), the data were stacked using a single stacking velocity of 350 m s^{-1}. This value is the velocity of first layer (overburden) as given in the refraction analysis (Figure 3.25). A summary of the processing flow used in this approach is given in Table 3.16.

Figure 3.43 Raw (left) and pre-processed data (right) showing severe front mute applied in approach-I.

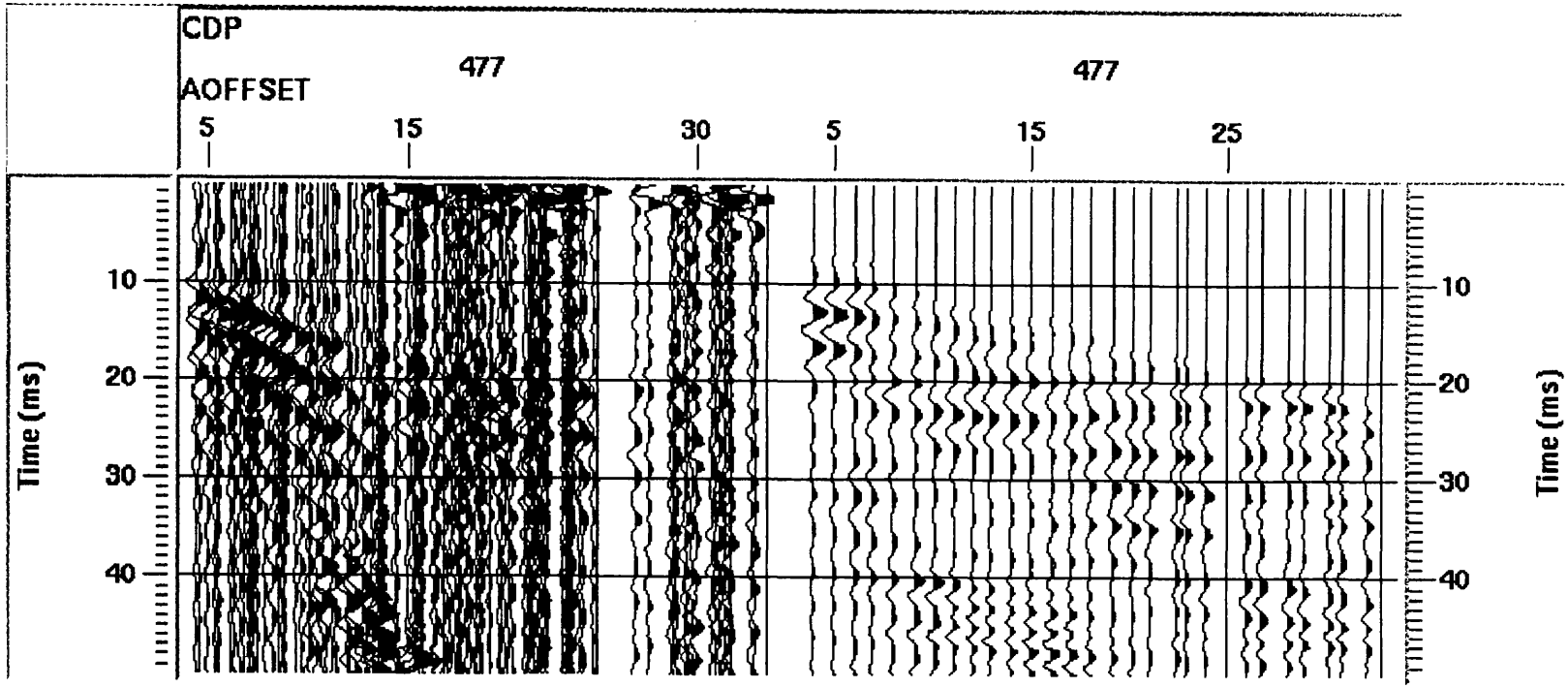

Table 3.16 Approach-I processing flow.

Data	200-700 Hz Lab Correlated 0-50 ms time <5 m offset only reversed polarity (matches the field correlated polarity)
Elevation Static	Datum 37 m; replacement velocity 350 m s^{-1}
AGC	20 ms centred windows
Spectral Shaping	200-500 Hz
NMO / Stack	Constant velocity stack at 350 m s^{-1}
AGC	10 ms centred windows
Pad stack volume	
Output	

Approach-I: results and comments

Since the polarity of the data was reversed, a positive impedance contrast is represented in displays by a black peak. The results of this approach are shown in Figure 3.44a, where it represents a pair of typical sections – inline I33 and crossline X16 from the data volume. There are no clear indications of any reflector, however there is one fairly continuous signal at a very early time (<20 ms TWT). This is interpreted as the base of clay or the top of the bedrock. This reflection wavelet is clearly made up of peak – trough – peak – trough – peak, spanning 10 ms. Thus the dominant frequency is about 200 Hz.

The geology of the site is very simple, a glacial deposit un-conformably overlying gently dipping Carboniferous rocks. The velocity of the overburden is less than the velocity of the bedrock, which means the reflecting interface has a positive impedance contrast, marked by the black peak. The central peak was picked as the top bedrock reflector and marked by a red circle (Figure 3.44b). The picks are very jittery, indicating a low signal to noise ratio.

The contour map of the bedrock horizon is shown in Figure 3.45. The time on the map is represented as un-migrated TWT (two way time). The values range from 6 ms to about 18 ms and a division by 3 gives an approximate depth in meters below the datum of 37.0 m. Thus the depths vary from about 2 m to about 6 m below the datum.

Figure 3.44a Sample inline and crossline sections – approach-I.

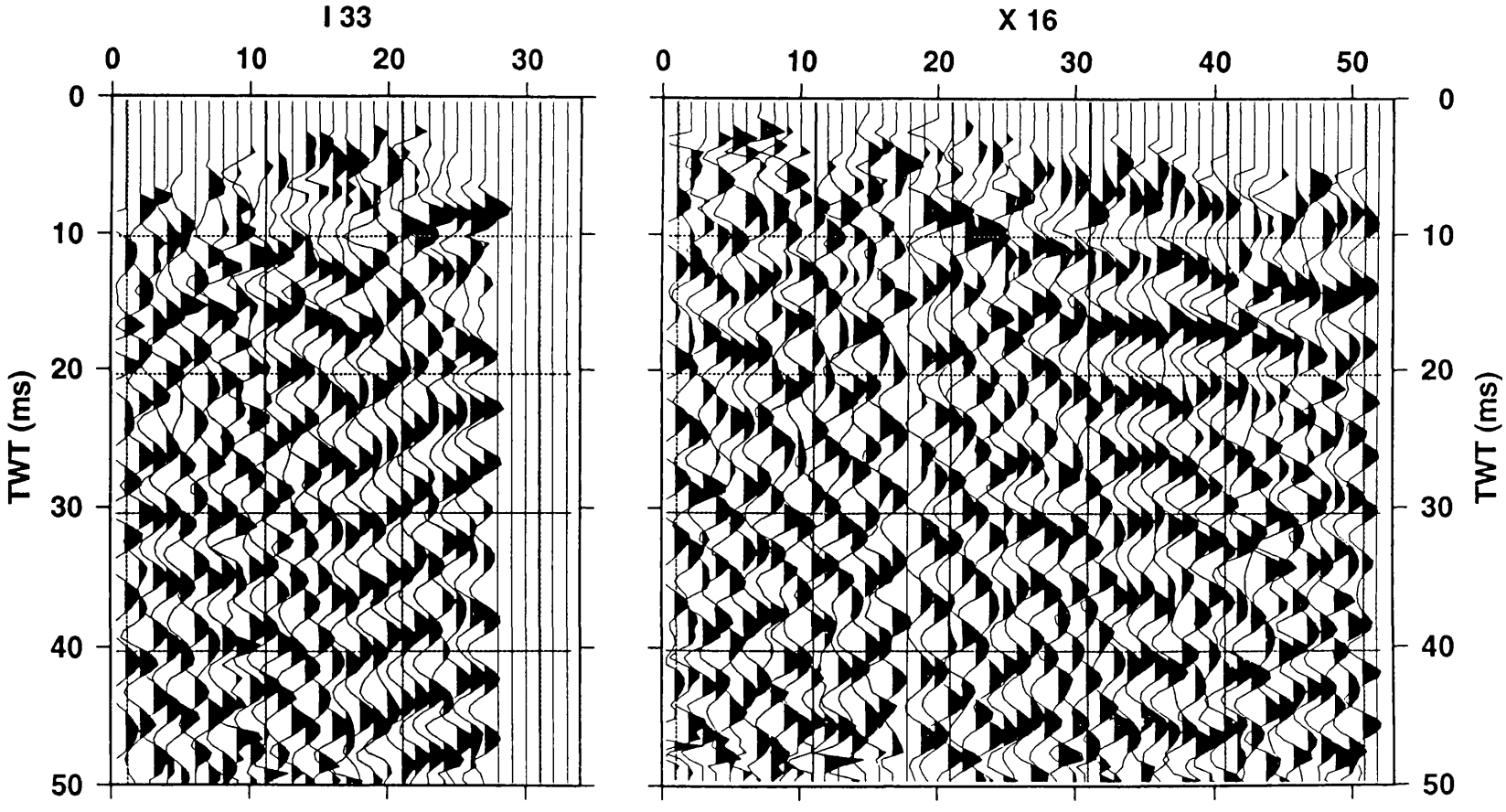

Figure 3.44b Sample inline and crossline sections – approach-I (interpreted).

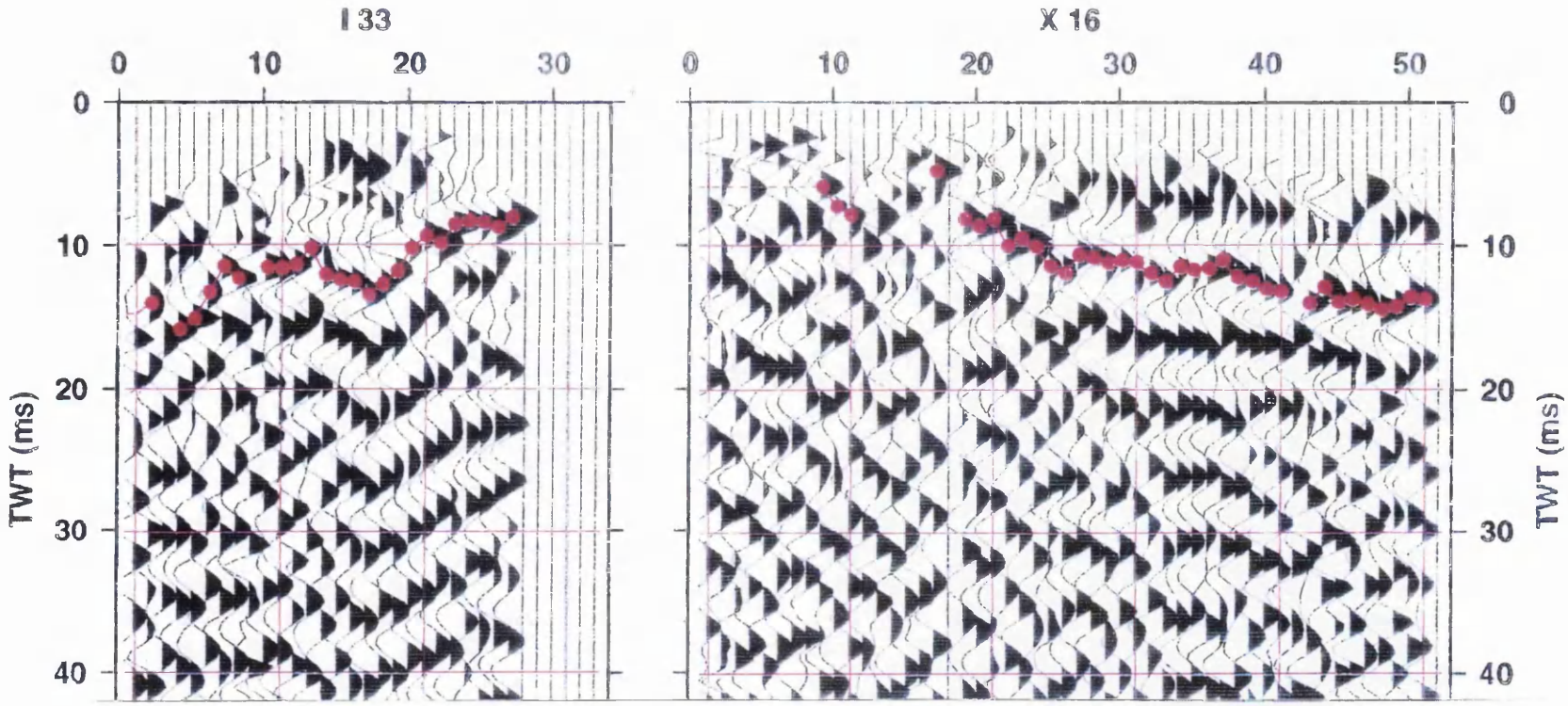

Red dots mark the interpreted base of the boulder clay.
The polarity is reversed, which is why a peak and not a trough is picked.

Figure 3.45 Contour map of base of clay horizon based on approach-I results.

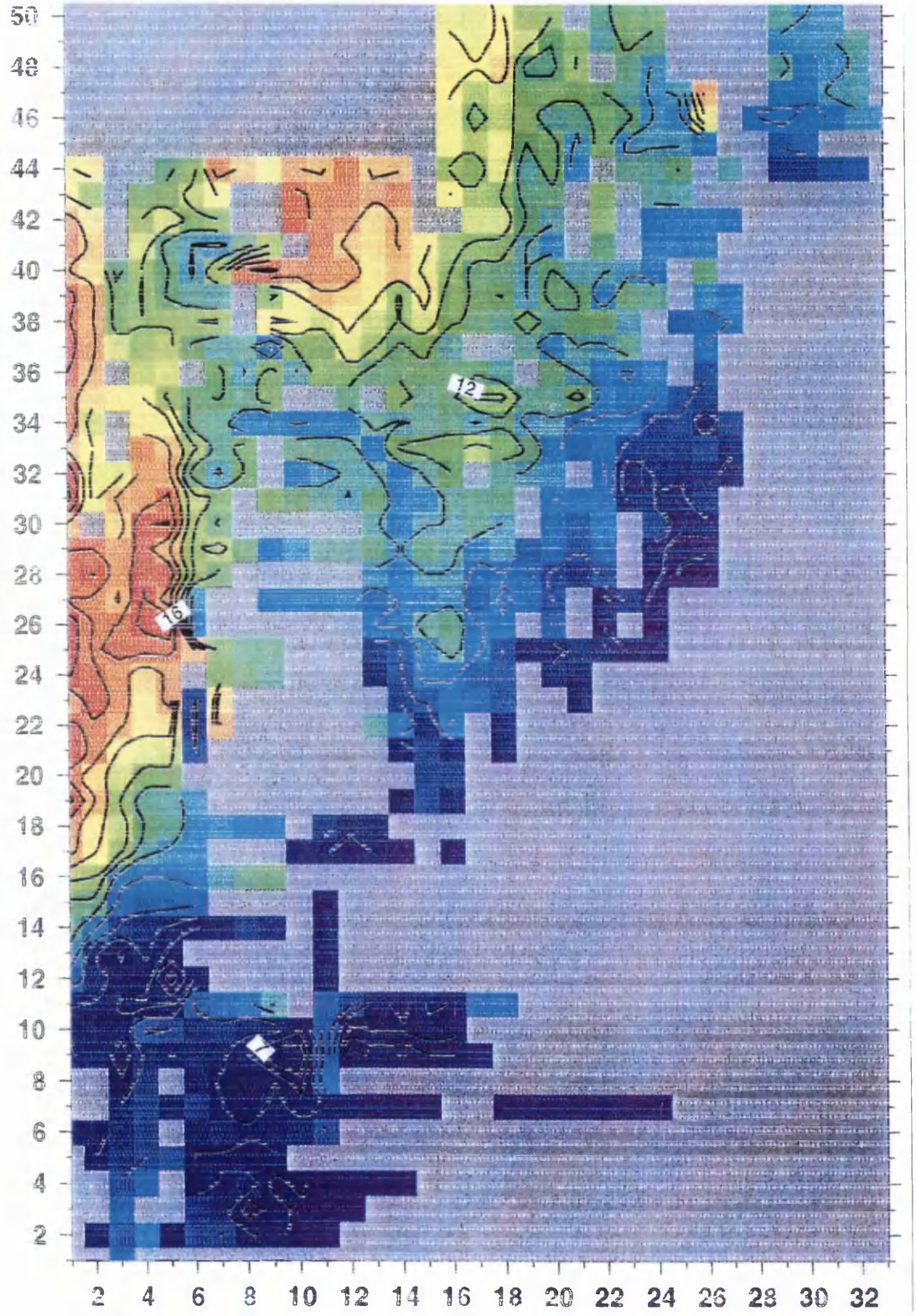

Contour interval 1 ms TWT. Dark blue – 6 ms, Dark orange – 18 ms, grey –no pick.

Processing - approach-II

Unlike the first approach where the aim was to image the very shallow clay/bedrock interface, this second approach aimed to image the deeper section. For that the broader bandwidth dataset (100-700 Hz Lab Correlated) was used. It also decided to use the whole 150 ms long trace, as hopefully some deeper structure would be imaged.

In this approach, the polarity of the data is kept as recorded, so the positive impedance contrast is now represented as a white trough instead of black peak as in approach-I. The long offset traces are also used instead of short offset traces as in approach-I. In order to correct the topography errors, an elevation static correction with 37.0 m datum and 350 m s^{-1} replacement velocity was applied to the data.

Like the first approach, spectral shaping was applied to whiten the zero phase vibroseis wavelet. This process retains the zero phase character while at the same time scales up all frequency components within the desired window to the same amplitude. The air blast and later arrivals were muted from the data. The first arrivals were not muted in order to keep any early reflections arriving soon after the refracted first arrivals (Figure 3.46). To avoid stacking the refracted signals as if they were reflections, a low stacking velocity at early times was used. For that, a 1-D velocity function (listed in Table 3.17) with 60 % NMO stretch was used.

Table 3.17 1-D time velocity pairs used for NMO stack in approach-II.

Time (ms)	Velocity (m s^{-1})
0	350
10	800
20	1200
50	1500

The stacked section was padded with zero traces to produce 52 inlines and 33 crosslines before they were migrated and transferred to GMA-plus for interpretation. Table 3.18 lists the processing flow for this approach.

Figure 3.46 Raw (left) and pre-processed data (right) showing only bottom mute applied in approach-II.

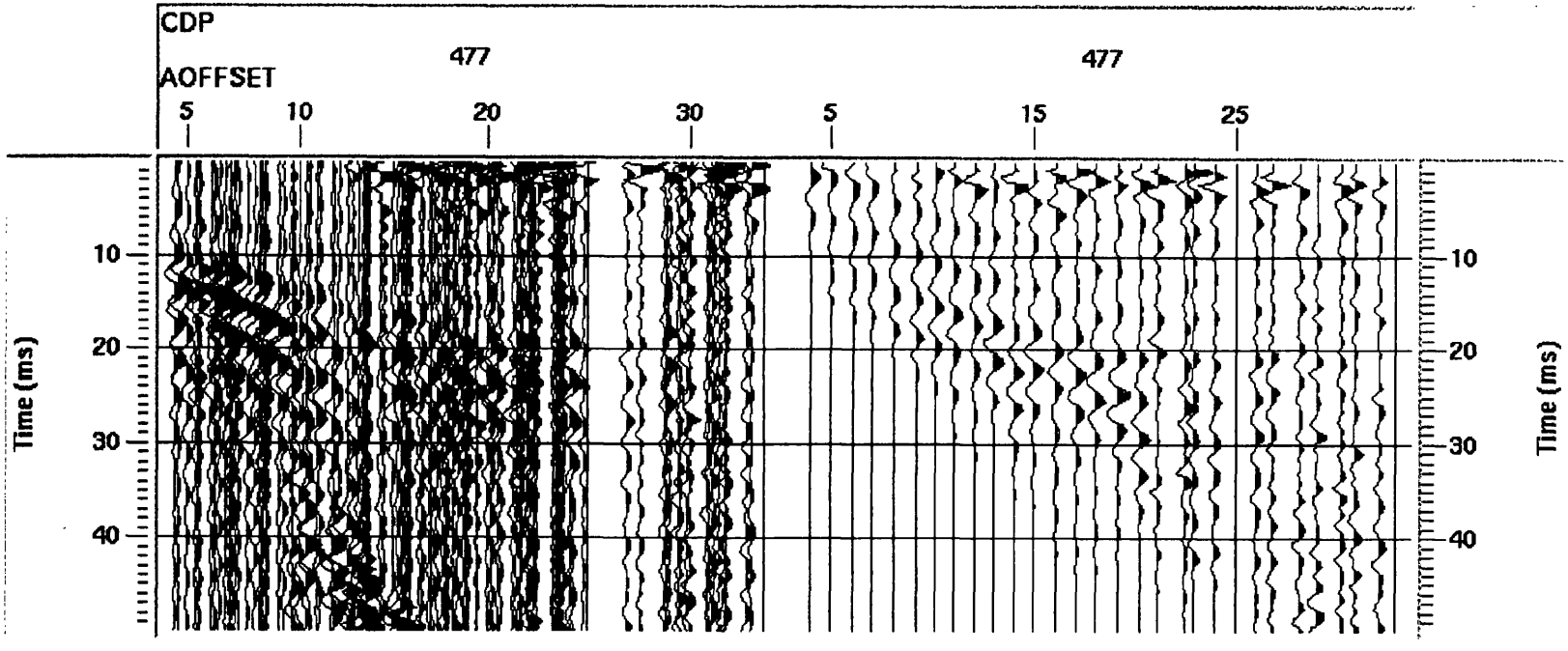

Table 3.18 Approach-II processing flow.

Dataset	100-700 Hz Lab Correlated, 0-150 ms
Elevation Static	Datum 37.0 m; Replacement velocity 350 m s^{-1}
Spectral Shaping	100-400 Hz
AGC	30 ms centred window
Muting	Air blast and later arrivals
NMO / Stack	1-D velocity function; 60% NMO stretch
AGC	40 ms centred window
Pad stack volume	
Migration	Kirchhoff time migration (same velocity as used in NMO stack)
Spectral Shaping	100-400 Hz

Approach-II: results and comments

Four examples of the vertical sections resulting from this approach are presented as two separate figures. Figure 3.47a shows examples of two inline sections - inline 17 and 29, while Figure 3.47b shows examples of two crossline sections - crossline 6 and 20. These examples reveal two reflectors between 5 ms and 30 ms TWT. A hint of deeper reflectors also appears in some inline sections.

Interpreted versions of the same four vertical sections are shown in Figure 3.48a and 3.48b. The first reflector is a very shallow strong trough and is picked as red circles. This reflector is picked as the shallowest identifiable consistent event. Because the data have a polarity corresponding to the SEG convention, the trough represents an increase in impedance contrast, or the boundary between the upper low velocity layer and the higher velocity layer below. This reflectors may represent the clay/bedrock interface. Figure 3.49 shows the migrated time structure map of this red horizon. Not surprisingly, it shows similarities to the map produced from the first approach (Figure 3.45).

The second identifiable consistent event is the strong peak just below the red picked trough. This reflector is marked by yellow circles (Figure 3.48a, Figure 3.48b). The black peak represents a negative impedance contrast, or in other words the upper medium has a higher acoustic impedance than the lower. A condition where such a reversed polarity event would occur is at the top of a water- or air-filled underground void. Thus the yellow reflector might represent in some form the old mine workings.

The overall structure of the mapped yellow horizon (Figure 3.50) shows a general deepening to the top right hand corner of the 3-D area, cut across by possible fault zones (or trough-like features) trending WNW to ESE. This strike is same as the strike of the Carboniferous bedrock below the overburden boulder clay. The yellow event reaches a maximum reflection time of 25 ms at the top right hand corner of the area, which corresponds to about 16 –17 m depth.

Figure 3.47a Samples from two inline sections – approach-II.

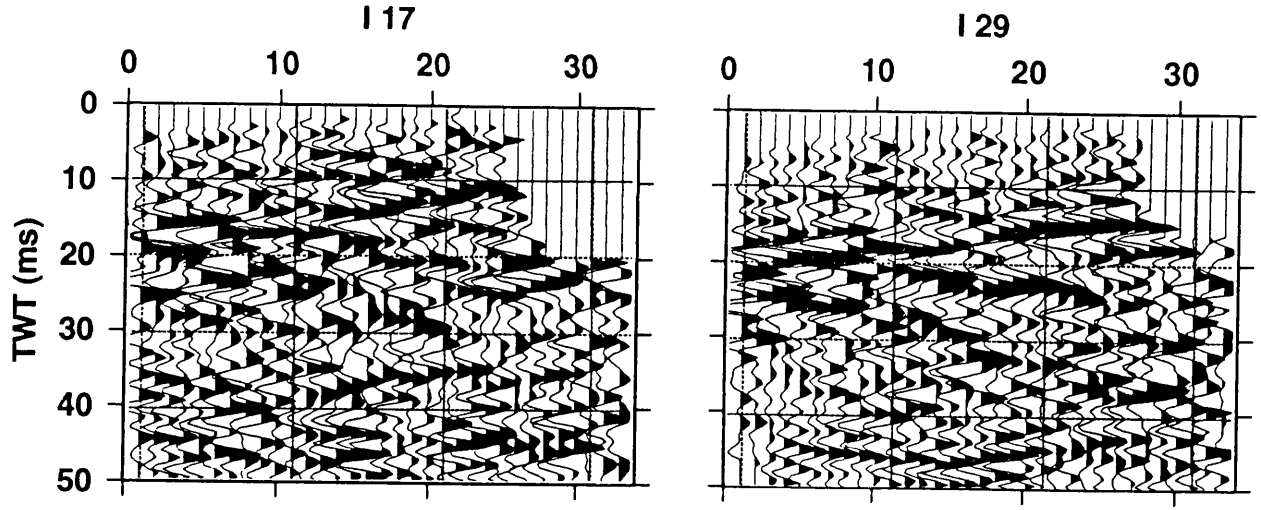

Figure 3.47b Samples from two crossline sections – approach –II.

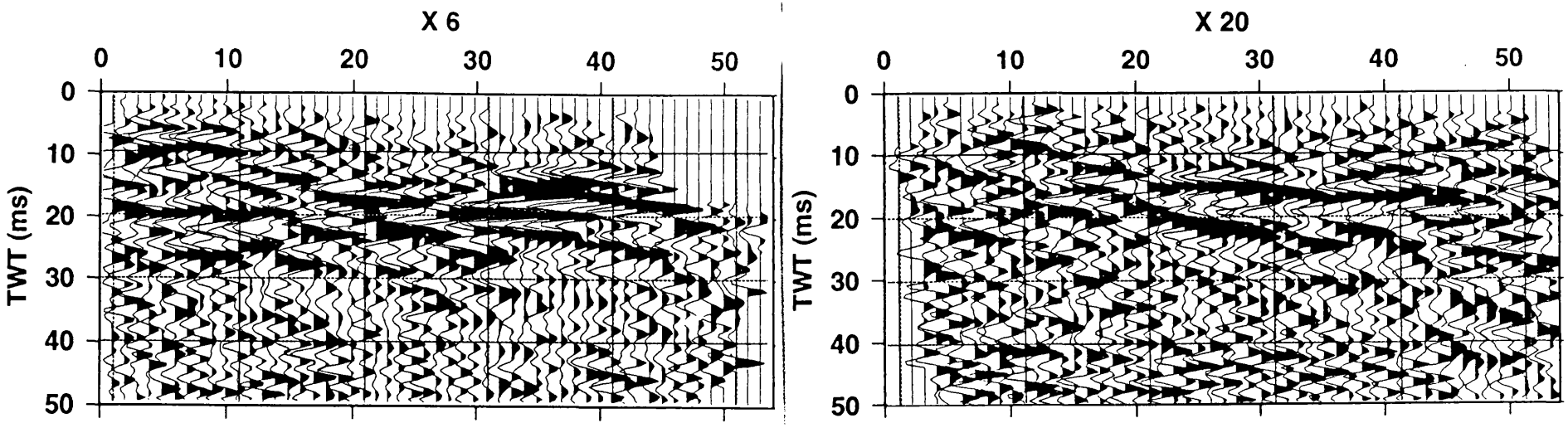

Figure 3.48a Samples from two inline sections – approach-II (interpreted).

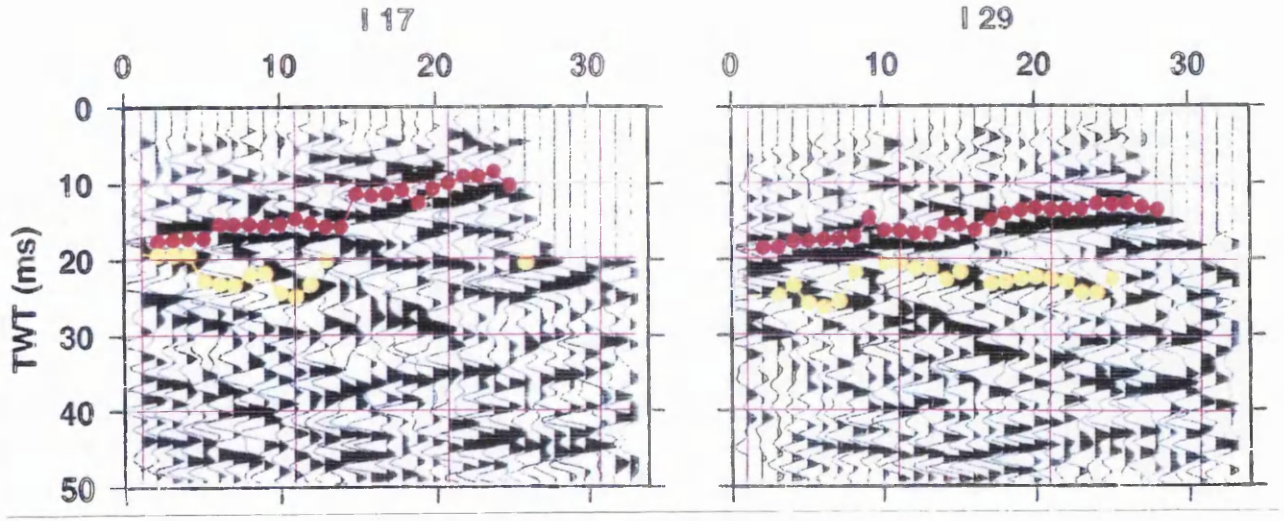

Figure 3.48b Samples from two crossline sections – approach-II (interpreted).

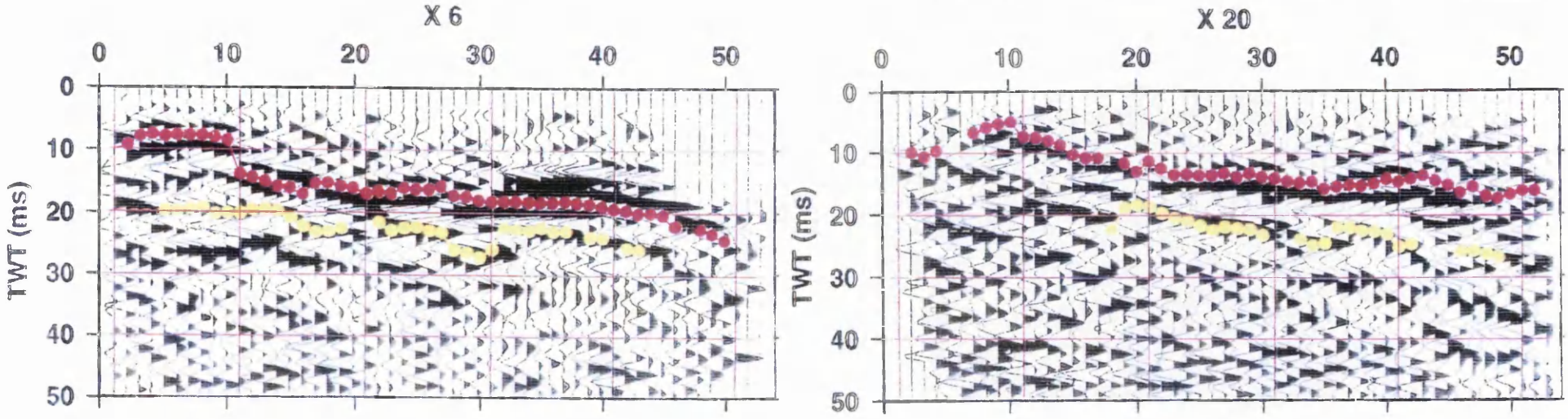

Figure 3.49 Bedrock or base clay (red horizon) map – approach-II.

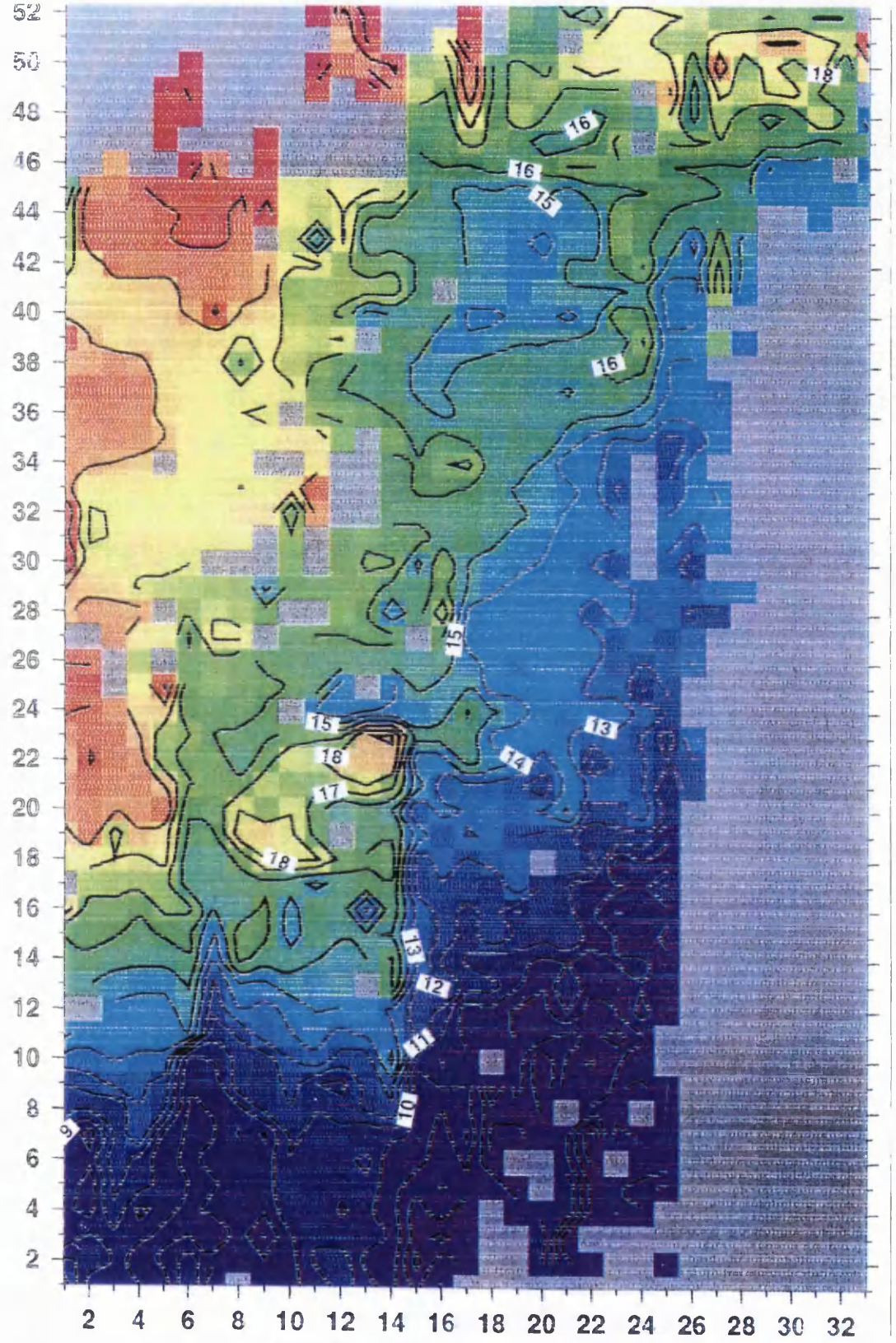

Contour interval 1 ms TWT. Dark blue – 8 ms, dark orange – 20 ms, grey – no picks.

Figure 3.50 Yellow horizon (possibly underground voids) – approach-II.

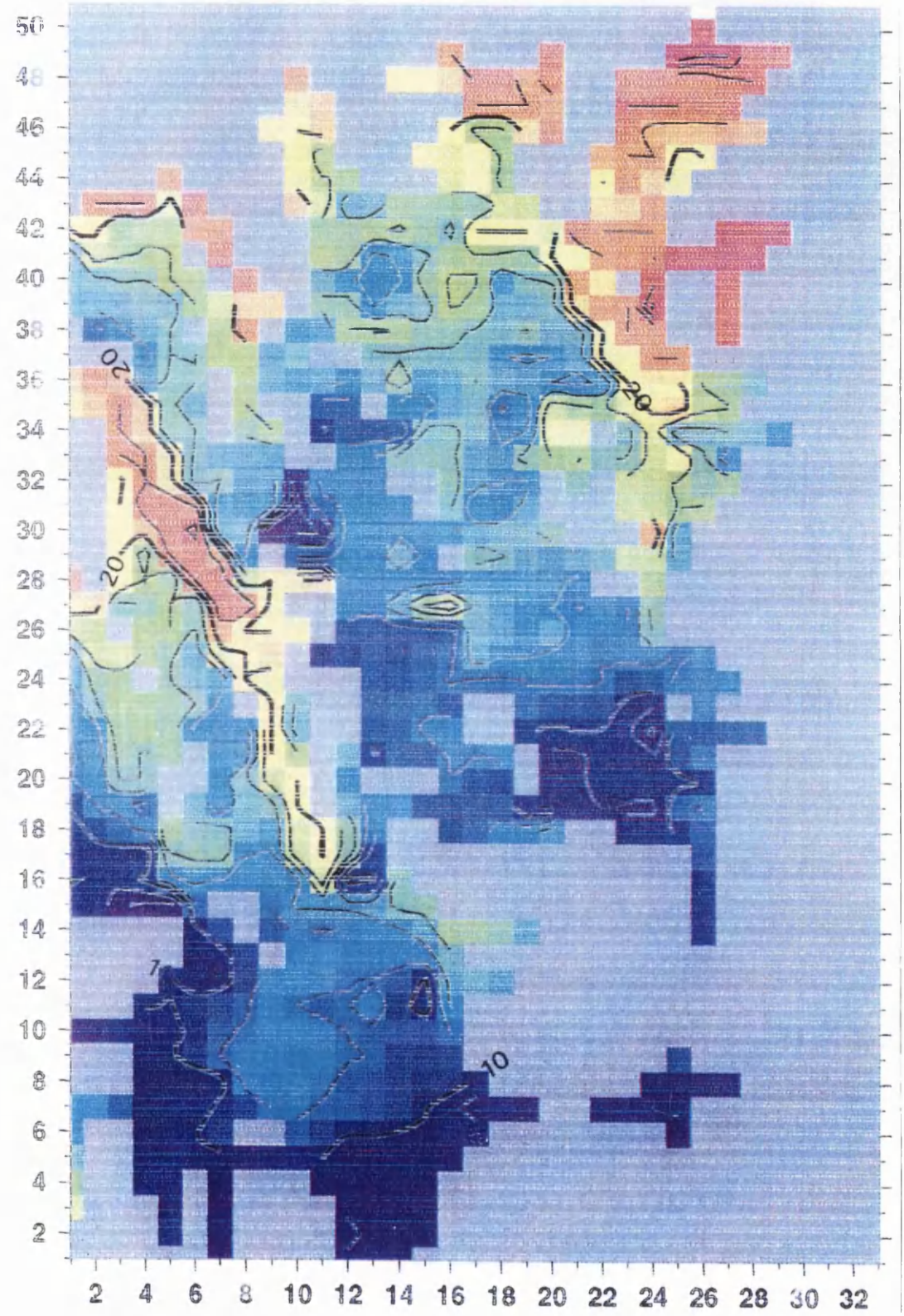

Contour interval 1 ms TWT. Dark blue – 9 ms, dark orange – 22 ms, grey – no picks.

Although the overall trend of the yellow horizon follows the general direction of the strike in the Carboniferous, there remain questions to be answered. For example, there is no independent evidence for fault-like structures. Furthermore, there is still much of area where picks cannot be made. These problems lead to reprocessing the data using a third approach.

Processing – approach-III (reprocessing of approach-II)

In a 2-D survey, the spread is normally laid parallel to the perceived general dip of the layers to obtain a true dip cross-section. The same principle can be applied to designing a 3-D survey. To get the best image of the subsurface, the inlines and crosslines should be chosen to be parallel to either the strike or dip direction of the layers.

In the first and second approaches, the data were binned such that the inlines are parallel to the rows and crosslines are parallel to the columns of the surface peg geometry. However, the directions of these rows and columns are somewhat oblique to the general dip and strike direction of the layers, but this binning strategy was chosen to avoid lots of empty bins. Results from the second approach (yellow horizon), show an interesting pattern, where the contour lines are elongated in the NW-SE direction, parallel to the general strike of the layers within the Carboniferous. The results might be improved if the data are re-binned with respect to the geological dip and strike. Such re-binning is a freedom available from the randomised CMP distribution shown in Figure 3.40, but would not have been possible if the sources had been arranged on a regular grid like the receivers.

This third approach is a modification of the second approach. Using the same data (100-700 Hz Lab Correlated), the data were re-binned, based on the results of the second approach. The bin grid was rotated clockwise until the crosslines were parallel to the strike.

Compared to the second approach in which we have 53 inlines and 33 crosslines (or 1749 bins), the rotated binning grid changes the number of inlines and crosslines to 50 and 57 (or 2850 bins), respectively (Figure 3.51a). Obviously this rotation also increases the number of empty bins. Figure 3.51b shows the relation of the inline and crossline system with respect to the National Grid coordinate system.

The data (100-700 Hz rotated bin) were processed in the same style as the second approach. The elevation static of 350 m s^{-1} replacement velocity with 37.0 m datum was also applied to the data to correct for elevation differences. No change of trace polarity was made. The main difference between this (third) and the previous (second) approach was in the way that the data were stacked. Unlike in previous two approaches, in this approach we have decided to apply both top and bottom mute (Figure 3.52). This hopefully will ensure that only the reflection signals will be stacked. Instead of stacking using a 1-D velocity function, as in the second approach, these data were stacked using a 3-D velocity function.

The reason of using the 3-D velocity function instead of 1-D velocity function is because of the presence of lateral velocity variations. By using this velocity function, it is hoped that the data would be stacked with the appropriate stacking velocity, thus giving a better image of the subsurface. Finally, the data were not migrated, as in the second approach. A summary of the processing flow for this approach is given in Table 3.19, while Table 3.20 is a summary of all processing flows for the three different approaches.

Figure 3.51a CMP coverage with rotated 2 m binning grid – approach-III.

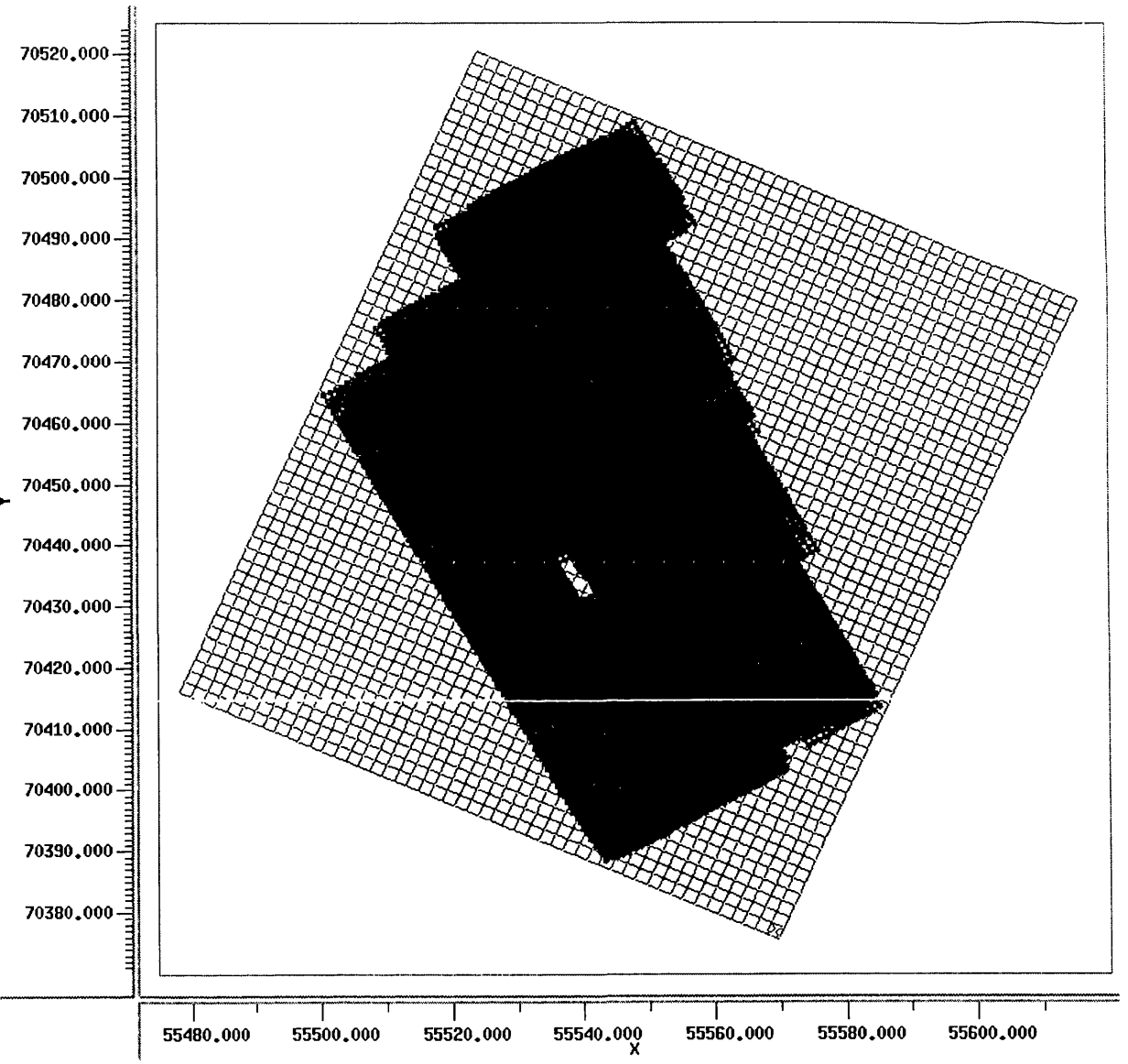

Figure 3.51b Relation between inline-crossline and National Grid (E-N) coordinates for approach-III.

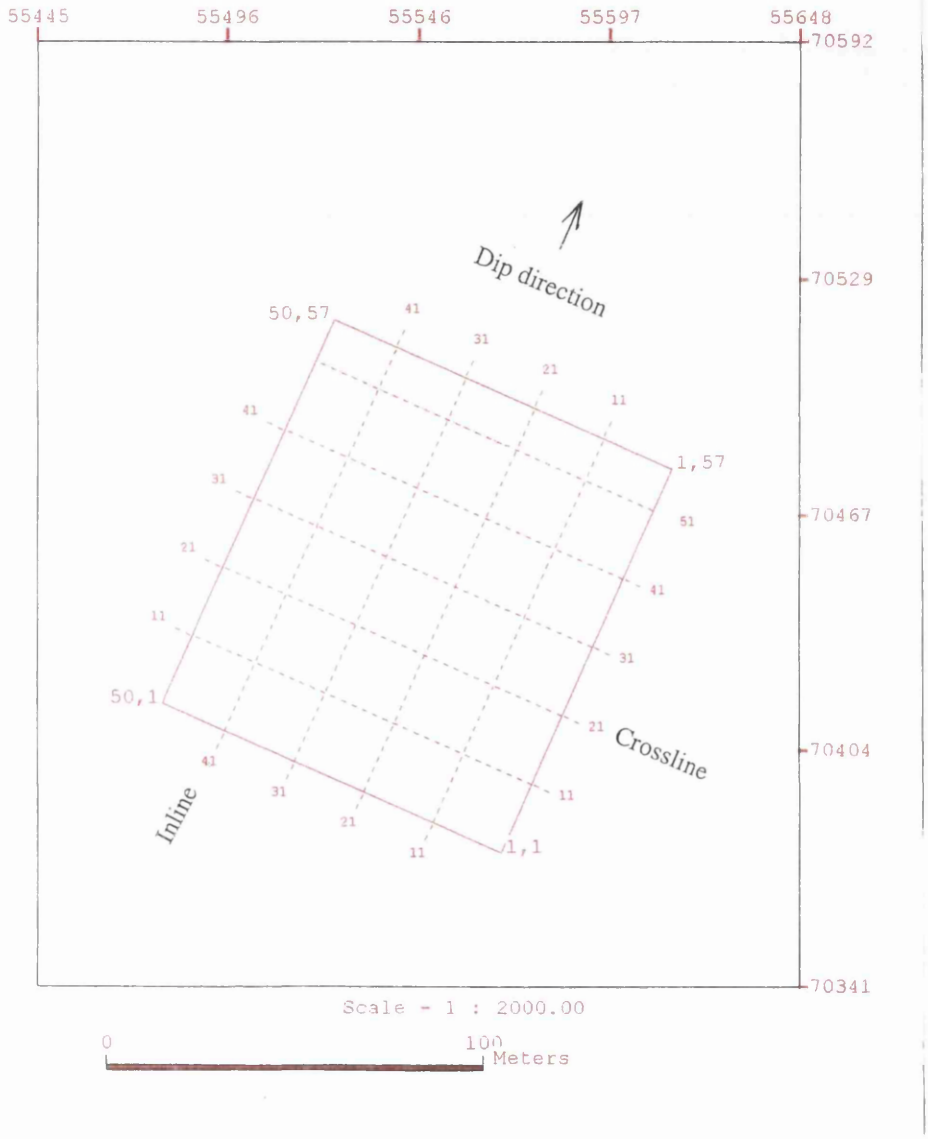

Figure 3.52 Raw (left) and pre-processed data (right) showing severe front and bottom mute applied in approach-III.

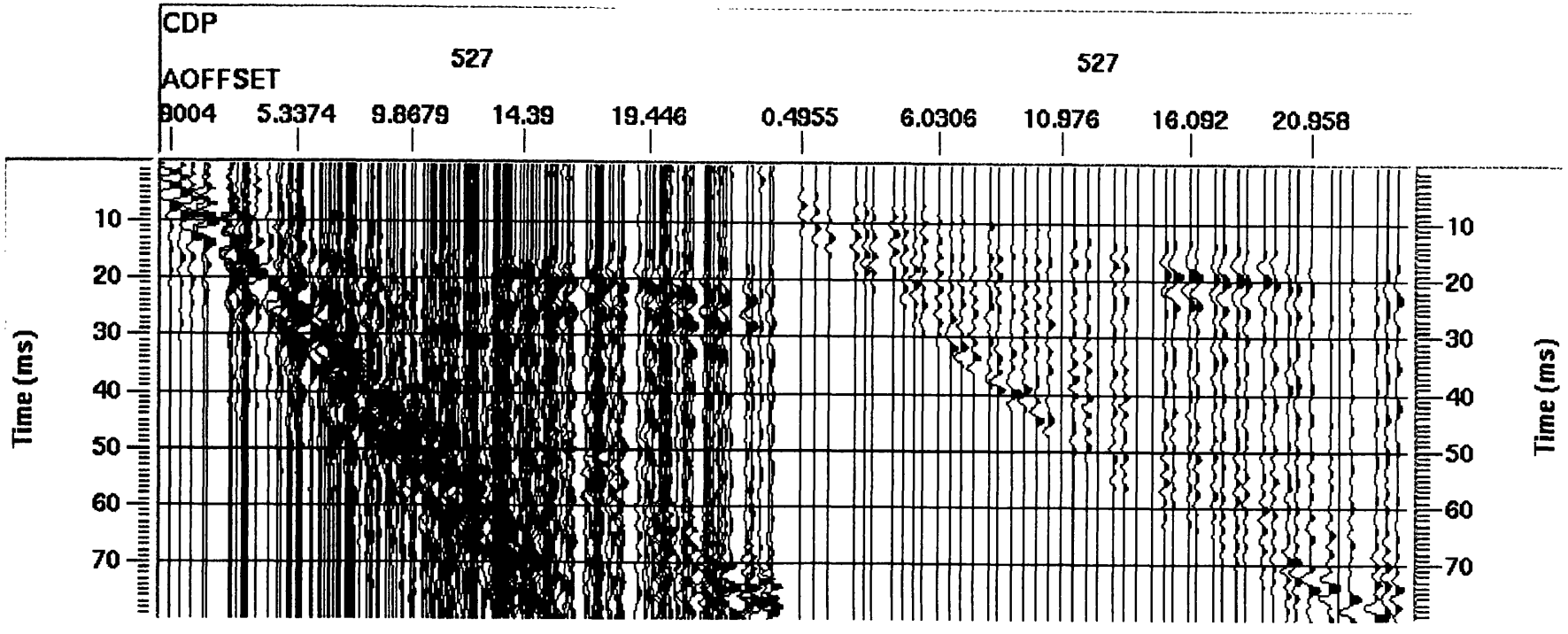

Table 3.19 Approach-III processing flow.

Dataset	100-700 Hz Lab Correlated; 2 m bin rotated, 0-150 ms
Elevation Static	Datum 37.0 m; Replacement velocity 350 m s^{-1}
Spectral Shaping	100-400 Hz
AGC	30 ms centred window
Muting	Air blast and later arrivals
NMO / Stack	3D velocity function; 60% NMO mute
AGC	40 ms centred window
Pad stack volume	
Spectral Shaping	100-400 Hz

Table 3.20 Approach-I, -II and -III processing flows – similarities and differences.

Parameters	Approach-I	Approach-II	Approach-III
Data	200-700 Hz Lab. Corr. 2 m bin 0-50 ms traces 0-5 m offset traces	100-700 Hz Lab. Corr. 2 m bin 0-150 ms traces 0-20 m offset traces	100-700 Hz Lab. Corr. 2 m rotated bin 0-150 ms traces 0-20 m offset traces
Elevation Static	Datum 37.0 m; Rep. velocity 350 m s^{-1}	Datum 37.0 m; Rep. velocity 350 m s^{-1}	Datum 37.0 m; Rep. velocity 350 m s^{-1}
Polarity	Reverse	Normal	Normal
Muting	Refraction first break	Air blast; later arrivals	Air blast; later arrivals
NMO / Stack	CVS; 60% NMO stretch	1-D vel. function; 60% NMO stretch	3-D vel. function; 60% NMO stretch
Spectral Shaping	200-500 Hz	100-400 Hz	100-400 Hz
Migration	None	Kirchhoff time	None

Approach-III: results and comments

As in Approach-II, examples of vertical sections resulting from this approach are also presented as two separate figures. Figure 3.53a shows examples of two inline sections – inlines 28 and 37, while Figure 3.53b shows examples of two crosslines – 19 and 31. All these examples also show the presence of two reflectors, but they are slightly deeper (between 12 and 35 ms TWT). The first reflector is a horizontal strong trough around 16 – 20 ms TWT and is marked by red circles. The second reflector is a strong peak dipping towards a higher value of crossline number (i.e. in a NE direction). This reflector is marked by yellow diamond marker. Interpreted versions of the same four vertical sections are shown in Figure 3.54a and Figure 3.54b.

The data were interpreted in a same way as in second approach. Because the polarity of these data is not reversed, according to the SEG convention the trough is represents an increase in impedance contrast. This means that the upper layer has a lower velocity than the deeper layer, assuming that density changes are less important than velocity changes. As the area has a relatively simple geology, this condition occurs at the boundary between overburden and bedrock. So it is assumed that this red reflector represents the clay/bedrock interface. From the geological map cross section (Figure 3.3), this interface is drawn as a flat glacial erosion surface.

The second reflector, marked by the yellow marker, is a peak. This means that this reflector has a negative impedance contrast. In most common conditions the velocity increases with increasing depth, but here the situation is reversed. The negative impedance contrast is a result of a higher velocity layer sitting on top of a relatively low velocity layer. Since this site is over an abandoned coal mine, a condition where such a reversed polarity event would occur is at the top of a water- or air-filled underground void. Besides that, it also can occur at the top of a thick coal seam as coal has lower velocity compared to sandstone or shale (Carboniferous rock). Thus, it can be inferred that the yellow reflector might represents, in some form, the top of the old minework or a thick coal seam.

Figure 3.53a Samples from two inline sections – approach-III.

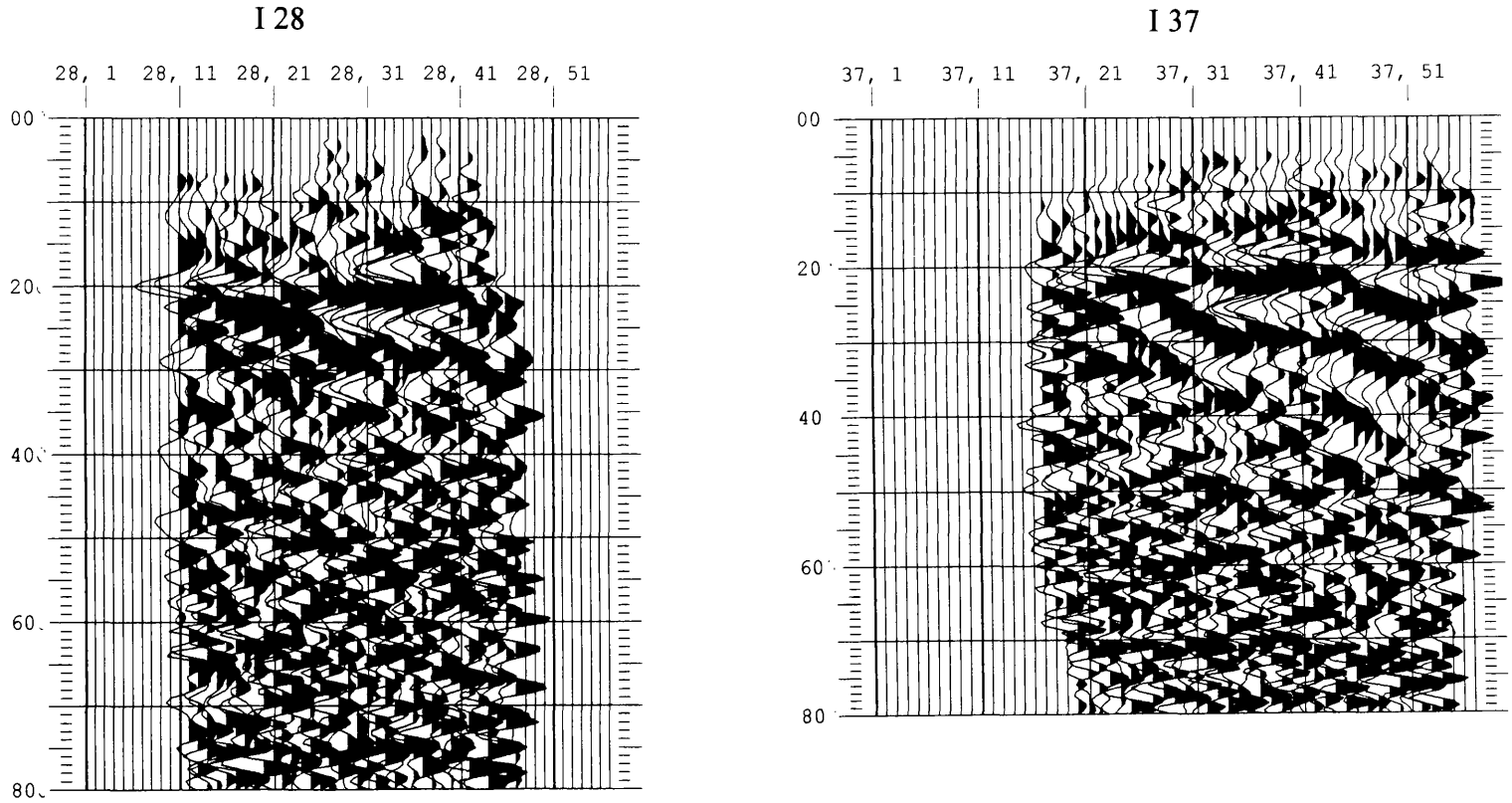

Figure 3.53b Samples from two crossline sections – approach –III.

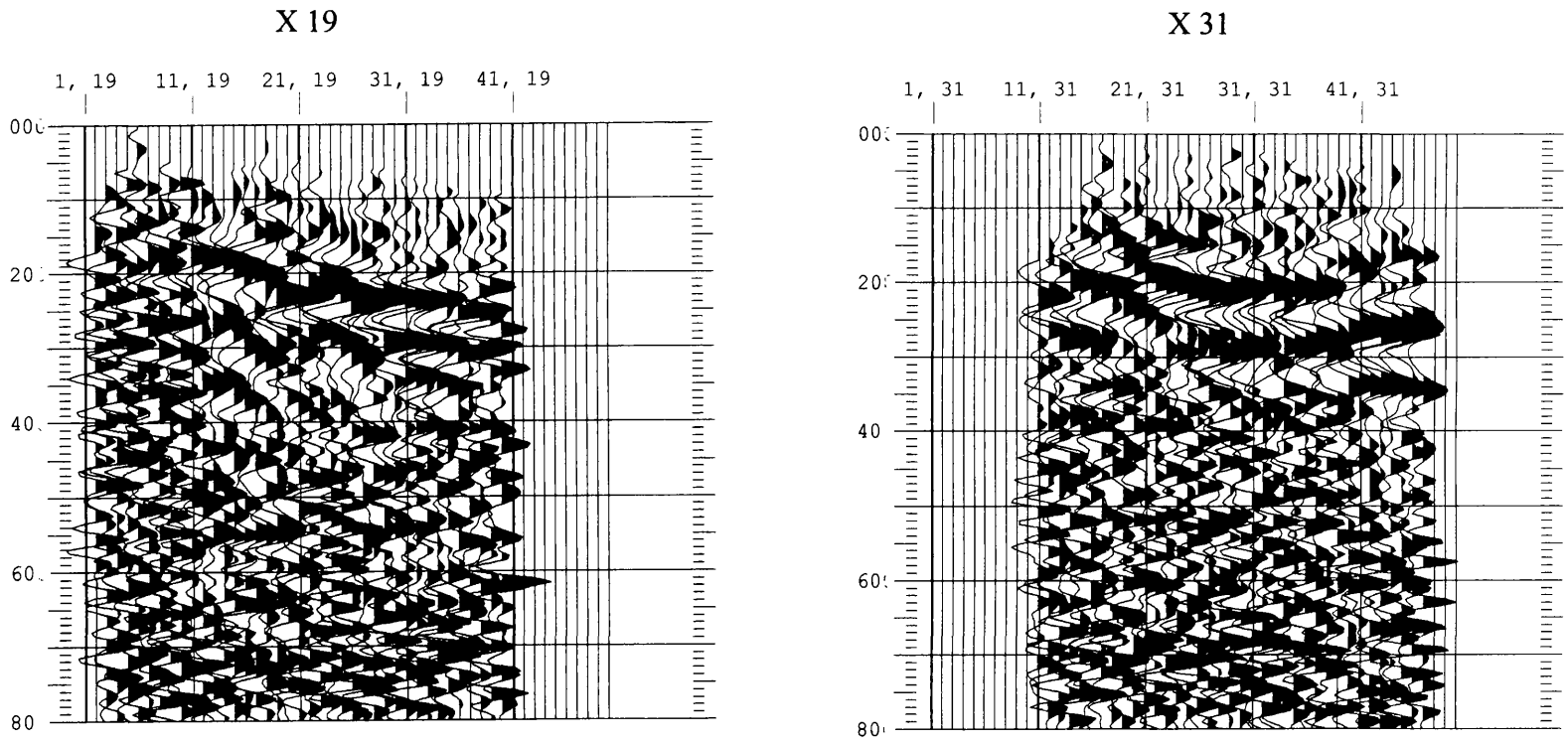

Figure 3.54a Samples from two inline sections – approach-III (interpreted).

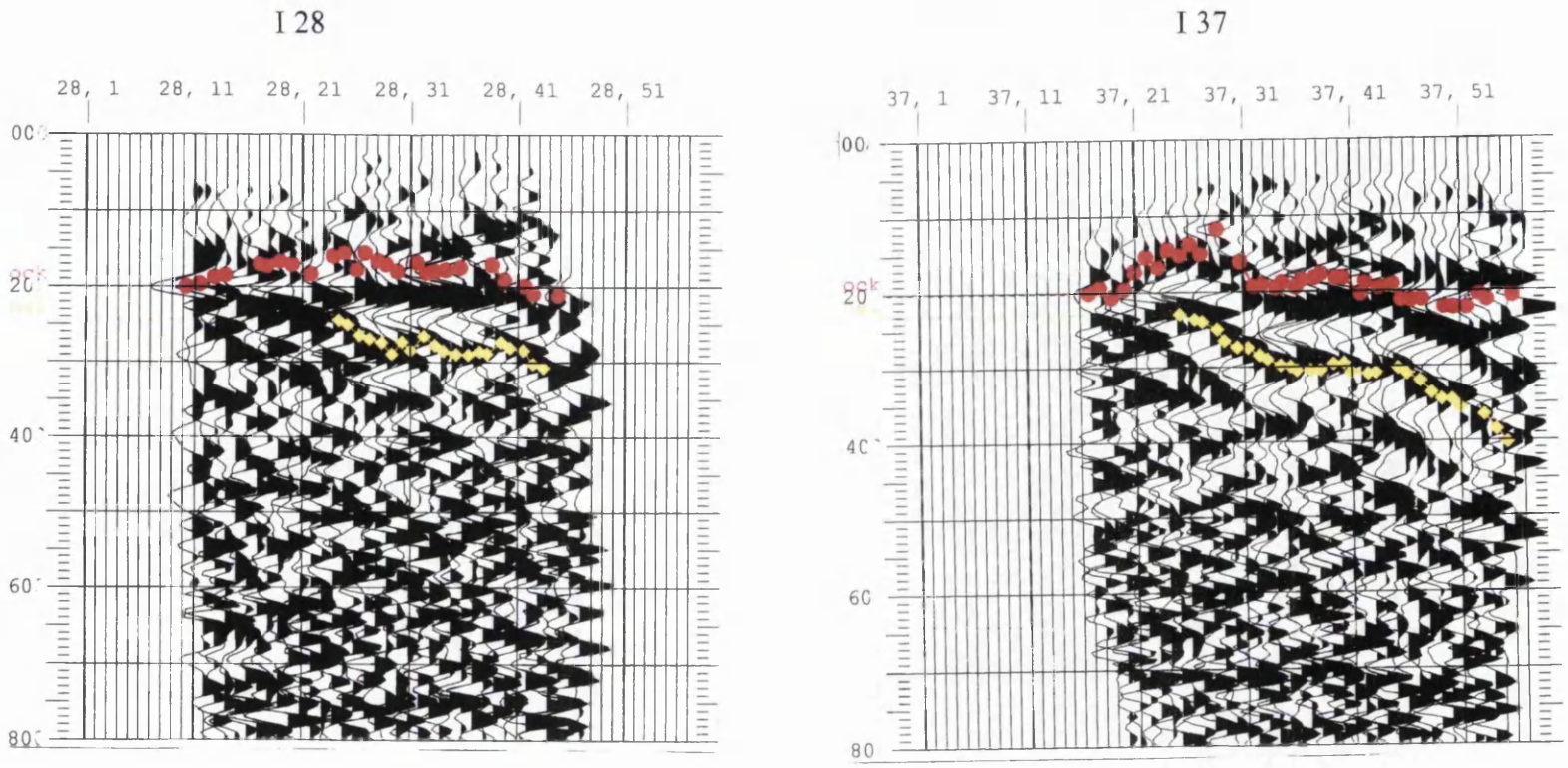

Figure 3.54b Samples from two crossline sections – approach-III (interpreted).

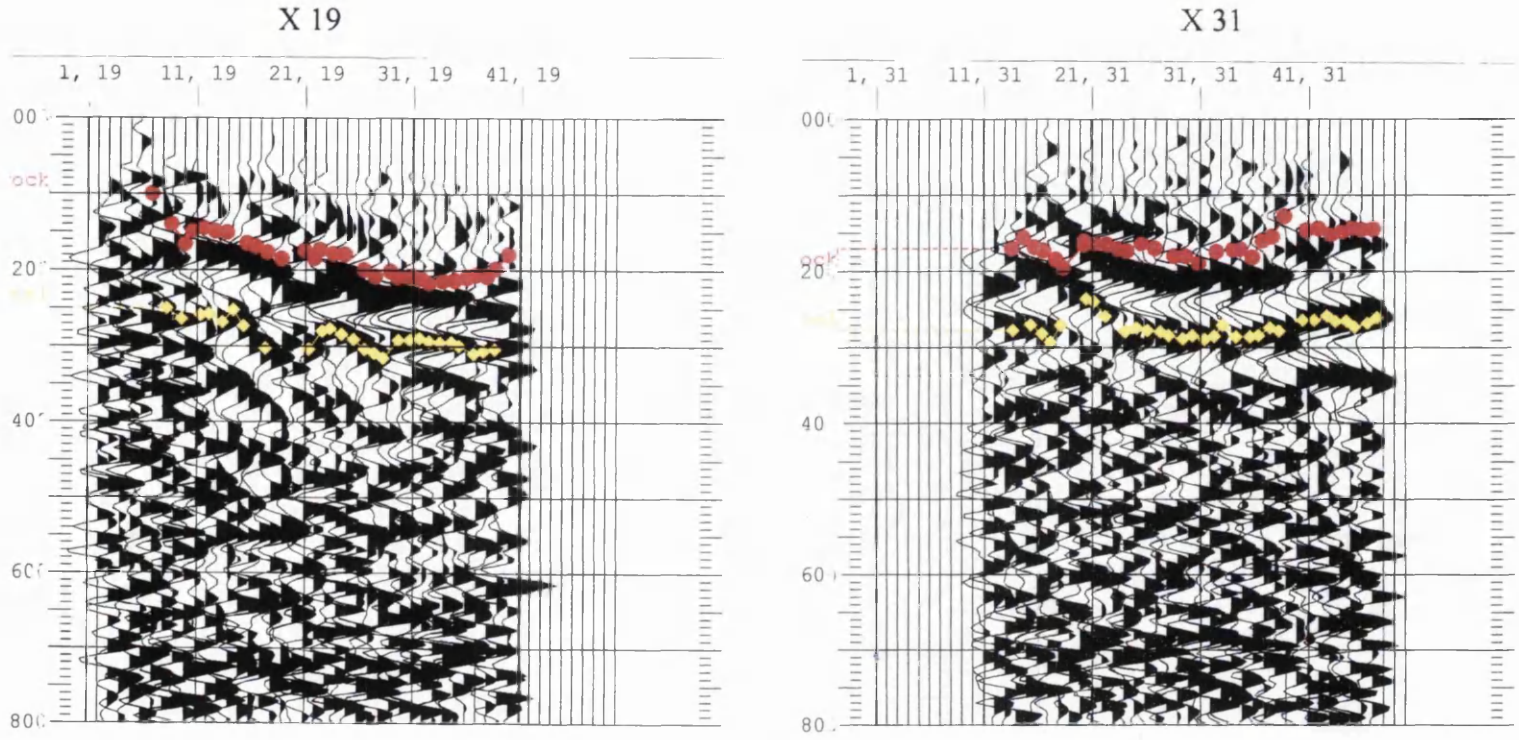

Only those two reflectors are picked as our aim is to image the underground workings. No attempts were made to pick the topsoil/clay boundary, as this reflector is too shallow. Furthermore the reflected signal from this boundary is masked by the first arrivals. The other reason of limiting the picking is that no direct well tie could be made. The picking was based only on the continuity of the signals.

The picking of the red reflector is relatively easy, as it can be picked almost on all vertical sections. In contrast, the picking of yellow reflector is not as easy. To see the behaviour of these reflectors and guide the picking, the 3-D data volume was sliced at different times. Figure 3.55a to Figure 3.55f are examples of six time slices at 17.5, 20.0, 24.0, 25.5, 30 and 35.0 ms TWT of the data processed under the third approach. These time slices show the distribution of positive and negative amplitudes at a constant time. The positive amplitudes or peaks are coloured as red, while the negative amplitudes or troughs are coloured as blue. Picks are also displayed on these time slices.

The time slice at 17.5 ms (Figure 3.55a) shows an irregular area of blue (as marked by the red pick marker) over most of the section. This feature becomes clearer in on the 20 ms slice (Figure 3.55b), however, it is absent from the deeper slices (Figure 3.55c, d, e and f). This feature corresponds to the trough picks (red marker) on the vertical section. The distribution of these picks indicates that this reflector is almost flat/horizontal. Figure 3.56 shows the plan view (structure map) of the red horizon. The red horizon is picked with reference to the trough, thus it is represents the boundary of glacial clay and Carboniferous rock (bedrock). The time (TWT) variation ranges from approximately 10 ms to 24 ms TWT, which corresponds to approximately 3 m to 7.2 m deep (assuming the velocity for the layer above this reflector is 600 m s^{-1} – glacial till). The map of this reflector shows an alternating curved region of blue (shallow) and red (deep), with the overall trend dipping towards the N-NW. This shows that the bedrock reflector is not totally flat but it is rather an undulating surface. This curved feature however is not observed in approach-II processing result (Figure 3.49).

Figure 3.55a Time slice at 17.5 ms TWT.

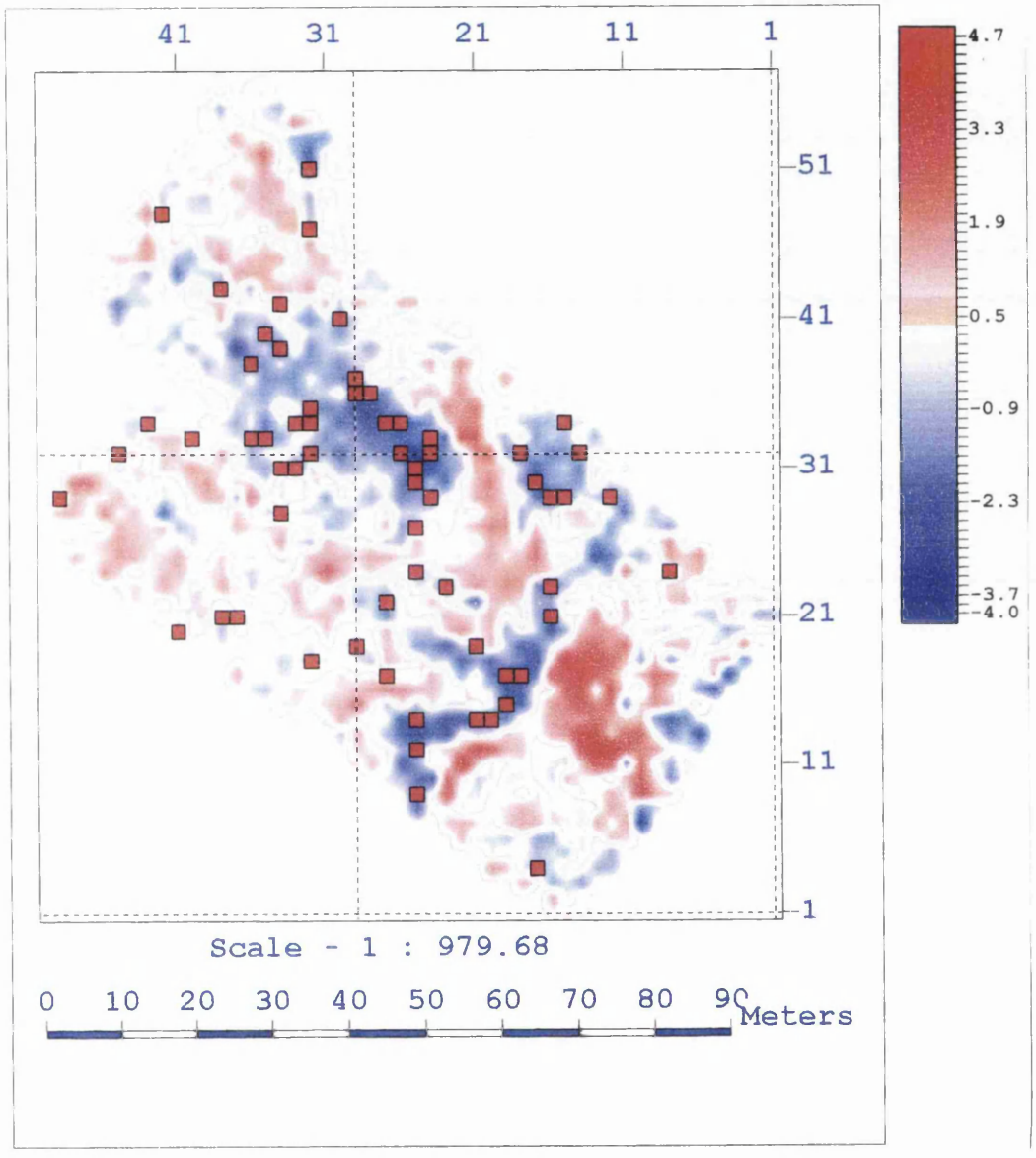

Figure 3.55b Time slice at 20.0 ms TWT.

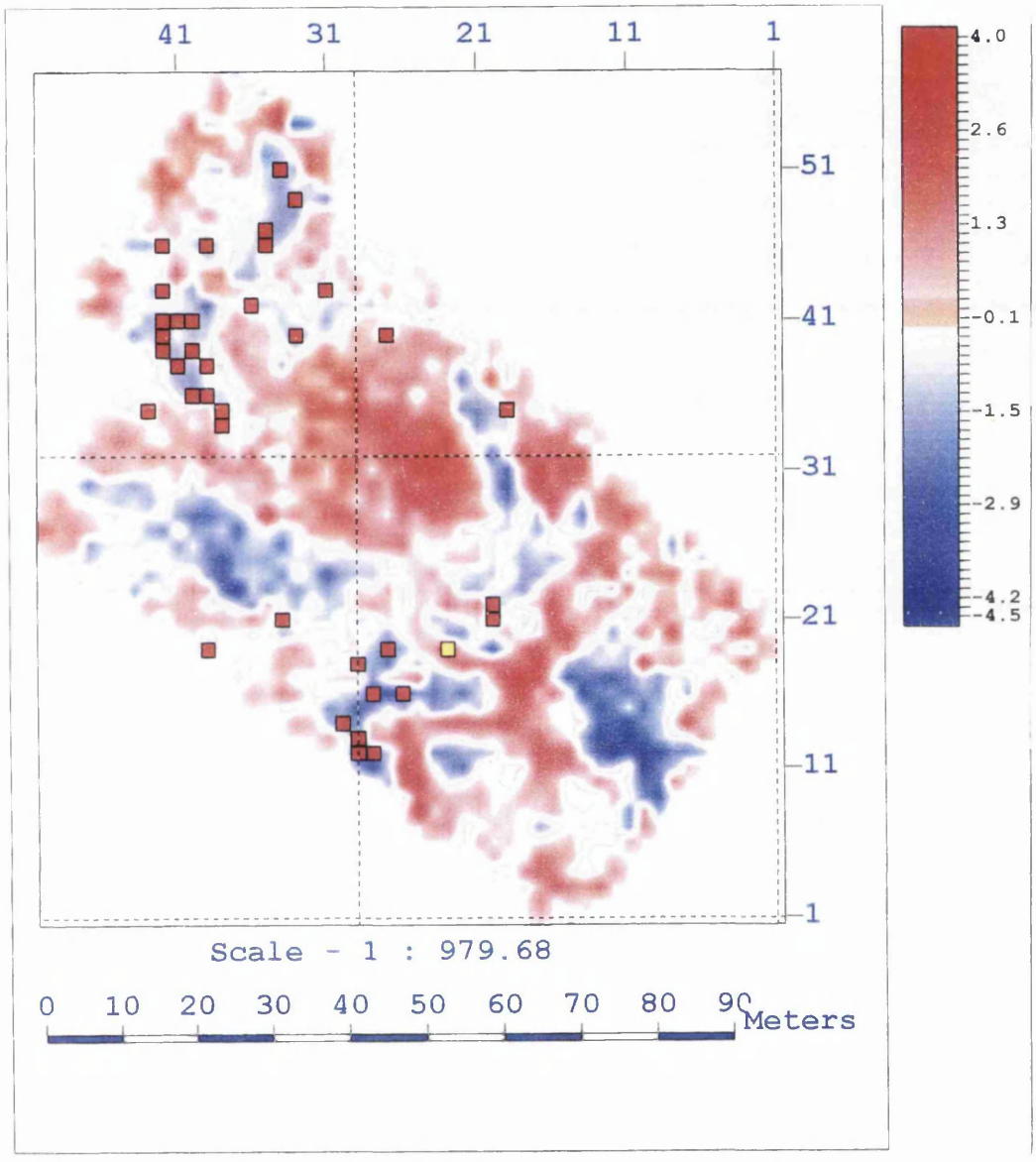

Figure 3.55c Time slice at 24.0 ms TWT.

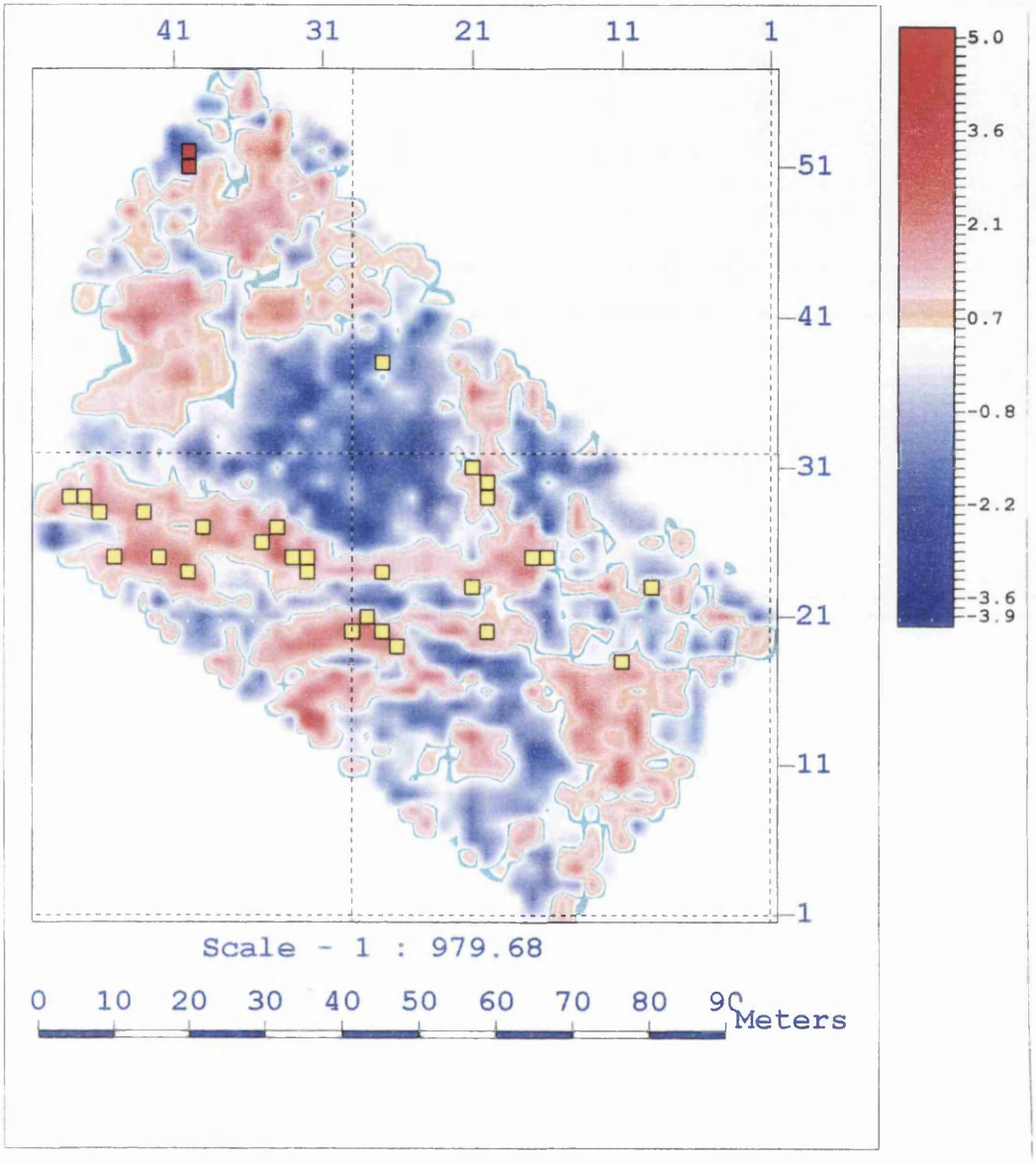

Figure 3.55d Time slice at 25.5 ms TWT.

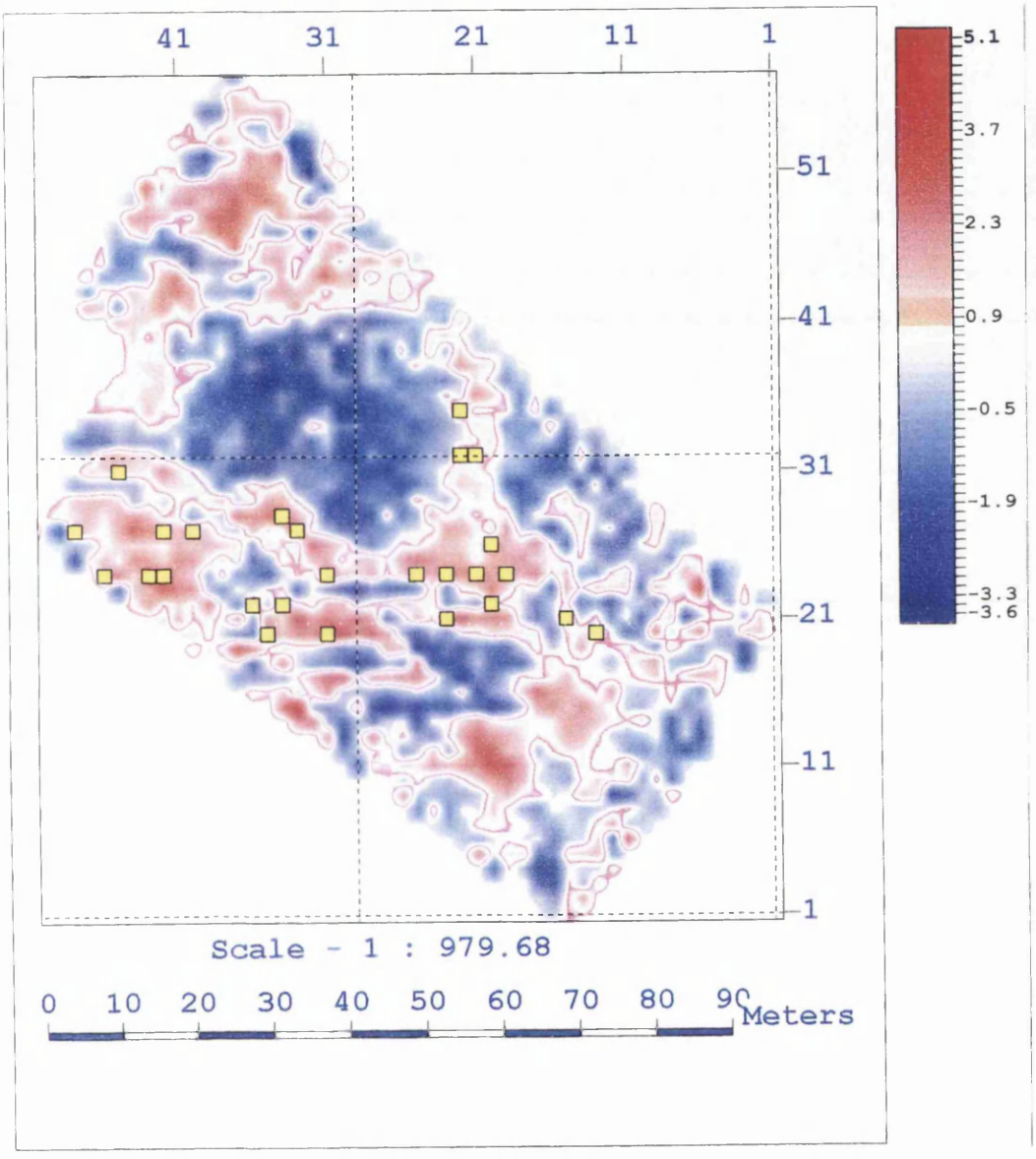

Figure 3.55e Time slice at 30 ms TWT.

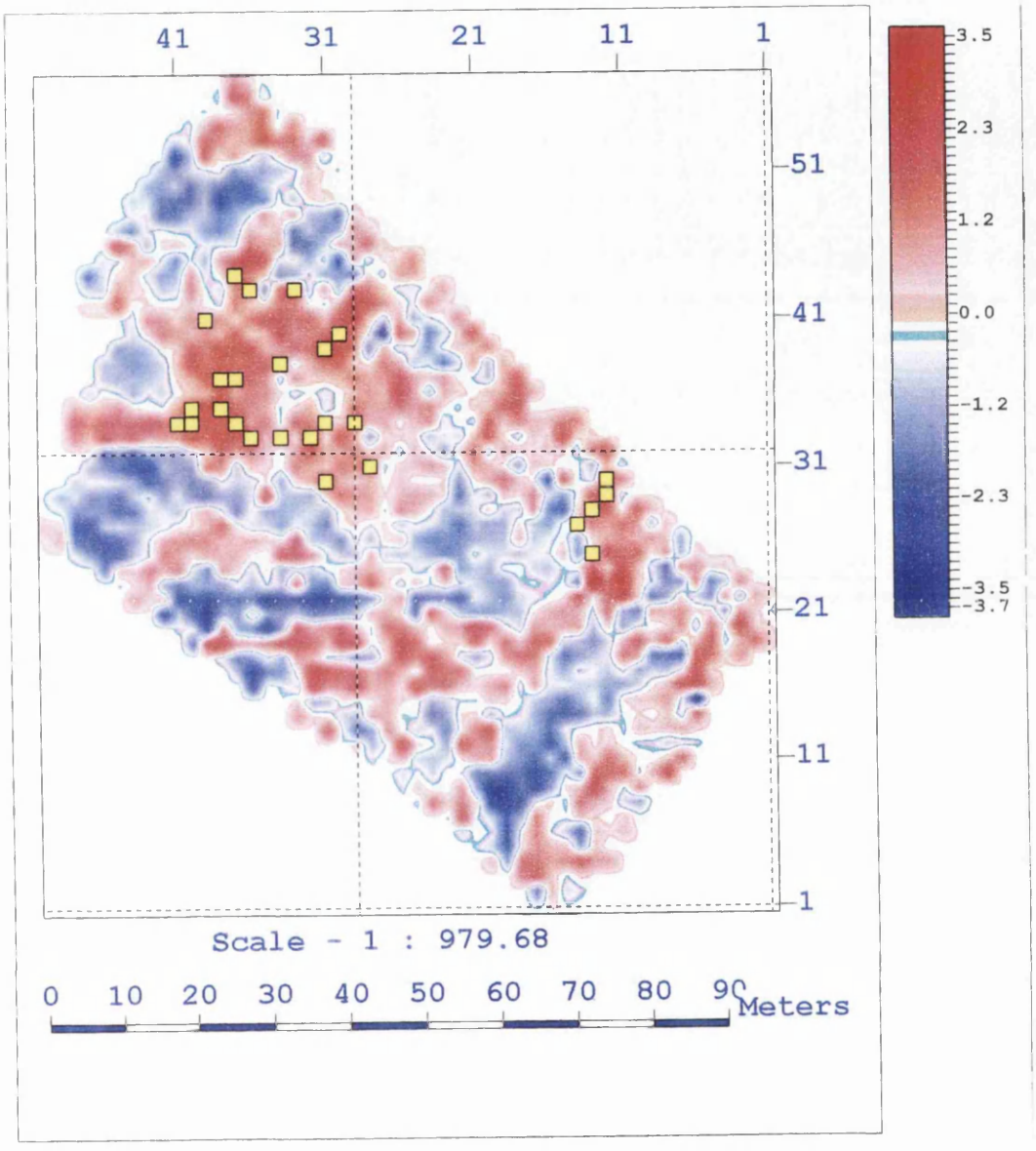

Figure 3.55f Time slice at 35.0 ms TWT.

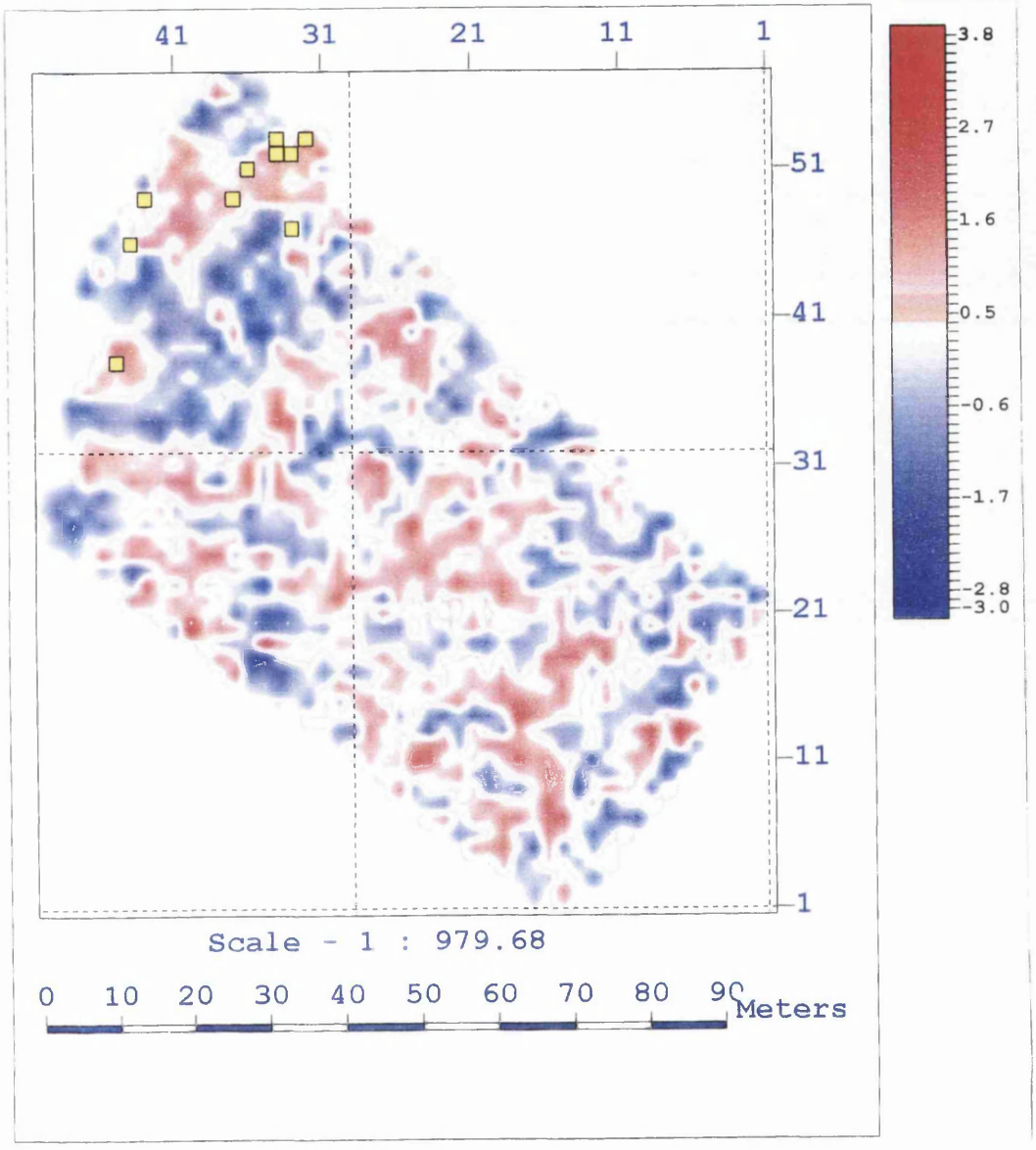

Figure 3.56 Plan view of the red (clay/bedrock) reflector.

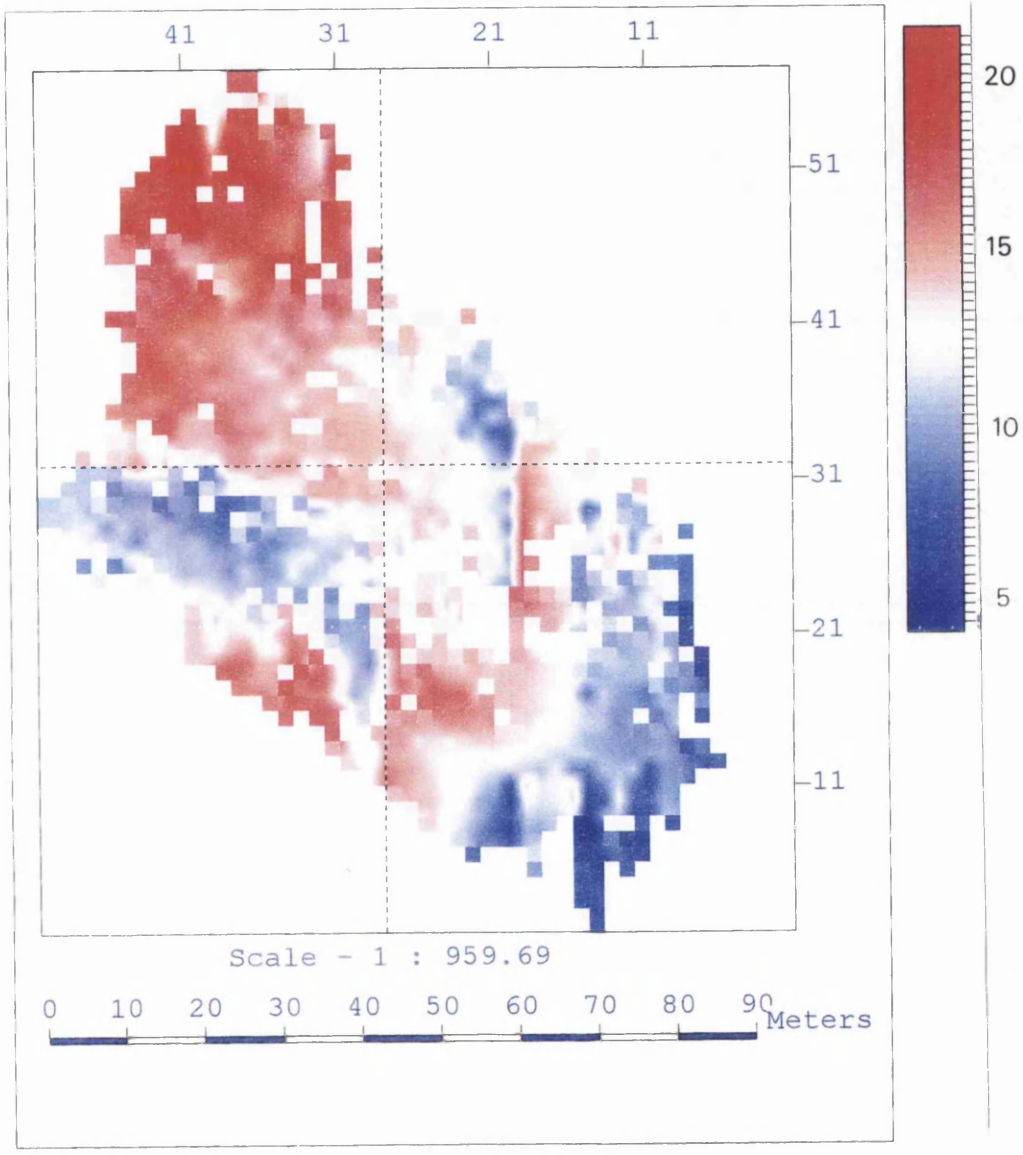

The main target of this work is to map out the reflector from a shallow mineworks such as tunnels or thick coal seams. This target is deeper than the bedrock reflector and can be recognised by a strong continuous peak, representing the expected negative impedance contrast. Vertical sections of the data (Figures 3.53 and 3.54) show that it appears at around 22 to 35 ms TWT, thus analysing the time slices of the 3-D data volume around these time should show interesting features.

The slice at 24.0 ms TWT (Figure 3.55c) shows a strong red coloured line parallel to inline No 23. This feature corresponds to a peak, and is marked with the yellow pick marker. As the bins have been rotated so that the crosslines are aligned parallel to the strike, this line is parallel to strike. This is an indication of either air- or water-filled mineworking or a thick coal seam, as both of these can produce a strong peak parallel to the strike direction. The next deeper slices (25.5 ms (Figure 3.55d) and 30 ms (Figure 3.55e)) show the band moving towards the NE of the area, which means that it is dipping towards that direction. Tracing this reflector back to shallower slices (e.g. the time slice at 17.5 ms TWT) shows that this reflector is absent, thus it can be assumed that this reflector originates somewhere within the range of 17.5 ms to 20.0 ms TWT.

Unlike the red horizon, the yellow reflector shows a NE dipping structure (Figure 3.57), and it is much deeper (approximately 22 – 40 ms TWT). This is in concordance to what is being shown in the time slices, i.e. it starts to appear clearly in or around inline 23 and dips to the NE. As this reflector is truncated by the red reflector around inlines 20 to 23 (time slices 17.5 and 20.0 ms TWT), the picking of this reflector from inline 1 to 20 cannot be done. This is why the structure map (Figure 3.57) is blank SW of inline 22.

Time slices at 35.0 ms TWT (Figure 3.55f) and deeper show a mixed of blue (trough) and red (peak) without any structural pattern. Nothing can be deduced from these slices except that it is all noise. The vertical sections also confirm that no reflectors can be picked at these deeper times.

Figure 3.57 Plan view of the yellow (? mineworkings or thick coals) reflector.

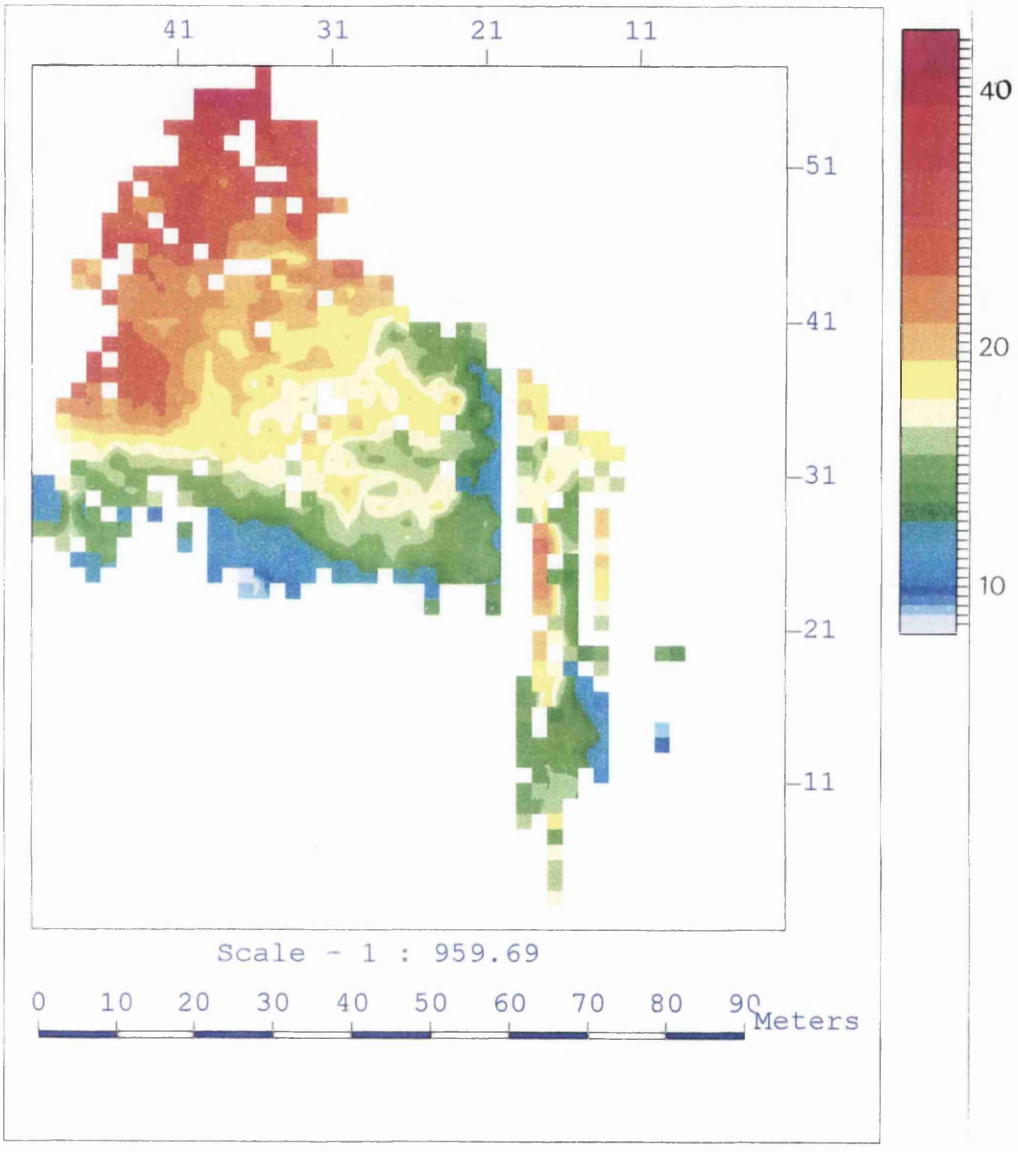

3.11 Discussion and conclusion

The use of seismic investigation in shallow engineering surveys normally involves finding or calculating the depth of the bedrock. For this purpose, the refraction technique is the primary choice, as it is simple and easy to be conducted. In the area where the geological conditions are simple such as an overburden overlying flat bedrock, this technique (with some borehole information) may be enough in answering the depth of the bedrock problem. However today, the aims of shallow seismic investigation diverge into wider areas such as investigating movement of shallow contaminants (aquifer study), imaging dangerous underground tunnels or voids, or even in searching for underground water reservoirs. The seismic refraction method is thus becoming more and more inadequate as it has several shortcomings, such as the hidden layer problem.

As the refraction technique becomes unsuitable for these new tasks, shallow seismic investigators are now using the reflection technique in much of their work. Seismic reflection can be used to image the subsurface more accurately if the acoustic impedance contrast is big enough to be detected. To date, seismic reflection, especially the 2-D technique, has widely been used for shallow seismic investigation either to accurately map the bedrock or to study shallow water reservoirs. The reasons are mainly that it is simple to conduct, and involves little computational time. As the technology becomes increasingly more advanced, the previously exclusive techniques (used in petroleum exploration) are now also available for shallow seismic investigation usage. These include the 3-D seismic reflection method.

This study is involved with transferring one previously exclusive petroleum exploration technique – 3-D seismic reflection – to shallow seismic engineering investigation work. This work is one of the pioneering works in this field, thus descriptions on the acquisition processing techniques have been discussed in detail.

The aim specific of this work is a case study or trial to image shallow underground mining tunnels, which have been abandoned for decades. These areas are considered dangerous and not suitable for development. However, because of the increasing demand for land for either housing or industrial estates, these previously dangerous areas are now considered to have potential for development. Before they can be developed, the unstable ground needs to be treated, normally by grouting. For this remediation work to be economical, an estimate of how much grouting material is needed to stabilise the area is important, as this is the most expensive cost involved. To estimate the volume of grouting material needed, a reliable method for imaging the unstable ground is important. The 3-D seismic reflection method may be one of the solutions.

With a grant of some £13K, the 3-D survey was planned over a 6000 m^2 area that is known to have been extensively mined. This amount is small compared to the cost of closely spaced boreholes (a more traditional engineering method of continuously imaging the subsurface) survey, since the average drilling cost of each borehole – e.g. rotary coring in rock – is £40 / m with an additional £50 per hole and £400 to supply the rig to the site (Waltham 1994). For example, the total cost to conduct a grid of 50 m deep boreholes (using a rotary coring method) at a regular 10 m spacing to cover an area of 6000 m^2 is about £120K.

The 3-D data were processed using three different approaches. The results of the second approach indicate the presence of two possible reflectors that have been marked as red and yellow reflectors. The red reflector is interpreted to be the clay/bedrock interface, while the yellow reflector is within the bedrock. The yellow reflector shows a strong reverse polarity characteristic which is interpreted as the reflection from a mineworking or a thick coal seam. The reason for this interpretation is the reversed polarity, which could only happen in the presence of a negative impedance contrast. This condition (in the site) could occur at the upper boundary between solid rock and an underground void, or at the upper boundary between the solid rock such as sandstone and a thick coal seam. No boreholes were drilled to confirm these pickings.

An attempt to improve the result leads to the third processing approach. In this approach the data were re-binned so that the inline/crossline direction are parallel to the dip/strike directions respectively. The randomness of the CMPs and their azimuths allows this re-binning to be done. This is the advantage of the data collected using this kind of survey. The disadvantage, on the other hand, is that it produced lots of zero trace bin, which increases the number of dead traces in the vertical sections. The processing sequences were kept same as the second processing approach with a difference in the way the data were stacked. In this approach the data were stacked using 3-D velocity function. The result of this approach shows an improvement in quality. As in the second approach two reflectors are recognised and picked. The consistency in picking the reflectors become easier as the reflectors are clearly recognised either on the vertical section or the time slices.

The structure maps of these two reflectors show interesting information. The red reflector (clay/bedrock boundary) is undulating with two deep areas. The overall pattern is dipping in a N or NW direction. More interesting is the structure map of the yellow horizon (? tunnel or thick coal seams). The contours strike in the NW-SE direction, which is the same direction of the solid geology. The horizon dips NE.

Although this 3-D seismic reflection survey failed to produce a detailed picture of the target, it did however manage to image the presence of the general pattern of possible underground voids or thick coal seams. Information such as the depth of the underground minework is important for remediation work, because it can limit the area to be grouted, as only a shallow unstable area needs to be grouted. Thus the volume of grouting material can be estimated by assuming the average height of the minework.

The results of this 3-D seismic reflection survey show that this method is also feasible for a shallow engineering site survey. The cost and time consumed to conduct this survey also proved that it is very cost-effective.

The delay in producing any result from this trial survey was due to the fact that lots of time was spent to find the best way to process the very shallow seismic data. Clearly the processing time would have to be reduced to a month or less for the method to become acceptable and useful to engineering contractors. Time was also spent on introducing a new mapping method as a by-product of the 3-D seismic reflection, named as 'surface tomography'. This new mapping technique is discussed in Chapter Four.

CHAPTER FOUR

SURFACE TOMOGRAPHY

4.1 Introduction

Tomography by definition means a picture of a cross section of an object. Like a loaf of slice bread, stacks of neighbouring cross sections can give a 3-D picture of an object. A computerised axial tomography or CAT scan is one of the famous examples of this concept. A CAT scan is used to define normal or abnormal structure in the body as well as assisting in procedure by helping to guide accurately the placement of instruments or treatments. In a CAT scan, a large doughnut-shape X-ray machine takes X-ray images (closely spaced X-ray slices or cross-sections) at many different angles around the body over a full range of penetration angles in a controlled manner. The rays pass through different materials of the body such as bones and soft tissue. Different body materials show different X-ray attenuation characteristics. The loss of intensity due to the unequal absorption by different parts of the body is measured and reconstructed to give the picture of the part that has been scanned or examined. In order to reconstruct the intensity of the X-ray recorded, four major reconstruction algorithms have been introduced which are: (1) summation methods, (2) convolution methods, (3) Fourier methods and (4) summation-expansion methods (Peterson *et al.* 1985).

Deep-earth geophysicists, in studying the internal structure of the earth also use this technique. It was first introduced into this field by Aki *et al.* (1977) and known as seismic tomography. Seismic tomography uses the same principles as in a CAT scan but rather than using the attenuation characteristic, the travel-times of the signals are observed (Lowrie 1997). In most cases, the recorded arrival time (travelled from a source location - normally an earthquake epicentre to an observation centre around the globe) is different from the theoretical times calculated based on a homogeneous mathematical earth model. Seismic tomography is concerned with studying this difference. The main reason for this difference is that the waves travel through inhomogeneous earth materials. Using a modelling technique – adjusting the velocity of the model until it give an observed travel time - a velocity model of the earth's interior can be obtained. Therefore seismic tomography may be described as the three

dimensional modelling of the velocity distribution of seismic waves in the Earth (Lowrie 1997).

The success of seismic tomography in mapping the velocity structure of the Earth leads to smaller scale work which is known as refraction tomography (Lanz *et al.* 1998). Like seismic tomography, refraction tomography also involves analysing the arrival times of the rays travelling from sources to receivers. However instead of utilising the seismic energy from natural sources such as an earthquake, refraction tomography utilises controlled seismic sources, and the receivers can be arranged over a small area of interest.

Crosshole tomography is another method where the tomography concept is used. It is used primarily in the petroleum industry to describe the lateral velocity variation in the reservoir description phase of exploration and production. Unlike both a CAT scan and seismic tomography – where rays are detected by exterior detectors (receivers), crosshole tomography studies need two neighbouring boreholes, one for the sources and the other for the receivers. The sources and receivers are placed at various depths and as in seismic tomography, the arrival times are observed. The arrival times from each source-receiver pair are then reconstructed to give a picture in terms of velocity distribution of the reservoir. Three forms of reconstruction methods are normally used which are: (1) algebraic reconstruction technique (ART), which was developed from the summation-expansion technique used in medicine, (2) simultaneous reconstruction technique (SIRT) and (3) Gauss-Seidel method methods (Sheriff 1990). Details of the mathematics involved in seismic tomography can be found in many tomography textbooks.

Although CAT-scanning, seismic tomography and cross-hole tomography each study a different characteristic of the rays, they share one thing in common, which is that they need to have lots of rays travelling through the medium. The rays radiating from the source in a fan-like path are similar to a simple fan-shooting survey used in detecting or

delineating localised anomalous zone such as salt domes and mine shafts (Kearey and Vine 1990).

In this chapter, we are going to introduce a new and simple surveying method employing the tomography technique, named herein as surface tomography. Surface tomography involves analysis of the arrival times from lots of ray paths (using the tomography concept) that travel by refraction along a very shallow interface, but without applying any reconstruction technique. The data used in this study are the same as the data used in the 3-D seismic reflection studies (Chapter 3), however instead of whole records, only the first arrivals are used.

4.2 The concept

All the tomography techniques, regardless their field of application, share the same basic idea, where the properties of rays (travelling through different media) are studied to give a picture of the target object. Surface tomography is, in effect, a development of the old concept of the fan-shooting refraction method.

In fan-shooting refraction methods, receivers are located such that raypaths form fan-like arrays radiating from the shot location (Figure 4.1). Normally an approximate location of the target is known prior to the survey, and the survey is designed so that the target can be placed in the middle of the fan. The source-receiver offsets are approximately constant, except for a normal or control linear profile. The arrival time for each receiver is then compared to the control profile (a profile taken from the area where no anomalies are present). Whenever the ray travels through an anomalous velocity zone, it will be subjected to a time lag or time lead depending upon whether the zone has a lower or higher velocity anomaly respectively, compared to the surrounding velocity.

Figure 4.1 Fan shooting refraction, a basic idea of surface tomography.

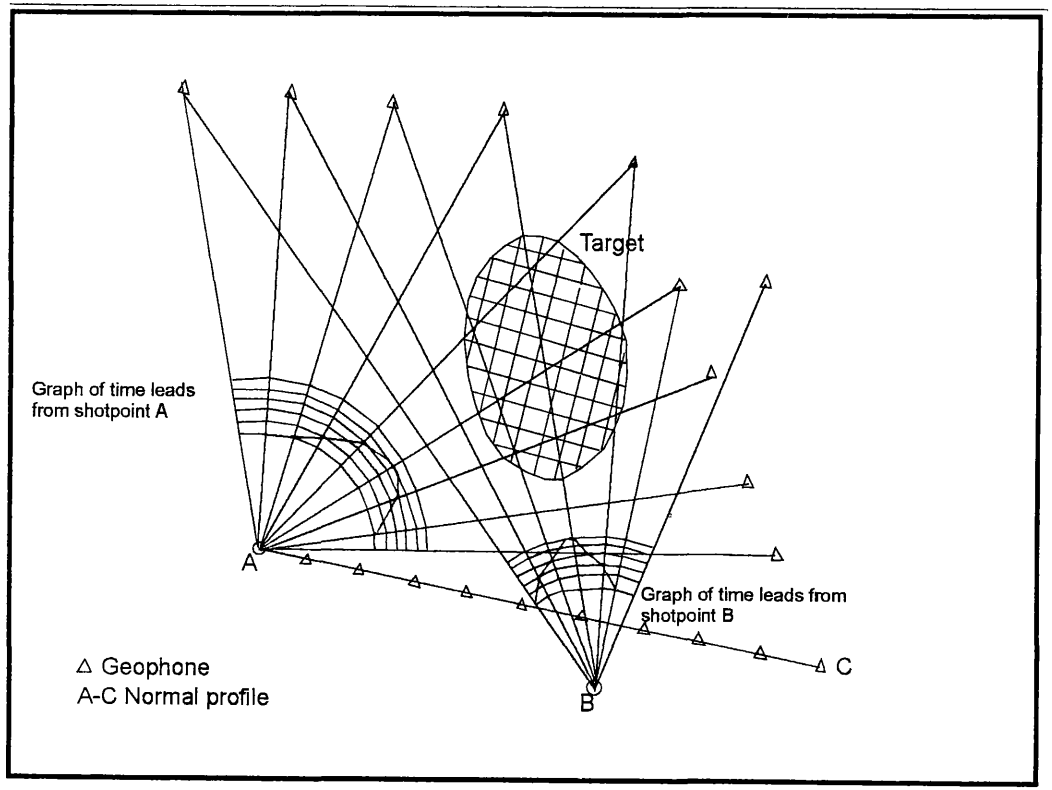

Detectors are located roughly on the arc of a circle centred at the source point in different directions. Expected arrival times are determined from a normal travel time curve established from a calibration or normal profile made where no local high velocity body is present. An early arrival with respect to normal indicates that part of the travel path is at an abnormally high velocity, signifying the present of a local body such as a dome of high velocity salt.

Surface tomography also shares the same idea – whenever the ray path encounters an anomalous zone, it will be subject to a time lead or time lag. However, the approximate location of the anomalous zone is not known. Furthermore, source-receiver offsets are not constant, and no normal (control) profile is needed. The main characteristic of surface tomography is that it needs to have lots of random raypaths. Details of the travel time differences due to the anomalous velocity which form the basic idea of this technique are explained in Appendix 1.

Unlike the fan shooting method, in surface tomography the arrival time for each source-receiver pairs are not compared to their corresponding control arrival time (to determine the time lag or lead); instead all the arrival times for each source-receiver pairs are 'reduced' to be relative to one velocity value which represent the datum or reference velocity. The difference between the observed arrival time and the arrival time as if only one material had been present gives the total delay time (Sheriff 1973), which can be higher or lower than the datum reduced time.

The reduced travel time (graphical detail will be explained in section 4.5.3) is a function of velocity and of the structure (velocity, thickness) of the overlying layers. Consider these three two-layer models situations:

1) The control situation where the velocity of the first and second layers is 600 m s^{-1} and 2400 m s^{-1} respectively, and the thickness of the first layer is 2 m. The arrival time at 10 m distance is 10 ms. The reduced time for this point at a 2400 m s^{-1} reduction velocity is 6 ms.
2) The first and second layer velocities are 600 m s^{-1} and 1200 m s^{-1} respectively, with the thickness of the first layer being 2 m. The arrival time at 10 m distance is 14 ms. The reduced time for this point at 2400 m s^{-1} reduction velocity is 9 ms, or 3 ms slower than the control time.
3) The first and second layer velocities are 600 m s^{-1} and 2400 m s^{-1} respectively, with the thickness of the first layer being 4 m. The arrival time at 10 m distance is 17 ms. The reduced time for this point at 2400 m s^{-1} reduction velocity is 12 ms, or 6 ms slower than control.

Thus, instead of being due to low velocity anomalies, a time lag could also be due to thicker overlaying layers. This is a drawback of the technique.

This drawback is not crucial to the success of the method, as the bedrock interface (the layer of interest) is assumed to be roughly horizontal. The assumption is based on the general geological cross-section (Figure 3.3) as well as the information from boreholes and the preliminary study (Section 3.6, Figure 3.6). The physical properties of the overlying layer are consistent throughout the area, thus the velocity is also consistent. The effect of the topography variation has been corrected for (by elevation and static corrections) during the seismic data processing. So the time lag or lead is not influenced too much by the structure (the thickness and velocity) of the overlying layer.

4.3 Previous work

As mentioned in Section 4.1, most tomography applications are in medical imaging (CAT-scanning), reservoir characterisation (crosshole tomography) and in understanding the internal structure of the earth (seismic tomography). Impressive results from crosshole tomography studies in describing the petroleum reservoirs have influenced many geophysicists to adopt the technique for shallow geophysical investigations. Peterson *et al.* (1985) and Cottin *et al.* (1986) used the crosshole tomography technique to image the area for a radioactive waste repository and foundation quality, respectively. Lytle and Dines (1980) also used the crosshole tomography technique in mapping buried voids, shaft and tunnels.

Kilty and Lange (1990) used the tomography technique to detect shallow ore mineral zones. In contrast to conventional crosshole tomography, they used a surface to surface technique where the sources and receivers were positioned along two parallel profiles with the target approximately in the middle. First arrivals from the waves that travelled through the bedrock (vertically bedded high velocity material covered by alluvium)

were reconstructed using transform reconstruction methods to give an image of the ore mineralization zone.

Lanz *et al.* (1998) used the tomography concept in mapping the depth and geometry of landfill. They studied the first arrival times from several neighbouring 2-D refraction profiles. The first arrival times were then reconstructed using a tomographic algorithm that employs a fast finite-difference eikonal solver for propagating wavefronts through 2-D heterogeneous media, and an inversion method that incorporates appropriate damping and smoothing constraints (Lanz *et al.* 1998) to produce a tomogram for each refraction line.

Although the surface tomography introduced here also employs a surface to surface technique, it is different from the techniques of Kilty and Lange (1990), and Lanz *et al.* (1998). Instead of placing the sources and receivers along parallel lines like them, the sources and receivers are placed randomly. This allows the rays to travel a full range of azimuths. This technique also examines the first breaks from the wave that travels through the bedrock, however, instead of applying an algebraic or transform reconstruction technique, the author uses a simple mathematical manipulation performed using a spreadsheet. We compare the time taken to travel through different materials with the time taken as if it travels through only one type of material. The time lead and time lag are mapped instead of the velocity.

4.4 Aims

The site (refer to Chapter 3 for a detailed description) is situated on an abandoned coalmine. It has a relatively simple geology comprising NE-dipping coal bearing Carboniferous sandstones and shales overlain by Quaternary glacial deposits and covered by a loamy top soil (Figure 4.2). In the study area, two recorded and one previously unrecorded mineshaft have been found and treated (Photo 4.1). The size of the shaft is approximately two meters square.

Figure 4.2 Schematic cross-section of the study area showing the relatively simple geology.

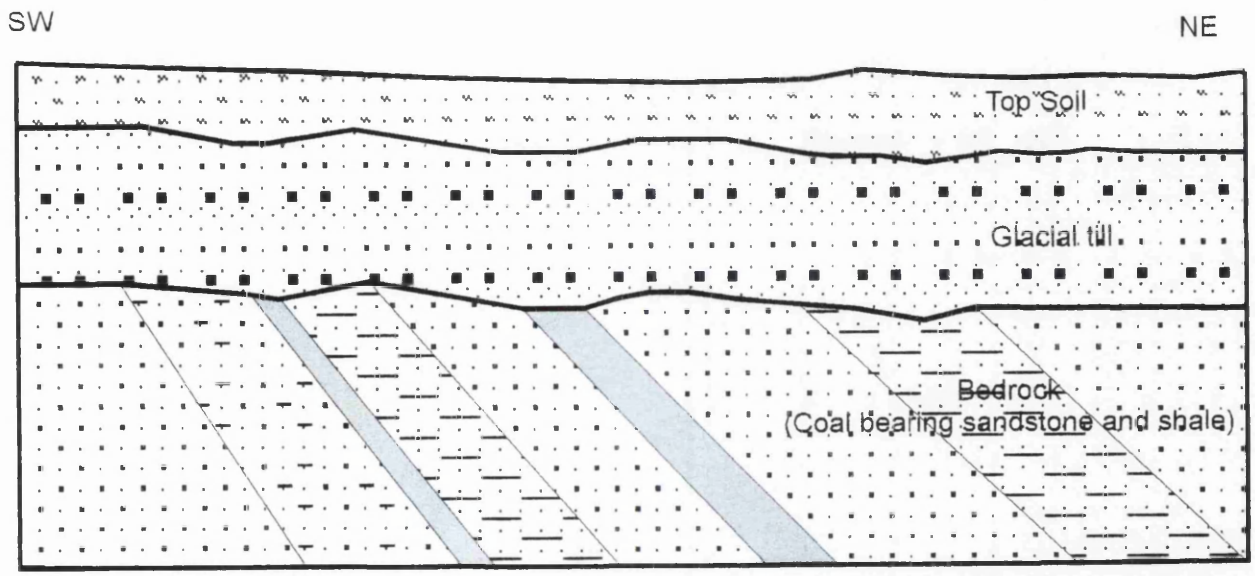

Photo 4.1 An abandoned mineshaft at the Todd Campus West site during treatment for stabilisation.

The aim of this technique is to detect anomalous velocity zones. Mineshafts, which have a very low velocity compared to the surrounding material, would be an ideal target, although it is also hoped that the technique will pick up geological effects such as the variations in velocity of sandstone, shale and coal.

4.5 First breaks

4.5.1 Picking

Since surface tomography deals primarily with analysing first arrival times, accurate picking of the first arrival times is very important. Inconsistency in picking will result in huge errors. The dataset used for this study is same as the one used in the 3-D shallow seismic reflection, and was gathered using a portable OYO minivibrator as a source and 30 Hz single geophones as receivers. Detailed descriptions of the acquisition methods have been presented in Chapter 3.

At large offsets unwanted signals (noise) degrade the data quality. For the near offset traces where the energy (of the signal) is stronger than the noise level, the data quality is good. In order to minimise errors, picking of the first-arrivals has only been done on the good data, where they are clearly identified. Since the long offset traces were contaminated by unwanted noise, the first break picking was limited to offsets of less than 10 m. As the aim of this technique is to pinpoint any anomalies of a size of approximately 2x2 m^2, such as a buried mine shaft, there are enough such near offset traces to serve this purpose.

Prior to first break picking, the polarity of the signal needed to be confirmed. This was done by comparing the vibroseis data to the data gathered using hammer and weight drop (impulsive source) from the 2-D survey carried out on the same area. The first trough was picked on all shot gathers and CDP gathers (Figure 4.3) when it is clearly recognised. All the first arrivals were picked manually using ProMAX/3D and then exported to a Microsoft Excel 97 spreadsheet for simple manipulation.

Figure 4.3 Example of first break picking on a 3-D CMP gather.

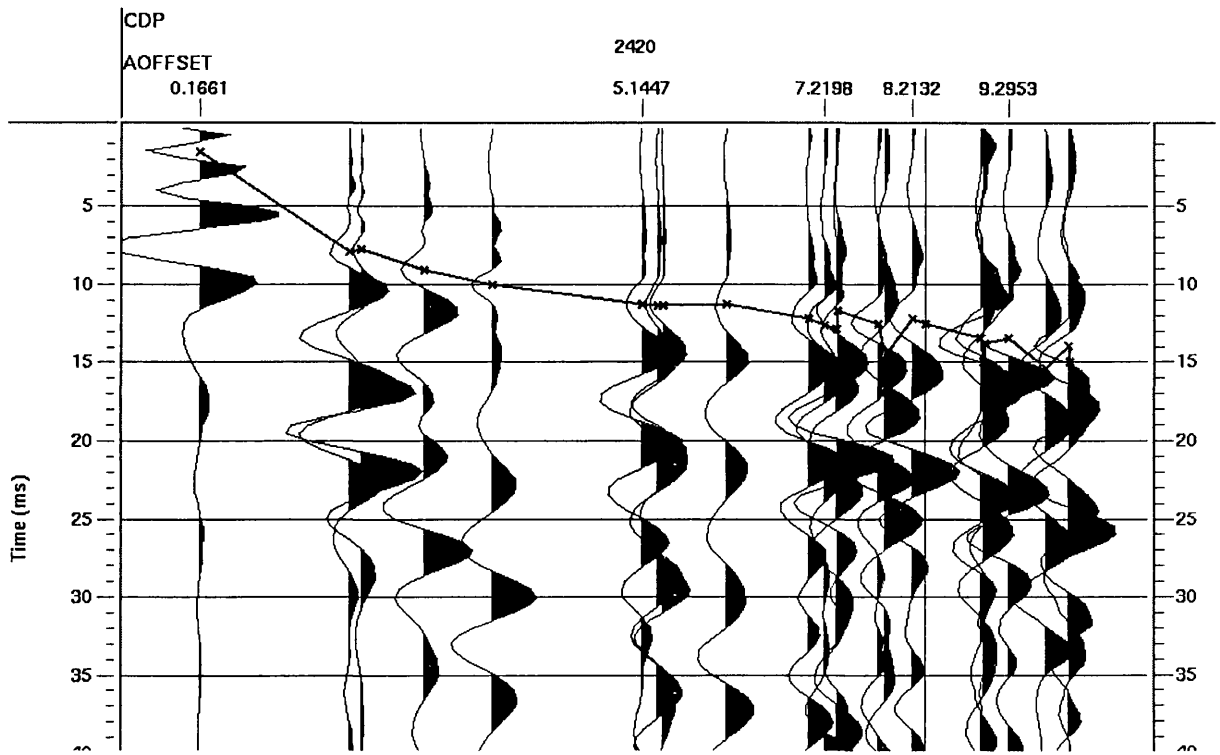

Traces are spaced proportional to the source-receiver offset.
Only offsets of less than 10 m are used.

4.5.2 Time distance curves

Picked first arrival times were then plotted against their offset (distance) to produce a time-distance curve. All the time-distance pairs were initially plotted onto the same graph (Figure 4.4). This is known as the all-points time-distance plot. The advantage of this plot is it gives an idea (first impression) of the geological information such as the layers present, their average velocity and their estimated thickness or depth. This information is sufficient for surface tomography studies since there is no intention of mapping the structure of the refracting interface.

The all-points time-distance plot shows that the variation of the first arrivals (Figure 4.4) increases with offset. At very near offsets it is small (±2 to 4 ms from the mean), however the variation for the far offsets is big, between ±6 to 8 ms around the mean. As the energy of the signal decreases with offset and the noise level increases relatively, this increase in variation with offset is to be expected. One of the reasons for the variation is the difficulty in recognising the first breaks on the far offset traces. This is also the reason why the first break picking is restricted to the near offsets (less than 10 m) only.

Inhomogeneity of the medium (lateral variations in velocity) is, of course, another explanation of this variation. Because the rays have to travel through different velocity layers, the time-distance curve will show a scattered plot rather than a classical straight line section.

What information can we gather from the all-points time-distance plot? Based on best-fit lines drawn onto the travel-time plot, there are three different segments or layers which can be recognised. The first and third segments are clearly seen on the curve. The first is determined by drawing a least-squares best-fit line through the origin. It has a slope of approximately 5.45×10^{-3} s/m. The third segment dominates most of the graph; it has a least-squares best-fit slope of approximately 6.06×10^{-3} s/m, and crosses the time axis at 10 ms.

Figure 4.4 Time-distance curve for all source-receiver pairs.

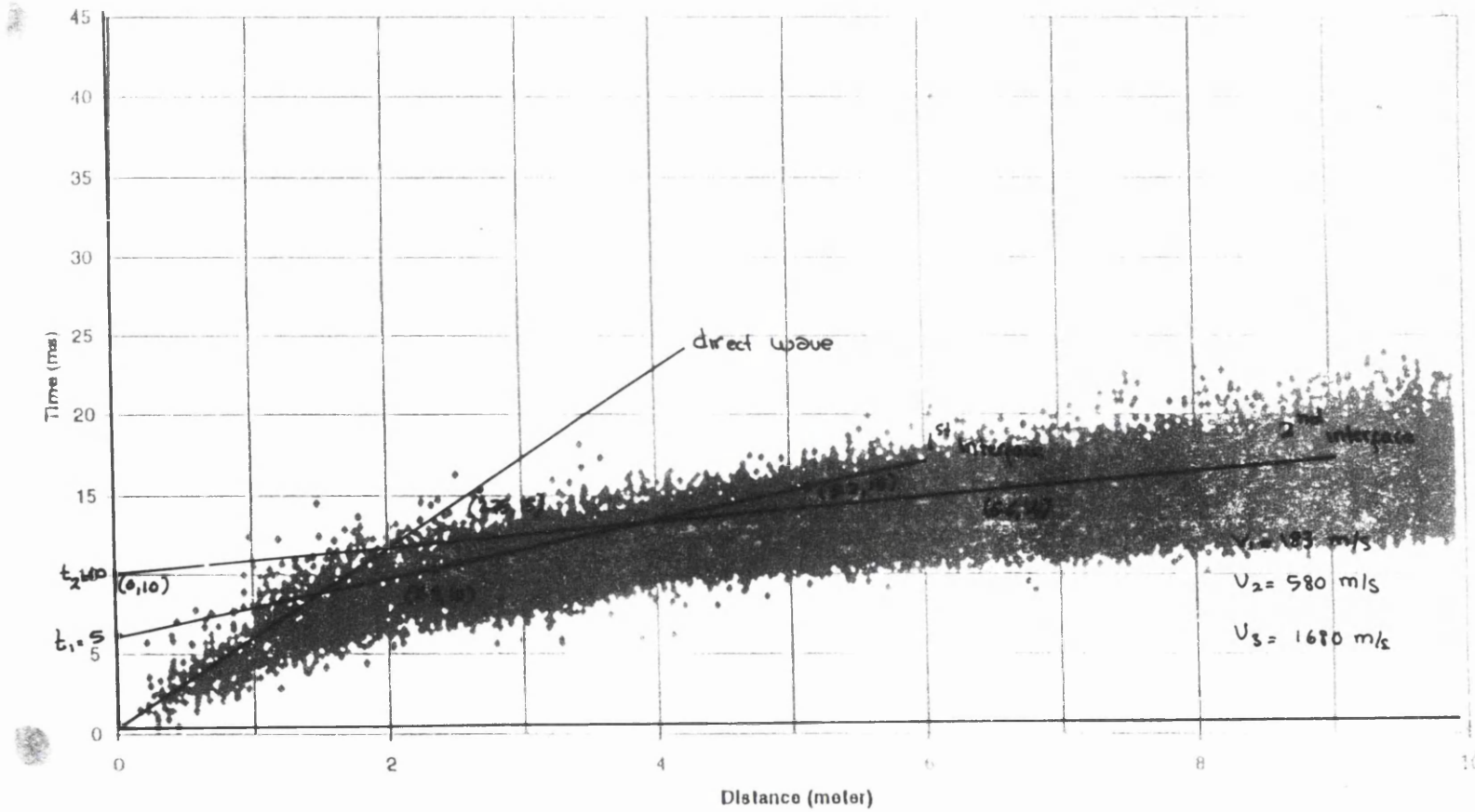

The second segment is more subjective, however, based on the knowledge of the local geology, a best-fit line with a slope of approximately 1.74×10^{-3} s/m can be drawn in between the first and third segments. It intercepts the time axis at 4.9 ms. The crossover distances between the three line segments thus obtained are at approximately 1.5 and 4 m, respectively.

In a normal refraction work, data from forward and reverse shots are observed for the same line. The differences in intercept time indicate the structure of the interface. The interface is flat if the intercept times are the same, otherwise it is dipping. The direction of dip is towards the higher intercept time. However, in the case where only one direction is shot, the interface must be assumed to be horizontal. A plot of all-pairs travel-time graph can be considered as the case where only one direction is shot in a normal refraction survey. Therefore, it has to be assumed that the interface is horizontal.

As the plot indicates a three-layer model, the thickness of the first and second layer can be obtained. Equation 4.1 below needs information on the intercept time and the velocities for all the layers in order to calculate the layer thicknesses. Assuming no dip, the thickness of the first layer is 0.47 m and that of the second layer is 1.51 m.

Equation 4.1 Thickness of the Z_1 & Z_2 for a horizontal interface.

$$Z_1 = \frac{t_1 V_2 V_1}{2(V_2^2 - V_1^2)^{1/2}}$$

$$Z_2 = \frac{t_2 V_2 V_3}{2(V_3^2 - V_2^2)^{1/2}} - \frac{Z_1 V_2 (V_3^2 - V_1^2)^{1/2}}{V_1 (V_3^2 - V_2^2)^{1/2}}$$

where Z_1, Z_2 are the thicknesses of layers 1 and 2

V_1, V_2, V_3 are the velocities of layers 1, 2, and 3

t_1, t_2 are the intercept times for layers 2 and 3

The geological map (Geological Survey of Great Britain, sheet 30, Figure 3.3) shows this area is situated over low angle NE-dipping inter-laminated Carboniferous sandstones and shales with seams of coal of various thickness. This Carboniferous rock is overlain by Quaternary glacial deposits. The contact between these two groups is drawn as a flat erosion surface. On top of the glacial deposits are thin black and loamy materials known as topsoil.

Prior to the 3-D survey, a week of third year geophysical fieldwork (refraction and resistivity survey) was conducted on the site under the supervision of the geophysics lecturers and the author. The students were divided into four groups. All groups gathered their data using the same inline spread geometry pattern - a line of 24 geophones with a 2 m interval. At least five shots were recorded for each group. The shots were placed 2 and 5 m away from both ends and in the middle of the spread (Figure 4.5). Group A and B aligned their spread parallel to the strike while the other two aligned theirs perpendicular to the strike. The result of these refraction surveys is shown in Table 4.1.

Figure 4.5 Third year refraction spread geometry.

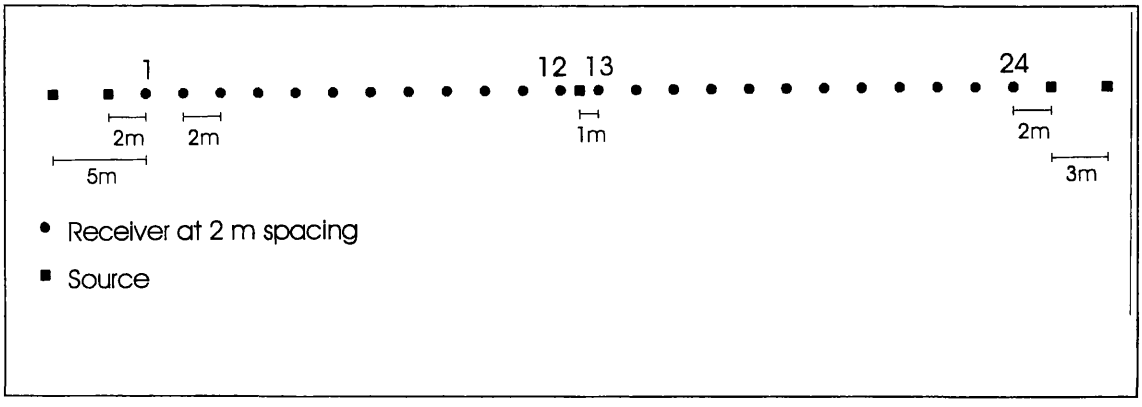

Table 4.1 Results of the refraction survey undertaken by the third year students.

Group	Layers	Velocities	Thicknesses
A	2	440 m s^{-1}; 2000 m s^{-1}	4.5 m
B	2	425 m s^{-1}; 2370 m s^{-1}	2.8 m
C	3	441 m s^{-1}; 1349 m s^{-1}; 2778 m s^{-1}	1.8; 8.9 m
D	2	370 m s^{-1}; 2300 m s^{-1}	2.3 m

A week before the 3-D reflection survey was done, the loamy topsoil was stripped from the area where the injection grouting boreholes were to be drilled (Photo 4.2). Between 0.3 and 0.7 m of the topsoil were stripped off. The daily drilling logs from the grouting operation were also available for reference. They show that the rockhead – the rock underneath the glacial deposit - is approximately 3 m beneath the surface.

Based on direct evidence from the geological and drilling records, the site clearly comprises three layers as graphically shown in Figure 4.2. If so, why do three of the four student refraction surveys only detect two layers? To explain this contradiction, the author re-analysed each of the student groups' datasets and their results. One of the reasons that can be deduced lies in the spread geometry.

The travel-time curve (Figure 4.4) indicates that the crossover distance between segments one and two is approximately 1.5 to 2 m offset. The crossover distance is the distance where the refracted wave has travelled through a higher velocity medium and has arrived at the same time as the direct arrival, or the refracted arrival which has travelled through a lower velocity interface. The crossover distance is different from the critical distance (the distance at which the reflection time equals the refraction time). The critical distance is less than crossover distance; however in designing a seismic survey, the crossover distance is often taken as an approximation of the critical distance (Milson 1989). The critical time is obtained by dividing the crossover distance by the direct wave velocity (Milson 1989). This will avoid the detection of unimportant signals such as the direct wave.

Photo 4.2 Area of stripped topsoil, where grouting holes were to be drilled.

Since the nearest offset receiver is at 1 m, and the receiver spacing is 2 m while the approximate critical distance is 1.5 m, only one receiver can detect the direct arrival, an arrival from the first layer (top soil). In an area with a lateral variation in velocity like this area, drawing a best-fit line was not an easy job. The problem is, to which line segment does this single point belong?

Without any prior knowledge of the layers and their velocity, there is a high possibility that this single point was considered as a part of the second segment which means that only two segments were recognised. Drawing the best-fit line through the origin and honouring all the points will decrease the slope, which implies an increase in the velocity. Depending on the slope of the best-fit line drawn in this way, the velocity should give the value of approximately 183 m s^{-1} (first layer velocity), 580 m s^{-1} (second layer velocity) and 1680 m s^{-1} (third layer velocity) based on the time distance curve of Figure 4.4.

An average velocity value for the sandstone-shale (typical rock type for the third layer) is 1500 to 4000 m s^{-1} (Waltham 1994). Pennant Sandstone of Carboniferous age however has a higher velocity value in the range of 4000 – 4500 m s^{-1} (Kearey and Brooks 1991). However, because rockhead or bedrock is very shallow (approximately 3 m), it is subjected to weathering, which will reduce the velocity. The weathering effect may be the reason why the velocity for the third layer (Carboniferous rock of sandstone-shale type) is as low as 1600 m s^{-1}.

4.5.3 Reduced time distance curves

A reduced time distance curve is another way to display time-distance pairs. Reduced time where the travel time corresponding to a single constant velocity is subtracted from the recorded time (Equation 4.2). The constant velocity is known as the reduction velocity. The reduced time plot is normally used to display large-scale refraction data, which are concerned with late arriving phases such as wide-angle reflections or S-wave arrivals (Kearey and Brooks 1991).

Equation 4.2 Reduced time equation.

$$T = t - \frac{x}{V_r}$$

T = Reduced time

t = Observed time
x = Offset
V_r = Reduction velocity

Six different reduction velocities – 400, 600, 800, 1400, 1600 and 1800 m s^{-1} were chosen in order to estimate velocities for the second and third layers. The first three were chosen to estimate the velocity for the second layer, and the other three were used for estimating of the velocity of the third layer.

Figure 4.6a and 4.6b show all-points plots reduced by the six different reduction velocities. The middle part of the plot in is flattened at a 600 m s^{-1} reduction velocity (Figure 4.6a), while the end section (third segment) is flattened when 1600 m s^{-1} of reduction velocity is applied (Figure 4.6b).

Inspection of the 600 m s^{-1} reduced time plot also reveals evidence of the existence of three layers, since there appear to be three different segments with positive, flat and negative slopes, respectively. These estimates of velocity for the second and third layers, of 600 and 1600 m s^{-1}, respectively, are clearly very approximate, in view of the scatter of points.

Figure 4.6a Test of three different reduction velocities (400, 600, and 800 m s^{-1}) in order to estimate velocity of second layer.

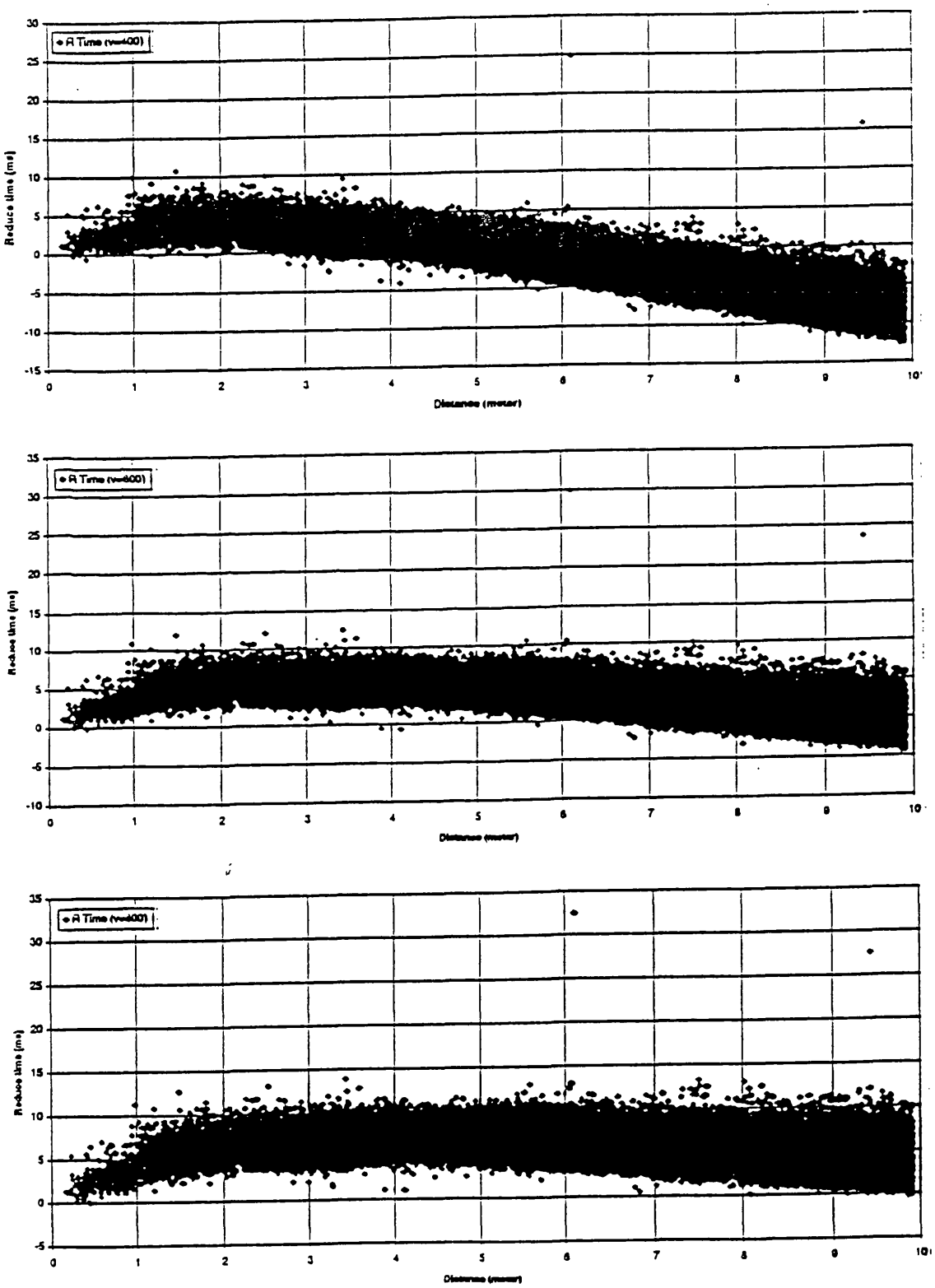

Figure 4.6b Test of three different reduction velocities (1400, 1600, and 1800 m s^{-1}) in order to estimate velocity of third layer.

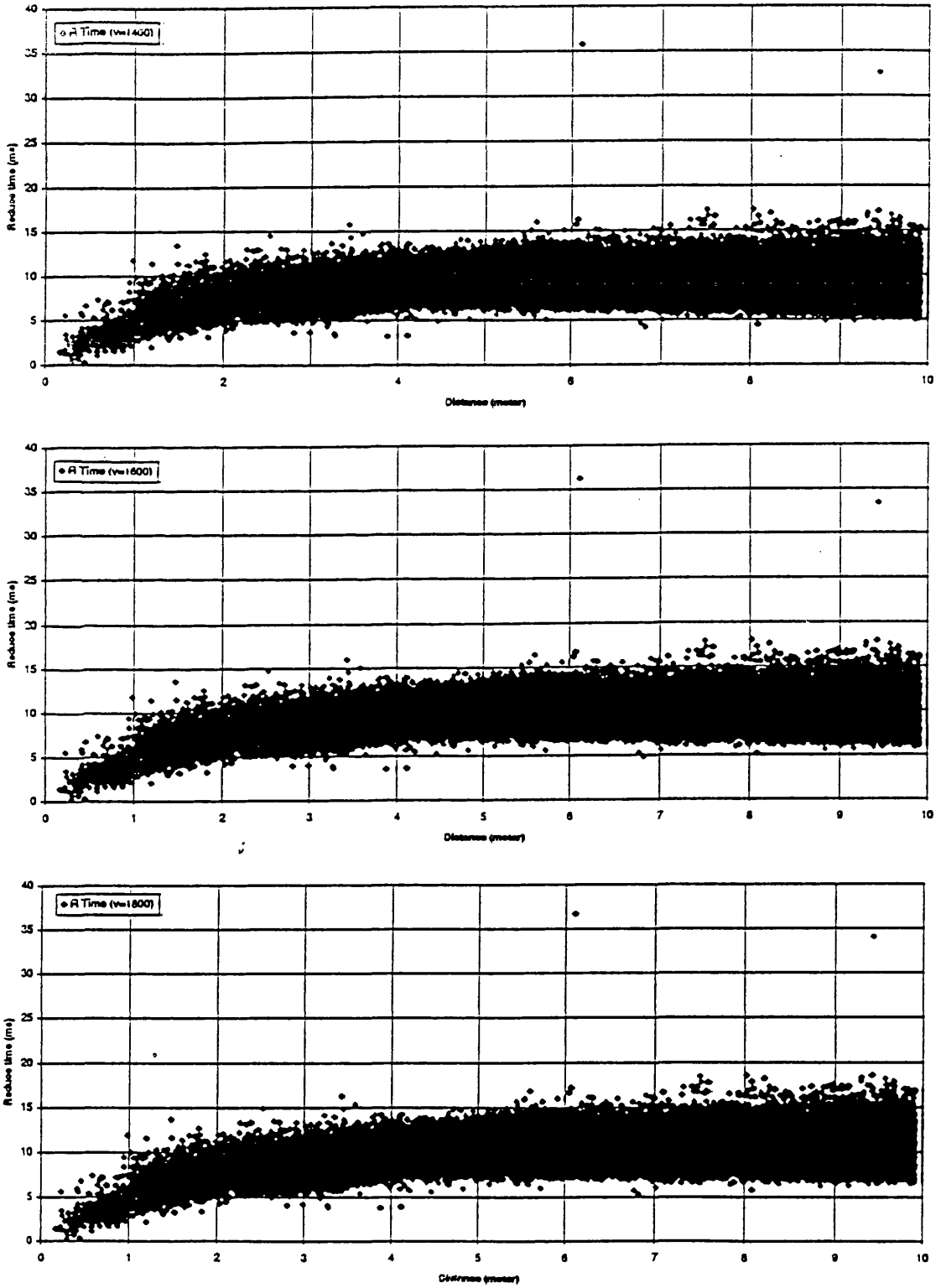

4.6 Surface tomography

The surface tomography method is a simple and robust way of mapping the velocity of a refractor, using the first arrivals from a 3-D survey. The arrival times from many ray paths are displayed along a projection (map) of the respective ray paths along the refractor. Each ray will show either a time lag or lead relative to a reference time, depending on the medium within which it is travelling. These time lags or leads are assigned an appropriate color scheme to make them easy to recognize. In calculating a time lag or time lead, only three basic pieces of information are needed, which are: (1) source and receiver location, (2) azimuth (which can also be calculated from source and receiver location) and (3) first break time. Using these, the surface length of the raypath, an average velocity and the direction of travel can be obtained.

As the dataset used in this study is the same as that used in the 3-D reflection survey, all these data are already available in the database (the first breaks having already being picked during the data processing phase). The surface length (the distance between source and receiver) represents a projection of the propagation path from source to receiver through all the media (topsoil, glacial till and Carboniferous). However, as the main target (e.g. a hidden mineshaft) extends only up to the second interface (between glacial till and Carboniferous bedrock), only the portion of the raypath travelling along that interface is useful in detecting the anomaly related to the shaft. The projection of the raypath through the first and the second layers should be edited out.

The length of the path along the second interface (refracting along the top of the third layer) can be obtained by subtracting the critical distance from the surface length. A crossover distance from the all-points time-distance curve gives a good approximation to the critical distance. Re-calculating the travel path also means shortening the surface length, however the direction is still the same. In order to draw an accurate third layer path, the subsurface projected coordinate (vertically projected from the entry point to the third layer) is calculated using Equation 4.3. Figure 4.7 shows a schematic relation between the surface path and the surface projected third layer path.

Equation 4.3 X & Y coordinate for the projected third layer entry point.

$$S_x^{'} = S_x + \frac{x_c \sin(\alpha)}{2}$$

$$S_y^{'} = S_y + \frac{x_c \cos(\alpha)}{2}$$

where X_c = Critical distance

α = Azimuth

S_x, S_y = X & Y coordinate for original point

$S_x^{'}, S_y^{'}$ = X & Y coordinate for projected point

Figure 4.7 Schematic relation between surface path and the surface projected path within the third layer.

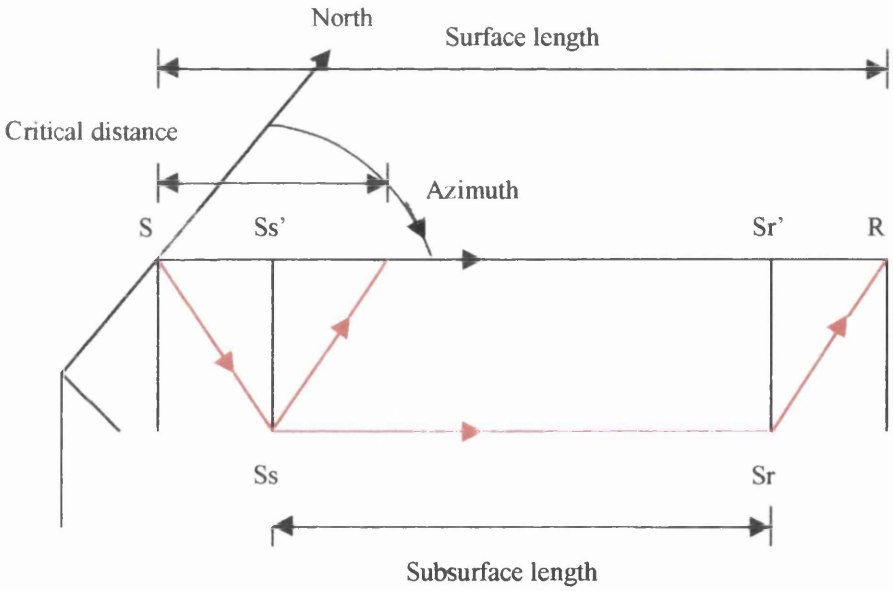

Where S = source
R = receiver
Ss = subsurface equivalent of S
Sr = subsurface equivalent of R
Ss' = surface projected Ss
Sr' = surface projected Sr

4.7 The display

The best way to look at the surface tomography had to be found by producing different kinds of maps such as vector and raster image maps. All these maps were produced on a UNIX Sun workstation using the GMT (Generic Mapping Tools) programs. Because the target is small (approximately two meters square) a useful map must be big enough to see those anomalies. The decision has been made to produce maps with 1:50 scale, i.e. 1 m on the ground is equal to 2 cm on the map. Therefore, any anomalies of 4 cm^2 (2 by 2) on the map (1 m^2 on the ground) should be recognised without any difficulties.

Three types of maps were produced. Each of them aims to tell a different story. All these maps were plotted using a Hewlett Packard Design Jet 350C plotter. Because the original maps were too big to be plotted as a single file, the size had to be reduced (for presentation purposes) to an appropriate size prior to sending to the plotter. The scale used for three main back-pocket maps is approximately 1:192, which means the original size of the map is reduced by a factor of four (approximately).

4.7.1 Reduced time (vector) map

Figure 4.8 (Back pocket 1) shows a reduced time map for the whole dataset. All the rays travelling through the second interface are represented by vectors. There is a small arrowhead showing the travel direction, but this is only visible on larger-scale plots or screen displays.

The aim of this map is to show the zones of time lead and time lag with respect to their path so that anomalous zones can be identified. The data, which comprise the third layer's (X, Y) coordinates of the point Ss' (Figure 4.7), the azimuth from source to receiver, the path length and the reduced time, were sorted by their reduced time and binned into several files.

Each file was assigned a different colour. The datum or average time was assigned as green. The time lag, or time bigger than the datum, was assigned blue increasing in intensity towards higher times, whereas the time leads were assigned red increasing in intensity towards lower values (Figure 4.9). This colour code was used for all surface tomography maps.

4.7.2 Reduced time (vector) anisotropy map

The solid geology of this area is north-easterly dipping coal bearing sandstones and shales of Carboniferous age, striking NW-SE. Because of the heterogeneous nature of the stratigraphy, rays travelling along the strike direction are likely to have a different velocity from those travelling across the strike. This is a form of anisotropy.

The reduced time (vector) anisotropy map displays this anisotropy. This reduced time (vector) anisotropy map is produced in the same way as a reduced time (vector) map. The individual files which had been previously sorted by reduced time were sorted once again, this time by their azimuth. All raypaths with azimuths between 0° to 90° and 180° to 270° (i.e. down- or up-dip) were stored into different files from the ones with azimuths of 90° to 180° and 270° to 360° (i.e. along strike).

Figure 4.10a (Back pocket 2) is the resulting map where the azimuths lie between 0° to 90° and 180° to 270°, representing all the rays that travelled roughly perpendicular to the strike. Figure 4.10b (Back pocket 3) represents all the rays travelling more or less parallel to the strike.

Figure 4.9 Colour code as used in all reduced time maps.

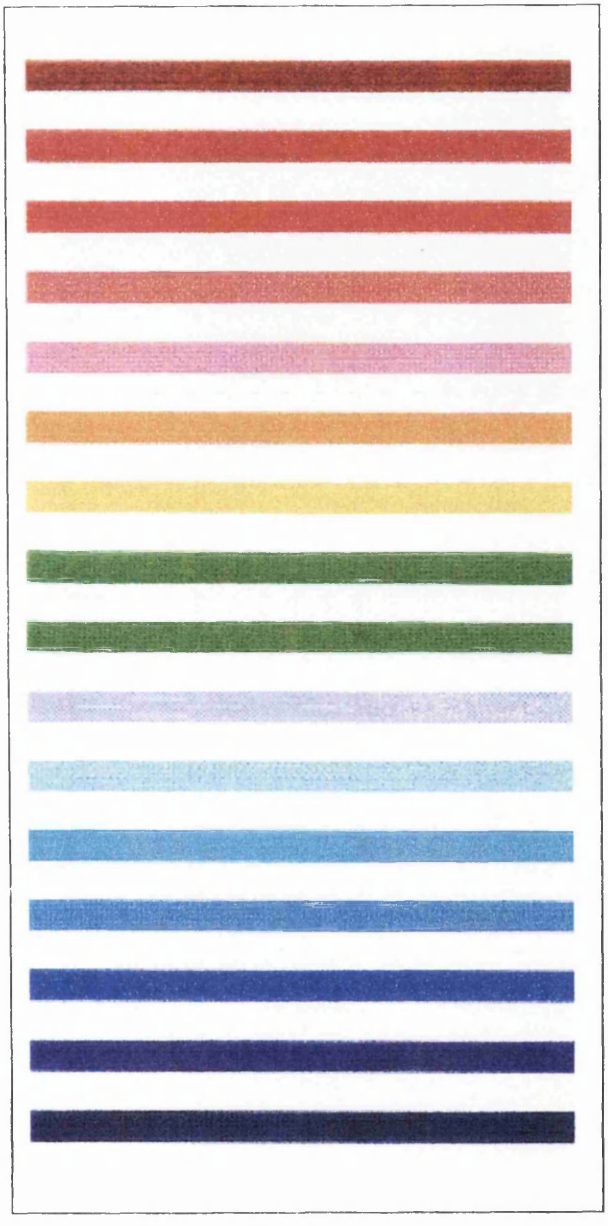

4.7.3 Reduced time (image) map

The reduced time (vector) map is produced by plotting lots of thin lines with an appropriate colour representing each source-receiver vectors. Where there is lots of vector covering the area (e.g. southern parts of the area, Figure 4.8), finding a small clustering of different colour (small anomaly) is not a problem. On contrary, where the number of vectors is not sufficient to cover the area, it create gaps (e.g. middle part of the map, Figure 4.8), thus it is hard to recognise any small anomalies. This is the drawback of the reduced time (vector) map.

The reduced time (image) map is produced to overcome this problem. Instead of using lines, the area is coloured by different colours corresponding to the local reduced times. Instead of lines, points were used. For each vector, coordinates for a series of points at 2 m intervals were calculated. The points were calculated using Equation 4.3, but instead of using the critical distance, a 2 m crossover distance was used. Figure 4.11a shows an example of two lines (vectors) and the series of 2 m interval points along the lines. The points were then gridded onto a 0.25 m equal grid with a 1.0 m search radius (Figure 4.11b), thus giving fine pixels for producing an image map. The reduced time values of all the points inside the circle were averaged. Using the same colour code as before, these new points were then used to produce a raster image map (Figure 4.12, Back pocket 4).

4.8 Interpretation

How do we interpret these maps? As the map is produced using different colours to show the time lag and the time lead, interpretation is qualitative. The differences in the general pattern (of colour) and the concentration of blue (time lag) are the main observations. The pattern difference will hopefully indicate the bedrock geology while a small concentration of time lag colour (blue) may reveal the location of a low velocity anomalous zone, such as a mineshaft.

Figure 4.11a An example of a series of 2 m interval points (red crosses) calculated along two corresponding vectors (solid lines).

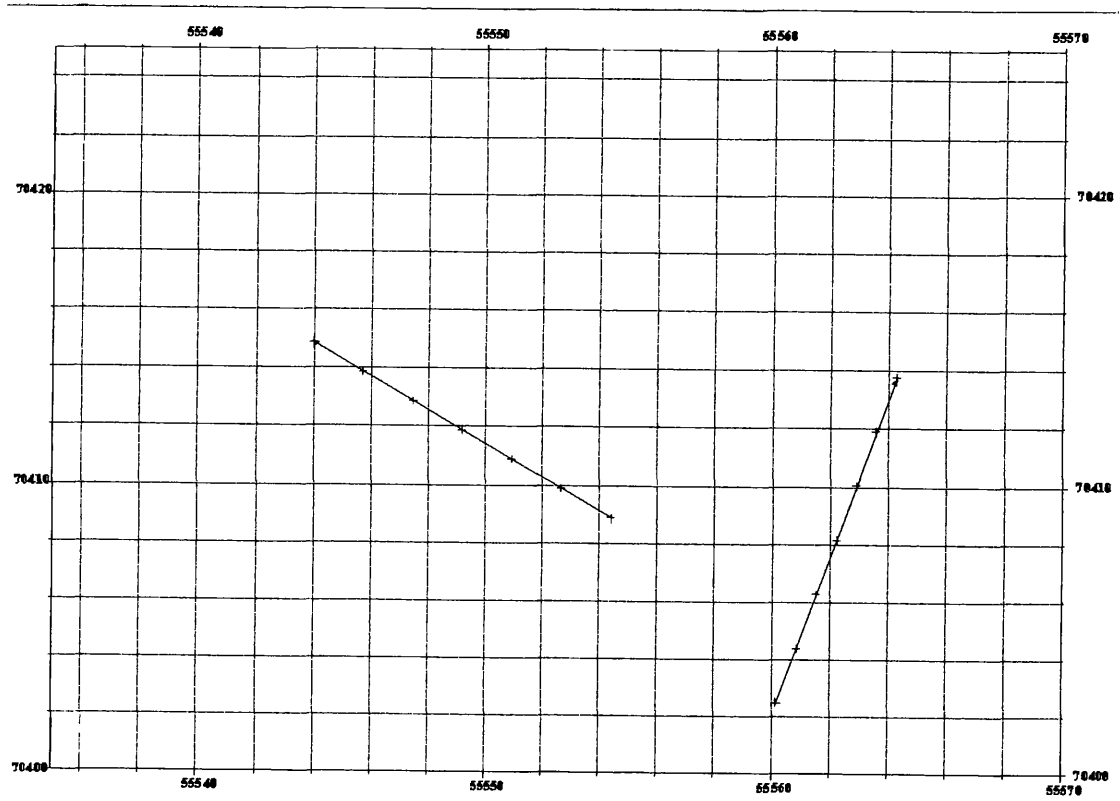

Grid is 2 m square.

Figure 4.11b Details of the points (left) and 0.25 m pixels of different colours (right) used to produce the image maps.

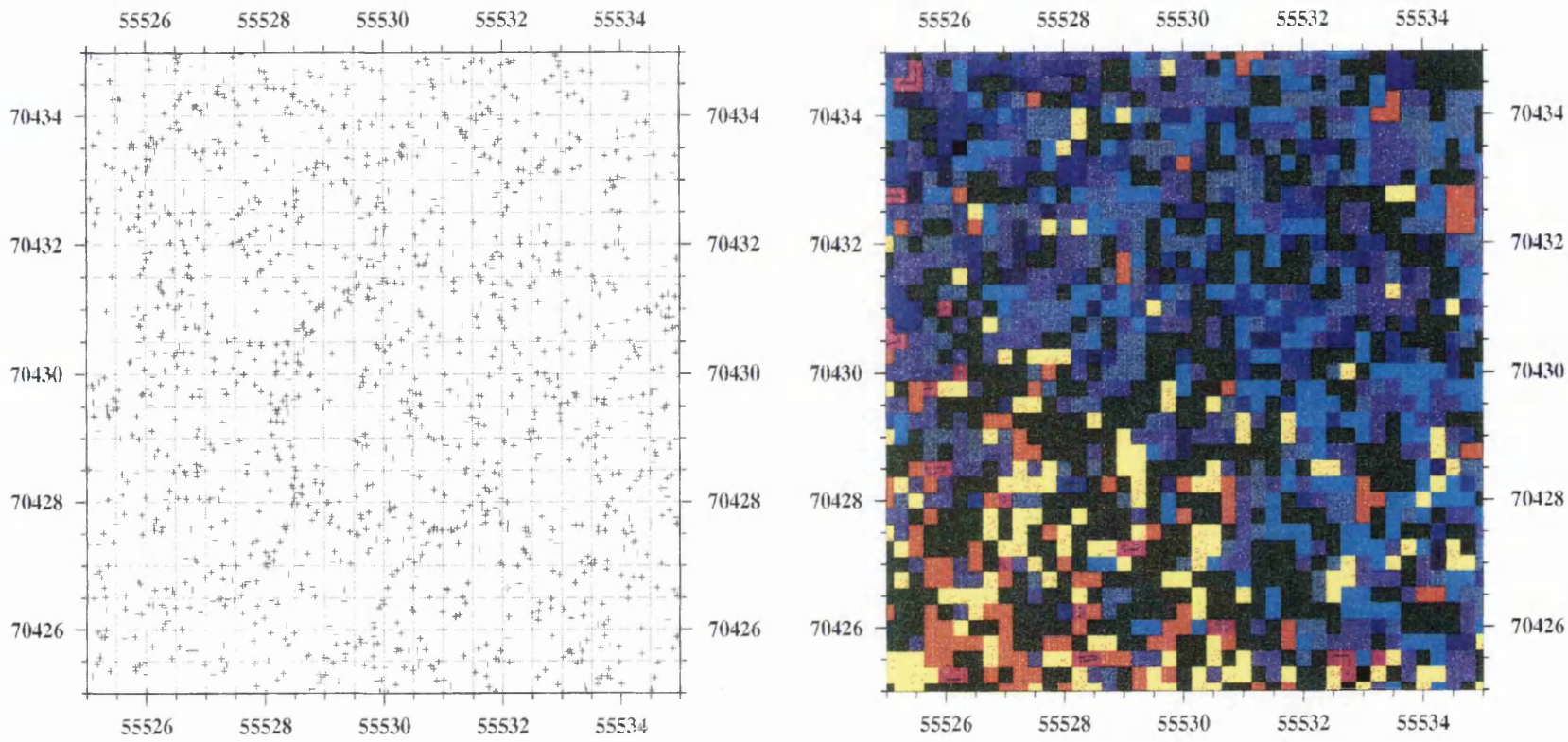

4.8.1 Control

Because the interpretation of these maps is qualitative, the controls on the interpretation are very important to make it meaningful. Our controls are based on all information available such as: (1) the geological map (Figure 3.3), (2) the 1966 and 1981 boreholes and mineral report, (3) the 1995 boreholes and geotechnical report, and (4) the plan view of working coal seams as abandoned in 1897 (Figure 3.4). An attempt is also made to correlate these maps with the result of the 3-D seismic reflection study (Figures 3.52 to 3.54).

The bedrock geology is known to be a low angle NE-dipping Carboniferous sandstone and shale sequence with seams of coal of various thicknesses. The general strike is NW-SE. Extensive drilling in 1981 identified several coals, as listed in Table 4.2. Based on this, a map with conjectural coal outcrop was drawn (Figure 4.13). Among these, only two coals were conjectured to crop out at the site - Twechar no. 1 and Twechar no. 2, which have an average thickness of 0.38 m and 0.16 m, respectively (Table 4.2).

Borehole information from the 1995 drilling programme was not useful because most of the drilling was terminated once bedrock was encountered. The only useful information that can be gathered from these boreholes is the depth to bedrock and its type.

Figure 3.4 shows two superimposed plans of the worked coals as abandoned in 1897. The blue outline is the plan of the Jubilee Coal working, while the green outline shows the plan of the combined Meiklehill Main and Meiklehill Wee Coals (also known as Possil Main Coal). The Jubilee coal was deeper (113 m) than the green outline workings (41-46 m). The working of the green coals was more extensive, where the working pattern started in the middle of the study area and extended in the NW-SE (parallel to the general strike direction) and moved in the NE direction (down-dip direction). The working pattern for blue (deeper) outline is more subtle where it recorded two main working areas connected by a tunnel. Both blue and green workings were terminated at the NW part with the same pattern (abruptly at a NE-SW line).

Figure 4.13 Conjectural outcrop (red dashed lines) of various coal seams in and around the study area.

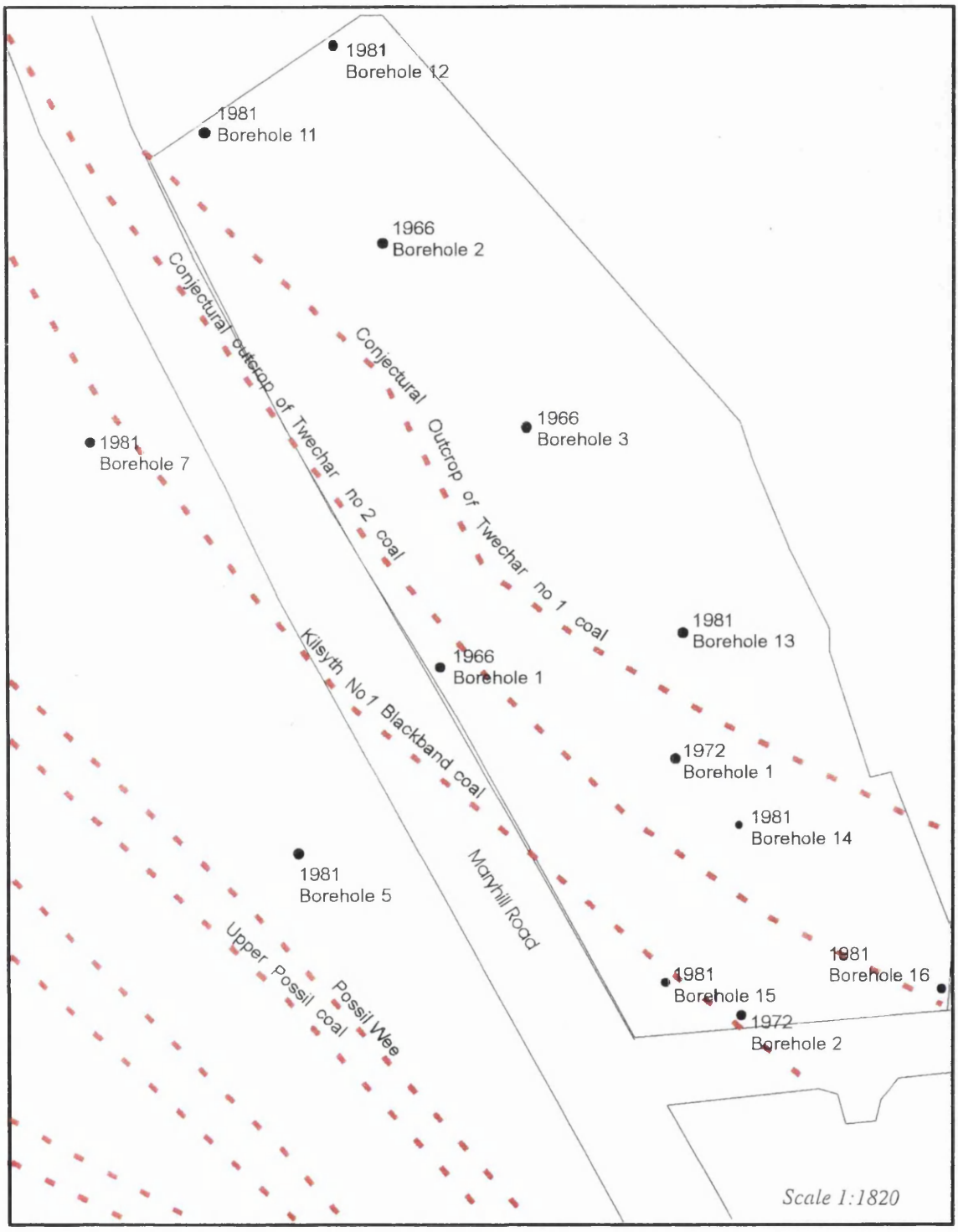

The time slices of the 3-D seismic reflection survey show a continuous peak (red) parallel to the strike direction (see for example Figures 3.55c and 3.55d). This peak is interpreted as an indication of the tunnel or low velocity layer such as the coal layer (refer to Chapter 3 for detailed discussion).

Table 4.2 The general sequence of the underlying seams together with their average thickness and their approximate depth (in m). Green and blue colours are the worked coals whose plan views are shown in Figure 3.4.

Seam	**Average Thickness (m)**	**Approximate depth (m)**	**Note**
Twechar no. 1 Coal	0.38	0	Datum
Twechar no. 2 Coal	0.15	8	
Kilsyth no 1 Blackband Coal	0.69	15	Worked
Kilsyth no 1 Blackband Under Coal	0.46	21	
Possil Wee Coal	0.61	38	
Upper Possil or Meiklehill Main Coal	0.92	41	Worked
Upper Possil Ironstone or Meiklehill Wee Coal	0.46	46	Worked
Lower Wee Coal	0.69	53	
Fourteen Inch Ironstone and Coal	0.15	59	
Fourteen Inch Under Coal	0.46	66	
Ashfield Cooking Coal	0.33	73	
King Coal	0.46	79	
Possil Main Coal	0.99	84	Worked
Cloven Coal	0.46	95	
Shale Coal	0.92	108	Worked
Jubilee Coal	0.61	113	Worked
Knightswood Coal	0.76	122	Worked

4.9 Discussion

The discussion is based on (1) the reduced time (vector) maps, (2) the reduced time (image) map and (3) the reduced time (vector) anisotropy maps with an assumption of a horizontal interface and constant thickness. The interpretations of these maps were controlled by all information available as mentioned in Section 4.8.1.

The reduced time maps, whether vector (Figure 4.8, Figure 4.10a, Figure 4.10b) or image (Figure 4.12), show an interesting pattern of colours – alternating strips of blue and green striking NW–SE. They also show two areas – one of orange and the other of blue in the very south of the area. These are shown at a larger scale (1:128) in Figure 4.14a, back pocket 5. All these features are enhanced in the reduced time (vector) anisotropy maps for vectors along strike. For example, Figure 4.14b, (Back pocket 6) and Figure 4.14c (Back pocket 7) show enlargements of reduced time anisotropy maps associated with the zones of orange and blue at the south end of the area, as shown in Figure 4.14a. Figure 4.14b shows a map of the vectors propagating in the 90°-180° direction while Figure 4.14c shows the more limited propagation direction. It is found that, by limiting the vector to a certain propagation angle (Figure 4.14b, Figure 4.14c) the separation between bands of colours becomes clearer. These features (alternating strips) also show up on the map of bedrock resulting from the 3-D seismic reflection survey, Figure 3.56). What do these patterns mean?

Assuming the bedrock is flat (as discussed in section 4.2), the time lag or lead is a function of velocity alone, which means that a time lead corresponds to a higher velocity layer, and *vice versa*. This assumption is based on the depth to the bedrock information obtained from the boreholes (Figure 3.6) where it is consistently recorded around 2.5 m to 5.0 m. Without any information on the geology of the bedrock, it can be concluded that these patterns reflect the main bedrock geology (inter-laminated sandstone and shale). This is based on the fact that P-waves to travel faster in sandstone than in shale.

The result of 3-D survey for bedrock (Figure 3.56), however, does not entirely support the assumption (flat bedrock) where the presence of the undulating bedrock surface is mapped. One of the possible explanations is that the bedrock detected by this survey is most likely to be the boundary between the weathered and unweathered rock and not the boundary between the glacial deposit and the weathered rock. This is based on the fact that the impedance contrast between weathered and unweathered rock is larger than that between the glacial deposit and weathered rock (bedrock surface). The boundary between the weathered and unweathered rock is deeper than the boundary between the glacial deposit and the weathered rock. Furthermore, the weathering effect on shale is more pronounced than the effect on sandstone because clay (main component in shale) is less resistant to weathering compared to silica (main mineral composite in sandstone), thus producing an uneven weathered-unweathered boundary.

The red colour on the bedrock map (Figure 3.56) represents the deeper area while the blue is shallower. In geological terms based on the argument above, the red is related to shale, as shale shows less resistance to weathering compared to sandstone, and thus may have a deeper weathered-unweathered boundary. On the other hand, the blue is related to the sandstone. The depth to the weathered-unweathered boundary variation also could be in a more resistant rock such as sandstone due to the presence of different amounts of water, as water is a good weathering agent.

Comparing this map (Figure 3.56) with the reduced time (image) map (Figure 4.12), there is a good correlation between the deeper area (red on Figure 3.56) with the blue or time lag area (Figure 4.12). The shallow area (blue on Figure 3.56) in contrast corresponds to the red (time lead) on Figure 4.12.

To test this idea, information on the type of bedrock (the rock type underneath the glacial till) from the boreholes is analysed and is presented as Figure 4.15. Most of the boreholes in the blue area showed that weathered sandstone is the bedrock except 1995-3 and 1981-14 where shale is recorded.

Figure 4.15 Bedrock types from 1966, 1981 and 1995 boreholes.

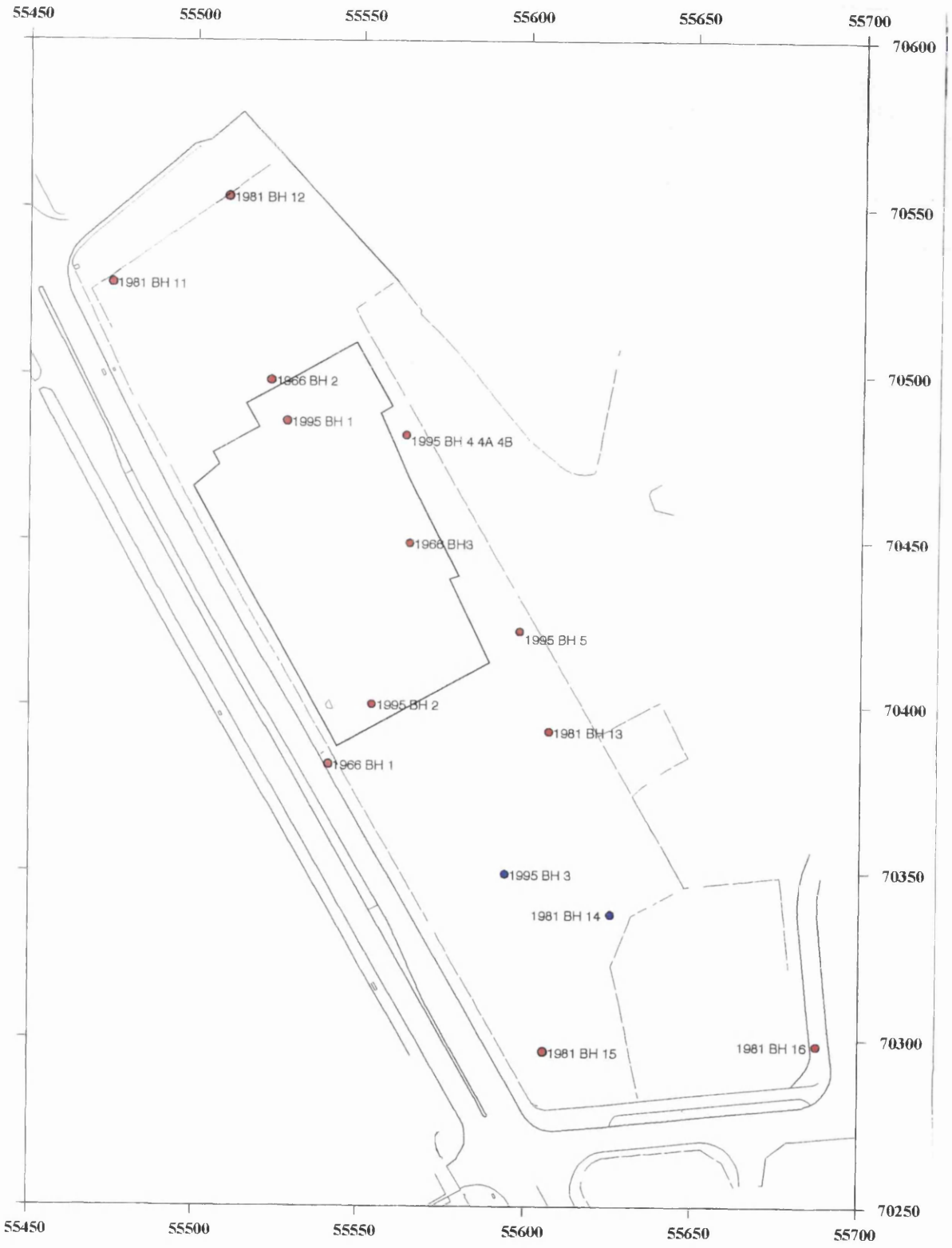

Red and blue circles represent sandstone and shale respectively.

This physical evidence contradicts the idea of blue corresponding to shale, thus an alternative explanation is that those bands are related to more weathered sandstone possibly caused by to the presence of more water. This idea agrees with the fact that the northern part of the area is nearer to the River Kelvin (Figure 3.4). Although we know that the P-wave velocity increases in a water saturated rock, it is still true that the velocity of P-wave velocity is less in the saturated weathered rock compare to the saturated unweathered rock (if the rock is same).

Can we correlate the surface tomography results with the 3-D seismic reflection results? Time slices around 24 and 25 ms (Figure 3.55c, Figure 3.55d) of 3-D seismic reflection data show a continuous peak (indicated by red marker) striking NW-SE and dipping NE. Based on the geological map (Figure 3.3) the general strike is NW-SE and dipping approximately 18° toward the NE. This general strike and dip was confirmed by analysing the three point problem for several coal seams identified during the 1981 drilling programme (Appendix 2). The calculations of strike and dip are attached as Appendix 3.

The 3-D seismic results show that the strong continuous red marker corresponds to the general dip and strike of the area. As discussed in Chapter 3, this strong continuous peak (reverse polarity) occurs at the boundary with a negative acoustic impedance contrast, which means that the upper layer has a higher acoustic impedance value than the lower layer. In the study area, a high negative impedance contrast can occur at the top of a thick coal seam or at the top of water- or air-filled tunnels/mineworkings. The general strike of the coal seams is parallel to the general strike of the bedrock. As the red stripe (Figure 4.12) is parallel to the general geology strike direction, it also reflects the geology/structure within the bedrock, thus this red stripe may indicate of the presence of thick coals or tunnels.

The idea that the strike is parallel to the red stripe (seen on the reduced time maps) or continuous peak (red) in the 3-D time slices contradicts the drawn outcrop strike of Twechar no. 1 in which it was drawn oblique to this direction (Figure 4.13). The

conjectural strike of Twechar no. 1 has been drawn in an open S-shape. This conjectural outcrop is based on the 1981 drilling report in which it was only reported in two boreholes, 1981-12 and -13.

As the regional dip is to the NE, any borehole to the NE of that conjectural outcrop should therefore intersect the Twechar no. 1 coal. Borehole 1981-11 was drilled between the conjectural outcrop and borehole 1981-12. In theory, it should record the Twechar no. 1 coal at shallower depth compared to the depth in borehole 1981-12, but it did not record any. The position of this conjectural outcrop is rather peculiar in being placed SW of borehole 1981-11 (Figure 4.13).

As a check on this conjectural outcrop, we can use the depth at which it was recorded in boreholes 1981-12 and –13, together with the regional dip (approximately 18° to the NE). The calculation of these points is attached as Appendix 4. Twechar no. 1 should then crop out 29 m and 16 m up-dip from boreholes 1981-12 and -13, respectively, assuming a horizontal surface (Figure 4.16). The calculated outcrop location for borehole 1981-13 lies on the conjectural outcrop. However for the borehole 1981-12, it lies to the NNE of borehole 1981-11 (Figure 4.16). This explains why there was no Twechar no. 1 recorded in borehole 1981-11.

The conjectural outcrop of Twechar no. 2 also was drawn to the SW of boreholes 1981-11, -12, -13, -14 and -16 (Figure 4.16). Using the same arguments as above, these boreholes should have recorded this coal unless the drilling depth was too shallow. From the list (Appendix 2) Twechar no. 2 coal was indeed recorded in boreholes 1981-11, -12 and -13, but was absent from boreholes 1981-14 and -16. As boreholes 1981-14 and -16 are nearer to the drawn conjectural outcrop compared to borehole 1981-13, these boreholes should have recorded Twechar no. 2, but they did not. So what is wrong with that drawn outcrop?

Calculating the outcrop location from their depths in boreholes 1981-11, -12 and –13, and using the regional dip, Twechar no. 2 coal should outcrop at 53, 51 and 43 m up-dip

from those boreholes, respectively (Figure 4.16). The calculated distance for borehole 1981-13 matches the location of the drawn outcrop, but the distances for the other two boreholes do not fit at all. The calculated outcrop of Twechar no. 2 for borehole 1981-12 lies to the NE of the conjectural outcrop while for borehole 1981-11 it lies to the SW (Figure 4.16).

To check this mis-match between the re-calculated outcrop of Twechar no. 2 points based on boreholes 1981-11 and 1981-12, and the drawn conjectural outcrop supplied by the contractor, the dip and strike of Twechar no. 2 coal is re-examined. Calculating the dip of the Twechar no 2 using three points (boreholes 1981-11, -12 and -13) shows an anomalous strike of NE-SW and a dip of 1.52° towards the NW (Figure 4.17). This strike and dip is totally different from the regional dip and strike of the area, and suggests that there may be an error during the logging or mineral identification. If it is true, which of those three sources of information is the most likely to cause the problem?

In order to solve the problem, drilling logs for boreholes 1981-11 and 1981-12 were re-examined. Borehole 1981-11 drilling log recorded the presence of coal at the depth of 16.99 m below ground level. From the GDA list (Appendix 2), this coal has been identified as Twechar no. 2 coal. Examination of drilling log 1981-12 showed that only one coal was encountered. However in the list given in the GDA report (Appendix 2), two coals were identified named as Twechar no. 1 and Twechar no. 2 coal at the depth of 9.49 m and 16.50 m, respectively. The coal found during the drilling (at 9.49 m deep) is related to the Twechar no. 1, whereas at the depth where they identified Twechar no. 2, the drilling log recorded 'sandy mudstone'. No trace of coal was recorded at this depth.

Figure 4.16 Calculated outcrop points for the Twechar no. 1 and Twechar no. 2 coals based on boreholes 1981-11, -12, and -13.

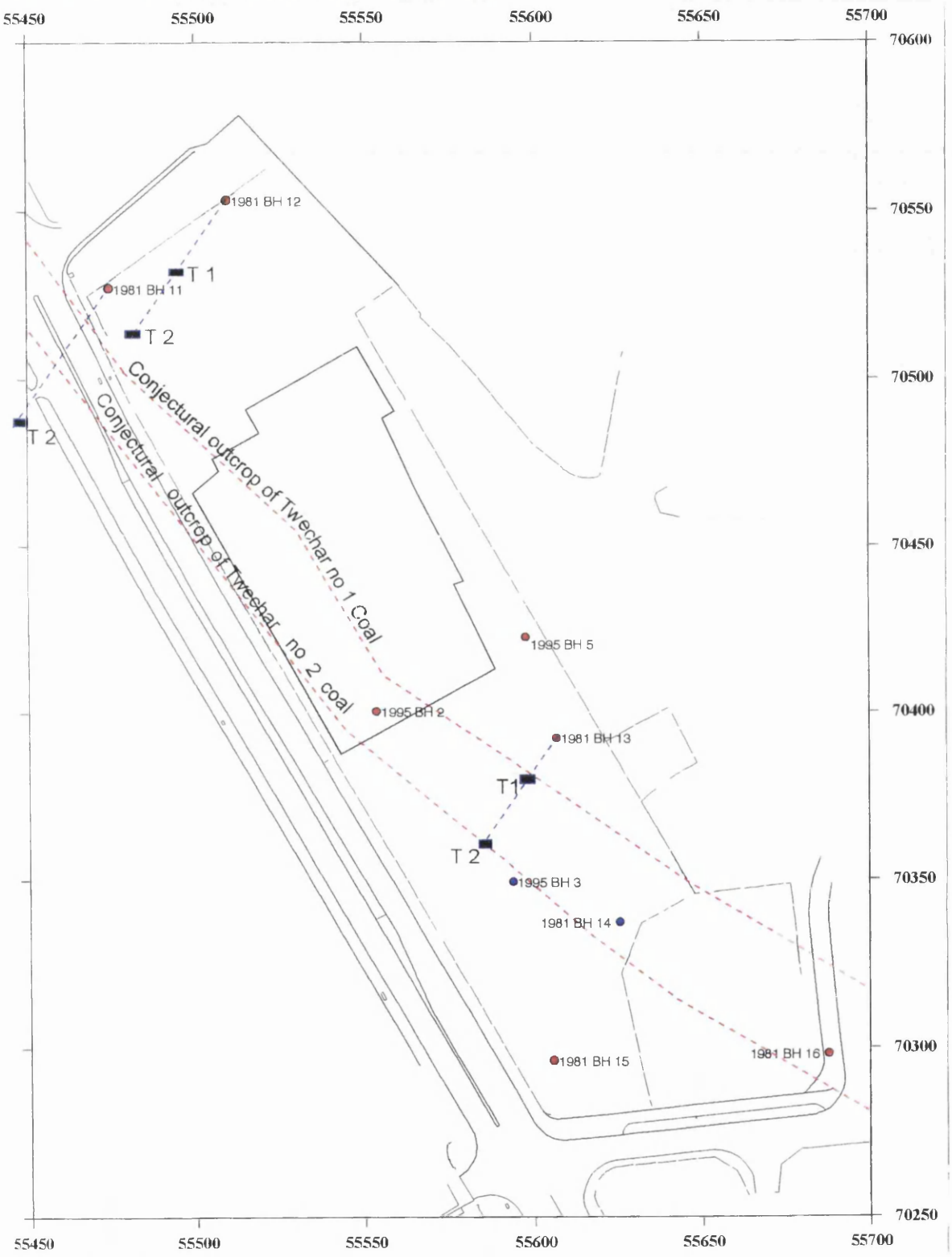

T1 and T2 are the calculated outcrop points for Twechar no. 1 and 2 Coals.

Figure 4.17 The 3-point problem calculation showing anomalous strike and dip for Twechar no. 2 Coal.

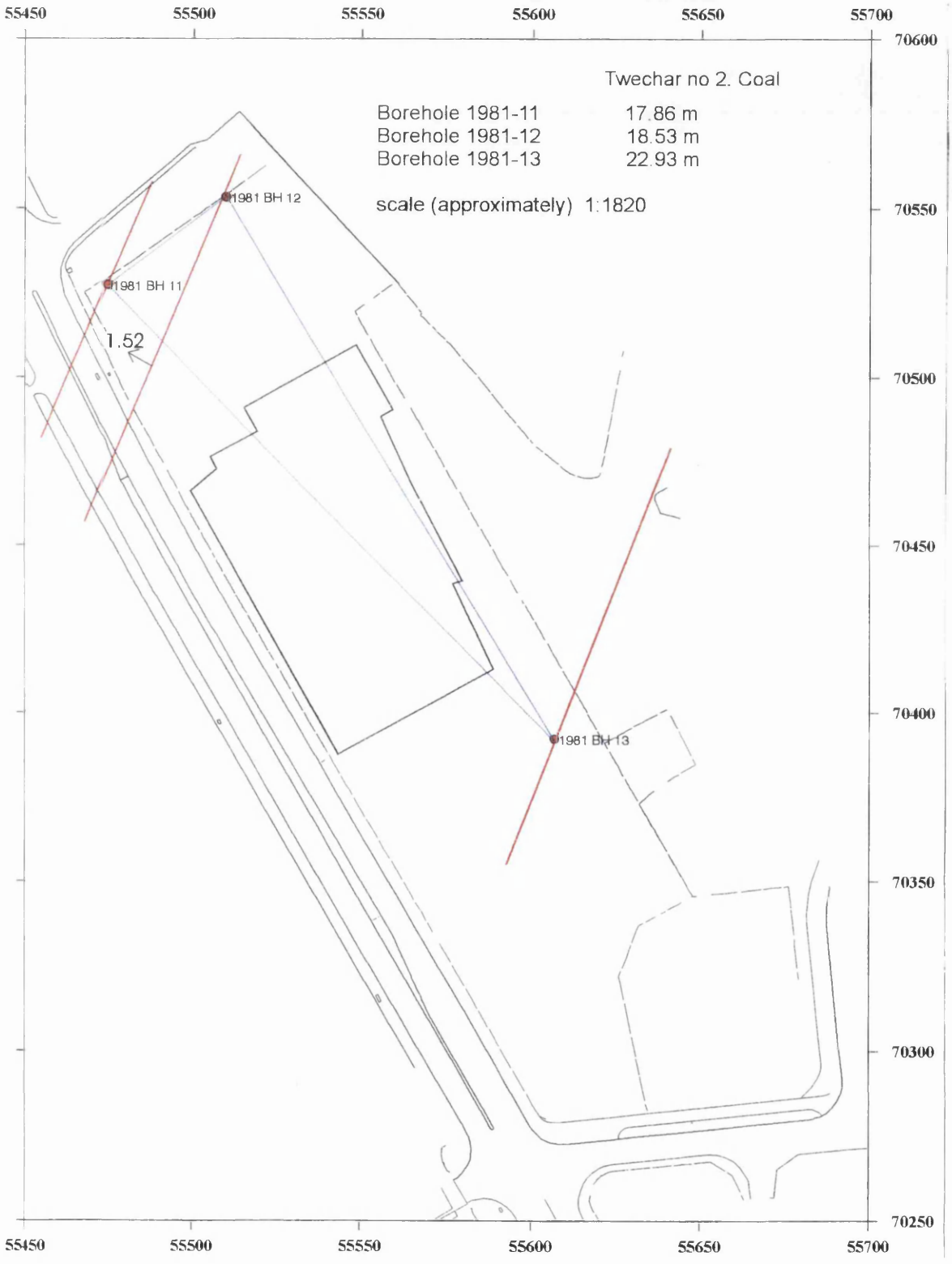

Although the Twechar no. 2 is not identified in borehole 1981-14 and 1981-16 (refer to Appendix 2), the drilling logs from these boreholes were also re-examined as the conjectural outcrop of Twechar no. 2 was drawn to the SW of these boreholes. This is because they should record the presence of Twechar no. 2. Extrapolating down dip from the drawn conjectural outcrop of Twechar no. 2, the coal should be logged at around 4 m and 2 m depth in boreholes 1981-14 and 1981-16, respectively. However at those depths, both drilling logs showed the presence of sandy mudstone.

In all three drilling log examined (1981-12, 1981-14 and 1981-16), where there should be Twechar no. 2 coal found, all of them recorded the presence of sandy mudstone without any evidence of coal. This raises the question whether the Twechar no. 2 coal identified in 1981-11 is actually the Twechar no. 2 or a deeper coal. To check this, based on the drawn conjectural line of Twechar no. 2, a down dip extrapolation was done for 1981-11 and shows that the Twechar no. 2 should be found at a more shallower depth (around 4 m deep below ground level). The drilling log for 1981-11 borehole at this depth logged the presence of the sandy mudstone, which is consist with other boreholes (1981-12, 1981-14 and 1981-16).

The other question about the Twechar no. 2 identified in 1981-11 is that it was found deeper than in borehole 1981-13 or in borehole 1981-12. Yet, the location of 1981-12 borehole is to the west of those boreholes. Thus the Twechar no. 2 in 1981-11 should be found at a shallower depth.

This simple analysis shows that although the coal found in borehole 1981-11 was identified as the Twechar no. 2 coal, this should be treated with care as it may be confused with the deeper coal. To avoid any confusion, the Twechar no. 2 information from boreholes 1981-11 and 1981-12 was did not considered for modelling or discussion.

As the drawn conjectural outcrop for Twechar no. 1 and Twechar no. 2 coal (from the GDA report) are questionable, can we revise the conjectural outcrop to satisfy all the

conditions? To re-draw the new outcrop line for Twechar no. 1 and 2 we have to consider all strike/dip direction information as well as the calculated outcrop points for both Twechar no. 1 and 2 coals for 1981-13 and Twechar no. 1 in 1981-12 borehole (Figure 4.16). The information from the 3-D time slices at 20 –25 ms (Figures 3.55b, 3.55c, and 3.55d) and the strike of the tunnels/mineworks (or thick coal layers) across the survey area in the NW-SE direction should also be taken into account.

In boreholes 1981-13, -14, -15, and -16 there is record of the presence of Kilsyth no. 1 Blackband (0.69m thick) or Blackband Under (0.46m thick) Coal at an approximate depth of 10-20 m (Appendix 2). It is also recorded that the Kilsyth no. 1 Blackband Coal was being mined (Table 4.2).

If the peak signal detected by the 3-D survey is related to these two coals or related mineworks, then the strike of the upper coal such as Twechar no. 1 and 2 should also be drawn parallel to this strike direction. Drawing of the outcrop line for Twechar no. 1 by connecting two calculated points (Borehole 1981-12 and -13) produces a NNW-SSE direction line, which is oblique to the strike direction. This is unlikely as the strike of Twechar no. 1 should parallel the regional strike direction.

The second alternative is to introduce a fault or faults running across the field. Although there was no evidence of faults recorded in any of the reports available, judging from the extensive fault system shown on the geological map (Figure 3.3) the possibility of faults being present in the area cannot be ruled out.

The existence for the east fault across the field is the NE-SW (across strike) continuous red signature on some of the 3-D time slices (e.g. Figure 3.55c). The second supporting evidence of the east fault is more subtle and was deduced by analysing the plan view of the abandoned Jubilee coal mine (Figure 3.4), where it shows a strange pattern, where instead of one continuous working field, there are two fields separated by a tunnel system in the middle of the field – as if they were the same seam separated by fault.

The existence of the west fault was also deduced from analysing the pattern of the workings. The plan view for both mineworks (Figure 3.4) also shows an abrupt termination parallel to the NE-SW direction, as if they also had been faulted. The location of the west fault was placed so that it coincides with the edge of the mine workings.

Based on the calculated outcrop points for both Twechar no. 1 and 2 coals, and the possible existence of two faults, the new revised Twechar no. 1 conjectural outcrop is drawn as shown in Figure 4.18. If we accept this fault model, then an explanation is needed to explain why the fault did not show on any reduced time map. One possible explanation is, since the reduced time map is based on analysing the refractions from the top of bedrock, which in most of the survey area is sandstone, the differences in velocity are negligible, thus the differences in velocity did not show up on the reduced time maps.

On the image map (Figure 4.12) the conjectural outcrop of Twechar no. 1 is drawn on the blue stripe (time lag) rather than on the red (time lead). The reason for this is, if the conjectural outcrop shows the presence of the coal (Twechar no. 1, 0.38 m thick) and coal has relatively lower velocity than sandstone, then the blue zone is an appropriate place to draw it. The effect of this coal also will slow down the travel time of any raypath crossing this coal, thus creating a zone of very slow (dark blue) travel times. The width of this blue stripe (approximately 6-10 m) is also appropriate to the time lag zone created by this coal although it is only 0.38 m thick. Figure 4.19 shows the relation between the thickness of the coals and the time lag zones created by them.

Figure 4.18 Revised outcrop lines for Twechar no. 1 and 2 Coals.

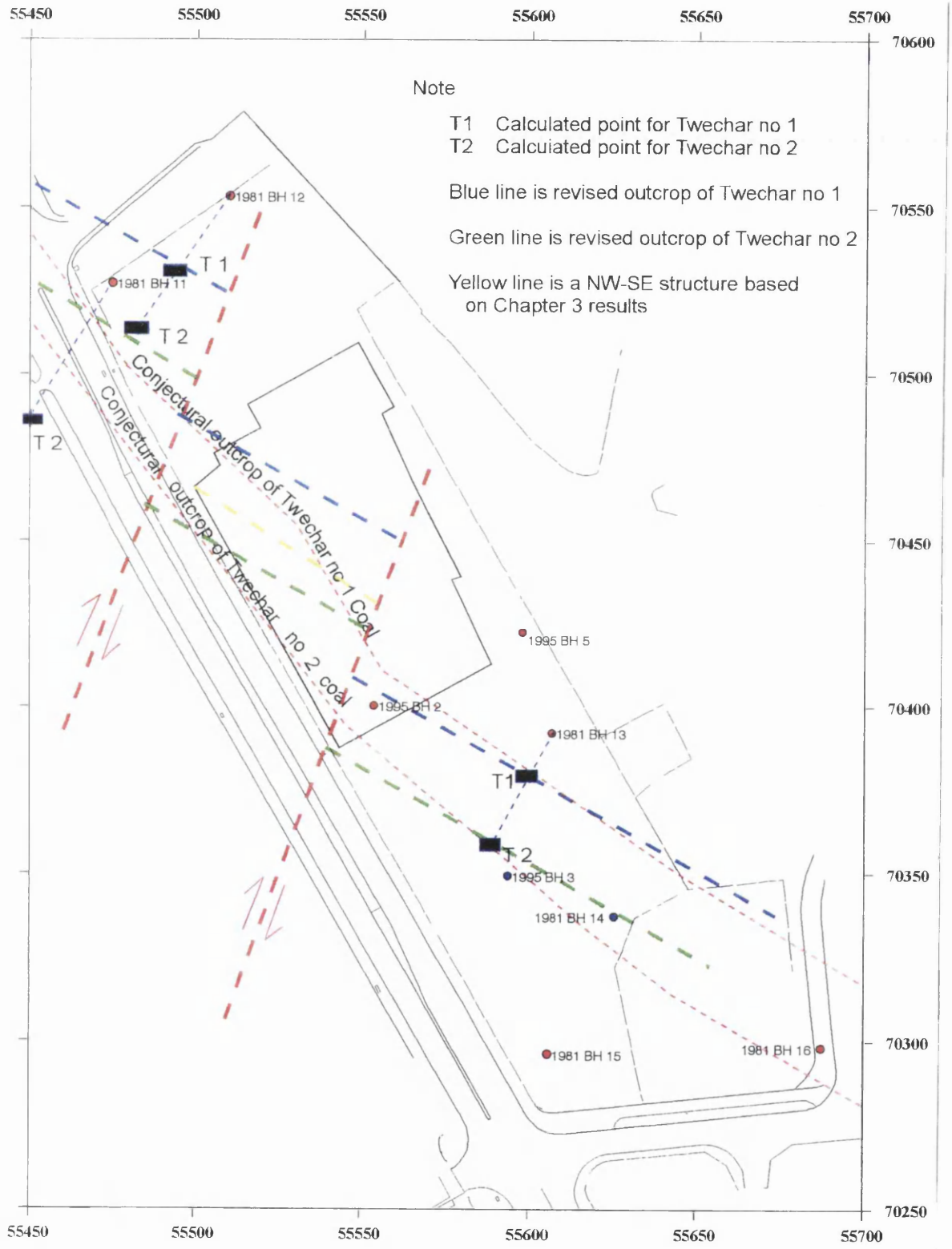

Figure 4.19 Relation between the true thickness, horizontal thickness and maximum width of the blue zone. Red lines represent the dipping layer. Wm represents the maximum width of the vector band on the surface.

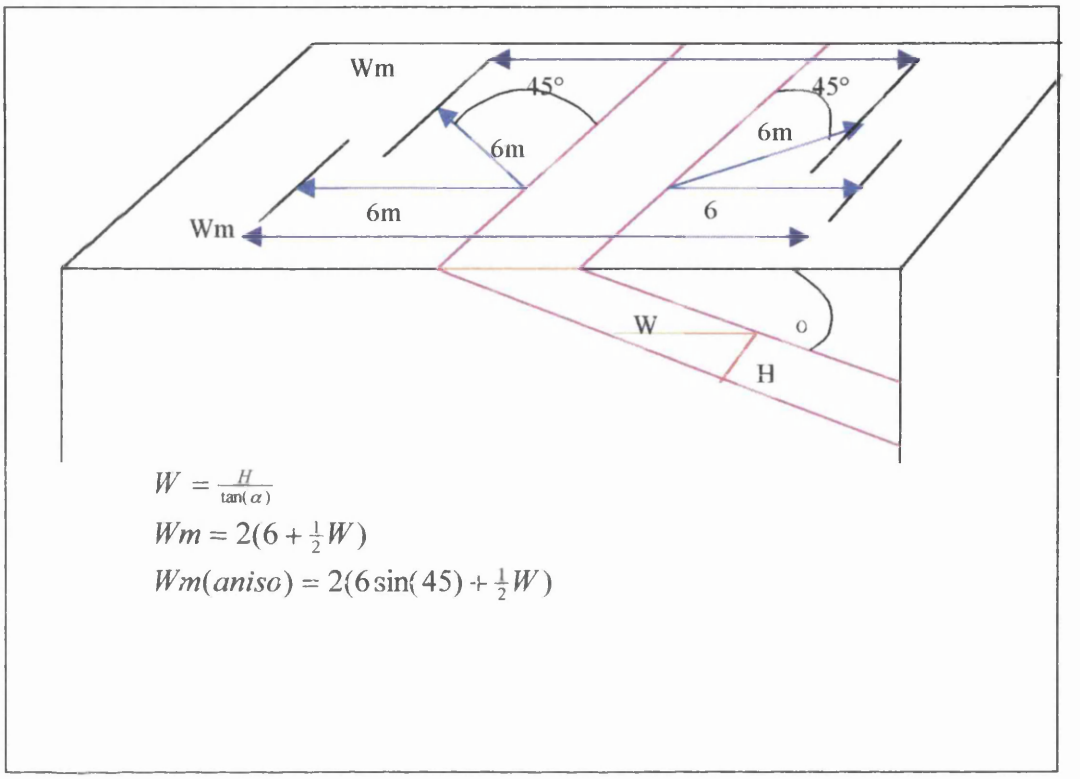

The width (horizontal thickness) of the layer is controlled by its true thickness and dip. Assuming the topography is flat, the relation is $W = \frac{H}{\tan(\alpha)}$ where W is the width; H is the true thickness and α is the dip.

Based on the geological map and investigation reports, the average thickness of Twechar no. 1 is 0.38 m and it dips at 18° to the NE. This means the horizontal thickness is approximately 1.2 m; however this is still too narrow compared to the width of the blue strip (6-10 m). To explain this, instead of the horizontal thickness of the coal, the total vector (raypath) lengths should be considered. Any raypath originating in or passing through this zone will experience a delay. Because we are dealing with the raypaths, the width of the blue does not necessarily represent the width of the low

velocity layer, in this case the Twechar no. 1 coal. Instead, it represents the maximum length of the path which is travelled perpendicular to the strike in either direction. As the maximum length of the path is 6 m (maximum offset 10 m, less the critical distance 4 m), the maximum width will be approximately 13 m.

The discussion so far relates the blue stripe to a thick coal layer sandwich by a more weathered sandstone. This particular coal is may be related to the Twechar no. 1 and Twechar no. 2 coals. If we accept this idea than we have to explain with what velocity does the P-wave travelled through the coal? As has been shown above, the horizontal thickness (h) of the Twechar no. 1 is approximately 1.2 m. If we take the maximum reduced (RT) delay time for the P-wave to travel through 1.2 m of coal is 5 ms (refer to Figure 4.9), then from a calculation shown below the P-wave velocity through coal is approximately 200 m s^{-1}.

$$RT = \frac{h}{Vcoal} - \frac{h}{Vref}$$

$$5ms = \frac{1.2m}{Vcoal} - \frac{1.2m}{1600m/s}$$

$$Vcoal \approx 200m/s$$

This value is far too small for the velocity of P-waves in coal. Thus, it is impossible to relate the blue strip to the presence of a coal seam alone.

Since the coal alone cannot be exclusively responsible for the blue strip, another possible explanation for it is it represents the area where the weathered rock is thicker. In section 4.2 the author discussed how this could occurs. The first model represents a control condition where the overburden with 600 m s^{-1} velocity over laying Carboniferous sandstone-shale bedrock (of 2400 m s^{-1} velocity). The second model represents the condition where the bedrock velocity is lower than normal, thus reflecting a low velocity anomaly. The third model on the other hand was discussed in order to

explain the effects of a thicker overburden over the bedrock. The discussion of these models was based on two assumptions which are 1) the bedrock interface is flat and, 2) no variation in topography – thus the thickness of overburden is constant. The conclusion drawn from this discussion shows that the delay time (blue zone) could be caused by either a geological anomaly (model one) or the variation in thickness of overburden (model three).

Picking of the first arrival was done on all shot gathers after the data were corrected for field statics. The second assumption is based on the fact that the field static correction corrects all the errors resulting from the differences in elevation and weathering effects. All the picked first arrivals are therefore referred to a common datum.

The first assumption on the other hand was based on the geological cross-section of the area (Figure 3.3). However, this assumption is not entirely consistent with the information from boreholes, the preliminary geophysical survey (Figure 3.6) and the result of refraction modelling from the Technical University of Vienna (Figure 3.25) that indicate the bedrock is not flat. Figure 3.25 clearly shows that the top layer (overburden) varies in thickness by approximately 2 m from West to East along the 60 m long line with a velocity of only 370 m s^{-1}. As the thickness variation is approximately 2 m over the 60 m line, the dip of this reflector is approximately 2°. If the dip is constant the maximum variation over the 10 m length (the maximum offset of the data used in this studies) is 0.35 m. The conditions discussed above are presented graphically as shown in Figure 4.20.

Figure 4.20 Graphical representation of the variation of the overburden.

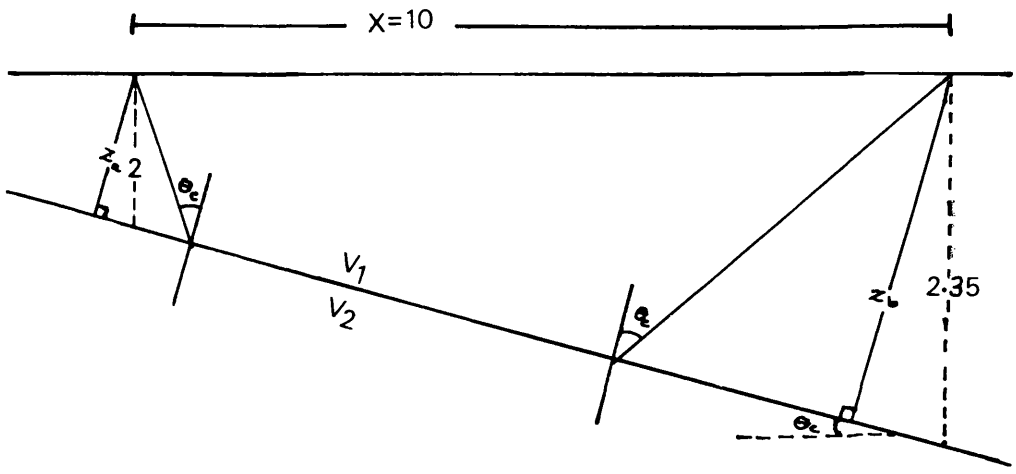

What is the effect of a variation in thickness of overburden on this study? Consider model one, discussed in section 4.2 where the velocity of the overburden is 600 m s^{-1} and the velocity of underlying layer (bedrock) is 2400 m s^{-1}. Depending on if the ray propagates up-slope or down-slope, the arrival time will differ. The up-slope travel time (t_u) and the down-slope travel time (t_d) are given by the expression below (Reynolds 1997).

$$t_u = \frac{x[\sin(\theta_c - \alpha)]}{v_1} + \frac{2z_b(\cos\theta_c)}{v_1}$$

$$t_d = \frac{x[\sin(\theta_c + \alpha)]}{v_1} + \frac{2z_a(\cos\theta_c)}{v_1}$$

where $\theta_c = \sin^{-1}\left(\frac{v_1}{v_2}\right)$

$\approx 14.5^0$

If the minimum thickness is 2 m, then the maximum thickness at the deeper end of the 10 m line will be 2.35 m. Therefore the z_a and z_b thickness will be approximately 2 m and 2.35 m, respectively (referring to Figure 4.20).

From the expression above, the total up-dip travelled time is 11 ms which gives a reduced time of 7 ms. This means the time taken to travelled up-dip is delayed 1 ms compared to the average time. The total down-dip travelled time on the other hand is 12.3 ms which gives the reduced time of 8.3 ms, and a delay of 2.3 ms.

From the discussion above, both up-dip and down-dip reduced time show a delay time, which could cause the blue zones. Thus, it is fair to say that the observed variations (blue and red zones) could also be substantially due to variations in drift thickness.

CHAPTER FIVE

CONCLUSIONS AND RECOMMENDATIONS

5.1 Seismic reflection as a tool for archaeological survey

5.1.1 Conclusions

A number of geophysical techniques are very useful in archaeological studies either in looking for valuable buried artifacts/objects or in locating archaeological sites. These include ground penetrating radar (GPR), resistivity, and magnetics or even gravity. GPR and resistivity are normally used in locating buried ditches while the magnetic method is used to detect any iron-related objects, which are often associated with the ancient site. The gravity method is not as popular as those three methods, but has sometimes been used in locating buried building foundations such as Roman buildings or roads.

Unlike the above-mentioned four techniques, the seismic method has found itself least favourite among the usage of geophysical technique in archaeological investigation. This perception, however, is now changing. To date, some work has been done in this field utilizing the seismic method. The main target is normally to detect buried ditch-like structures. The success of the seismic method in archaeological work depends on the size of the target and the impedance contrast between the host material and the foreign material filling in the structure. The main seismic technique used in archaeological work is seismic refraction, as it is easier than the reflection technique.

The work described here was done to prove that the seismic reflection technique also can be used as an archaeological investigations tool despite its bad reputation among the 'archaeo-geophysicists'. The aim of this work as to a Roman fort ditch which has been buried a couple of meters deep. The target itself has a V-shape with a size of approximately 10 m wide and couple of meters deep. Because the target is very small and shallow (for the normal reflection survey), the author introduced the highly condensed acquisition technique where a total of 208 shots were taken along a 50 m - long 2-D profile. The results of this very shallow seismic reflection survey were then

compared to the results (re-interpreted) of the resistivity survey (the more common archaeo-geophysical survey method) which had been done by Baker (1996).

The resistivity survey shows the presence of four low resistivity anomalies, with two of them most likely being ditch-related anomalies. However from excavation records, the fort is surrounded by only one ditch, which is unusual for a Roman fort as most of them were typically surrounded by at least two ditches. The two ditch-related anomalies seen on the resistivity profiles show that the resistivity profiles alone cannot solve the problem, although it narrowed down the options on where to lay the excavation trenches.

The results from the highly condensed 2-D seismic reflection profile also shows the presence of two structure-like ditches. These two ditch-like structures on the seismic reflection data are found to be correspond well to the two possible ditch-related resistivity anomalies. The size of one of the ditch-like structure on the seismic reflection data is approximately same as the excavation records and more interestingly it lies a few meters off from the expected location (based on excavation records).

Unlike the resistivity result, where the anomalies were interpreted qualitatively and ambiguously, the seismic reflection result shows an image of the ditch-like structures itself. Furthermore a quantitative interpretation can also be made based on the image produced. This means that a more confident determination of the target location can be archieved using the seismic reflection survey method.

Comparing the results of these two methods, it can be concluded that the seismic reflection method gives a better result, despite the pre-perception that this method is very difficult to conduct and the chances of failure are high for a very shallow investigation.

5.1.2 Recommendations

To increase the chances of success, the physical properties of the target and the surrounding area need to be understood, as the seismic reflection method only works best in an area where the contrast in acoustic impedance is high.

Although the result of this reflection survey (together with the resistivity results) gave the possible location of the buried Roman fort ditch, as well as confirming the existence of only one ditch, the seismic image can still be improved to show the existence of the target beyond any doubt.

To produce a clear image, instead of using hammer to generate the seismic source, higher frequency sources should be considered. This includes the buffalo-gun or even detonators. The source should also be placed a few feet under the surface (inhole sources) to avoid the noise contamination. The inhole sources also reduce the attenuation of the high frequency energy component by the top layer.

Besides the choices of the source used, any future similar survey also should consider a 'walk-away test' to determine the optimum window and design the acquisition parameters based on this window. The combination of a highly condensed CDP and optimum window concept will concentrate recording of the less contaminated reflection arrival zone, thus reducing the failure rate.

This work was done using an OYO McSeis 1600 recording instrument (seismograph). This particular seismograph only has 16 bits of dynamic range (the ratio of the highest and smallest recoverable signals can be recovered by the system). The smallest recoverable signal is often taken to be the noise level of the system. However, signals often can be extracted even though they are buried in the noise. So in future, a recording system with a higher dynamic range such as OYO DAS-1 which has 24 bit dynamic range should be considered as it can increases the recoverable ratio, thus increases the chances of extracting useful signals from high-amplitude noise.

5.2 3-D seismic reflection for engineering-scale site survey

5.2.1 Conclusions

Seismic reflection exploration is deployed mainly by deep seismic explorationists to map possible petroleum accumulations, and also to investigate the deep interior of the Earth. The applications of this technique to shallow work are relatively new, but it became more familiar to shallow geophysical investigators in the 1980's as seismic recordings system become smaller and more portable, without reducing their capability. Today's high-resolution seismic recording systems are very important in shallow seismic investigations, as high frequencies (up to 1 KHz or more) can readily be recorded. Beside the development of high-resolution recording systems, advances in computer technology have enabled more data to be processed, and in less time.

Today seismic reflection is widely used to investigate targets of less than 200 m depth. Most of such work is aimed at mapping the depth of the bedrock interface in engineering foundation studies, or in mapping the aquifer zone in groundwater studies. Current applications of this technique, together with case studies, are regularly documented in the Proceedings volumes of the annual symposia or in house journals of learned societies in the fields of geophysics, engineering geology, groundwater or even archaeometry. Mostly, a simple 2-D CDP technique is used; however, with the increasing availability of high-resolution portable seismographs, in the last three years or so there has developed a trend amongst the geophysicists to try more advanced techniques such as the 3-D seismic method. This technique is now considered essential in identifying and mapping hydrocarbon accumulation targets in petroleum exploration.

The major part of thesis is a discussion of a new imaging method in shallow seismic investigation – a full 3-D shallow seismic survey. At the time this project was initiated (early 1996), it was believed to be the first full 3-D seismic reflection survey that had ever been done for engineering purposes, despite the fact that other shallow 3-D projects had started at around the same time (referred to in Chapter 3). Most of these, however,

have turned out to be not much more than an extension of a 2-D line reflection survey, or in other words, 2-D lines with offset sources. In contrast, the high fold of coverage and range of azimuths and offsets used in the present trial survey are even greater than in most full-scale 3-D deep seismic reflection surveys.

The aim of the present 3-D work was to image underground mine workings at depths of approximately 20–35 m. The roofs of the tunnels and rooms are probably collapsed, as the workings were abandoned on hundred years ago. Besides imaging the tunnels, it was also hoped to image the bedrock geology.

The results of this work show promising images. The top bedrock, made of inter-layered Carboniferous sandstone and shale, at very shallow depths (less than 10 m) was partly mapped over much of the 2 m grid (Figure 3.53). However, the positive identification of the old mineworkings is much less certain. Reliance has been made on the reversed polarity of the mapped reflector (Figure 3.54) as an indication of the upper surface of a void or a thick coal layer as coal, has lower velocity than the sandstone.

The main problem of this work occurred during the acquisition phase, as time was very limited. The data were collected intensively within a week. There was no time for extended source suitability comparisons, as only three sources were available, the 7 kg sledgehammer, weight drop and mini-vibroseis. The condition of the top layer (covered by thick grass and containing lots of moisture) also contributed in degrading the data quality. The hammer and weight drop sources did not yield a broad or high enough frequency range, as was expected. On the other hand the surface materials absorbed most of the high frequency signal produced by the mini-vibrator despite it being placed in a 5 to 10 cm deep pre-prepared hole. Besides the absorption problems, the data were also contaminated heavily by unwanted noise, in particular, the several drilling rigs operating simultaneously during the acquisition.

The data were processed using industry standard seismic data processing software. The processing largely followed the standard practice in the petroleum industry, with a few

minor differences. Only 150 ms of data were recorded, as only the top 50 m was the region of interest. The shallow bedrock interface meant that the corresponding reflection arrival was very early. This early reflection arrival tended to overlap with earlier arriving signals such as the direct wave and refraction first arrivals. Spiking deconvolution (or spectral whitening for vibroseis data) is ineffective at separating these closely-spaced signals unless there is a wider-frequency bandwidth than was recorded.

The combination of short trace length (150 ms), lateral changes and small impedance contrast with depth created problems in analyzing the velocity variation. The choice of stacking velocity functions was very difficult. A constant velocity stacking technique was found to be the best way to stack the data.

5.2.2 Recommendations and further work

Despite the fact that good images of the primary target were not produced, this full 3-D seismic reflection experiment can be considered a success. However, in retrospect, the site conditions and target of the Todd Campus West site may have been too complex for a preliminary trial 3-D survey. However the experiment shows that it is logistically feasible, even in the presence of other site contractors. A better target for future experimentation would be a somewhat deeper target set of voids in a flat-lying geological structure, and without the presence of contractors on site.

The results presented here may be improved by further processing, especially in separating the refraction first arrivals from the early reflection signals. Preliminary work in this respect has been started, using wavelet packet transform filtering applied to the present 3-D dataset (Watts *et al.* 1998).

In a future trial survey, the acquisition phase is very important, and there should be more effort in choosing a suitable seismic source. Perhaps a buffalo gun placed down a hole 0.3-0.5 m deep can be investigated as a source. This may eliminate (to some

extent) the loss of high frequency signal due to the absorption by the loose surface material, which is inevitable with a surface source such as the minivibrator. Besides the choice of source used, it is also vital to study what (minimum) fold is required to obtain good results from a full 3-D survey. This will minimize the cost of conducting the survey, or alternatively, more area can be surveyed in the same time and at similar costs.

In view of cost of grouting suspected or known mine workings, and the fact that the 3-D seismic method might become useful as a pre- and post-grouting imaging tool, it is believed to be the most promising geophysical survey method available today.

5.3 Surface tomographic mapping – a new tool

5.3.1 Conclusions

This dissertation has also introduced a new robust and simple tomographic method for mapping the velocity of the top bedrock. The basic concept of this technique is same as the fan shooting refraction technique, which requires only the first arrival time from each source and receiver pair. However, the data are not acquired especially for the purpose, but are a by-product of the 3-D reflection survey. The aim was to develop a semi-automated quick process, with minimum user input, to reveal small-scale velocity anomalies at the level of (say) the top bedrock.

The surface tomography maps, which use colour-coding to reveal the velocity anomalies, show some interesting results. Bands of different colours were observed striking parallel to the strike of the Carboniferous rock. More interestingly, one of the low-velocity bands closely follows the re-interpreted outcrop of the Twechar no. 1 coal. There was some disagreement on the location of the conjectural outcrop lines for Twechar no. 1 and 2 coals (as supplied by the geotechnical investigators in their reports), thus revised outcrop lines for these coals are presented (Figure 4.18).

This new method is a robust surface mapping technique. The results (in the form of reduced time maps) show that it can successfully image the bedrock surface geology. Besides the success in imaging the bedrock, the technique is also shows potential for detecting any localized anomaly such as a mine shaft or even surface mineralization related anomalies. This is based on the presence of a few 'blobs' of different colours surrounded by different colours. Unfortunately the author could not prove any shaft-related anomaly on the map. But after the survey was completed, the geotechnical investigation found one previously un-recorded shaft, which unfortunately lay just outside the survey area.

In conclusion, this technique shows potential as a by-product of a 3-D reflection survey especially in investigating an area which has a complex surface geology such as the study area. The technique is also can be used to image or study the surface anisotropy.

5.3.2 Recommendations

The reduced time (image) map is produced based on an average reduced times at every 0.25 m grid within 1 m search radius, thus all the point within the search radius contributes the same weight, regardless their location with respect to the central point. For example, consider three theoretical points A, B and C (Figure 5.1). Point A, B and C are one out of a series of 2 m interval points (from 3 corresponding vector lines) with a reduced time of 5, 8 and 9 ms. An average time out of these three value that contribute to the central point is 7.3 ms. This value is higher than the nearest reduced time value which is 5 ms (point A). This value is not appropriate to represent the reduced time for the central point as it should have a value nearer to 5 ms. This problem becomes more serious if one of the point in the area has an extreme value.

Figure 5.1 Points within 1 m search radius which contribute to the average value of the central point (red dot).

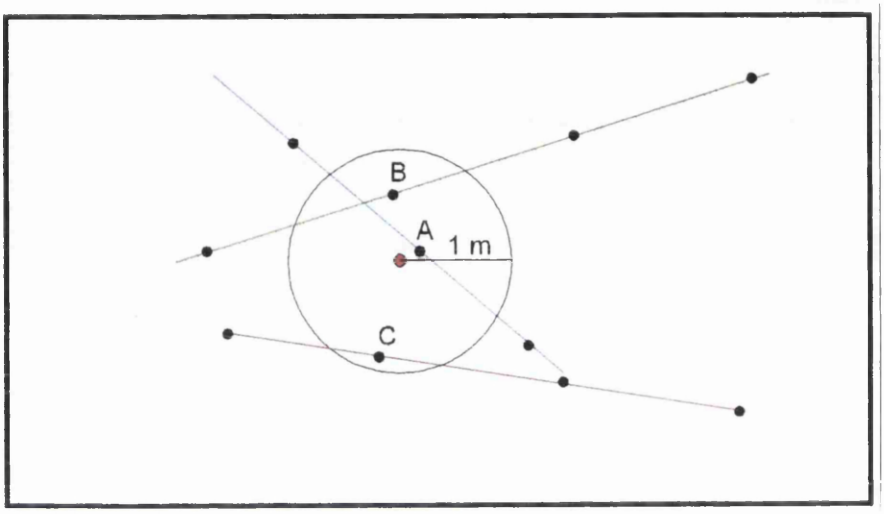

To overcome this problem, a different kind of averaging technique, which takes into account the effect of distance from the centre of the averaging area should be considered. Such a method should maximize the near centre contribution and at the same time minimize the contribution of the far (from centre) points. This means that the value carried out by the centre point will reflected the conditions of the small centered area. One of the technique can be used to carry out this task is by using a Gaussian (normal) distribution function and could be developed in future.

LIST OF REFERENCES

Aki K., Christofferson A., Husebye E., 1977. Determination of three dimension seismic structure of the lithosphere. *Journal of Geophysical Research* **82**, 277–296.

Allen S. J., 1980. Seismic method. *Geophysics* **45**, 1619–1633.

Al-Rawahy S. Y. S., and Goulty N. R., 1995. Effect of mining subsidence on seismic velocity monitored by a repeated reflection profile. *Geophysical Prospecting* **43**, 191-201.

Baker G. S., Steeples D. W., and Drake M., 1998. Muting the noise cone in near-surface reflection data: An example from southeastern Kansas. *Geophysics* **63**, 1332-1338.

Baker L. M., 1996. *The application of geophysical techniques to locate the defences of the Roman Fort at Inveresk, Midlothian.* Unpublished BSc dissertation, University of Glasgow.

Barnes M. K., and Mereu R. F., 1996. An Application of the 3-D Seismic Technique for Mapping Near-Surface Stratigraphy near London, Ontario. *Journal of environmental engineering geophysics (JEEE)* **1**, issue 3, 171-177.

Bay Geophysical Inc., 1998. Company web-page, http://www.baygeo.com/

Bee M. F., Bearden J. M., Herkenhoff E. F., Supiyanto H., and Koestoer B., 1994. Efficient 3D seismic surveys in a jungle environment. *First Break* **12**, 253-259.

Bell F. G., 1979. *Methods of treatment of unstable ground.* The Butterworth Group Ltd.

Betrelli C., Mascarin B. and Salvador L., 1993. Planning and field techniques for 3D land acquisition in highly tilled and populated areas – today's results and future trends. *First Break* **10**, 23-32.

Birkelo B. A., Steeples D.W., Miller R. D., and Sophocleous M., 1987. Seismic Reflection Study of a Shallow Aquifer During a Pumping Test. *Groundwater* **25**, 703-709.

Breeze D. J., 1983. *Roman Forts in Britain.* Aylesbury, Shire Publication.

Brown A. R., 1991. *Interpretation of three-dimensional seismic data (third edition).* AAPG Memoir 42, AAPG Publishing.

Brown A. R., 1996. *Interpretation of three-dimensional seismic data (fourth edition).* AAPG Memoir 42, AAPG Publishing.

Brückl E., Castillo E., Madhusudan, and Salzmann H., 1997. Detection of abandoned underground coal mine workings by seismic methods. Unpublished article.

Bühnemann J., and Holliger K., 1998. Comparison of high-frequency seismic sources at the Grimsel test site, central Alps, Switzerland. *Geophysics* **63**, 1363-1370.

Büker F., Green A. G., and Horstmeyer H., 1998a. Shallow seismic reflection study of a glaciated valley. *Geophysics* **63**, 1395-1407.

Büker F., Green A. G., and Horstmeyer H., 1998b. Shallow 3-D seismic reflection surveying: Data acquisition and preliminary processing strategies. *Geophysics* **63**, 1434-1450.

Burger H. R., 1992. *Exploration geophysics of the shallow subsurface.* Prentice Hall Ltd.

Chiu S. K. L., and Stewart R. R., 1987. Tomographic determination of three-dimensional seismic velocity structure using well logs, vertical seismic profiles and surface seismic data. *Geophysics* **52**, 1085-1098.

Chiu S. K. L., Kanasewich E. R., and Phadke S., 1986. Three-dimensional determination of structure and velocity by seismic tomography. *Geophysics* **51**, 1559-1571.

Clark J. C., Johnson W. J., and Miller W. A., 1994. The application of high resolution shear wave seismic reflection surveying to hydrogeological and geotechnical investigations. In *Proceeding of the Symposium on the Application of Geophysics to Engineering and Environmental Problems*, **vol. 1**, March 27-31.

Collingwood R.G and Richmond I., 1969. *The Archaeology of Roman Britain 3rd edition.* Methuen and Co Ltd.

Cottin J. F., Deletie P., Jacquet-Francillon H., Laksmanan, J., Lemoine Y., and Sanchez M., 1986. Curved ray seismic tomography: application to the Grand Etang Dam (Reunion Island). *First Break* **4**, 25-30.

Corsmit J., Versteeg W. H., Brouwer J. H., Helbig K., 1988. High-resolution 3D reflection seismics on a tidal flat: acquisition, processing, and interpretation. *First Break* **6**, 9-23.

Dana P. H., 1994, (revised 1998). *Global Positioning System Overview.* The Geographer's Craft Project, Dept. of Geography, The University of Texas at Austin.

Dennison E. P. and Coleman R., 1996. *The Scottish Burgh Survey, Historic Musselburgh: the archaeological implications of development.* Historic Scotland and the Scottish Culture Press.

Devaney A. J., 1983. A Computer Simulation Study of Diffraction Tomography. *IEEE Transactions on Biomedical Engineering* **30**, 377-386.

Dickinson J. A., Fagin S. W. and Weisser G. H., 1990. Comparison of 3-D Seismic Acquisition Techniques on Land. *SEG Expanded Abstract 1990 technical program* **vol. 1**, 60th annual international SEG meeting Sept 23-27 1990.

Dines K. A., and Lytle R. J., 1979. Computerised Geophysical Tomography. *Proceedings of the IEEE* **67**, 1065-1073.

Dolan F., and Pratt T. L., 1997. High-resolution seismic profiling of the Santa Monica Fault Zone, West Los Angeles, California. *Geophysical Research Letters* **24**, 2051-2054.

Doll W. E., Miller R. D., and Xia J., 1998. A noninvasive shallow seismic source comparison on the Oak Ridge Reservation, Tennessee. *Geophysics* **63**, 1318-1331.

Fessenden H. M., 1940. *Fessenden, Builder of tomorrow.* New York, Coward-McCann Inc.

Fessenden R. A., 1917. Patent no 1240328, Methods and apparatus for locating ore bodies. US Patent Office

Francese R. G., and Hajnal Z., 1997. Reflection seismic imaging of complex stratigraphic features in glacial deposits. *EAGE extended abstract*, 59th Conference and Technical Exhibition – Geneva, Switzerland, 26-30 May.

Gendzwill D, 1990. High-Resolution Seismic Reflections in an Underground Mine. *SEG Expanded Abstract 1990 technical program* **vol. 1**, 60th annual international SEG meeting Sept 23-27 1990.

George T. N., 1973. Geology Around Glasgow. In *Excursion guide to the geology of the Glasgow district, edited by Bluck, B. J., 1973.* Geological Society of Glasgow.

Ghose R., Nijhof V., Brouwer J., Matsubara Y., Kaida Y., and Takahashi T., 1998. Shallow to very shallow, high-resolution reflection seismic using a portable vibrator system. *Geophysics* **63**, 295-1309.

Gochioco L. M., and Cotton S. A., 1989. Locating faults in underground coal mines using high-resolution seismic reflection techniques. *Geophysics* **54**, 1521-1572.

Goulty N. R., and Hudson A. L., 1994. Completion of the seismic refraction survey to locate the vallum at Vindobala, Hadrian's wall. *Archaeometry* **36**, 327-335.

Goulty N. R., Gibson J. P. C., More J. G., and Welfare H., 1990. Delineation of the vallum at Vindobala, Hadrian's Wall, by a shear-wave seismic refraction survey. *Archaeometry* **32**, 71-82.

Green A., Pugin A., Beres M., Lanz E., Büker F., Huggenberger P., Horstmeyer H., Grasmück M., DeIaco R., Holliger K., and Maurer H. R., 1995. 3-D high-resolution seismic and georadar reflection mapping of glacial, glaciolacustrine and glaciofluvial sediments in Switzerland. *Annual symposium environmental engineering geophysics soc. (SAGEEP)* Expanded abstracts, 419-434.

Greenberg, J., 1997. Activity buoys new technology. *AAPG Explorer* **Nov 97**, 8-9&18.

Hasbrouck Geophysical Inc., 1994. Shallow 3-D reflection seismic example. Hasbrouck Geophysical Inc. homepage http://www.hasgeo.com

Heliker, Griggs, Takahashi, and Wright, 1986. Volcano monitoring at the US Geological Survey's Hawaiian Volcano Observatory. *Earthquake Information Bulletin* **18**, 35.

Hewitt, 1980. *Seismic Data Acquisition.* SEG Continuing Educational Program, Soc. Exploration Geophysics, Tulsa.

Hill, I. A. and Ali, J. W., 1988. Application of shallow seismic reflection methods to site investigation. *Trans. Inst. Min. Metall. (Sect. B: Appl. Earth sci)* **97**, B29-B35.

Hoover, G. M. and O'Brien, J. T., 1980. The influence of the planted geophone on seismic land data. *Geophysics* **45**, 1239-1253.

House J. R., Boyd T. M., and Haeni F. P., 1996. Haddam Meadows, Connecticut: A case study for the acquisition, processing, and relevance of 3-D seismic data as applied to the remediation of DNAPL contamination. In *AAPG studies in Geology no 42 and SEG Geophysical development series no 5, edited by Weimer P and Davis L.* AAPG/SEG publication, Tulsa, 257-266.

Hunter J. A., Pullan S. E., Burns R. A., Good R. L., Harris J. B., Pugin A., Skvortsov A., and Gorianiov N. N., 1998. Downhole seismic logging for high-resolution reflection surveying in unconsolidated overburden. *Geophysics* **63**, 1371-1384.

Hunter J. A., Pullan, S. E., Burns, R. A., Gagné, R. M. and Good, R. L., 1984. Shallow seismic reflection mapping for the overburden–bedrock interface with an engineering seismograph - Some simple techniques. *Geophysics* **49**, 1381-1385.

Hunter J. A., Pullan, S. E., Burns, R. A., Gagné, R. M. and Good, R. L., 1987. Applications of a Shallow Seismic Reflection Method to Groundwater and Engineering Studies. *Proc. of exploration 87, Ontario Geological Survey Special Volume: an application of geophysics and geochemistry*, 704-715.

Hyde E. D., 1987. *Coal Mining in Scotland.* Scottish Mining Museum, Edinburgh.

Jefferson R. D., Steeples D. W., Black R. A., and Carr T., 1998. Effects of soil-moisture content on shallow seismic data. *Geophysics* **63**, 1357- 1362.

Jeng Y, 1995. Shallow seismic investigation of a site with poor reflection quality. *Geophysics* **60**, 1715-1726.

Johnson W. J., and Clark J. C., 1992a. High resolution S-wave Reflection Surveying for Groundwater Characterisation. In *Proceedings of RD 92, National research and development conference on the control of hazardous materials, Feb. 2-6*, 1996 San Francisco.

Johnson W. J., and Clark J. C., 1992b. Improving subsurface resolution with the seismic reflection methods: Use S-wave. In *The Proceedings of the 6th national outdoor action conference national ground water assoc.,* May 11-13 1992, Las Vegas.

Karastathis V. K., and Papamarinopoulos St. P., 1997. The detection of King Xerxes' Canal by the use of shallow refraction and reflection seismics - Preliminary results. *Geophysics Prospecting* **45**, 389-401.

Kearey P., and Brooks M., 1991. *An Introduction to Geophysical Exploration (second edition).* Blackwell Science Publications.

Kearey P., and Vine F. J., 1990. *Global Tectonics (first edition).* Blackwell Scientific Publications.

Kidd D. F., Kruppenbach J. A., and Ricketts B., 1990. Multidiscipline Approach to Very Shallow Exploration Targets. *SEG expanded abstract 1990, tech. program* **1**, 60th annual international SEG meetings, Sept 23-27 1990, San Francisco.

Kilty K. T., and Lange A. L., 1990. Acoustic Tomography in Shallow Geophysical Exploration Using a Transform Reconstruction. In *Geotechnical and Environmental Geophysics, edited by Stanley H. Ward.* Society of Exploration Geophysicists.

Knapp R. W., and Steeples, D. W., 1986a. High-resolution common-depth point seismic reflection profiling. Instrumentation. *Geophysics* **51**, 276-282.

Knapp R. W., and Steeples D. W., 1986b. High-resolution common-depth-point reflection profiling: Field acquisition parameter design. *Geophysics* **51**, 283-294.

Kourkafas P., and Goulty N. R., 1996. Seismic reflection imaging of gypsum mine workings at Sherburn-in-Elmet, Yorkshire, England. *European Journal of Environmental And Engineering Geophysics* **1**, 53-63.

Lamer A., 1970. Couplage sol-geophone. *Geophysical Prospecting* **18**, 300-319.

Lankston R W., 1989. The seismic refraction method: A viable tool for mapping shallow targets into the 1990s. *Geophysics* **54**, 1535-1542.

Lanz E., Maurer H., and Green A. G., 1998. Refraction tomography over a buried waste disposal site. *Geophysics* **63**, 1414-1433.

Lanz E., Pugin A., Green H., and Hurstmayer H., 1996. Results of 2- and 3-D high-resolution seismic reflection surveying of surficial sediments. *Geophysical Research Letters* **23**, 491-494.

Leick A., 1992. Delineating Theory for GPS Surveying. *Journal of Surveying Engineering* **118**, 33-42.

Lepper C. M., 1981. *Guideline for Selecting Seismic Detectors for High-Resolution Applications.* Bureau of Mines Ref. Of Investigation 8500, US Dept of the Interior.

Lowrie W., 1997. *Fundamentals of Geophysics.* Cambridge University Press.

Lytle R. J., and Dines K. A., 1980. Iterative Ray Tracing Between Boreholes for Underground Image Reconstruction. *I.E.E.E Trans. Geosci. Remote Sensing.* **GE-18**, 234-240.

MacGregor M. and MacGregor A.G., 1948. *British Regional Geology: The Midland valley of Scotland, 2nd edition.* Her Majesty's Stationary Office.

Miller R. D., and Xia J., 1998. Large near-surface velocity gradients on shallow reflection data. *Geophysics* **63**, 1348-1356.

Miller R. D., Pullan S. E., Steeples D. W., and Hunter J. A., 1994. Field comparison of shallow P-wave seismic sources near Houston, Texas. *Geophysics* **59**, 1713-1728.

Miller R. D., Steeples D. W., and Brannan M, 1989. Mapping a bedrock surface under dry alluvium with shallow seismic reflections. *Geophysics* **54**, 1528-1534.

Miller R. D., Steeples D. W., and Mazzella A., 1990. Reflection from geologic interface shallower than 30 m at the Pittman Lateral, Henderson, Nevada. *SEG expanded abstract, 1990 technical program* **vol. 1**, 60th Annual International SEG meeting Sept 23-27 1990 San Francisco.

Miller R.D., Villela A., Xia J., 1997. Shallow High-Resolution Seismic Reflection to Delineate Upper 400 m around a Collapse Feature in Central Kansas. *Environmental Geoscience* **4**, 119-126.

Milson J., 1989. *Field Geophysics.* Open University Press.

Narbutovskih S. M., Michelsen F. B., Clark J. C., and Christensen E. W., 1995. High resolution seismic reflection test at the DOE Hanford site. *Proc. Symp. Application Geophysics to Engineering and Environmental Problems*, 947-951.

Norminton E. J., 1990. Seismic Model Studies of the Overburden Bedrock Reflection: P-wave and S-wave. *SEG expanded abstract, 1990 technical program* **1**, 60th annual international SEG meeting Sept 23-27 1990.

Ongkiehong L., and Askin H. J., 1988. Towards the universal seismic acquisition technique. *First Break* **6**, 46-63.

Owen T. R. E., and Sinha M. C., 1990. A PC-based seismic acquisition system. *First Break* **8**, 57-62.

Peterson J. E, Paulsson B. N. P., and Mc.Evilly T. V, 1985. Applications of algebraic reconstruction techniques to crosshole seismic data. *Geophysics* **50**, 1566-1580.

Pullan S. E., and Hunter J. A., 1985. Seismic model studies of the overburden-bedrock reflection. *Geophysics* **50**, 1684-1688.

Pullan S. E., and MacAullay H. A., 1987. An in-hole shotgun source for engineering seismic surveys. *Geophysics* **52**, 985-996.

Pullan S. E., Hunter J. A., and Neave K. G., 1990. Shallow Shear-Wave Reflection Tests. *SEG expanded abstract, 1990 technical program* **1**, 60th annual international SEG meeting Sept 23-27, 380-382.

Reynolds J. M., 1997. *An Introduction to Applied and Environmental Geophysics.* John Wiley and Son Publication.

Rice J. A, Krohn C. E., and Houston L. M., 1990. Shallow Near-Surface Effects on Seismic Waves. *SEG expanded abstract, 1990 technical program* **1**, 60th annual international SEG meeting Sept 23-27, 747-749.

Richmond I. A. (the late), (1978). A Roman Fort at Inveresk, Midlothian, edited and prepared by W. S. Hanson. *Proc. Soc. Antiq. Scot.* **110**, 286-304.

Ritchie J. N. G. and Ritchie A., 1972. *Regional Archaeologies: Edinburgh and Southeast Scotland.* Heinemann Educational Books Ltd.

Rogers A. W., 1981. Determination of static correction. In *Development in Geophysical Exploration Method-2, edited by Fitch A. A.* Applied Science Publication.

Sheriff R. E., 1973. *Encyclopaedic Dictionary of Exploration Geophysics, 1st edition.* Society of Exploration Geophysics, Tulsa.

Sheriff R. E., 1990. *Encyclopaedic Dictionary of Exploration Geophysics, 3rd edition.* Society of Exploration Geophysics, Tulsa.

Sheriff R. E., and Geldart L. P., 1995. *Exploration seismology, 2nd edition.* Cambridge University Press.

Siahkoohi H. R., and West G. F., 1996. 3-D seismic imaging of complex structures in glacial deposits. *SEG Expanded Abstract, 60th Annual International Mtg.*, 873-876.

Smythe D. K., 1994. *3-D seismic reflection trial- data acquisition report.* Unpublished NIREX report no 622.

Smythe D. K., 1995. The 3D structural geology of the PRZ in *Radioactive waste disposal at Sellafield, UK, edited by R S Haszeldine and D K Smythe.* Department of Geology and Applied Geology, University of Glasgow.

Steeples D. W., 1990. Spectral Shaping during Acquisition of Seismic Reflection Data. *SEG expanded abstract, 1990 technical program* **1**, 60th annual international SEG meeting Sept 23-27, 917-921.

Steeples D. W., and Miller R. D., 1986. Some shallow seismic-reflection pitfalls. *SEG Expanded Abstracts with Biography,* 56th Technical Program, 101-104.

Steeples D. W., Green A. G., McEvilly T. C., Miller R. D., Doll W. E., and Rector J. W., 1997. A workshop examination of shallow seismic reflection surveying. *The Leading Edge* **16**, 1641-1647.

Steeples D. W., Knapp R. W., and McElwee C. D., 1996. Seismic reflection investigations of sinkholes beneath Interstate Highway 70 in Kansas. *Geophysics* **51**, 295-301.

Stefanic V., 1997. Seismic industry rides the waves, plenty of work and success but where are the new hires. *AAPG Explorer* **June 1997**, 1,6,10.

Stone G. D., 1994. *Designing Seismic Surveys in Two and Three Dimensions, edited by Meeder C. A.* SEG publishing.

Stright M. J., 1986. Evaluation of archaeology site potential on the Gulf of Mexico continental shelf using high-resolution seismic data. *Geophysics* **51**, 605-622.

Thomas K., 1997. Faster, better, data is industry goal. *AAPG Explorer* **June 97**, 8-9.

Veen, M. van der, and Green A. G., 1998. Land streamer for shallow data acquisition: Evaluation of gimbal-mounted geophones. *Geophysics* **63**, 1408-1413.

Waltham A. C., 1997. *Foundation of Engineering Geology.* Blackie Academic and Professional.

Watts D. R., Smythe D. K., and Deighan A. J., 1998. Removal of airblast from a 3-D engineering seismic survey with a wavelet packet filter. *SEG expanded abstract with biographies*, 1998 technical program **1**, 821-824.

Whiteley R. J., Hunter J. A., Pullan S. E., and Nutalaya P., 1998. "Optimum offset" seismic reflection mapping of shallow aquifers near Bangkok, Thailand. *Geophysics* **63**, 1385-1394.

Wright C., 1996. A note on the computation of the offset distance XY in the generalized reciprocal method of seismic refraction interpretation. *Geophysical Prospecting* **44**, 41-53.

Wu J., 1996. Potential pitfalls of crooked-line seismic reflection surveys. *Geophysics* **61**, 277-281.

Wynn J. C., 1986. Archaeological Prospection: An introduction to the special issue. *Geophysics* **51**, 533-537.

Yilmaz O., 1987. *Investigations in Geophysics. Vol. 2: Seismic data processing.* SEG publication.

APPENDICES

Appendix 1

The Basis of surface tomography (after Lowrie 1997).

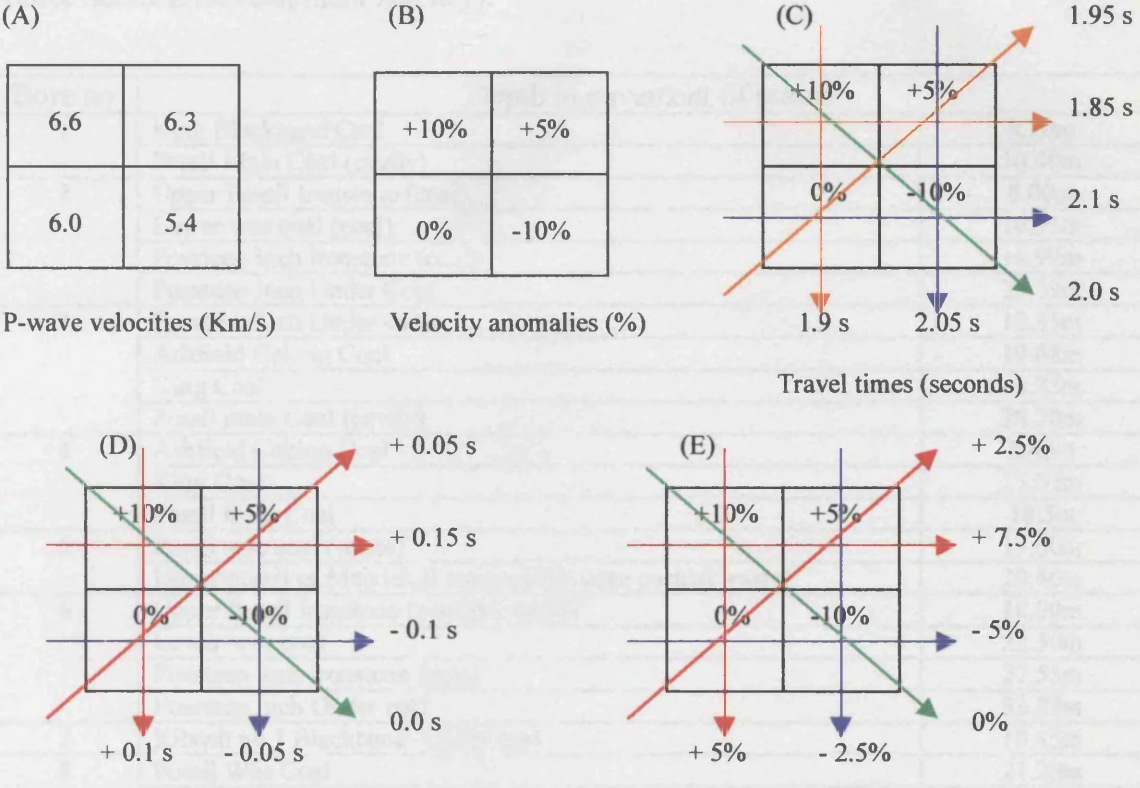

Consider the passage of rays in six directions through a square region containing four equal areas with P-wave velocities 5,4 km s^{-1}, 6.0 km s^{-1}, 6.3 km s^{-1} and 6.6 km s^{-1} (App. 1a). Let the expected velocity in the region be 6.0 km s^{-1}. The velocity anomaly in each area is found by subtracting the reference value and can be expressed as a percentage of the expected value. This gives zones that are 10% and 5% fast, a zone that is 10% slow and a zone with no anomaly (App. 1b). Suppose that six seismic rays traverse the square region (App. 1c), and let the expected travel time be 2.0 s for each ray; some of the observed travel times are shorter and some are longer than the expected value. The travel time anomaly is computed by subtracting the observed times from the expected travel time (App. 1d); it is positive or negative depending on whether the ray travels faster or slower than average. The travel time residual is obtained by expressing the anomaly as a percentage of the expected travel time (App. 1e). A positive residual result for an early arrival that has travelled through a fast zone with positive velocity anomaly; a negative residual corresponds to passage through a slow zone with negative velocity anomaly. The set of travelled time residual forms the database for topographic inversion, which is designed to yield the original velocity structure (App. 1a), or, more commonly, the distribution of fast and slow regions (App. 1b).

Appendix 2

Correlation of coal seams and strata encountered in boreholes 1981-1 to -29 inclusive (after Scottish Development Agency).

Bore no	Depth to pavement of seams	
1	King Blackband Coal	8.20m
	Possil Main Coal (cavity)	10.40m
2	Upper Possil Ironstone (coal)	8.00m
	Lower wee coal (coal)	10.91m
	Fourteen Inch ironstone (coal)	16.97m
	Fourteen Inch Under Coal	25.09m
3	Fourteen Inch Under coal	12.35m
	Ashfield Coking Coal	19.68m
	King Coal	26.25m
	Possil main Coal (cavity)	28.20m
4	Ashfield Coking Coal	8.43m
	King Coal	15.03m
	Possil main Coal	18.5m
5	Possil wee coal (waste)	17.00m
	Upper possil or Meiklehill main coal (Loose packed waste)	20.40m
6	Upper Possil Ironstone (possible waste)	18.00m
	Lower wee coal	22.50m
	Fourteen inch Ironstone (coal)	27.55m
	Fourteen Inch Under coal	33.85m
7	Kilsyth no 1 Blackband Under coal	10.45m
8	Possil Wee Coal	21.20m
	Upper Possil or Meiklehill main coal	22.90m
9	Lower wee coal	9.40m
	Fourteen Inch ironstone (coal)	15.55m
	Fourteen inch Under coal	22.40m
10	King coal (or King coal (waste))	9.75m (13.60m)
	Possil Main Coal (waste)	13.60m or 17.85m
11	Twechar No 2 Coal	17.37m
12	Twechar No 1 Coal	9.49m
	Twechar No 2 Coal (position)	16.50m
13	Twechar No 1 Coal	5.20m
	Twechar No 2 Coal	13.92m
	Kilsyth No 1 Blackband Coal (possible closed waste)	19.70m
14	Kilsyth No 1 Blackband (waste)	15.30m
	Kilsyth No 1 Blackband Under Coal (waste)	22.30m
15	Kilsyth No 1 Blackband Under Coal	9.96m
16	Kilsyth No 1 Blackband (waste)	14.50m
	Kilsyth No 1 Blackband Under Coal (position)	20.90m
17	Possil Main	3.5m
	Cloven Coal	10.56m
	Shale Coal (collapsed waste)	22.42m
	Jubilee Coal	28.67m

18	Shale Coal (void)	13.65m
	Jubilee Coal	20.08m
	Knightswood Gas Coal (waste)	27.68m
19	Cloven Coal	5.47m
	Shale Coal (waste)	18.3m
	Jubilee Coal (waste)	24.20m
20	Possil Main Coal	5.49m
	Cloven Coal	12.48m
	Shale Coal (waste)	26.56m
21	Shale Coal	3.91m
	Jubilee Coal	9.66m
	Knightswood Gas Coal (void)	18.71m
22	Jubilee Coal	3.66m
	Knightswood Gas Coal (void)	13.06m
23	Shale Coal (waste)	6.91m
	Jubilee Coal	11.69m
	Knightswood Gas Coal	20.59m
24	Knightswood Gas Coal	7.55m
	Knott Coal	26.92m
25	Knott Coal	21.17m
26	Knott Coal	13.98m
27, 28, 29	Penetrated strata referred to as the Black Metals known to underlie the Knott Coal	

Appendix 3

Calculation of 3-point problem to establish regional strike and dip.

a) Strike and dip of Blackband Coal based on boreholes 1981-13, -14, and –16.

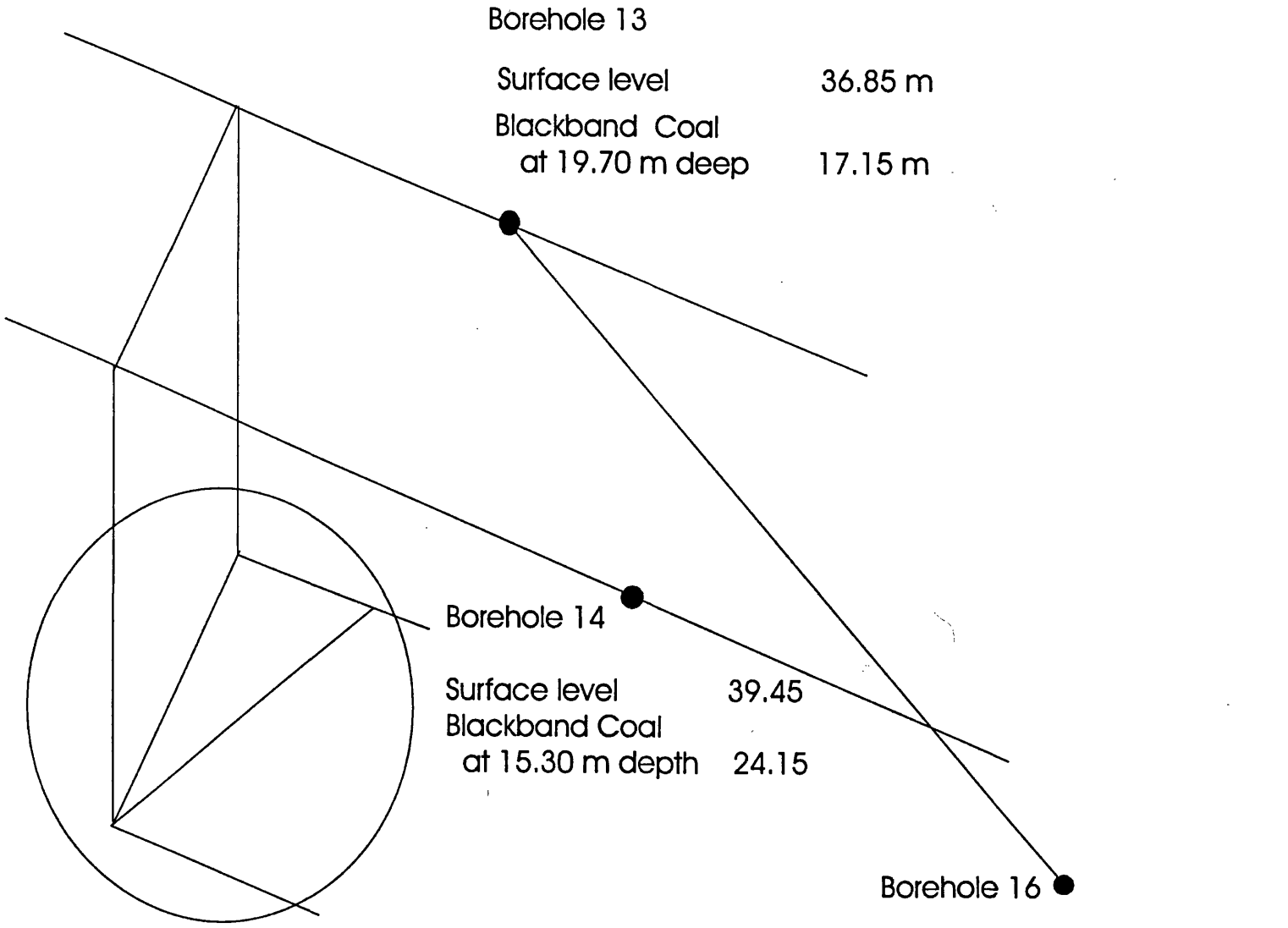

Dip of the layer is

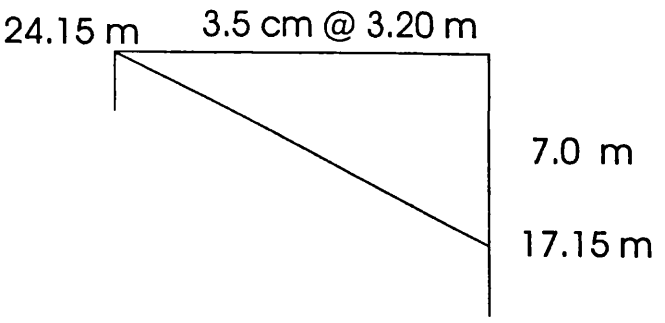

Tan O = 7.01/3.20
= 2.18
O = 65.4 degrees.

Diff. Between Bh. 13 and 16 is 9.15 m
Dist. Between Bh. 13 and 16 is 10 cm

which means

1 cm = 0.915 m or
1 m = 1.090 cm

Diff between Bh 14 and 16 is 2.17 m
On map 2.17 m is equal to 2.4 cm from Bh 16

b) Strike and dip of Blackband Under Coal based on boreholes 1981-14, -15, and –16.

Diff. Between Bh. 14 and 15 is 12.97 m
Dist. Between Bh. 14 and 15 is 3.8 cm

which means

1 cm = 3.4 m or
1 m = 0.3 cm

Diff. Between Bh. 14 and 16 is 2.17 m
on map, 2.17 m is equal to 0.65 cm from Bh. 14

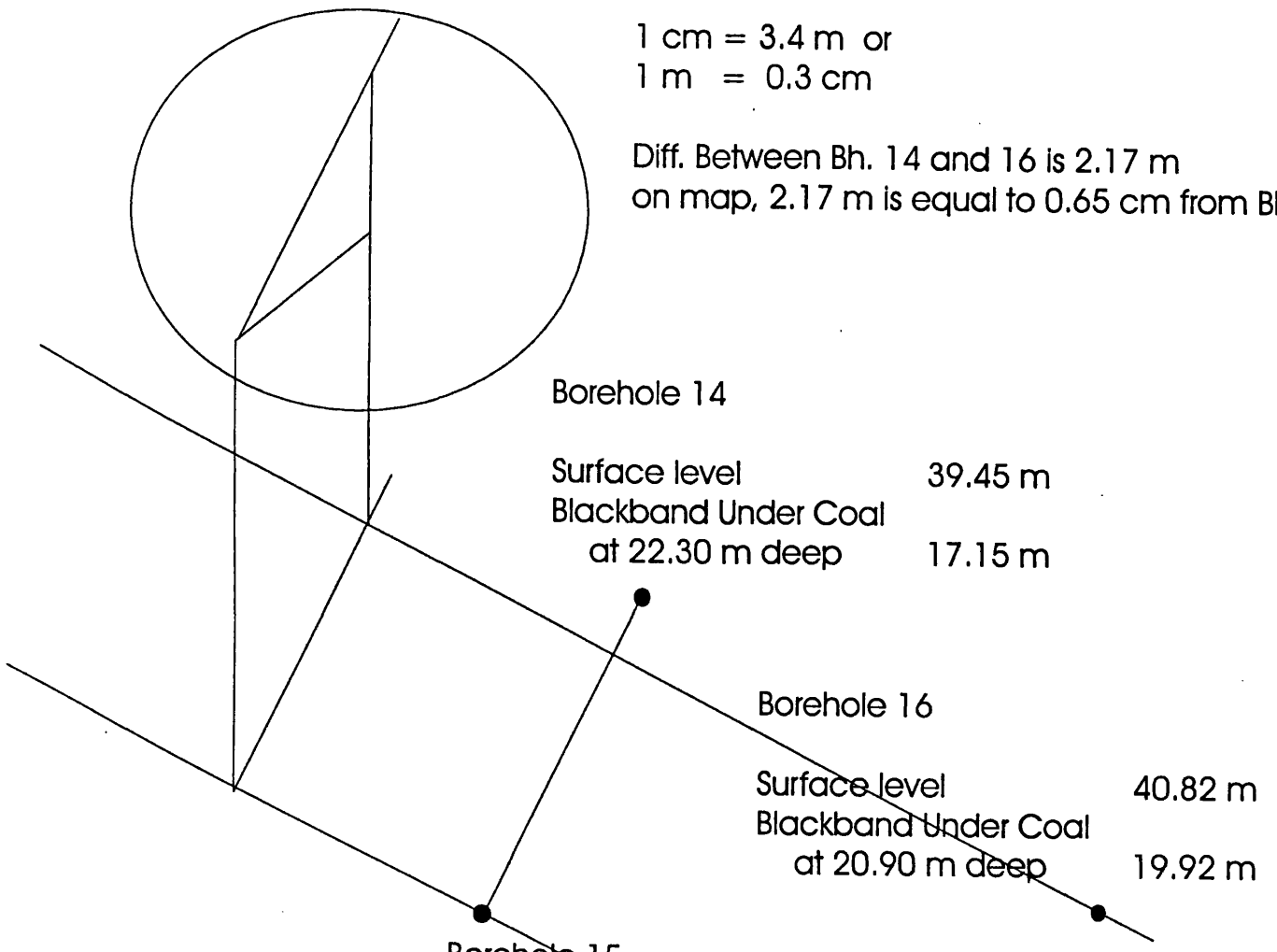

Dip of the layer is

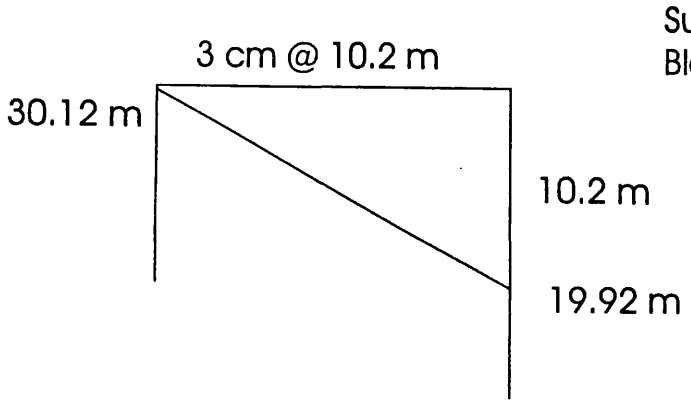

Tan O = 10.2/10.2
= 1
O = 45 degrees.

c) Strike and dip of Blackband Under Coal based on boreholes 1981-7, -14, and –15.

Borehole 7

Surface level 33.56 m

Blackband Under Coal at 10.45 m deep 23.11 m

Diff. Between Bh. 14 and 15 is 12.97 m
Dist. Between Bh. 14 and 15 is 3.7 cm

which means

1 cm = 3.5 m or
1 m = 0.28 cm

Diff between Bh 7 and 14 is 5.96 m
On map 5.96 m is equal to 1.67 cm from Bh 14

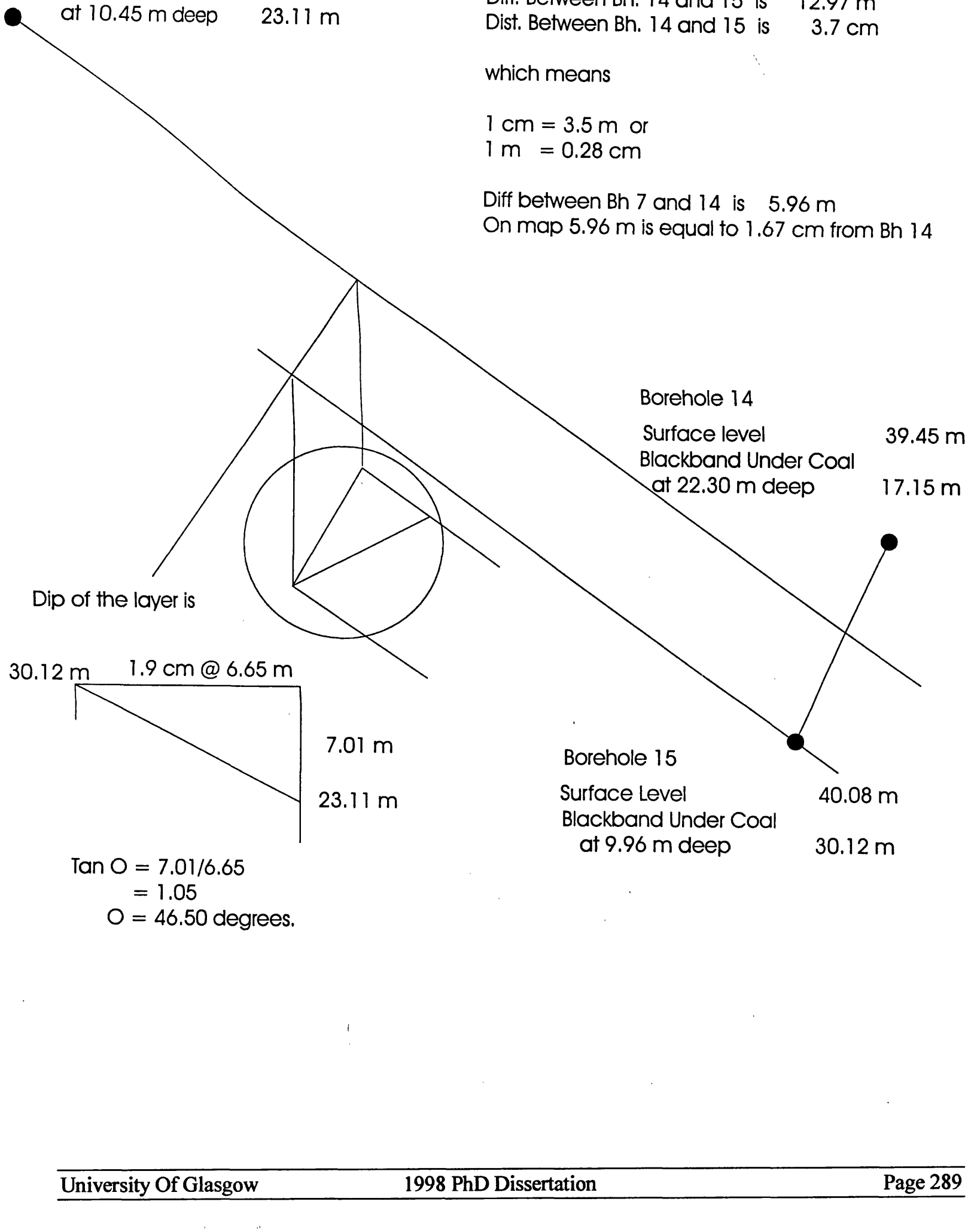

Dip of the layer is

Tan O = 7.01/6.65
= 1.05
O = 46.50 degrees.

Appendix 4

Calculations of conjectural outcrop points of Twechar no. 1 and Twechar no. 2 Coals.

Calculation of the conjectural outcrop of Twechar no. 1 and no. 2 based on the presence of these coals in boreholes 1981-11, -12, and -13. Note that the dip of these layers (18°) is taken from the geological map and documentation reports as the readings calculated from the three point problem using the deeper coal horizon shows a rather steep dip (>42°, appendix 3).

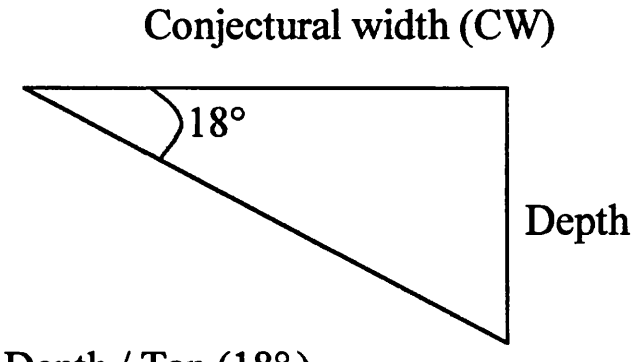

CW = Depth / Tan (18°)

Scale (Figure 4.16)

5.5 cm (on map) = 100m (on surface) or
1 cm (on map) = 18.2 m (on surface) or
0.05 cm (on map) = 1 m (on surface)

Twechar No 1 Coal

	Borehole 11	Borehole 12	Borehole 13
Surface level (m)	35.23	35.03	36.85
Twechar No 1 at (depth, m)		9.49	5.20
Twechar No 1		25.54	31.65
Conjuctural Outcrop (m) (depth/tan 18)		29.20	16.00
Conjuctural on map (cm)		1.5	0.8

Twechar No. 2 Coal

	Borehole 11	Borehole 12	Borehole 13
Surface level (m)	35.23	35.03	36.85
Twechar No 2 at (depth, m)	17.37	16.50	13.92
Twechar No 2	17.86	18.53	22.93
Conjuctural Outcrop (m) (depth/tan 18)	53.45	50.78	42.84
Conjuctural on map (cm)	2.7	2.5	2.1

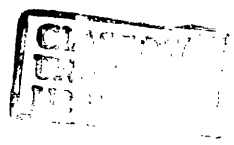

WEST of SCOTLAND SCIENCE PARK
(TODD CAMPUS WEST)

REDUCED TIME (VECTOR) MAP

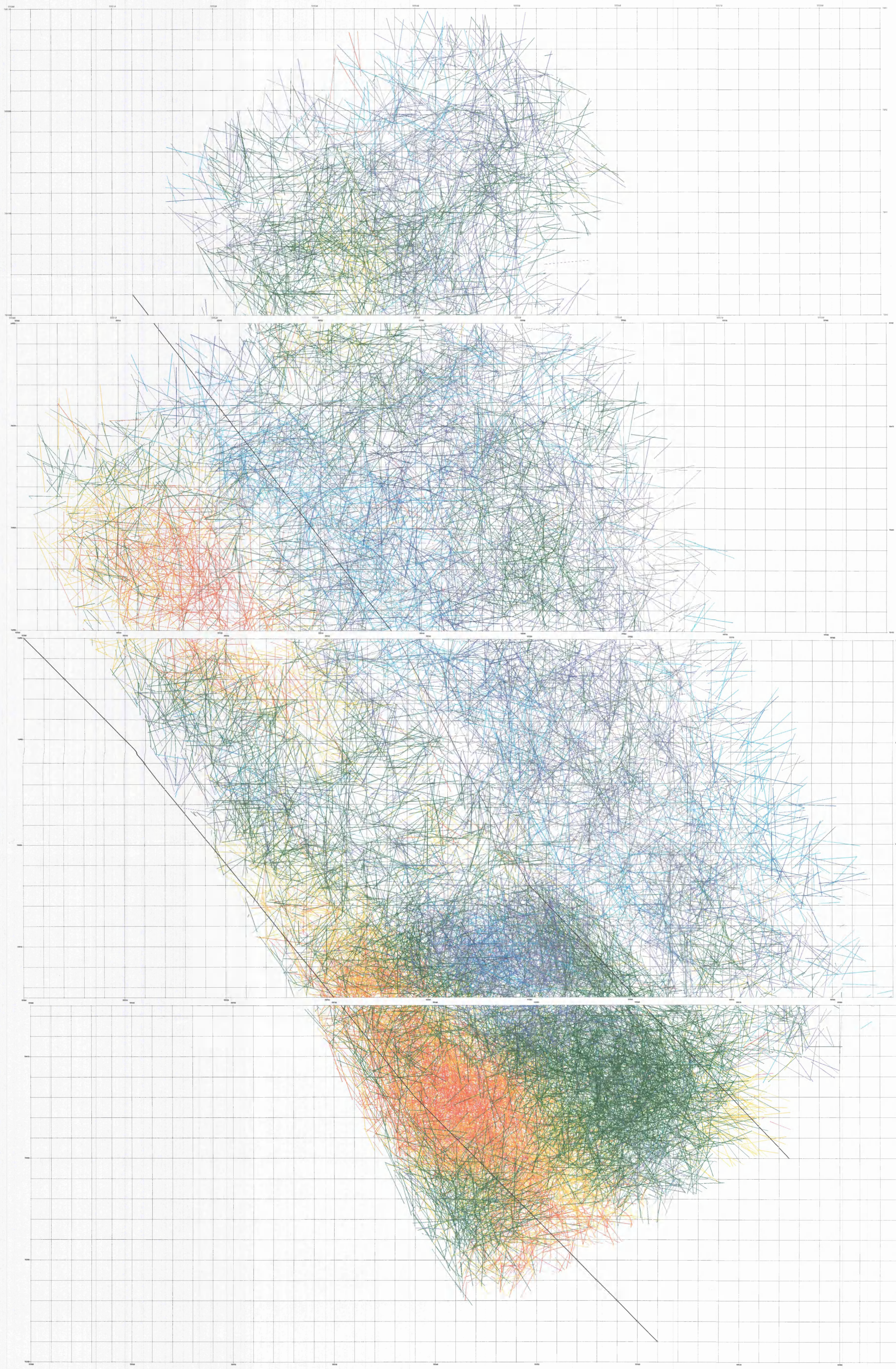

Figure : 4.8

Back pocket : 1

Grid : 2 m x 2 m

Reduction velocity : 1600 m/s

WEST of SCOTLAND SCIENCE PARK
(TODD CAMPUS WEST)

REDUCED TIME (VECTOR) MAP
(0-90 anisotropy map)

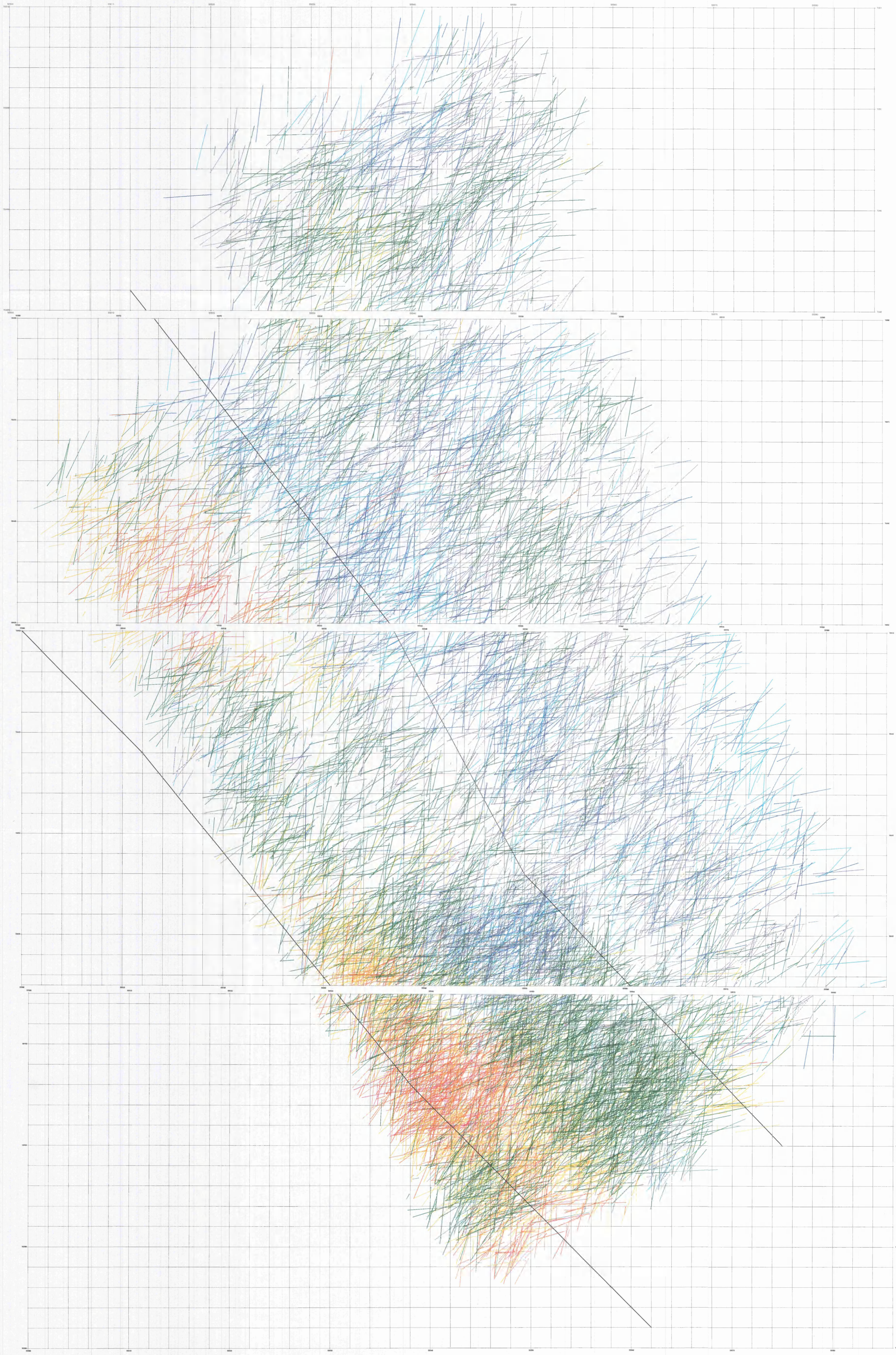

Figure : 4.10a

Back pocket : 2

Grid : 2 m x 2 m

Reduction velocity : 1600 m/s

Datum

WEST of SCOTLAND SCIENCE PARK
(TODD CAMPUS WEST)

REDUCED TIME (VECTOR) MAP
(90-180 anisotropy map)

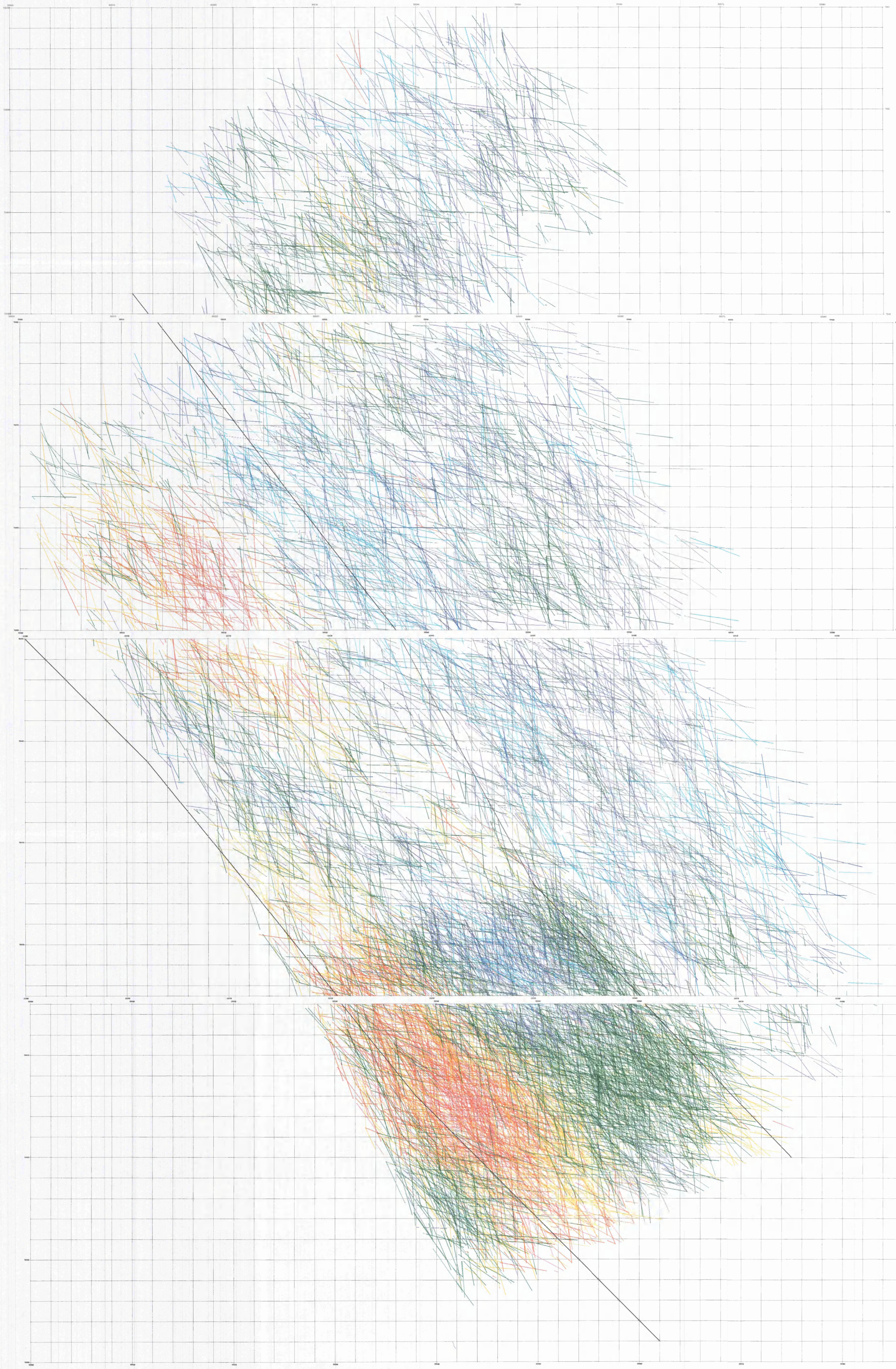

Figure : 4.10 b

Back pocket : 3

Grid : 2 m x 2 m

Reduction velocity : 1600 m/s

WEST of SCOTLAND SCIENCE PARK
(TODD CAMPUS WEST)

REDUCED TIME (IMAGE) MAP

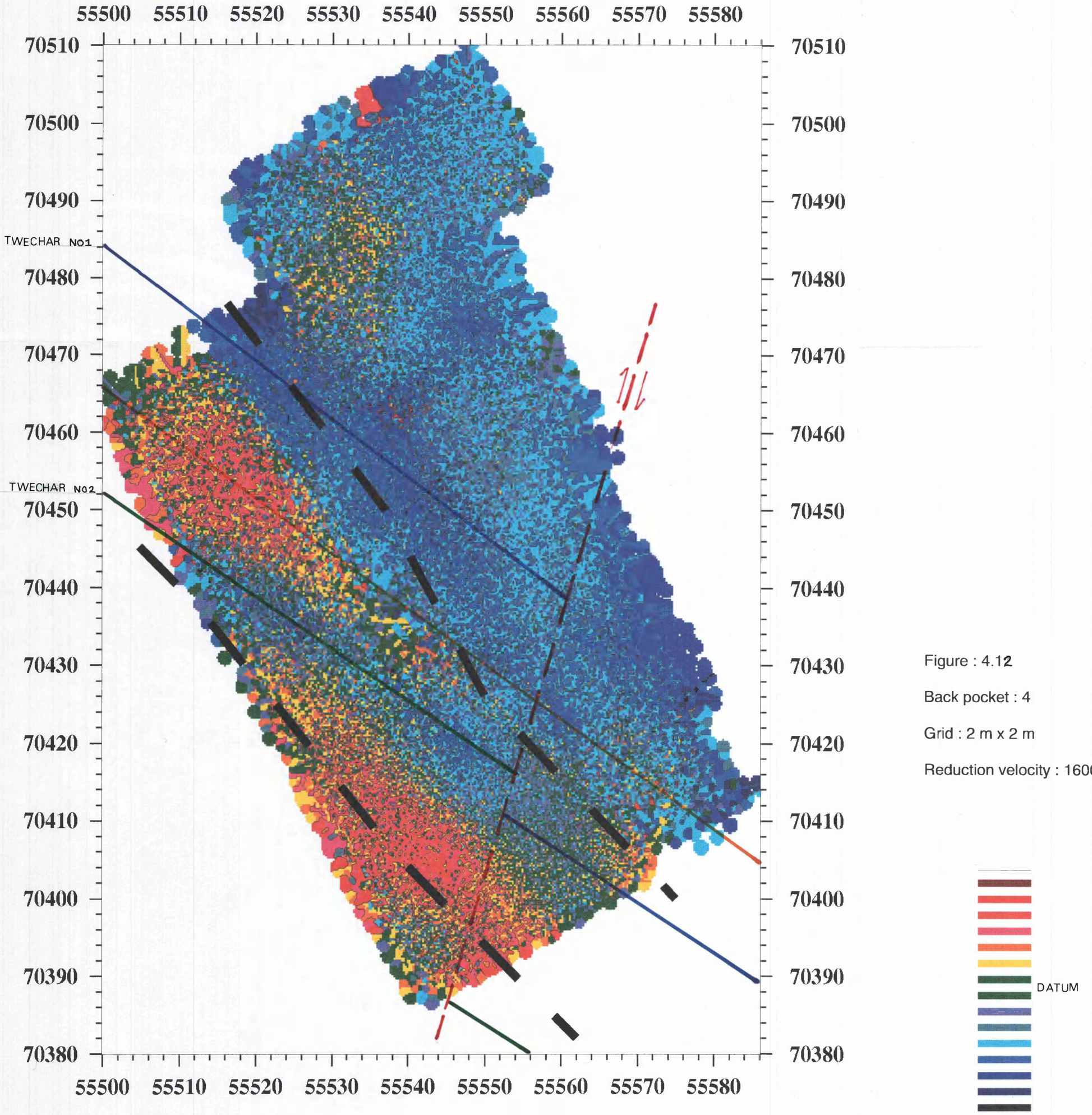

Figure : 4.12

Back pocket : 4

Grid : 2 m x 2 m

Reduction velocity : 1600 m/s

Filename: Figure4_11.cgm
Date: 98-09-12 14:54
Panel 1 of 1
Rotate=0

WEST of SCOTLAND SCIENCE PARK
(TODD CAMPUS WEST)

REDUCED TIME (VECTOR) MAP

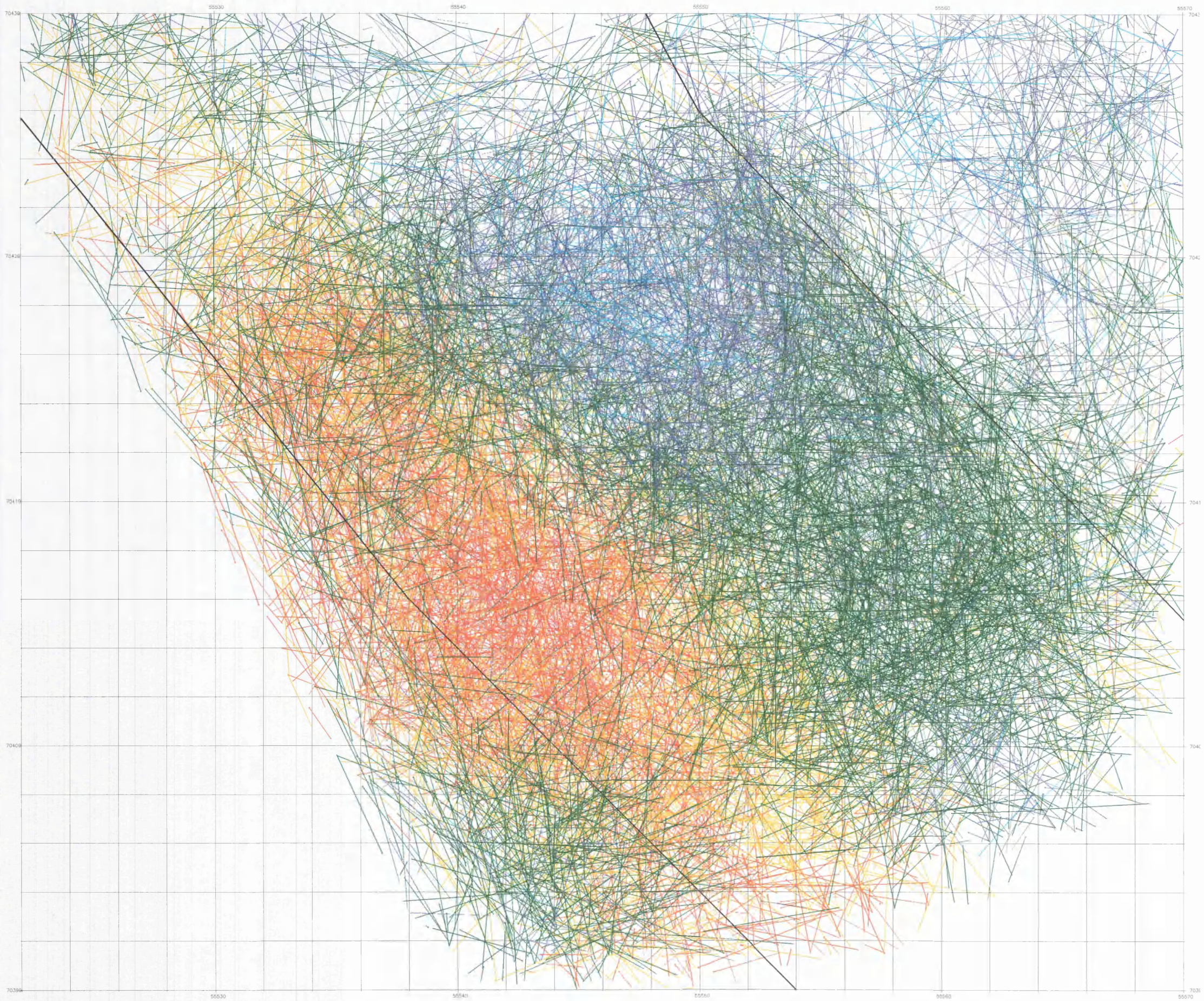

Figure : 4.14a

Back pocket : 5

Grid : 2 m x 2 m

Reduction velocity : 1600 m/s

WEST of SCOTLAND SCIENCE PARK
(TODD CAMPUS WEST)

REDUCED TIME (VECTOR) MAP
(90-180 anisotropy map)

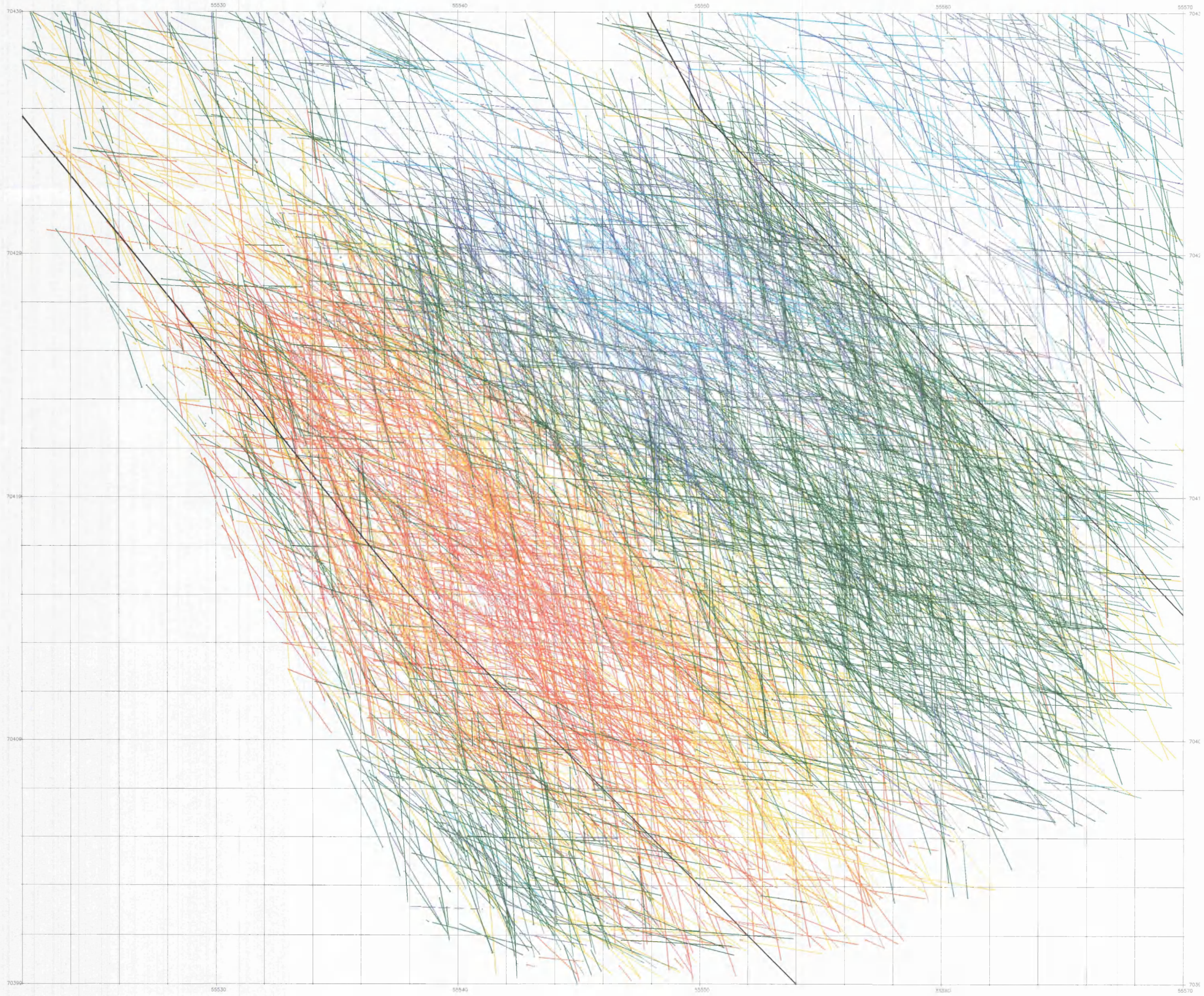

Figure : 4.14b

Back pocket : 6

Grid : 2 m x 2 m

Reduction velocity : 1600 m/s

WEST of SCOTLAND SCIENCE PARK
(TODD CAMPUS WEST)

REDUCED TIME (VECTOR) MAP
(110-155 anisotropy map)

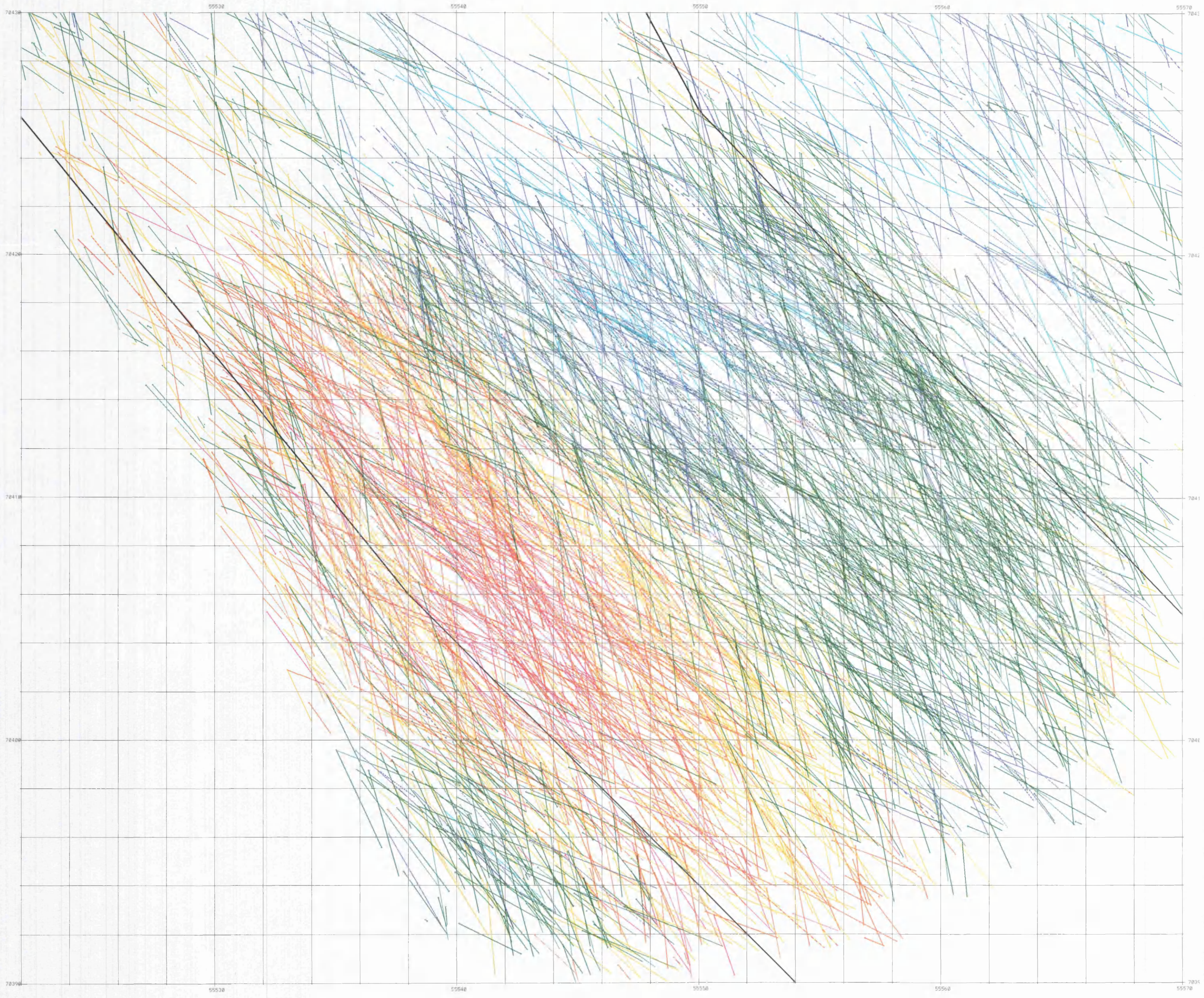

Figure : 4.14c

Back pocket : 7

Grid : 2 m x 2 m

Reduction velocity : 1600 m/s